NASA TT F-9331

RADIATION PROCESSES IN STRATUS CLOUDS

Ye. M. Feygel'son

Translation of pages 1-59, 66-68, & 121-229 of:
"Radiatsionnyye protsessy v sloistoobraznykh oblakakh".
Izdatel'stvo "Nauka", Moscow, 1964

NATIONAL AERONAUTICS AND SPACE ADMINISTRATION
WASHINGTON MAY 1965

RADIATION PROCESSES IN STRATUS CLOUDS

Ye.M.Feygel'son

33800

The propagation of radiant energy in stratus clouds and the role of this energy in cloud formation and development are discussed and calculated. The problem of scattering and absorption in clouds is investigated from the viewpoint of radiation transfer. Absorption spectra of water droplets and ice crystals are given and experiments on light scattering in clouds are discussed. The role of radiant energy in the physical processes connected with cloud formation and the influence of the re-radiation from clouds to the surrounding atmosphere are discussed and programmed on an electronic computer ("Ural-1"). The problems are formulated with and without allowance for radiation. The results are compared with the calculations by other authors and with actual experiments. Numerous graphs, tabulations, and references are included. author

INTRODUCTION

*/3

This monograph is devoted to the investigation of the propagation of radiant energy in clouds and to elucidation of the role of radiant energy in cloud formation and development.

The laws of radiant energy transfer in a cloudy and cloudless atmosphere differ, since the optical properties of such atmospheres differ.

The main features of clouds as optical media are:

1. Radiant energy is absorbed in a cloud by water vapor, and also by liquid water droplets and ice crystals, whose absorption in the long-wave region of spectrum is one order of magnitude - or more - greater than that of water vapor.

2. Droplet water shows extensive absorption in the 8-12 μ spectrum band, i.e., in the "transparent window" of the atmosphere for which the absorption of water vapor is low. This is of primary importance in the heat exchange between a cloud and the atmosphere surrounding it.

3. Liquid water and ice have continuous absorption spectra, in contrast to water vapor, which has a line spectrum.

4. Long-wave radiation undergoes considerable scattering by liquid water

---

* Numbers in the margin indicate pagination in the original foreign text.

and ice, while such scattering is negligible in the cloudless atmosphere.

5. The scattering coefficient of droplet water in the short-wave region is several orders greater than that of the cloudless atmosphere.

6. The scattering of light by water droplets is characterized by a very elongated scattering indicatrix.

The need for taking account of scattering as well as absorption, the elongation of the indicatrix of clouds, and the great optical thickness make the radiation transfer problem in clouds considerably more difficult than in the cloudless atmosphere. This problem belongs to the specialized field of radiation transfer theory - which studies transfer in strongly scattering media, including such objects of geophysical study as clouds, oceans, or snowfields, and in many cases demanding the development of special methods of research. Problems in the optics of powders and colloids are also related to this general subject matter.

The studies reported in this monograph, in their general direction, can be classified into two groups:

1. Investigations of the optical regime of clouds, and of the angular and spectral distribution of the radiation emitted by them (Chapters II-IV).

2. Elucidation of the role of radiant energy in the physical processes connected with cloud formation and atmospheric thermodynamics.

In the concluding part of the book (Chapters V-VII, especially Chapters III and IV), two aspects of the phenomena are likewise distinguished: the influence of radiation on the state of a cloud, and the influence of a cloud, by virtue of its radiational properties, on the surrounding atmosphere. /4

The following is a brief summary, Chapter by Chapter.

Chapter I is an introductory review of the basic facts on the cloud as an optical medium, for use in subsequent Chapters.

Chapter II investigates the scattering, in clouds, of solar energy in the visible spectrum range (0.35-0.75 μ); develops an approximate method for determining the radiation intensity and flux; calculates the mean radiant flux on the boundaries of stratus clouds of various forms, together with their albedo; and gives the directional distribution of the radiation reflected and transmitted by clouds. We also consider the propagation of light from a directed source through a cloud, estimate the correction to the direct light of the source for multiple scattering, and propose a method for determining the spectrum of the particles by measuring the attenuation of the direct beam.

Chapter III gives a method of calculating the radiation flux with allowance for the absorption and calculates the spectral flux on the boundaries of a cloud in the near-infrared region of the spectrum ($0.70 \leq \lambda < 2.5$ μ). The quantity of solar radiation absorbed by a cloud layer is also estimated.

Chapter IV determines the spectral albedo and characteristic radiation of clouds in the long-wave region ($3 \leq \lambda \leq 30\ \mu$) and estimates the degree to which the radiation from cloud boundaries approaches black-body radiation. In this Chapter (and in Chapter V) we elucidate the qualitative features of the effect of a cloud layer on the vertical temperature distribution in the atmosphere.

Chapter V, for the case of an atmosphere containing a cloud layer, considers a classical problem in radiation transfer theory: the vertical temperature distribution under conditions of radiative equilibrium. Our calculations demonstrate the influence of the cloud on the temperature conditions of the atmosphere and the interaction of various factors of radiation transfer in the development of the radiation temperature.

Chapter VI is devoted to the nonstationary thermal regime of stratus clouds after their formation. We study the radiative cooling of the upper part of a cloud, considered in isolation or in conjunction with other forms of heat exchange. We investigate the development, above the clouds, of temperature inversions of radiative origin. We define the ability of a cloud layer to form spontaneously and maintain itself, by means of radiative transfer, in the neighborhood of the upper boundary.

Finally, Chapter VII investigates the role of radiative heat transfer in the initial stage of cloud formation. Here, we pose the general problem of the formation of a cloud layer as a result of interaction between all the principal factors of heat exchange and moisture exchange. However, we give only the very first preliminary results of the solution.

In this monograph we consider only those stratus clouds that constitute sufficiently simple optical media, i.e., clouds that are plane-stratified and are of great horizontal extension. These clouds are interesting, since they are stable, typical for the middle latitudes, and cover large areas. A number of the results obtained for stratus clouds may be applied to clouds of other forms.

In conclusion, we note that the primary method of investigation has been the numerical solution of the equations of radiation transfer and heat exchange. The approximate solutions obtained are often rather rough (mainly in Chapters III-IV); an error estimate is given in all cases where it could be made. /5

The work on which this monograph is based was performed with the participation of M.A.Kuznetsova and Ye.P.Petrova, Laboratory Assistants, Institute of Atmospheric Physics, USSR Academy of Sciences, who did most of the calculations. M.A.Kuznetsova also took part in compiling the survey of physical properties of stratus clouds (Chapter I, Section 1). Junior Scientist O.N.Dobrova, Institute of Atmospheric Physics, took part in working out the method of solving the transfer equations given in Chapter II, Sections 2-5, and in the calculations. Junior Scientist L.V.Petrova, Institute of Atmospheric Physics, did the programming of the problems given in Chapter VII, and obtained the numerical results on an "Ural-1" computer. I express my thanks to all these colleagues.

I also wish to thank Prof.G.V.Rozenberg, Senior Scientist M.S.Malkevich

and L.M.Romanov, Candidate in Physical and Mathematical Sciences, for a number of useful suggestions.

This monograph is the result of investigations by the author during the last 12 years. The work before 1958 has been reviewed and substantially revised.

The first stage of this work was done under the guidance of Prof.Yevgraf Sergeyevich Kuznetsov. I also express my profound appreciation to Ye.S. Kuznetsov.

TABLE OF CONTENTS

/230

SYMBOLS /6

In this paper the following symbols are used:

z - height,
r - direction of propagation of energy characterized by the polar angle θ, and azimuth ψ, $\mu = \cos\theta$,
t - time,
t° - temperature in Centigrade,
T - absolute temperature,
T_d - dew point temperature,
γ - vertical temperature gradient,
γ_a - adiabatic temperature gradient,
c_p - heat capacity at constant pressure,
ρ - air density,
ρ_w - density of water vapor in the atmosphere, or humidity,
ρ_{CO_2} - same for carbon dioxide,
ρ_v - same for droplet water, or liquid water content,
ρ_a - same for aerosol,

$q_w = \frac{\rho_w}{\rho}$ - specific humidity,

$q_v = \frac{\rho_v}{\rho}$ - specific water content,

$q = q_w + q_v$ - specific total moisture content,
u - relative humidity,
w - vertical velocity,
k_t - kinematic coefficient of turbulent mixing,
α - effective coefficient of absorption of real air per unit mass,
n - refractive index,
$\varkappa$ - absorption index,
α_w - mass coefficient of absorption of water vapor,
α_{CO_2} - same for carbon dioxide,
α_v - same for water,
α_a - same for aerosol,
$\tilde{\alpha}$, $\tilde{\alpha}_w$, $\tilde{\alpha}_v$; $\tilde{\alpha}_{CO_2}$; $\tilde{\alpha}_a$ - volumetric coefficient of absorption for the same cases,
$P(m)$ - function of radiative transfer in the layer containing m gm/cm^2 of the absorbing substance.

Analogous symbols are used for mass and volume coefficients of scattering making use only of σ, σ_v, and σ_a as well as coefficients $\tilde{\sigma}$, $\tilde{\sigma}_v$, and $\tilde{\sigma}_a$. In addition, we also will have σ_R and $\tilde{\sigma}_R$ which are purely molecular or Rayleigh scattering coefficients. Accordingly, the following are defined:

$\gamma(\varphi)$ - function of scattering (we will denote this by indicatrix of scattering) of a real atmosphere,

$\gamma_v(\varphi)$ - function of scattering of droplet water,

$\gamma_a(\varphi)$ - same for aerosol.

We note that the values α, σ, and γ for all substantions given here are, /7 generally speaking, functions of the wavelength λ (or of the frequency ν). The relation to the wavelength is denoted by α_λ, σ_λ, γ_λ. Furthermore, the function and coefficient of scattering of droplet water both depend on the size of the droplets; the symbols given above relate to a combination of droplets of different sizes. In the case of a single droplet with a radius a, the symbols $\sigma_v(a)$, $\gamma_v(a, \varphi)$ are used.

D - coefficient of total attenuation of radiation,
τ - optical thickness measured from the lower boundary of the atmosphere,
τ' - optical thickness measured from the upper boundary,
τ^* - total optical thickness of the atmosphere: $\tau^* = \tau + \tau'$,
τ_0 - total optical thickness of the cloud layer,
A_e - albedo of the earth's surface,
A - albedo of the cloud layer,
$I(z, r)$ - intensity of radiation at the point z, in the direction r,
$F(z)$ - radiation flux,
I_i and F_i - intensity and flux of ascending (i = 1) and descending (i = 2) radiation,
$r_\odot$ - direction of propagation of solar light,
ζ - zenith distance of the sun, $\mu_\odot = \cos \zeta$,
πS - solar constant,
a - droplet radius,
$\pi a^2 K_s(a, \lambda)$ - effective cross section for scattering,
$\pi a^2 K_a(a, \lambda)$ - same for absorption,
$\pi a^2 K_1(a, \lambda)$ - effective cross section for integral back scattering,
$\pi a^2 K(a, \lambda)$ - effective cross section for attenuation,
v - meteorological visibility range.

All formulas, illustrations, and Tables are designated by three numbers: The first (Roman) indicates the Chapter number, the second - the Section number, the third - the formula, Figure, or Table number.

CHAPTER I

/8

THE CLOUDY ATMOSPHERE AS AN OPTICAL MEDIUM

Section 1. Survey of the Physical Properties of Stratus Clouds

This review contains a summary of the basic concepts on the physical properties of stratus clouds. More complete information can be found in monographs (Bibl.1-3) and in the compendium (Bibl.4).

1.1 Forms of Stratus Clouds

Stratus clouds include cirrostratus designated below as Cs (Cirrostratus), high stratus designated as As (Altostratus), stratus-rain designated as Ns (Nimbostratus), Sc (Stratocumulus) and St (Stratus). Similar to these in their physical properties are also Ac (Altocumulus).

Stratus clouds of the upper-layer Cs appear as a white or light-blue rather thin veil. They are observed singly or in combination with other cloud forms. With the passage of frontal cloudiness, Ci (Cirrus) increase in quantity and gradually cover the entire sky, changing into Cs which, in turn, are replaced by As after compacting and lowering.

As clouds belong to those of the middle layer. They have the appearance of a grayish or bluish homogeneous layer of fibrous structure; As may cover the entire sky. Weakly defined waves are sometimes noted along the lower base of the sheet. As clouds often are similar to Ac clouds in cases when Ac have the appearance of a continuous sheet.

Clouds of the lower layer include the St, Sc,and Ns clouds. The nimbostratus clouds Ns form a continuous gray or dark-gray sheet with various bluish-yellowish hues; the highly amorphous and locally translucent Ns are of great thickness. Usually, Ns are formed from As whose layers gradually become compacted and sink until they are converted to Ns. Such clouds produce extensive precipitation and are almost always connected with fronts.

Together, the Ns and As clouds form the frontal system of Ns-As clouds (sometimes Ns-As-Cs) distinguished by great thickness. Because of precipitation, the base of the Ns is always washed out and ragged. Internally, Ns are quite nonuniform with occasional interspersed individual cumulonimbus clouds.

Stratus clouds St appear as a low gray or grayish-yellow sheet of almost homogeneous form resembling fog rising above the earth's surface. The lower surface of the clouds is quite ragged with irregular wisps hanging from it.

Stratocumulus clouds Sc consist of large globular masses, waves, or gray /9 shrouds. Between these elements, the cloud cover thins out, forming interstices.

1.2 Levels, Thickness, Temperature, Moisture

In this and the following Sections provisional data on stratus clouds are compiled.

Table I.1.1 [assembled from data of the monograph (Bibl.1)] gives the distribution with height and the thicknesses of various forms of clouds.

TABLE I.1.1

Type of Cloud	Height of Base km	Thickness of Layers, km
Cs	6—8	1.5—2.5, at times from 0.1 to several km
As	2—6	1—2
Ac	2—6	~0.3
Ns — As	0.1—1	2—3 (at times 5—6)
St	0.1—0.7	0.2—0.8
Sc	0.6—1.5	0.2—0.8
Ns — As — Cs	~1	5—6 (to 12)

Temperature data are given below.

Table I.1.2 shows the temperatures of Ci clouds according to data in another report (Bibl.5).

TABLE I.1.2

Lower Boundary		Upper Boundary	
Limits of Observed Temperature	Most Frequently Recurring Temperatures	Limits of Observed Temperature	Most Frequently Recurring Temperatures
—23°; —62°	—40°; —45°	—40°; —75°	—46°; —48°

The Ns-As cloud systems are characterized principally by negative temperatures (Bibl.1). Temperatures of $+5^{\circ}$ and -5° occur most frequently at the lower boundary. The temperature gradient within the system is, on the average, somewhat smaller than the moist-adiabatic and increases with height: 0.47 at the lower boundary, 0.49 in the middle, and 0.55 in the upper boundary. The range of temperature from -8° to -12° predominates inside the cloud.

In individually occurring As layers, temperatures from -4° to -6° predominate, while in As clouds temperatures of -6° to -8° predominate. These data are taken from another report (Bibl.1) and obviously refer to the summer period.

For St-Sc clouds the temperature distribution given in Table I.1.3 (Bibl.1)

is typical.

In interpreting Table I.1.3, we indicate that for St and Sc clouds the presence of above-cloud inversion, partly wedged into the cloud itself, is characteristic. The nature and character of both parts of the inversion (within the cloud and above it) are different. This question is considered in more detail in Chapter VI. Lines 5 and 6 in Table I.1.3 relate to the first part of the inversion while lines 7 and 8 refer to the second part.

A detailed analysis of moisture in the clouds is made difficult by the low accuracy of hygrometers and their large inertia (especially at a humidity close to 100%; it is usually assumed that the relative humidity in clouds is equal to 100% because reliable measurements of supersaturation are as yet almost unavailable). /10

TABLE I.1.3

	December-February	March-May	June-August	September-October	Average for the year
1. Temperature gradient under the cloud, °/100 m	0.69	0.80	0.77	0.76	0.76
2. Temperature on the lower boundary, °C	—9.0	—5.0	+3.5	—0.8	—2.8
3. Temperature gradient in clouds without inversion, °/100 m	0.66	0.62	0.65	0.71	0.66
4. Temperature on the upper boundary, °C	—10.0	—6.9	+1.2	—3.1	—4.7
5. Thickness of inversion wedging into the cloud, km	0.136	0.134	0.149	0.147	0.139
6. Temperature gradient in this inversion, °/100 m	—3.3	—1.74	—0.74	—2.05	—1.94
7. Thickness of the inversion layer above cloud, km	0.31	0.27	0.39	0.36	0.3
8. Temperature gradient in this layer, °/100 m	—0.35	—0.13	+0.20	—0.84	—0.28

1.3 Phase Composition, Liquid-Water Content, Microstructure

The clouds of the lower and middle layer are mainly all liquid water or mixed.

In Fig.I.1.1 taken from Borovikov (Bibl.1), the lower curve delimits the region of recurrence of all-water clouds and the upper curve, of mixed types. Let us compare this diagram with the temperature data given above. We see that St-Sc clouds are all-water clouds in no less than 50% of the cases and are almost never all-crystalline. Frontal Ns-As systems are more often mixed than are St and Sc. The phase composition of individual As and Ac layers has not yet been sufficiently investigated. However, there are reasons to believe (Bibl.1) that the As are mixed clouds while the Ac are predominately crystalline (see also Chapter II, Sect.1). The Cs clouds of the upper layer are always

crystalline.

The liquid-water content of the cloud ρ_v depends on the temperature and /11 on the temperature gradient of the cloud layer (increasing with the increase of

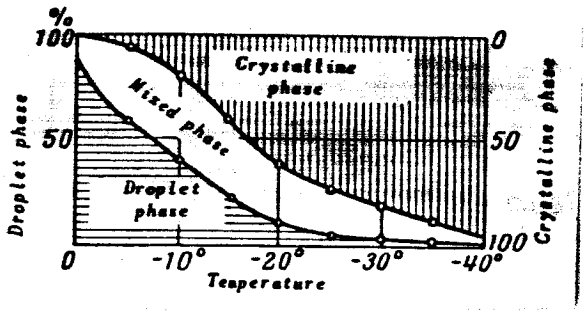

Fig.I.1.1 Correlation of the Phase Composition of Clouds with the Temperature

the latter), on the height of the lower boundary, on the form of the clouds, on the phase of its state, and on the thermodynamic conditions of formation of the cloud. Within the limits of the cloud, the liquid-water content changes sub-

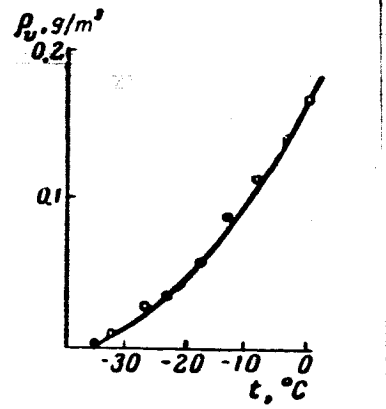

Fig.I.1.2 Average Liquid-Water Content as a Function of Temperature

stantially along the vertical. Figure I.1.2 shows the correlation of the liquid-water content of stratus clouds with the temperature (the circles represent experimental data, while the solid curve gives theoretical data) obtained from 493 measurements of liquid-water content in the region of Leningrad. These data are presented in Table I.1.4.

Table I.1.5 gives the data obtained at the TsAO [Central Aerological Observatory; (Bibl.1)]. The average liquid-water content $\rho_{v,av}$ and the maximum liquid-water content $\rho_{v\ max}$ are compiled for two groups of St, Sc, Ac and Ns, As clouds; the measurements were made at Riga, Minsk, and Vnukovo (average data

for the three indicated points are given in Table I.1.5).

A comparison of Tables I.1.4 and I.1.5 with the above characteristic temperatures, together with other information, permits a general conclusion as to the

TABLE I.1.4

	Temperature Interval, °C							
	−35÷ −30	−30÷ −25	−25÷ −20	−20÷ −15	−15÷ −10	−10÷ −5	−5÷0	0÷ +5
Number of Cases, n	7	10	22	29	44	105	222	54
ρ_v, g/m³	0.005	0.024	0.030	0.055	0.084	0.110	0.137	0.161

characteristic water content of clouds of various types. These results are summarized in Table I.1.6.

TABLE I.1.5

t, °C	St, Sc, Ac			Ns, As		
	n	ρ_v, av., g/m³	ρ_v, max., g/m³	n	ρ_v, av., g/m³	ρ_v, max., g/m³
15—19	15	0.29	1.14	—	—	—
10—14.9	108	0.27	1.18	26	0.36	1.66
5—9.9	301	0.33	3.14	96	0.32	1.30
0.0—4.9	663	0.30	3.00	295	0.30	1.07
−5.0—(−0.1)	1542	0.21	1.53	644	0.22	1.11
−10.0—(−5)	1344	0.18	0.99	328	0.17	0.90
−15.0—(−10.1)	710	0.14	1.47	175	0.17	0.67
−20.0—(−15.1)	163	0.13	0.82	66	0.15	0.48
−25.0—(−20.1)	47	0.12	0.39	23	0.15	0.33
−30.0—(−25.1)	3	0.09	0.15	1	0.22	0.22
−35.0—(−30.1)	1	0.15	0.15	—	—	—

The distribution of the water content within the cloud with height differs for clouds of various types.

In Sc, Ac, and St clouds lying below the inversion layer which inhibits the turbulent exchange, the water content increases with height and reaches a maximum value in the upper third of the cloud [Fig.I.1.3; (Bibl.6)]; at the very top boundary, the liquid-water content decreases sharply.

It should be said, however, that recent measurements by G.M.Zabrodskiy /12 (Bibl.7) made with more up-to-date apparatus show an increase in liquid-water content all the way to the upper boundary.

In Ns-As clouds [Fig.I.1.4; (Bibl.6)] the maximum liquid-water content is reached in the lower part of the layer when the cloud is thick and in its middle part when the cloud is only of moderate thickness.

TABLE I.1.6

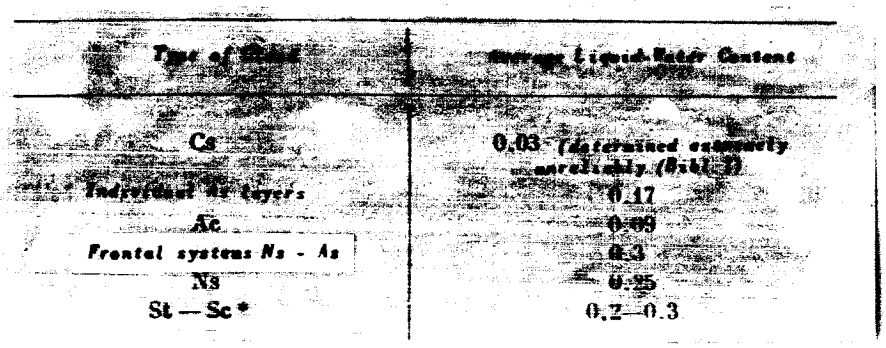

* In another report (Bibl.1) the average value of liquid-water content for St-Sc is given, equal to 0.2 gm/m^3, while (Bibl.2) gives test data by various authors; the value 0.3 gm/m^3 is considered as average.

A seasonal variation in the liquid-water content of stratus clouds is observed, apparently due to the above-mentioned correlation between liquid-water content and temperature.

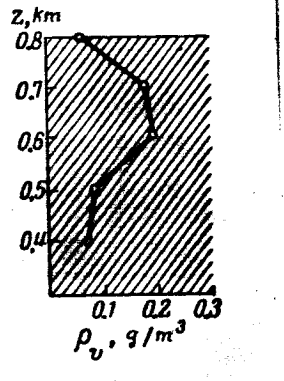

Fig.I.1.3 Distribution of Liquid-Water Content with Height in St, Sc, and Ac Clouds

Mean monthly values of liquid-water content and of temperatures in Sc and Ns clouds, obtained by V.Ye.Minervin (Bibl.8) from a large number of observations at a series of points, are given in Table I.1.7. /13

The correlation between liquid-water content and temperature was also con-

firmed in observations by A.I.Voskresenskiy and A.L.Dergach (Bibl.9) according to which the liquid-water content of St and Sc clouds in Arctic regions is lower

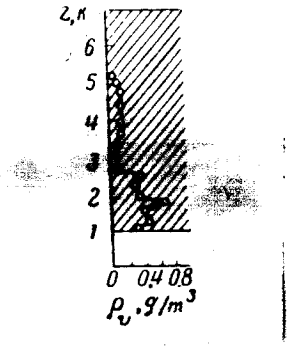

Fig.I.1.4 Distribution of Liquid-Water Content with Height in Ns-As Clouds

than in temperate latitudes (see Table I.1.8). The observed difference in liquid-water content is apparently explained by the lower temperatures in the

TABLE I.1.7

		Jan.	Feb.	March	April	May	June
Sc	ρ_v, g/m³	0.17	0.165	0.15	0.19	0.22	0.29
	t, °C	−8.0	−8.2	−7.3	−2.7	−1.1	3.4
Ns	ρ_v, g/m³	0.17	0.22	0.16	0.20	0.21	0.33
	t, °C	−7.8	−6.1	−5.0	−2.5	0.0	2.9
Sc	ρ_v, g/m³	0.305	0.33	0.27	0.23	0.20	0.17
	t, °C	5.4	5.9	−0.1	−5.1	−5.1	−7.8
Ns	ρ_v, g/m³	0.36	0.35	0.23	0.225	0.20	0.20
	t, °C	3.8	4.1	−1.3	−2.2	−4.8	−4.7

Artic as compared with those in the ETC (European Territory of the Soviet Union). Attention is directed to the difference in liquid-water content of St and Sc clouds as shown in Table I.1.8. The same conclusions are drawn elsewhere (Bibl.10) where it is shown that, in the Arctic, the liquid-water content

of Sc clouds is higher than that of St clouds.

In conclusion, we shall show that the liquid-water content is a rather unstable value which fluctuates irregularly within the cloud, with time and from case to case.

TABLE I.1.8

Cloud Type	Arctic ρ_v, g/m³	ETC* ρ_v, g/m³
St	0.10	0.14
Sc	0.23	0.29

* ETC — European Territory of the USSR

An example of changes in the liquid-water content during horizontal flight of an aircraft at a speed of 275 km/hour in stratus layers on the lee of a cold front is given in Table I.1.9, taken from another paper (Bibl.10).

TABLE I.1.9

Time	5 h 20 min	5 h 20.5 min	5 h 21 min	5 h 21.5 min	5 h 31 min	5 h 31.5 min	5 h 43 min	5 h 43.5 min
ρ_v, g/m³	0.19	0.29	0.3	0.02	0.08	0.19	0.02	0.09

The droplet composition of stratus clouds is characterized in Figs.I.1.5 and I.1.6 and also in the summary Table I.1.10, taken from another paper (Bibl.2). The size distribution of droplets is presented in Fig.I.1.5. The contribution of droplets of various sizes to the liquid-water content is shown in Fig.I.1.6. The symbols used in Table I.1.10 are a_m - average radius, i.e., the sum of all radii of the droplets, divided by their total number; a_d - the modal radius corresponding to the most frequently occurring radius of droplets in the given aggregate; a_p - the prevailing radius, i.e., the radius corresponding to the maximum contribution to liquid-water content.

An analysis of more detailed and up-to-date data of measurements carried /14 out at several locations was made at the Central Aerological Observatory. Unlike in previous papers in the processing of the observational data, here a correction was introduced for the coefficient of capture of droplets by the scoop. As a result, the percentage of fine droplets was increased and the corresponding average radius decreased. These data are shown in Table I.1.11 (Bibl.1).

TABLE I.1.10

Type of Cloud	Concentration (No. of Droplets, in 1 cm³)	a_m, μ	a_d, μ	a_p, μ	Measuring Interval, μ
Sc	340	4	3.5	6.5	1—12
	500	—	—	10.20	3—25
	310	8	—	—	—
As	450	5	4.5	7	1—13
Ns	330	6	4.0	12	1—20
	175	11	—	--	—
St	260	6	4.0	9	1—22
	664	5.3	7.0	—	2—40

Some information on the changes in the average droplet radius in the cloud are given in Table I.1.12 for clouds of various types (Bibl.1).

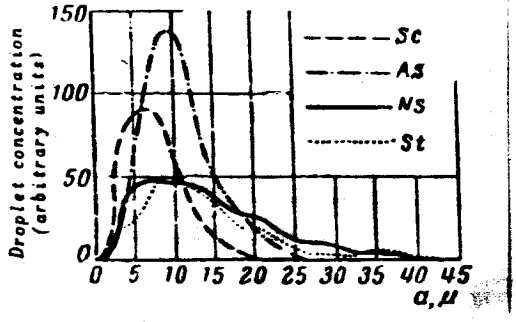

Fig.I.1.5 Droplet-Size Distribution

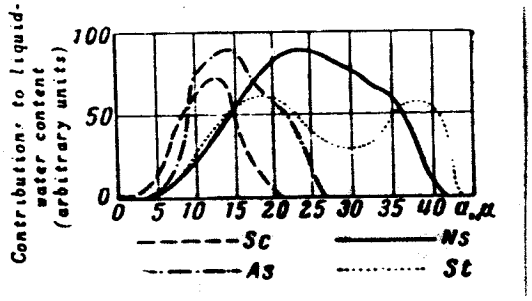

Fig.I.1.6 Contributions to Liquid-Water Content by Droplets of a Given Size

We note that Table I.1.12 is recommended elsewhere (Bibl.1) for practical use, as it represents average values. It does, however, give for Ns clouds a_{av} values which substantially differ from the values in Table I.1.11 taken from the same paper (Bibl.1).

The spectrum of droplets in clouds is just as variable a quantity as /15

the liquid-water content and depends on the stage of formation of the cloud, on the considered level, and the thickness. The subject of the variability in drop sizes is discussed in detail in (Bibl.1) where it is shown that averaged

TABLE I.1.11

Cloud Type	Average Diameter, μ
St	5.2
Sc	5.0
Ns	5.5
Ac	4.8

TABLE I.1.12

Type of Clouds*	a_{av}, μ	Type of Clouds*	a_{av}, μ
St	5.0	Sc	5.0
St_1	3.9	Sc_1	4.0
St_2	4.5	Sc_2	4.8
St_3	5.3	Sc_3	5.5
Ns	6.0—7.0	As	4.5—5.0

* Subscripts indicate lower (1), middle (2), and upper (3) parts of the cloud

characteristics of clouds of various shapes show less differences than the characteristics of individual clouds of the same shape or even of the same

TABLE I.1.13

Type of Clouds	Brikar (Bibl. 1)	Borovikov (Bibl. 1)	Vin (Bibl. 1)	Lewis (Bibl. 1) (Pacific Coast)		Lewis (Bibl. 1) (Other Regions of the USA)		Bullrich (Bibl. 11)	
	a_{av}	a_{av}	a_{av}	a_{av}	N	a_{av}	N	a_{av}	N
St	4.2	4.6	6.0	9.9	100	5.4	320	6	275
Sc	7.6	8.2	5.4					4	770
Ns	9.8	12.0	6.0	—	—	—	—	—	—
As	—	—	—	9.4	35	7.1	75	8	100
Ac	—	7.1	—						

cloud at various stages of its formation or at various levels. This partially explains the difference in the value of average radii obtained by various

authors. As an illustration, the values for a_{av} and the droplet concentrations N based on various data are given in Table I.1.13.

It should be noted, however, that the discrepancies in the values could be due also to the different methods of measuring the dimensional spectrum or, what is important, the shortcomings of these methods. We do not intend to analyze the existing methods, referring the reader to monographs (Bibl.1), and wish to point out only the following which is important for problems of cloud optics. Basically, up to now cloud-drop scoops have been used that are unsuitable for trapping very small particles ($a \leq 2 - 3\mu$). As a result, the drop-size distribution curves often have the appearance of those in Fig.I.1.5, i.e., they have a maximum in the region of average size. In all cases in which methods without this drawback were used, a second, much stronger maximum appeared in the region of small sizes.

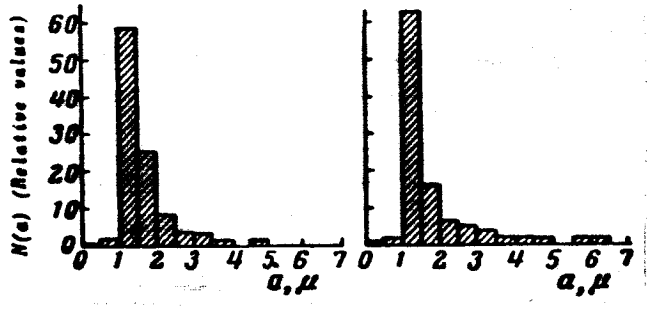

Fig.I.1.7 Examples of the Spectrum of Droplets in Clouds

Thus, in the paper by Keily and Millen (Bibl.12) several examples of spectra, obtained with a device trapping droplets of any size, are given. The method is based on identifying the droplets by an electric charge induced by /16 an artificial source. Spectra obtained for St clouds are presented in Fig.I.1.7.

The results of determination of the droplet spectrum by the optical method in clouds of the Sc type on the slopes of Mt. Washington are described in an article by Eldridge (Bibl.13). The data are compiled in Table I.1.14 giving the number of droplets of various sizes, contained in one cubic centimeter.

It should be pointed out that both of the latter articles were subjected to severe criticism in the literature (Bibl.14, 15, 16). Nevertheless, the revealed fact of the existence in clouds of small so-called "submicroscopic" particles is undisputable. Changes in optical characteristics of clouds due to very small particles are discussed elsewhere (Bibl.13, 17, 18).

It is interesting that, as indicated in Table I.1.13 (first, second, and last columns) Sc clouds have a larger average droplet radius and a larger concentration than do St clouds; this was also noted (Bibl.10) for Arctic conditions. Such a difference between St and Sc clouds is apparently real and

TABLE I.1.14

Droplet Radius · P	Ordinal Number of Measurements									
	1	2	3	4	5	6	7	8	9	10
0.5	34 600	47 900	15 100	1 910	34 400	61 100	22 100	25 600	45 600	21 300
1.5	2 400	830	3 790	380	1 050	1 580	4 410	6 170	4 560	4 680
2.5	350	—	770	130	—	—	370	1 550	370	850
3.5	—	—	80	640	—	—	550	—	—	—
4.5	—	—	230	130	—	—	370	510	—	420
5.5	140	30	150	—	—	—	70	1 060	370	1 700
6.5	230	110	80	—	200	220	—	510	730	850
7.5	80	220	—	—	480	1 140	40	—	—	—
8.5	—	80	—	—	70	140	40	—	—	—
9.5	—	30	—	—	—	—	—	—	—	—
10.5	—	—	—	—	—	—	—	—	—	—
11.5	—	—	—	—	—	—	40	—	—	—
12.5	—	—	—	—	—	—	110	—	180	—
Total number of droplets	37 800	49 200	20 200	3 190	36 200	64 100	28 100	35 400	51 800	29 800

characteristic since it agrees well with the greater reflectivity of Sc clouds (see Chapter II, Sect.1).

In conclusion, we would like to mention that several formulas were proposed for describing the spectrum of cloud droplets. Of these, two are widely accepted:

a) Formula by A.Kh.Khrgian and I.P.Mazin (Bibl.1)

$$n(a) = a_1 a^2 e^{-b_1 a}, \tag{1.1}$$

where

$$b_1 = \frac{3}{a_{av}}, \qquad a_1 = 1{,}45\,\frac{\rho_v}{a_{av}^6};$$

b) Formula by L.M.Levin (Bibl.19)

$$n(a) = \frac{1}{\sigma\sqrt{2\pi}\,a} e^{-\frac{\ln^2\left(\frac{a}{a_0}\right)}{2\sigma^2}}, \tag{1.2}$$

where a_0 denotes the median radius and σ the mean-square deviation of the logarithm of the droplet radius.

A comparison of eqs.(I.1.1) and (I.1.2) with numerous observational data /17 showed that the accuracy of the second formula is somewhat greater.

The information on stratus clouds compiled in this Section makes it pos-

sible to determine the principal parameters. These data are shown in Table I.1.15.

At the same time, the material examined above shows that a certain caution is required with respect to the data given in this Table. The Table is useful

TABLE I.1.15

Type of Clouds	Thickness of Layer H, km	Height of Base, km	Average Water Content, gw/m^3	Average Temperature °C	Average Droplet Radius, μ	Total Droplet Concentration cm^{-3}
St	~0.5	0.1—0.7	0.2	—5; +5	5,2	275
Sc	~0.5	0.5—1.5	0,2—0.3	—5; +5	5,0	770
Ns — As	2—3	0.1—1	0.3	—8; —12	5.5 (6—7)	—
As	~0.9	2—6	0.17	—4; —6 (Summer-time)	4.8	
Ac	~0.3	2—6	0.1	—6; —8 (Summer-time)	4.5—5	100
Ns — As — Cs	5—6	1	—		—	
Cs	1.2	6—8	0.03	—40; —45;	—	

only for a rough description of clouds and does not permit a sufficiently clear separation of the microstructure and the liquid-water content of clouds of various types.

Section 2. Radiation Field in the Atmosphere

2.1 Fundamental Concepts

The process of propagation of radiant energy in clouds and in a cloudless atmosphere is investigated below on the basis of the phenomenological theory of radiative transfer (Bibl.20, 21).

The basic concept of this theory is the radiation field, i.e., the distribution of radiation intensity $I_\lambda(x, y, z, r)$ at each point in space (x, y, z) for a given wave.

The amount of energy dE_λ, pertaining to a spectrum interval $(\lambda, \lambda + d\lambda)$ and propagated within a solid angle $d\omega$ in the direction r in a time dt through an element of surface $d\sigma$ is related to the intensity of radiation $I_\lambda(x, y, z, r)$ by the relationship

$$dE_\lambda = I_\lambda \cos\vartheta \, d\lambda \, d\sigma \, d\omega \, dt, \qquad (I.2.1)$$

where ϑ is the angle included by the normal to the surface $d\sigma$ and the direction r. The quantity I_λ is called also the specific intensity. As shown by

eq.(I.2.1), the radiation intensity is the amount of energy in a single spectral interval, flowing in unit time within a unit solid angle through unit area perpendicular to the direction of propagation of the energy.

An important characteristic of the radiation field is the total energy flux (below, we will call it simply flux) which is equal to the total amount of energy propagated through unit area in all directions in unit time

/18

$$F_\lambda(x, y, z) = \int I_\lambda(x, y, z, r)\cos\vartheta\, d\omega, \qquad \text{(I.2.2)}$$

This flux is related to a single spectral interval.

In a system of polar coordinates with the axis directed along the exterior normal to the area the following equation holds

$$d\omega = \sin\vartheta d\vartheta\, d\psi,$$

and the expression of the flux can be written in the form

$$F_\lambda(x, y, z) = \int_0^{2\pi}\int_0^{\pi} I_\lambda(x, y, z, \vartheta, \psi)\sin\vartheta d\vartheta\, d\psi, \qquad \text{(I.2.3)}$$

We shall now introduce the characteristics of interaction of radiation with matter. Matter is able to absorb, scatter, and emit radiation.

The absorptivity of matter can be characterized by the absorption coefficient. If through an area $d\sigma$ in the medium there passes an amount of radiation energy equal to the value (I.2.1) then, by definition, the amount of energy absorbed in an infinitely small layer of thickness ds is equal to

$$\alpha_\lambda \rho\, d\sigma\, ds \cos\vartheta\, d\lambda\, d\omega I_\lambda(x, y, z, r), \qquad \text{(I.2.4)}$$

where ρ is the density of the substance (which may vary from point to point) and α_λ is the mass absorption coefficient.

In the scattering of radiation by matter, part of the radiation energy propagated in the direction r is redistributed in all directions r'. This part of the energy is, by definition, equal to

$$\sigma_\lambda \rho\, d\sigma\, ds \cos\vartheta\, d\lambda\, d\omega\, I_\lambda(x, y, z, r). \qquad \text{(I.2.5)}$$

In order to fully describe the scattering it is necessary to assign also the angular distribution of scattered energy; the corresponding function from the directions r and r' is called the angular function or the scattering index γ_λ (x, y, z, r, and r').

By definition, the quantity

$$\sigma_\lambda \gamma_\lambda \frac{d\omega'}{4\pi} \rho \, d\sigma \, ds \cos\vartheta \, d\lambda \, d\omega \, I_\lambda \tag{I.2.6}$$

represents the part of energy scattered in the direction of r'. Obviously, the scattering index is equated to unity:

$$\frac{1}{4\pi} \int \gamma(x, y, z, r, r') \, d\omega' = 1, \tag{I.2.7}$$

In what follows it is always assumed that this index depends only on the angle of scattering φ (and not on the direction of the incident and scattered light) and can be presented in the form of a series according to the Legendre polynomials:

$$\gamma(\cos\varphi) = \sum_{k=0}^{\infty} C_k P_k(\cos\varphi). \tag{I.2.8}$$

We recall here the Legendre theorem of adding polynomials /19

$$P_k(\cos\varphi) = 2 \sum_{m=1}^{k} \frac{|k-m|!}{|k+m|!} P_k^m(\cos\theta) P_k^m(\cos\theta') \cos k(\psi - \psi') + P_k(\cos\theta) P_k(\cos\theta'), \tag{I.2.9}$$

where θ, ψ, and θ', ψ' are the polar and azimuth angles of the directions r and r'.

The emissivity of matter is characterized by the radiation coefficient η_λ. By definition, the amount of energy of the wavelength interval $(\lambda, \lambda + d\lambda)$ emitted by a mass element of matter $dm = \rho d\sigma ds$ in the directions included within the elementary solid angle $d\omega$ for a time interval dt is equal to

$$\eta_\lambda \, dm \, d\omega \, d\lambda \, dt.$$

If the medium is in a state of thermodynamic equilibrium, then the emissivity and absorptivity of matter are correlated by Kirchhoff's law:

$$\eta_\lambda = \alpha_\lambda B_\lambda(T), \tag{I.2.10}$$

where $B_\lambda(T)$ is Planck's function:

$$B_\lambda(T) = \frac{2hc^2}{\lambda^5} \frac{1}{\exp\left(\frac{hc}{\lambda k T}\right) - 1}. \tag{I.2.11}$$

For the lower atmosphere* the condition of local thermodynamic equilibrium

*Here and below, by lower atmosphere we mean the troposphere.

is usually assumed, i.e., it is supposed that, at each locus, the relationship (I.2.10) exists for the temperature at this point.

We shall consider that the condition of local thermodynamic equilibrium is applicable to clouds.

In addition to the mass absorption coefficient and the scattering coefficient α and σ, volumetric coefficients are generally used, i.e., the coefficients $\tilde{\alpha}$ and $\tilde{\sigma}$ computed for unit volume, where $\tilde{\alpha} = a\rho$ and $\tilde{\sigma} = \sigma\rho$.

Equations (I.2.4) and (I.2.5) yield the dimensional correlations:

$$[\sigma] = [\alpha] = \left[\frac{l^2}{m}\right],$$
$$[\tilde{\sigma}] = [\tilde{\alpha}] = \left[\frac{1}{l}\right],$$

where $[l]$ is the dimension of length and [m] is the dimension of mass.

In the theory of scattering, also the effective cross sections for scattering $\pi a^2 K_s$ and for absorption $\pi a^2 K_a$ are introduced on the portion of the radius a, which are correlated with $\tilde{\sigma}$ and $\tilde{\alpha}$ by

$$\pi a^2 K_s N = \tilde{\sigma}, \qquad \text{(I.4.12)}$$
$$\pi a^2 K_a N = \tilde{\alpha}, \qquad \text{(I.2.13)}$$

where N denotes the number of particles per unit time. The dimensionless values K_s and K_a are designated as relative cross sections for scattering and absorption.

For a rough description of the angular distribution of scatter, the concept of integral scattering into the front hemisphere (with respect to the direction of propagation of light) /20

$$\Gamma_1 = 2\pi \int_0^{\frac{\pi}{2}} \gamma(\varphi) \sin\varphi d\varphi \qquad \text{(I.2.14)}$$

is sometimes introduced, and into the back hemisphere:

$$\Gamma_2 = 2\pi \int_{\frac{\pi}{2}}^{\pi} \gamma(\varphi) \sin\varphi d\varphi. \qquad \text{(I.2.15)}$$

The effective cross section for scattering into the back hemisphere which is denoted by $\pi a^2 K_1$ is also used.

The scattering index as a whole is often characterized by the degree of elongation of Γ which is equal to $\frac{\Gamma_1}{\Gamma_2}$.

2.2 The Transfer Equation

We will introduce the basic equation which describes the process of radiative transfer in a medium. In doing so, we will assume that the medium contains several substances with different radiation coefficients $\eta_{\lambda,i}$, absorption coefficients $\tilde{\alpha}_{\lambda,i}$, and scattering coefficients $\tilde{\sigma}_{\lambda,i}$ (and scattering functions $\gamma_{\lambda,i}$). On the ray r, we will select a small cylinder with a base $d\sigma \perp r$ and an altitude ds.

The variation in radiative energy in the wavelength interval $d\lambda$, transferred during the time dt over a distance ds through the selected cylinder, is equal to

$$\frac{dI_\lambda}{ds} d\sigma ds d\lambda d\omega dt. \tag{I.2.16}$$

This energy fluctuation is due to the loss of energy in absorption which is

$$\sum_i \tilde{\alpha}_{\lambda,i} d\sigma ds d\lambda d\omega dt I_\lambda, \tag{I.2.17}$$

or due to a reduction in energy flux in the direction r produced by scattering in all directions, equal to

$$\sum_i \tilde{\sigma}_{\lambda,i} d\sigma ds d\lambda d\omega dt I_\lambda. \tag{I.2.18}$$

or due to an increase in energy flux in the direction r produced by radiation of the medium

$$\sum_i \tilde{\eta}_{\lambda,i} d\sigma ds d\lambda d\omega dt, \tag{I.2.19}$$

or else due to an increase in energy flux in the direction r produced by scattering of radiation which is propagated in all directions r', equal to

$$\frac{1}{4\pi} \sum_i \tilde{\sigma}_{\lambda,i} \int I_\lambda (r') \gamma_{\lambda,i} (r, r') d\omega' d\sigma ds d\lambda dt d\omega. \tag{I.2.20}$$

Therefore,

$$\frac{dI_\lambda (x, y, z, r)}{ds} = \sum_i \tilde{\eta}_{\lambda,i} + \frac{1}{4\pi} \sum_i \tilde{\sigma}_{\lambda,i} \int I_\lambda (x, y, z, r') \gamma_{i\lambda} (r, r') d\omega' - \\ - \sum_i (\tilde{\alpha}_{\lambda,i} + \tilde{\sigma}_{\lambda,i}) I_\lambda (x, y, z, r). \tag{I.2.21}$$

If the direction cosines of the ray r are designated by l, m, and n, then /21

$$\frac{dI}{ds} = l \frac{dI}{dx} + m \frac{dI}{dy} + n \frac{dI}{dz}.$$

For the case of a plane-stratified medium the last expression is simplified to

$$I_\lambda(P, r) = I_\lambda(\ldots)$$

and

$$\ldots = \cos\theta \frac{dI_\lambda}{dz}$$

(Here the axis z is perpendicular to the boundaries of the medium and is directed from the lower boundary to the upper. The polar axis coincides with the z axis.)

We will introduce the optical thickness of the atmosphere at the z level, determined by the formula

$$\tau_\lambda = \sum_{i=1}^{n} \int_0^z [\tilde{\alpha}_{\lambda, i}(z) + \tilde{\sigma}_{\lambda, i}(z)]\, dz. \tag{I.2.22}$$

The optical thickness of the entire atmosphere τ^* is equal to

$$\tau_\lambda^* = \sum_i \int_0^\infty [\tilde{\alpha}_{\lambda, i}(z) + \tilde{\sigma}_{\lambda, i}(z)]\, dz. \tag{I.2.23}$$

Utilizing eq.(I.2.22) and taking into account eq.(I.2.10), the transfer equation can be presented in the form of

$$\cos\theta \frac{dI_\lambda}{d\tau_\lambda} = \left[1 - \varphi_\lambda(\tau)\right] B_\lambda(T) + \frac{1}{4\pi} \int I_\lambda(\tau, r')\, \hat{\gamma}_\lambda |\, \tau, r, r' |\, d\omega' - I_\lambda(\tau, r), \tag{I.2.24}$$

where

$$\varphi_\lambda(z) = \frac{\sum_i \tilde{\sigma}_{\lambda, i}}{\sum_i (\tilde{\alpha}_{\lambda, i} + \tilde{\sigma}_{\lambda, i})}, \tag{I.2.25}$$

$$\hat{\gamma}_\lambda(z, r, r') = \frac{\sum_i \tilde{\sigma}_{\lambda, i}\, \gamma_{\lambda, i}(z, r, r')}{\sum_i (\tilde{\alpha}_{\lambda, i} + \tilde{\sigma}_{\lambda, i})}. \tag{I.2.26}$$

In solving eq.(I.2.24), the natural boundary condition is the condition imposed on the intensity of radiation penetrating into the medium across the boundaries.

In the case of a plane-parallel medium, radiation passes in ascending directions $\left(0 \leq \theta \leq \frac{\pi}{2}\right)$ into the medium across the lower boundary $\tau = 0$ and in a descending direction $\left(\frac{\pi}{2} \leq \theta \leq \pi\right)$ through the upper boundary $\tau = \tau^*$. It is therefore convenient to consider separately the intensity of ascending radiation:

$$I_1(z, \theta, \psi) = I(z, \theta, \psi) \quad \text{at} \quad 0 \leqslant \theta \leqslant \frac{\pi}{2},$$

(here and below the symbol for the wavelength is omitted) and of descending radiation

$$I_2(z, \tilde{\theta}, \psi) = I(z, \theta, \psi) \quad \text{at} \quad \frac{\pi}{2} \leqslant \theta \leqslant \pi,$$

where

$$\tilde{\theta} = \pi - \theta \quad \text{and} \quad 0 \leqslant \tilde{\theta} \leqslant \frac{\pi}{2}.$$

/22

If, in addition, we introduce the functions

$$\hat{\gamma}_{11}(r, r') = \hat{\gamma}(r, r') \quad \text{at} \quad 0 \leqslant \theta \leqslant \frac{\pi}{2};\ 0 \leqslant \theta' \leqslant \frac{\pi}{2},$$

$$\hat{\gamma}_{12}(r, \tilde{r}') = \hat{\gamma}(r, r') \quad \text{at} \quad 0 \leqslant \theta \leqslant \frac{\pi}{2};\ \frac{\pi}{2} \leqslant \theta' \leqslant \pi,$$

$$\hat{\gamma}_{21}(\tilde{r}, r') = \hat{\gamma}(r, r') \quad \text{at} \quad \frac{\pi}{2} \leqslant \theta \leqslant \pi;\ 0 \leqslant \theta' \leqslant \frac{\pi}{2},$$

$$\hat{\gamma}_{22}(\tilde{r}, \tilde{r}') = \hat{\gamma}(r, r') \quad \text{at} \quad \frac{\pi}{2} \leqslant \theta \leqslant \pi;\ \frac{\pi}{2} \leqslant \theta' \leqslant \pi$$

(here, the angle $\tilde{\theta} = \pi - \theta$ corresponds to the ray $\tilde{r}$) then eq.(I.2.24) can be replaced by a system of equations which determines the functions I_1 and I_2:

$$\cos\theta \frac{\partial I_1}{\partial \tau} = [1 - \varphi(\tau)] B(T) + \frac{1}{4\pi} \int_+ I_1(\tau, r') \hat{\gamma}_{11}(\tau, r, r')\, d\omega' + \frac{1}{4\pi} \int_+ I_2(\tau, r') \hat{\gamma}_{1,2}(\tau, r, r')\, d\omega' - I_1(\tau, r), \tag{I.2.27}$$

$$-\cos\theta \frac{\partial I_2}{\partial \tau} = [1 - \varphi(\tau)] B(T) + \frac{1}{4\pi} \int_+ I_1(\tau, r') \hat{\gamma}_{21}(\tau, r, r')\, d\omega' + \frac{1}{4\pi} \int_+ I_2(\tau, r') \hat{\gamma}_{22}(\tau, r, r')\, d\omega' - I_2(\tau, r). \tag{I.2.28}$$

It is easy to see that $\hat{\gamma}_{11} = \hat{\gamma}_{22}$ and $\hat{\gamma}_{12} = \hat{\gamma}_{21}$ if the index depends only on the angle of scattering. The boundary conditions for eqs.(I.2.27) and (I.2.28) have the form

$$I_1(0, r) = \chi_1(r), \qquad I_2(\tau^*, r) = \chi_2(r), \tag{I.2.29}$$

where $\chi_1(r)$ and $\chi_2(r)$ are given functions.

In eqs.(I.2.27) - (I.2.28), the angular variables change within the limits $0 \leq \theta \leq \frac{\pi}{2}$, $0 \leq \psi \leq 2\pi$. Accordingly, the integration is extended over the surface of the upper hemisphere.

Along with the quantities I_1 and I_2 it is convenient to investigate the ascending flux of radiation F_1 and the descending flux F_2:

$$F_1(\tau) = \int_0^{2\pi} \int_0^{\frac{\pi}{2}} I_1(\tau, r) \cos\theta \sin\theta d\theta d\psi, \tag{I.2.30}$$

$$F_2(\tau) = \int_1^{2\pi} \int_0^{\frac{\pi}{2}} I_2(\tau, r) \cos\theta \sin\theta d\theta d\psi. \tag{I.2.31}$$

The complete or resultant radiation flux $F(\tau)$ is equal to

$$F(\tau) = \int_0^{2\pi} \int_0^{\pi} I(\tau, r) \cos\theta \sin\theta d\theta d\psi = F_1(\tau) - F_2(\tau). \tag{I.2.32}$$

2.3 Integral Form of the Transfer Equation

/23

For simplicity, we will consider a medium consisting of only one substance. Equations (I.2.27) and (I.2.28), in this case, assume the form

$$\cos\theta \frac{\partial I_1}{\partial \tau} = (1-k) B(T) + kK_1(\tau, r) - I_1(\tau, r), \tag{I.2.33}$$

$$-\cos\theta \frac{\partial I_2}{\partial \tau} = (1-k) B(T) + kK_2(\tau, r) - I_2(\tau, r), \tag{I.2.34}$$

where

$$k = \frac{\sigma}{\alpha + \sigma},$$

$$K_1(\tau, r) = \frac{1}{4\pi} \int_+ I_1(\tau, r') \gamma_{11}(\tau, r, r') d\omega' + \frac{1}{4\pi} \int_+ I_2(\tau, r') \gamma_{12}(\tau, r, r') d\omega', \tag{I.2.35}$$

$$K_2(\tau, r) = \frac{1}{4\pi} \int_+ I_1(\tau, r') \gamma_{21}(\tau, r, r') d\omega' + \frac{1}{4\pi} \int_+ I_2(\tau, r') \gamma_{22}(\tau, r, r') d\omega'. \tag{I.2.36}$$

We shall formally consider $B(T)$ and $K_1(\tau, r)$ to be known values. Then the solution of eqs.(I.2.33) and (I.2.34) for given boundary conditions can be presented in the form

$$I_1(\tau, r) = I_1(0, r) e^{-\tau \sec\theta} + (1-k) \sec\theta \int_0^{\tau} B(t) e^{-(\tau - t)\sec\theta} dt + k \sec\theta \int_0^{\tau} K_1(t, r) e^{-(\tau - t)\sec\theta} dt, \tag{I.2.37}$$

$$I_2(\tau, r) = I_2(\tau^*, r) e^{-(\tau^* - \tau)\sec\theta} + (1-k) \sec\theta \times \int_{\tau}^{\tau^*} B(t) e^{-(t-\tau)\sec\theta} dt + k \sec\theta \int_{\tau}^{\tau^*} K_2(t, r) e^{-(t-\tau)\sec\theta} dt. \tag{I.2.38}$$

The relations (I.2.37) and (I.2.38) for a known temperature T(z) and therefore for a known value B(t) represent a system of integral equations for the determination of $I_1(\tau, r)$ and $I_2(\tau, r)$. If T(z) is unknown, the systems (I.2.37) and (I.2.38) must be supplemented by still another equation, namely, that for the heat balance of the atmosphere.

2.4 The Radiative Heat Inflow

Let us compute the value of radiative inflow of heat into an element of volume*. For this it is obviously necessary to compute the full amount of absorbed and radiated energy and determine the balance between them.

The full amount of radiant energy absorbed by unit volume is equal to

$$\int_0^\infty \tilde{\alpha}_\lambda \int I_\lambda d\omega d\lambda.$$

The amount of energy radiated by a unit volume under conditions of local /24 thermodynamic equilibrium is

$$4\pi \int_0^\infty \tilde{\alpha}_\lambda B_\lambda (T)\, d\lambda.$$

From this, the radiative heat inflow $Q(\tau)$ becomes

$$Q(\tau) = \int_0^\infty \tilde{\alpha}_\lambda \int_\infty I_\lambda (\tau, r)\, d\omega d\lambda - 4\pi \int_0^\infty \tilde{\alpha}_\lambda B_\lambda (T)\, d\lambda. \qquad \text{(I.2.39)}$$

A state of radiant equilibrium exists at $Q = 0$. Otherwise, $Q(\tau)$ is one of the components of the total heat balance of the medium which can be written in the form of

$$c_p \rho \frac{\partial T}{\partial t} = Q + \tilde{Q}, \qquad \text{(I.2.40)}$$

where $\tilde{Q}$ is the heat inflow due to other forms of heat exchange. For instance, in the case of turbulent mixing:

$$\tilde{Q} = \frac{\partial}{\partial z} k_t c_p \rho \frac{\partial \theta}{\partial z}, \qquad \text{(I.2.41)}$$

where θ is the potential temperature.

The system of equations (I.2.37), (I.2.38), and (I.2.39) or (I.2.40) is a closed system and makes it possible to determine three unknown functions $I_1(\tau, r)$, $I_2(\tau, r)$ and $T(\tau)$.

---

* The radiative heat inflow is here determined for the case of one absorbing and scattering substance.

Let us substitute in the right-hand side of the relation (I.2.39) the expressions of intensity (I.2.37) and (I.2.38). This will yield

$$Q(\tau) = \int_0^\infty \tilde{\alpha}_\lambda \left\{ \int_0^{2\pi} \int_{\frac{\pi}{2}}^{\pi} [I_{1,\lambda}(0, r)\, e^{-\sec\theta\tau} + I_{2,\lambda}(\tau^*, r) \times e^{-\sec\theta(\tau^*-\tau)}] \sin\theta d\theta d\psi + \right.$$

$$+ k_\lambda \int_0^{2\pi} \int_0^{\frac{\pi}{2}} \sec\theta \left[\int_0^\tau K_{1,\lambda}(t, r)\, e^{-\sec\theta(\tau-t)} dt + \int_\tau^{\tau^*} K_{2,\lambda}(t, r)\, e^{-\sec\theta(t-\tau)} dt \right] \times$$

$$\left. \times \sin\theta d\theta d\psi + (1 - k_\lambda) \int_0^{2\pi} \int_0^{\frac{\pi}{2}} \sec\theta \int_0^{\tau^*} B_\lambda(t)\, e^{-\sec\theta|\tau-t|} dt - 4\pi B_\lambda(\tau) \right\} d\lambda. \tag{I.2.42}$$

We will introduce the so-called integral exponential functions or Gold's functions*:

$$E_n(x) = \int_1^\infty \frac{e^{-xy}}{y^n} dy. \tag{I.2.43}$$

Obviously,

$$\int_0^{\frac{\pi}{2}} \cos^n\theta e^{-x\sec\theta} \sin\theta d\theta = \int_1^\infty \frac{e^{-x\mu}}{\mu^{n+2}} d\mu = E_{n+2}(x) \quad (n = -1; 0; 1, \ldots).$$

From this, we have /25

$$\int_0^{\tau^*} B(t) \int_0^{\frac{\pi}{2}} \sec\theta e^{-|\tau-t|\sec\theta} dt = \int_0^{\tau^*} B(t)\, E_1(|\tau - t|)\, dt,$$

after which the radiative heat inflow can be presented in the form of

$$Q(\tau) = \int_0^\infty \tilde{\alpha}_\lambda \left\{ \int_0^{2\pi} \int_0^{\frac{\pi}{2}} \left[I_{\lambda,1}(0, r)\, e^{-\tau\sec\theta} + I_{\lambda,r}(\tau^*, r)\, e^{-(\tau^*-\tau)\sec\theta} + \right.\right.$$

$$+ k_\lambda \sec\theta \left(\int_0^\tau K_{1,\lambda}(t, r)\, e^{-(\tau-t)\sec\theta} dt + \int_\tau^{\tau^*} K_{2,\lambda}(t, r)\, e^{-(t-\tau)\sec\theta} dt \right) \Big] \times$$

$$\left. \times \sin\theta d\theta d\psi + 2\pi(1-k_\lambda) \int_0^{\tau^*} B_\lambda(t)\, E_1(|\tau - t|)\, dt - 4\pi B_\lambda(T) \right\} d\lambda. \tag{I.2.44}$$

If we assume

$$I_{1,\lambda}(0, r) = B_\lambda(0), \qquad I_{2,\lambda}(\tau^*, \tau) = 0, \qquad \gamma(\tau, r, r') = 1,$$

we will obtain the following expression for the radiative heat inflow

---

* The aspects of the Gold function are described elsewhere (Bibl.22, 23).

$$Q(\tau) = 2\pi \int_0^\infty \tilde{\alpha}_\lambda \left\{ B_\lambda(0) E_3(\tau) + k_\lambda \int_0^{\tau^*} K_\lambda(t) E_1(|\tau - t|)\, dt + \right.$$
$$\left. + (1 - k_\lambda) \int_0^{\tau^*} B_\lambda(t) E_1(|\tau - t|)\, dt - 2B_\lambda(\tau) \right\} d\lambda. \qquad \text{(I.2.45)}$$

Section 3. Special Form of the Transfer Equation

Below are considered three spectral regions: the visible ($0.35 \leq \lambda \leq 0.75\ \mu$), the near-infrared ($0.75 \leq \lambda \leq 2.5\ \mu$), and the long-wave ($2.5 \leq \lambda \leq 40\ \mu$) as well as two forms of media: a cloudless atmosphere and a cloud layer. We will select special forms of the transfer equation corresponding to each of the above cases. In this, we will always refer to monochromatic radiation (the subscript λ is omitted).

3.1 Cloudless Atmosphere

1. Visible region of the spectrum. Here no noticeable absorption bands of atmospheric gases occur. The atmosphere can be considered as a medium in which scattering of light takes place on molecules of air and on aerosol particles and apparently also absorption of solar radiation by the aerosol. We are talking about absorption by dust since water in the visible region of the spectrum absorbs even less than water vapor (see Sect.3.2). V.G.Kastrov (Bibl.24) investigated the integral absorption of solar radiation by dust and, in a number of cases, detected noticeable amounts of absorbed energy. However, in other cases there was no absorption. It is not known to what extent this absorption can be ascribed to the visible region of the spectrum. In addition, the absorptivity of dust is as yet almost uninvestigated. Therefore, absorption by dust is not considered in this book.

Under the described condition, eq.(I.2.24) assumes the form

$$\cos\theta \frac{\partial I}{\partial \tau} = \frac{1}{4\pi} \int I(\tau, r') \gamma(\tau, r, r')\, d\omega' - I(\tau, r), \qquad \text{(I.3.1)}$$

where /26

$$\tau = \int_0^z \tilde{\sigma}_\lambda(z)\, dz, \qquad \text{(I.3.2)}$$

$$\tilde{\sigma}(z) = \sigma_R \rho_R + \sigma_a \rho_a, \qquad \text{(I.3.3)}$$

$$\gamma(z) = \frac{\tilde{\sigma}_R \gamma_R + \tilde{\sigma}_a \gamma_a}{\tilde{\sigma}_a + \tilde{\sigma}_R}. \qquad \text{(I.3.4)}$$

In measuring the scattering properties of a real atmosphere, the values $\tilde{\sigma}$ and γ obviously can be directly determined.

The boundary conditions of the problem under consideration are as follows:

1. Condition of incidence of a parallel beam of solar rays on the upper boundary of the atmosphere:

$$I_2(\tau^*, r) = \pi s \delta(r, r_\odot) \tag{I.3.5}$$

where $\delta(r, r_\odot)$ is a delta function having the property

$$\int f(r)\,\delta(r, r_\odot)\,d\omega = f(r_\odot).$$

2. Condition of reflection of radiation from the Earth's surface

$$F_1(0) = qF_2(0). \tag{I.3.6}$$

If the light reflected from the Earth's surface is subject to Lambert's law, i.e., does not depend on direction, then the intensity of reflected radiation is determined from eq.(I.3.6):

$$I_1(0, r) = \frac{q}{\pi} F_2(0).$$

It appears convenient to separate, in the sought value $I(\tau, r)$, the scattered light from direct solar light. For this, we will assume that

$$I(\tau, r) = I_s(\tau, r) + I_r(\tau, r), \tag{I.3.7}$$

where $I_s(\tau, r)$ is the intensity of a parallel beam of solar rays, determined from the equation

$$\cos\theta \frac{dI_s}{d\tau} = -I_s. \tag{I.3.8}$$

The solution of eq.(I.3.8) for the boundary condition (I.3.5) has the form

$$I_s = \pi s \delta(r, r_\odot)\, e^{-\sec\theta(\tau^*-\tau)}. \tag{I.3.9}$$

After substituting eq.(I.3.7) for I_s expressed by eq.(I.3.9) in eq.(I.3.1) and separating the intensity of ascending scattered radiation $I_{1,r}$ from the descending radiation $I_{2,r}$, we will obtain the following system of equations for determination of the quantities $I_{1,r}$ and $I_{2,r}$ (in what follows, the subscript r is omitted):

$$\cos\theta \frac{\partial I_1}{\partial\tau} = \frac{1}{4\pi}\int_+ I_1(\tau, r')\gamma_{11}(\tau, r, r')\,d\omega' + \frac{1}{4\pi}\int_+ I_2(\tau, r')\gamma_{12}(\tau, r, r')\,d\omega' - I_1(\tau, r) + \frac{S}{4} e^{-\sec\zeta(\tau^*-\tau)}\gamma_{1.2}(\tau, r, r_\odot), \tag{I.3.10}$$

$$-\cos\theta\frac{\partial I_2}{\partial\tau}=\frac{1}{4\pi}\int_{+}I_1(\tau,r')\gamma_{21}(\tau,r,r')\,d\omega'+$$

$$+\frac{1}{4\pi}\int_{-}I_2(\tau,r')\gamma_{22}(\tau,r,r')\,d\omega'-I_2(\tau,r)+\frac{S}{4}e^{-\sec\zeta(\tau^*-\tau)}\gamma_{22}(\tau,r,r_\odot). \qquad (I.3.11)$$

2. Infrared region of the spectrum. Here, absorption by water vapor (in the bands a, 0.8 μ, ρστ, Φ,Ψ,Ω; see Sect.5) and scattering on aerosol particles occurs, with respect to which molecular scattering can be neglected. /27

Equation (I.2.24) assumes the form

$$\cos\theta\frac{\partial I(\tau,r)}{\partial\tau}=\frac{\varphi(\tau)}{4\pi}\int I(\tau,r)\gamma_a(\tau,r,r')\,d\omega'-I(\tau,r), \qquad (I.3.12)$$

where

$$\varphi(\tau)=\frac{\tilde{\sigma}_a}{\tilde{\sigma}_a+\tilde{\alpha}_w}, \qquad (I.3.13)$$

$$\tau=\int_0^z[\tilde{\alpha}_w(z)+\tilde{\sigma}_a(z)]\,dz. \qquad (I.3.14)$$

The boundary conditions in this case remain as before.

3. Long-wave or heat radiation region. Here it is essential to take into account the radiation of the atmosphere itself and the absorption in the bands of water vapor and carbon dioxide. Scattering can be neglected although, strictly speaking, it must be taken into account for large particles of aerosol.

Equation (I.2.24) is presented in the form of

$$\cos\theta\frac{\partial I}{\partial\tau}=B(\tau)-I, \qquad (I.3.15)$$

where

$$\tau=\int_0^z[\tilde{\alpha}_w+\tilde{\alpha}_{CO_2}]\,dz. \qquad (I.3.16)$$

We will discuss in more detail the formulation of the boundary conditions for this case.

When the density of all absorbing substances along the upper boundary of the atmosphere becomes zero, it is natural to assume that the intensity of the descending long-wave radiation at this level is also equal to zero:

$$I_2(\tau^*,r)=0,\qquad 0\leqslant\theta\leqslant\frac{\pi}{2}. \qquad (I.3.17)$$

The latter condition is assumed in all papers dealing with the investigations of long-wave transfer in the earth's atmosphere (see, for instance Bibl.25). However, in investigating the radiation transfer in the troposphere (and it is precisely with this case that the greater part of the work done so

far was concerned) the conditions (I.3.17) contradict the recent data on the distribution of water vapor with height and the results of measurements of radiation flux at the tropopause level.

Table I.3.1 gives the ratios of descending radiation flux F_2 to ascending flux F_1 at the tropopause level according to measurements made by Suomi et al (Bibl.26) in five cases: Case 1 represents a single summer night; Case 2 - also a single night but under winter conditions; Case 3 - a cloudy winter night (a cloud was observed from the upper boundaries at the 720 mb level); Case 4 - average winter data; Case 5 - average summer data.

TABLE I.3.1

n	1	2	3	4	5
F_2/F_1, %	31	39	38	27	20

We see that the ratio F_2/F_1 does not change significantly under various conditions and that the value F_2 is not small compared with F_1. /28

According to the paper by Brewer and Houghton (Bibl.27), the ratio F_2/F_1 can also be computed yielding a value of 6-7% in the case of a cloudless sky. However, this result must be approached with caution since the above paper (Bibl.27) gives no data for an accurate determination of F_2/F_1. From the data of this same paper, it also follows that a cloud located immediately below the tropopause will cause an increase in the ratio F_2/F_1 at the tropopause level by a factor of about 1.5 - 2.0. This can be explained by the decrease in F_1 from a value that brings certain components of radiation of the lower heated parts of the atmosphere up to the radiation of a black body at tropopause temperature.

Therefore, in considering the transfer of long-wave radiation in the troposphere at the upper boundary, it is necessary to prescribe an intensity of descending radiation other than zero and to estimate it from data of distribution of H_2O, CO_2, and of temperature in the lower stratosphere. An example of such an estimate will be given in Chapter VII.

In deriving the boundary condition at the Earth's surface one usually utilizes one of two hypotheses (see Bibl.25).

1. The Earth radiates like a black body, i.e.,

$$I_{1,\lambda}(0, r) = B_\lambda(T_0), \qquad \text{(I.3.18)}$$

where T_0 is the temperature at the Earth's surface.

2. The Earth radiates like a gray body, i.e., the radiation of the Earth, for each wavelength, differs by a constant factor δ from the radiation of a black body at the same temperature. In this case, according to Kirchhoff's law there must exist the relation

$$I_1(0, r) = \delta B_\lambda + \frac{1}{\pi}(1 - \delta) F_2(0). \qquad \text{(I.3.19)}$$

From the analyses of radiation of the Earth's surface made elsewhere (Bibl.25), it seems that the condition (I.3.18) is better satisfied so that we will use it below.

3.2 The Cloud Layer

1. Visible region of the spectrum. In the visible region of the spectrum within the cloud layer, there is scattering on water droplets with respect to which the molecular scattering can be neglected. The transfer equation assumes the form of eq.(I.3.1) where now $\tilde{\sigma}(z)$ and $\gamma(z, r)$ are the total coefficients of scattering and the scattering indicatrix of droplet water, taking the particle-size distribution spectrum into consideration (see Sect.4.2). The boundary condition consists in stipulating scattered radiation arriving at both boundaries of the cloud layer and a parallel beam of direct solar radiation incident on the upper boundary of the cloud.

We neglected the absorption of light on water droplets and water vapor in the clouds. It would seem that, in view of the large scattering power of clouds (see Sect.4) and the attendant large distances covered by the light inside the clouds, the amount of absorbed radiation would be appreciable even at a low absorptivity of the droplets and the vapor.

The computation carried out in Chapter III shows, however, that this is not so. Actually, Table I.4.3 together with eq.(I.4.1) gives values of $\alpha_{v,\lambda}$ in the visible regions of the spectrum which lie within the limits

$$3 \cdot 10^{-9}\ km^{-1} \leqslant \alpha_{v,\lambda} \leqslant 3 \cdot 10^{-8}\ km^{-1}.$$

Let us assume that the absorption coefficient of water vapor in the considered case is 50 times greater, as is more or less the case in bands a and $\rho\sigma\tau$ of the near-infrared region. Then, /29

$$10^{-7}\ km^{-1} (\tilde{\alpha}_{v,\lambda} + \tilde{\alpha}_{w,\lambda}) \leqslant 10^{-6}\ km^{-1}.$$

At $\tilde{\sigma} = 30\ km^{-1}$ (see Sect.4), this yields

$$(1 - 1 \cdot 10^{-8}) \leqslant k \leqslant (1 - 1 \cdot 10^{-7}),$$

where

$$k = \frac{\tilde{\sigma}}{\tilde{\sigma} + \tilde{\alpha}_v + \tilde{\alpha}_w}.$$

Comparing these values of k with those given in Chapter III and with the corresponding amounts of absorbed energy we see that, in the visible region, the absorption is negligibly small.

2. Near-infrared region of the spectrum. In this region, scattering and absorption on water droplets and also absorption in the water vapor bands takes place. The transfer equation assumes the form of

$$\cos\theta\frac{\partial I}{\partial\tau}=\frac{\varphi(z)}{4\pi}\int I(\tau, r')\,\gamma_v(\tau, r, r')\,d\omega' - I(\tau, r), \tag{I.3.20}$$

where

$$\tau=\int_0^z[\tilde{\alpha}_v(z)+\tilde{\alpha}_w(z)+\tilde{\sigma}_v(z)]\,dz, \tag{I.3.21}$$

$$\varphi(z)=\frac{\tilde{\sigma}_v(z)}{\tilde{\alpha}_v(z)+\tilde{\alpha}_w(z)+\tilde{\sigma}_v(z)}. \tag{I.3.22}$$

The boundary conditions here are the same as in the previous case.

3. Region of thermal radiation. Unlike under the conditions of a cloudless atmosphere, here the scattering of long-wave radiation must be taken into account along with absorption. The transfer equation then assumes the form of

$$\cos\theta\frac{\partial I}{\partial\tau}=(1-\varphi)B(\tau)+\frac{\varphi}{4\pi}\int I\gamma_v d\omega' - I, \tag{I.3.23}$$

where $\varphi(z)$ and τ are determined by means of eqs.(I.3.21) and (I.3.22).

In deriving the boundary conditions for this problem, it must be kept in mind that long-wave radiation is one of the components of the heat balance of the atmosphere. On the interface between cloud and ambient atmosphere, the conditions of equality of heat flow on both sides of the boundary must apply. According to Kuznetsov (Bibl.28), this condition (taking radiation and turbulent heat exchange into consideration) is presented in the form

$$F^{(1)}+c_p\rho k_t^{(1)}\frac{\partial T^{(1)}}{\partial z}=F^{(2)}+c_p\rho k_t^{(2)}\frac{\partial T^{(2)}}{\partial z}. \tag{I.3.24}$$

The relation (I.3.24) can be replaced by stricter conditions of equality of separate heat flows in the ascending and descending direction:

$$F_1^{(1)}=AF_2^{(1)}+(1-A)F_1^{(2)}+c_p\rho k_t^{(2)}\frac{\partial T^{(1)}}{\partial z}. \tag{I.3.25}$$

$$F_2^{(2)}=(1-A)F_2^{(1)}+AF_1^{(2)}-c_p\rho k_t^{(2)}\frac{\partial T^{(2)}}{\partial z}. \tag{I.3.26}$$

Section 4. Optical Properties of Clouds /30

The diversity of the problem described in the preceding Section requires for each solution information on the coefficients of absorption and scattering

and on the scattering indicatrix of atmospheric gases, water droplets, aerosols and ice crystals.

The optical properties of water droplets were investigated mainly from a theoretical viewpoint and almost no experimental data are in existence. The optical parameters of a cloudless atmosphere, conversely, were determined mainly experimentally. The optical properties of real clouds were insufficiently investigated experimentally and were almost never determined by calculation. The optical characteristics of ice crystals have never been investigated at all.

TABLE I.4.1

λ, μ	m	$\varkappa$	λ, μ	m	$\varkappa$	λ, μ	m	$\varkappa$
4.0	1.338	0.0015	10	1.196	0.0368 (0.056)	35	1.36	0.1680
4.5	1.343	0.0096 (0.016)	12	1.187	0.2221 (0.247)	40	1.36	0.1752
5.0	1.330	0.0100	14	1.300	0.4130	45	1.36	0.2606
5.5	1.300	0.0097	16	0.380	0.4720	50	1.36	0.3021
6.0	1.324	0.1341 (0.101)	18	1.505	0.4189 (0.427)	55	1.36	0.4797
6.5	1.334	0.0969	20	1.530	0.3599	60	1.37	0.5145
7.0	1.327	0.0224 (0.045)	22	1.530	0.3072	65	1.38	0.5028
7.5	1.310	0.0228	24	1.490	0.2608	70	1.40	0.4823
8.0	1.293	0.0232 (0.048)	26	1.410	0.2272	75	1.41	0.4645
8.5	1.280	0.0243	28	1.390	0.2114	80	1.41	0.4632
9.0	1.264	0.0261 (0.050)	30	1.380	0.1874	85	1.41	0.4641
9.5	1.240	0.0289				90	1.41	0.4815

In this Section, the optical properties of water droplets in real clouds are discussed. The next Section is devoted to absorption and scattering in a cloudless atmosphere.

4.1 Optical Properties of Water Droplets

The principal results of the theory of electromagnetic waves describing the scattering and absorption of light by a particle are outlined in the monographs by K.C.Shifrin (Bibl.29) and of Van de Hulst (Bibl.30).

On the basis of this theory, numerous calculations have been performed up to now on the optical characteristics of a water droplet*, which were tabulated according to the parameter $\rho = \frac{2\pi a}{\lambda}$ and according to the refractive index of

* By optical characteristics of a separate particle or of an element of volume are meant the absorption coefficient, scattering coefficient, and scatter indicatrix. In the case of an individual particle, the first two quantities can be represented by the corresponding effective cross sections.

a droplet $n = m - i\varkappa$.

For orientation purposes relative to the computation results, the values of m and $\varkappa$ for a droplet in relation to the wavelength $\lambda \geq 4\mu$ are given in Table I.4.1 (Bibl.31) and in relation to the wavelength $\lambda \leq 4\mu$ in Table I.4.2 (Bibl.32).

We note that the imaginary part $\varkappa$ of the refractive index (the so-called absorption factor) is related to the absorption coefficient of liquid water $\tilde{\tilde{\alpha}}_v$ by the relation

$$\varkappa = \frac{\tilde{\tilde{\alpha}}_v \lambda}{4\pi}. \qquad (I.4.1)$$

TABLE I.4.2 /31

Δλ, μ	m	$\varkappa$	Δλ, μ	m	$\varkappa$
0.4—2	1.33	0	3.4—3.8	1.42	0.014
2—2.4	1.29	0	3.8—5.5	1.33	0.013
3*	1.41	0.175			

* The values m and $\varkappa$, at $\lambda = 3\mu$ are taken from another report (Bibl.29) since Johnson (Bibl.32) gives no data for the interval $2.4 - 3.4\mu$.

Other reports (Bibl.29, 32) give values of $\varkappa$ based on older measurements of $\tilde{\tilde{\alpha}}_v$ carried out by Aschkinass (Bibl.54) and also by Rubens and Landenberg at

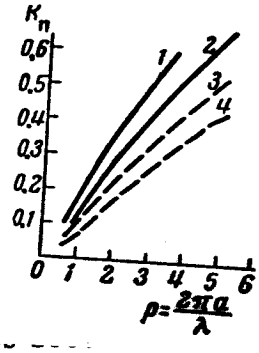

Fig.I.4.1 Cl... ...rption

1 — $\lambda = 10\mu$, $n = 1.22 - 0.061i$;
2 — $\lambda = 7\mu$, $n = 1.33 - 0.040i$;
3 — $\lambda = 10\mu$, $n = 1.20 - 0.037i$;
4 — $\lambda = 7\mu$, $n = 1.33 - 0.023i$

the end of the last and the beginning of the present century. Table I.4.1 is based on current data by Plyler and Acquista (Bibl.33) and by Cartwright (Bibl.34). The differences in the values of $\varkappa$ obtained on the basis of the old and new data can be judged from Table I.4.1, where the values of $\varkappa$ (Bibl.29)

which correspond to the old values of $\tilde{\tilde{\alpha}}_v$ are shown in parentheses. The Table shows a two-fold discrepancy in some cases.

Because of this discrepancy, the values of the cross section for absorption of the K_a droplets may differ greatly as is shown, for example, in Fig.I.4.1 (Bibl.35) where the values K_a are given for two wavelengths: $\lambda = 7\mu$ and $\lambda = 10\mu$ computed with the old (dotted curves) and the new (solid curves) values for $\varkappa$.

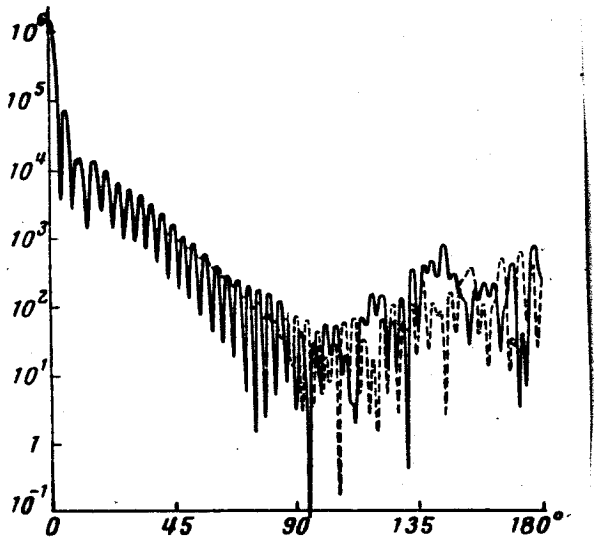

Fig.I.4.2 Fine Structure of the Scatter Indicatrix (ρ - 50, m - 1.33)

Table I.4.2 shows that in the visible and in the near-infrared region of the spectrum, up to $\lambda = 2.4\mu$, the refractive index n is a real value; moreover,

TABLE I.4.3

λ, μ	0.415	0.5	0.6	0.7	0.8	0.9	1.05	1.30
$\varkappa \cdot 10^8$	0.115	0.0596	0.511	1.67	13.0	115	299	1252

it is independent of the wavelength if $\lambda \leq 2\mu$. It follows from this that the optical characteristics of a droplet here also are independent of the wavelength and are determined only by the parameter ρ.

The absorption factor $\varkappa$ does not, strictly speaking, become zero anywhere in the examined region [see Table I.4.3 based on data by Shifrin (Bibl.29)]. However, everywhere except in the regions of the water absorption bands, at /32

$\lambda \geq 1.3\mu$ the absorption factor is small so that it can be neglected. At $\varkappa = 0$ the computation of the effective scattering cross section and of the scatter indicatrix is greatly simplified.

TABLE I.4.4

$\varphi°$	$\gamma(\varphi)$	$\varphi°$	$\gamma(\varphi)$	$\varphi°$	$\gamma(\varphi)$	$\varphi°$	$\gamma(\varphi)$
0	110768.6	70	547.27	140	1178.52	174	1198.165
10	76366.0	80	331.44	150	633.84	175	873.44
20	10142.7	90	99.640	160	643.554	176	458.67
30	5497.3	100	75.179	170	379.28	177	1765.50
40	6999.8	110	77.184	171	613.908	178	1740.38
50	2892.5	120	164.214	172	695.536	179	957.31
60	586.96	130	86.697	173	474.56	180	1031.34

Almost all computations made thus far relate precisely to the case of the true refractive index. A bibliography of pertaining papers can be found elsewhere (Bibl.29, 30, 36 - 40).

$\Delta\lambda$, μ	m	$\varkappa$	ρ									
			1.00	1.75	2.50	3.25	4.00	4.75	5.50	6.25	7.00	7.75
10.5—11.5	1.14	0.10	0.32	0.59	0.87	1.11	1.34	1.53	1.69	1.83	1.94	2.03
11.5—12.2	1.16	0.18	0.58	0.99	1.34	1.60	1.80	1.94	2.04	2.11	2.15	2.18
9.5—10.5	1.22	0.05	0.21	0.50	0.88	1.27	1.65	2.00	2.29	2.52	2.69	2.79
7.5—9.5	1.28	0.04	0.21	0.59	1.12	1.67	2.18	2.60	2.91	3.08	3.15	3.11
12.2—13	1.28	0.23	0.83	1.43	1.86	2.12	2.27	2.34	2.37	2.37	2.36	2.34
3.8—5.5	1.33	0.01	0.13	0.55	1.27	2.05	2.77	3.33	3.66	3.72	3.57	3.28
6.5—7.5	1.33	0.03	0.20	0.67	1.37	2.08	2.69	3.13	3.38	3.41	3.29	3.06
13.0—15.0	1.33	0.30	1.10	1.78	2.15	2.33	2.40	2.42	2.41	2.39	2.37	2.36
3.4—3.8	1.42	0.01	0.19	0.88	1.91	2.90	3.61	3.91	3.82	3.44	2.92	2.43

Detailed computations of the effective scattering cross section of a spherical particle at n = 1.33, 1.40, 1.44 and $\rho \leq 30$ are given by Penndorf (Bibl.36). In another paper (Bibl.37, 38), the computation of the scattering function is carried to values of $\rho = 400$, with special emphasis on large angles of scattering. Giese (Bibl.39) gives graphs of the fine structure of the scattering index. One of these graphs is reproduced in Fig.I.4.2.

K.S.Shifrin (Bibl.41) showed that the scattering indicatrix of a droplet, computed in first approximation of geometric optics for n = 1.33 and $\rho = 100$ passes along the center of the band enclosed by the upper and lower edges of /33

the curve of type (I.4.2) for the corresponding value of ρ. This means that for ρ ≈ 100 and n = 1.33 the scattering indicatrix of a water droplet is well described by the formulas of geometric optics without taking into account the fine structure.

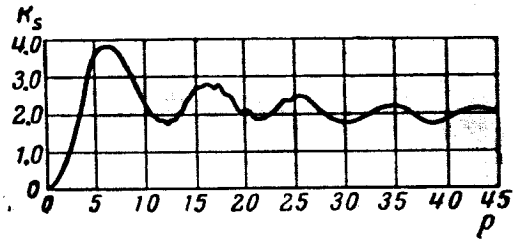

Fig.I.4.3 Cross Section for Scattering, at n = 1.33

Coefficients of the expansion of the scattering functions in a series according to Legendre polynomials were computed by Chu et al (Bibl.40) which makes this paper highly suitable for a numerical solution of the transfer equations. The expansions are given for $0.9 \leqslant n \leqslant 20$; $1 \leqslant \rho \leqslant 30$.

TABLE I.4.5

ρ												
8.50	9.25	10.00	10.75	11.50	12.25	13.00	13.75	14.50	15.25	16.00	16.75	17.50
2.10	2.15	2.19	2.22	2.24	2.24	2.25	2.25	2.24	2.24	2.23	2.22	2.21
2.20	2.21	2.21	2.21	2.21	2.21	2.20	2.20	2.19	2.19	2.19	2.18	2.18
2.84	2.84	2.80	2.75	2.65	2.57	2.48	2.41	2.34	2.29	2.26	2.23	2.22
3.01	2.85	2.68	2.51	2.38	2.28	2.22	2.20	2.21	2.23	2.27	2.30	2.32
2.33	2.31	2.30	2.29	2.28	2.27	2.26	2.25	2.25	2.24	2.23	2.23	2.22
2.92	2.56	2.26	2.06	1.97	1.98	2.07	2.22	2.39	2.53	2.63	2.64	2.57
2.80	2.54	2.34	2.21	2.16	2.16	2.21	2.29	2.36	2.42	2.45	2.44	2.40
2.34	2.33	2.31	2.30	2.29	2.28	2.27	2.27	2.26	2.25	2.25	2.24	2.23
2.09	1.96	2.07	2.28	2.50	2.65	2.69	2.60	2.43	2.24	2.11	2.07	2.11

From the viewpoint of cloud optics the lack of data for ρ > 30 constitutes a drawback (in the study of clouds it is necessary to know the scattering function for values of $\rho \lesssim 100$).

We will give two results of the theory of scattering on a spherical particle, covering the case of the true refractive index and extending the possibility of making use of Tables.

1. The optical characteristics of the droplets are invariant (with an error of the order of 1% with respect to the parameter)

$$\delta = 2\varrho\,(n-1). \tag{I.4.2}$$

2. Van de Hulst (Bibl.30) derived a formula which, while disregarding the fine structure, describes the dependence of the scattering coefficient on δ, within the entire range of variations in δ of interest here. This formula reads

$$K_s = 2\pi a^2\left[1 - \frac{1}{\delta}\sin 2\delta + \frac{1-\cos 2\delta}{2\delta^2}\right]. \tag{I.4.3}$$

This summary indicates that, in the region of pure scattering in which n = 1.33, the optical parameters of droplet water are known. As an example, a graph of the cross section for scattering, plotted with the computational data by Straton and Houghton [supplemented by Houghton and Chalker; (see Bibl.29)]. is given in Fig.I.4.3, while the angular distribution for scattering at n = 1.33 and ρ = 65 according to other data (Bibl.38) is given in Table I.4.4. Here, /34 Table I.4.4 gives the scattered light for λ = 0.5μ for an elementary volume of a monodisperse cloud containing droplets of a radius of a = 5.2μ.

The situation with regard to the long-wave region of the spectrum is considerably worse. Computations on the basis of Mie's theory for a complex refractive index are laborious, even for electronic computers and have thus far been carried out in an absolutely insufficient volume. It should be pointed out also that there is no invariance of the optical characteristics with respect to the parameter ρ or δ in the absorption region.

Tables I.4.1 - I.4.2 indicate the dependence of the refractive index on the wavelength, which makes it necessary to perform the computation separately for each value of λ and a.

The effective cross section for attenuation can be calculated in a very simple form:

$$K = K_s + K_a.$$

Table I.4.5 gives values of K for various m_λ and $\varkappa_\lambda$ at selected values of the parameter ρ. Shown also are the corresponding values of the wavelength intervals $\Delta\lambda$, μ. These data are taken from another paper (Bibl.32) and are based on "old" (see above) values of the absorption coefficient of liquid water.

In the solution of the simplest problems of the transfer theory, namely, determination of the transparency of clouds or attenuation of the light source over short distances where multiple scattering can be neglected (see Chapter II, Sect.7.1), it is sufficient to know the attenuation factor. In this case, the computation can be limited to the data in Table I.4.5. As shown by eqs.(I.3.1), (I.3.20), and (I.3.23) all other problems require a selective assignment of the attenuation factor, the scattering coefficient, and the scattering indicatrix. Until recently, the only data of this type for the case of a complex refractive index, i.e., in the region of absorption, were the results of computations by K.S.Shifrin (Bibl.42, 43). In one paper (Bibl.42), the effective cross sections for scattering K_s, for absorption K_a, and for back scattering K_1 are

computed by the Mie theory for a droplet radius of a = 6.265μ. The same is done for droplets with a radius of a = 12.53μ in his second report (Bibl.43).

TABLE I.4.6

λ_μ	K_s	K_a	K_1	Γ	Γ_s
3	1.110	0.894	0.128	8	
3.4	1.541	0.925	0.135	10	
4.5	2.146	0.500	0.131	15	16
6	1.743	1.127	0.047	36	
7	2.595	0.704	0.027	95	
8	2.967	0.234	0.042	70	
9	1.863	0.630	0.050	36	28
10	0.925	0.575	0.014	65	
11	0.465	0.768	0.008	56	
12	0.632	1.134	0.017	36	
13	0.792	1.236	0.024	32	
15	0.887	1.376	0.034	25	
18	1.013	1.416	0.046	21	24

With these data it is also possible to estimate the degree of elongation /35 of the scattering indicatrix in the absorption region:

$$\Gamma = \frac{K_s - K_1}{K_1}. \qquad \text{(I.4.4)}$$

TABLE I.4.7

λ_μ	K_s	K_a	K_1	Γ	Γ_s
9	2.052	0.910	0.548	3	16
10	1.590	0.777	0.223	6	—
13	1.864	1.261	0.083	21.5	28.5
15	1.450	1.063	0.128	10	—
18	1.193	1.379	0.040	29	28

Values of K_s, K_a, K_1 and of Γ for a = 6.265μ are given in Table I.4.6 (Bibl.43), and for a = 12.53μ in Table I.4.7 (Bibl.42). The last columns of these Tables contain the values of Γ_s which is the degree of elongation of the indicatrix in the region of pure scattering for n = 1.33 and the corresponding values of a and λ.

A comparison of Γ_s and Γ shows that, in the presence or absence of absorption, the indicatrices in many cases do not differ greatly with respect to the

integral effect. It is also shown (Bibl.40) that, at $\varkappa \leq 0.001$, the scattering indicatrix differs little from the case $\varkappa = 0$, i.e., from the case of pure

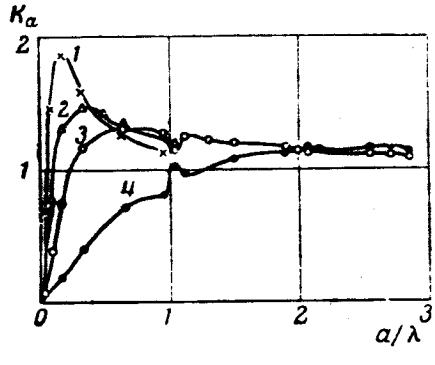

Fig.I.4.4 Cross Section for Absorption at n = 1.29
1 - $\varkappa$ = 1.29; 2 - $\varkappa$ = 0.645; 3 - $\varkappa$ = 0.322;
4 - $\varkappa$ = 0.0645

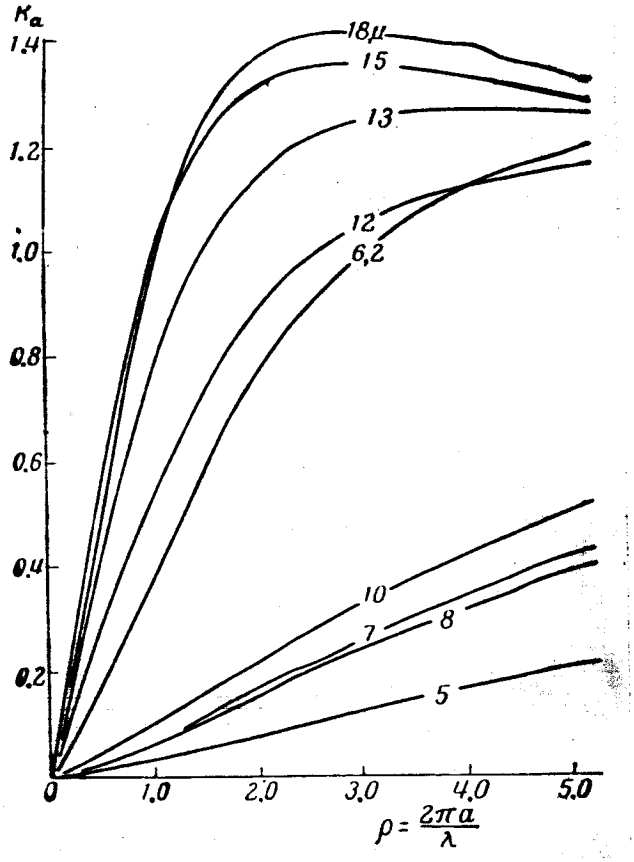

Fig.I.4.5 Cross Section for Absorption

scattering. In conformity with eq.(I.4.1) the scattering indicatrices which correspond to $\varkappa = 0$ can be utilized up to values of $\tilde{\tilde{\alpha}}_v$ which do not exceed

$\frac{40\pi}{\lambda}$ cm^2/gm, i.e., in the near-infrared region of the spectrum (up to $\lambda \approx$ $\approx 1.5\mu$).

The still-unpublished data of Houghton's computations of the value of K_a /38 for m = 1.29 and for different values $\varkappa$ are given by McDonald (Bibl.44). These values are shown in Fig.I.4.4. According to Table I.4.1, the values $\lambda = 8\mu$ and $\lambda = 14\ \mu$ correspond to m = 1.29. However, the values of $\varkappa$ selected by

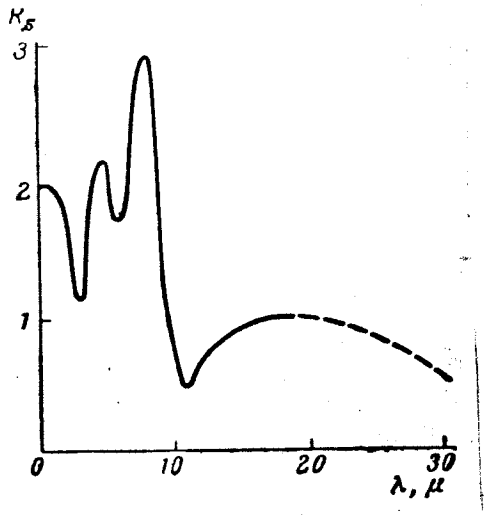

Fig.I.4.6 Cross Section for Scattering in the Absorption Region

Houghton make it possible to utilize his data only for $\lambda = 14\mu$. In this case, an interpolation between the curves $\varkappa = 0.322$ and $\varkappa = 0.645$ in Fig.I.4.4 makes it possible to determine the absorption cross section of droplets of any radius $a \leq 42\mu$.

The values of K_a for a series of wavelengths tabulated according to the parameter ρ within the range $0 \leq \rho \leq 5$ were computed approximately by Stephens (Bibl.31, 35) utilizing recent data on $\varkappa$. These results are presented in Fig.I.4.5 and in Table I.4.7. Unfortunately, Stephens did not compute the effective cross sections for attenuation K, so that his data must be used together with the data in Table I.4.5 which is not quite correct because of the difference in the wavelength and in the values of $\varkappa$ (see above). A comparison of the values of K_a in Tables I.4.6, I.4.7, and I.4.8 for the same values of a and λ shows that these values, in a number of cases, differ by a factor of 2 to 3, principally in the region of weak absorption. One of the causes of this discrepancy was discussed above - the difference in the values of $\varkappa$, in recent and old data on the absorptivity of liquid water. The second reason could be the approximate nature of the computation method used by Stephens which was developed by Aden (Bibl.35).

TABLE I.4.8

ρ	λ, μ								
	5	6,2	7	8	10	12	13	15	18
0.05	$1.192 \cdot 10^{-3}$	0.01632	$2.688 \cdot 10^{-3}$	$2.677 \cdot 10^{-3}$	$4.530 \cdot 10^{-3}$	0.02719	0.03854	0.04967	0.04125
0.10	$2.391 \cdot 10^{-3}$	0.03274	$5.391 \cdot 10^{-3}$	$5.368 \cdot 10^{-3}$	$9.075 \cdot 10^{-3}$	0.05446	0.07726	0.09964	0.08286
0.15	$3.603 \cdot 10^{-3}$	0.04936	$8.124 \cdot 10^{-3}$	$8.085 \cdot 10^{-3}$	0.01365	0.08189	0.1163	0.1501	0.1252
0.20	$4.835 \cdot 10^{-3}$	0.06625	0.01090	0.01084	0.01827	0.1095	0.1558	0.2014	0.1684
0.25	$6.094 \cdot 10^{-3}$	0.08351	0.01374	0.01365	0.02295	0.1374	0.1959	0.2536	0.2130
0.30	$7.387 \cdot 10^{-3}$	0.1012	0.01665	0.01652	0.02771	0.1560	0.2365	0.3067	0.2590
0.35	$8.719 \cdot 10^{-3}$	0.1194	0.01965	0.01947	0.03255	0.1941	0.2778	0.3609	0.3066
0.40	0.01010	0.1382	0.02275	0.02251	0.03749	0.2229	0.3198	0.4162	0.3561
0.45	0.01153	0.1577	0.02597	0.02566	0.04254	0.2520	0.3624	0.4725	0.4075
0.50	0.01302	0.1778	0.02932	0.02891	0.04772	0.2813	0.4055	0.5297	0.4609
0.55	0.01447	0.1969	0.03257	0.03200	0.05281	0.3089	0.4444	0.5790	0.5088
0.60	0.01612	0.2174	0.03617	0.03541	0.05797	0.3370	0.4855	0.6329	0.5619
0.65	0.01764	0.2384	0.03968	0.03888	0.06332	0.3658	0.5268	0.6855	0.6154
0.70	0.01932	0.2598	0.04342	0.04248	0.06874	0.3937	0.5665	0.7365	0.6685
0.75	0.02103	0.2814	0.04723	0.04610	0.07423	0.4208	0.6052	0.7853	0.7206
0.80	0.02278	0.3033	0.05114	0.04983	0.07982	0.4477	0.6428	0.8315	0.7716
0.85	0.02459	0.3250	0.05515	0.05365	0.08544	0.4736	0.6786	0.8749	0.8207
0.90	0.02643	0.3468	0.05922	0.05748	0.09115	0.4990	0.7127	0.9152	0.8677
0.95	0.02831	0.3684	0.06337	0.06138	0.09678	0.5234	0.7450	0.9526	0.9123
1.0	0.03020	0.3898	0.06755	0.06532	0.1024	0.5470	0.7755	0.9869	0.9543
1.05	0.03212	0.4109	0.07177	0.06927	0.1081	0.5697	0.8044	1.018	0.9939
1.1	0.03406	0.4318	0.07601	0.07325	0.1138	0.5916	0.8317	1.047	1.031
1.2	0.03798	0.4729	0.08458	0.08123	0.1251	0.6330	0.8820	1.099	1.099
1.3	0.04198	0.5135	0.09330	0.08930	0.1363	0.6720	0.9279	1.144	1.160
1.4	0.04613	0.5544	0.1023	0.09753	0.1475	0.7092	0.9706	1.184	1.213

TABLE I.4.8 (end)

ρ	λ, μ								
	5	6.2	7	8	10	12	13	15	18
1.5	0.05041	0.5959	0.1119	0,1061	0.1589	0.7448	1.010	1.220	1.257
1.6	0.05534	0.6378	0.1222	0.1152	0.1704	0.7791	1.047	1.251	1.293
1.7	0.06057	0.6787	0.1333	0.1249	0.1822	0.8119	1.080	1.277	1.321
1.8	0.06618	0.7169	0.1451	0.1351	0.1944	0.8426	1.109	1.299	1.343
1.9	0.07193	0.7507	0.1569	0.1456	0.2069	0.8710	1.135	1.317	1.363
2.0	0.07745	0.7798	0.1682	0.1559	0.2194	0.8969	1.156	1.331	1.381
2.2	0.08654	0.8285	0.1866	0.1743	0.2437	0.9414	1.191	1.351	1.409
2.3	0.09013	0.8515	0.1941	0.1820	0.2550	0.9606	1.205	1.358	1.419
2.4	0.09347	0.8752	0.2012	0.1894	0.2656	0.9784	1.218	1.363	1.424
2.5	0.09663	0.9001	0.2080	0.1962	0.2758	0.9951	1.229	1.367	1.428
2.6	0.1016	0.9246	0.2181	0.2040	0.2856	1.011	1.239	1.370	1.431
2.8	0.1124	0.9682	0.2397	0.2218	0.3057	1.038	1.256	1.374	1,436
3.0	0.1233	1.002	0.2607	0.2410	0.3266	1.064	1.269	1.376	1,440
3.2	0.1314	1.034	0.2765	0.2577	0.3477	1.086	1.279	1.373	1.436
3.4	0.1386	1.066	0.2912	0.2720	0.3677	1.104	1.285	1.369	1.428
3.6	0.1479	1.093	0.3095	0.2872	0.3866	1.120	1.289	1.364	1.421
3.8	0.1584	1.113	0.3289	0.3042	0.4050	1.133	1.292	1.358	1,416
4.0	0.1662	1.133	0.3434	0.3197	0,4233	1.145	1.293	1.352	1.407
4.2	0.1727	1.155	0.3562	0.3328	0.4409	1.155	1.293	1.344	1.409
4.4	0.1822	1.174	0.3745	0.3471	0.4577	1.163	1.292	1.336	1.386
4.6	0.1942	1.186	0.3954	0.3645	0.4747	1.171	1.290	1.329	1.377
4.8	0.2021	1.196	0.4091	0.3808	0.4920	1.177	1.288	1.321	1.367
5.0	0.2059	1.208	0.4169	0.3913	0.5089	1.182	1.285	1.314	1.357
5.2	0.2128	1.221	0.4307	0.4020	0.5245	1.186	1.281	1.306	1.346

TABLE I.4.9

a, μ	$\pi a^2 K$, μ²	$\pi a^2 K_s$, μ²	$\pi a^2 K_a$, μ²	$\pi a^2 K$, μ²	$\pi a^2 K_s$, μ²	$\pi a^2 K_a$, μ²
	$T = 253°$			$T = 263°$		
1.0	$8.16 \cdot 10^{-2}$	$6.27 \cdot 10^{-4}$	$8.10 \cdot 10^{-2}$	$8.13 \cdot 10^{-2}$	$7.14 \cdot 10^{-4}$	$8.06 \cdot 10^{-2}$
1.5	0.285	$6.79 \cdot 10^{-3}$	0.278	0.284	$7.69 \cdot 10^{-3}$	0.277
2.0	0.705	$3.49 \cdot 10^{-2}$	0.670	0.707	$3.93 \cdot 10^{-2}$	0.668
2.5	1.445	0.116	1.329	1.452	0.129	1.323
3.0	2.602	0.292	2.310	2.622	0.323	2.299
3.5	4.307	0.629	3.677	3.349	0.689	3.660
4.0	6.676	1.205	5.471	6.752	1.308	5.443
4.5	9.817	2.097	7.720	9.940	2.264	7.677
5.0	13.833	3.385	10.448	14.018	3.634	10.384
5.5	18.837	5.151	13.685	19.103	5.507	13.596
6.0	24.906	7.459	17.447	25.272	7.945	17.327
6.5	32.112	10.360	21.751	32.596	11.002	21.594
7.0	40.504	13.897	26.607	41.124	14.719	26.405
7.5	51.938	19.661	32.278	52.965	20.904	32.060
8.0	63.320	25.023	38.297	64.579	26.552	38.028
8.5	76.094	31.221	44.873	77.613	33.067	44.546
9.0	90.263	38.264	51.999	92.059	40.452	51.607
9.5	105.84	46.170	59.668	107.93	48.723	59.205
10.0	122.82	54.954	67.871	125.22	57.894	67.330
	$T = 258°$			$T = 268°$		
1.0	$8.15 \cdot 10^{-2}$	$6.69 \cdot 10^{-4}$	$8.08 \cdot 10^{-2}$	$8,11 \cdot 10^{-2}$	$7.606 \cdot 10^{-4}$	$8.034 \cdot 10^{-2}$
1.5	0,285	$7.23 \cdot 10^{-3}$	0.277	0,284	$8.175 \cdot 10^{-3}$	0.276
2.0	0,706	$3.71 \cdot 10^{-2}$	0.669	0,707	$4.161 \cdot 10^{-2}$	0.666
2.5	1.449	0.123	1.326	1,455	0.136	1.319
3.0	2,612	0.307	2.305	2,631	0.339	2.293
3.5	3.328	0.658	3.670	4,368	0.720	3.649
4.0	6,714	1.256	5.459	6,788	1.363	5.425
4.5	9,879	2.179	7.700	10,000	2.351	7.649
5.0	13,926	3.507	10.419	14,109	3.764	10.345
5.5	18.971	5.327	13.644	19,236	5.693	13.542
6.0	25,089	7.698	17.391	25,454	8.198	17.256
6.5	32,354	10.677	21.677	32,837	11.336	21.502
7.0	40,814	14.302	26.512	41,433	15.145	26.288
7.5	52,452	20.276	32.176	53,479	21.545	31.934
8.0	63,950	25.780	28.170	65,209	27.337	37.872
8.5	76,854	32.136	44.718	78,372	34.013	44.359
9.0	91.162	39.350	51.812	92,957	41.571	51.385
9.5	106.88	47.438	59.447	108,97	50.026	58.945
10.0	124.03	56.415	67.612	126,42	59.390	67.029
	$T = 273°$			$T = 283°$		
1.0	$8.08 \cdot 10^{-2}$	$8.09 \cdot 10^{-4}$	$8.00 \cdot 10^{-2}$	$8.02 \cdot 10^{-2}$	$9.13 \cdot 10^{-4}$	$7.94 \cdot 10^{-2}$
1.5	0.284	$8.68 \cdot 10^{-3}$	0.275	0.282	$9.75 \cdot 10^{-3}$	0.273
2.0	0.707	$4.40 \cdot 10^{-2}$	0.663	0.707	$4.91 \cdot 10^{-2}$	0.658
2,5	1.458	0.143	1.315	1.463	0.159	1.304
3.0	2.640	0.355	2.285	2.656	0.390	2.266
3.5	4.388	0.752	3.636	4.426	0.820	3.606
4.0	6.824	1.119	5.405	6.896	1.537	5.359
4.5	10.060	2.441	7.619	10.180	2.630	7.551

TABLE I.4.9 (end)

/40

a, μ	$\pi a^2 K$, μ²	$\pi a^2 K_s$, μ²	$\pi a^2 K_a$, μ²	$\pi a^2 K$, μ²	$\pi a^2 K_s$, μ²	$\pi a^2 K_a$, μ²
	$T = 273°$			$T = 283°$		
5.0	$14.200 \cdot 10^{-2}$	$3,898 \cdot 10^{-2}$	$10,302 \cdot 10^{-2}$	$14.384 \cdot 10^{-2}$	$4,179 \cdot 10^{-2}$	$10.206 \cdot 10^{-2}$
5.5	19.368	5.884	13.484	19.637	6.283	13.354
6.0	15.637	8.458	17.179	26.008	9.000	17.008
6.5	33.080	11.678	21.402	33.572	12.388	21.184
7.0	41.745	15.582	26.162	42.377	16.488	25.889
7.5	53.994	22.198	31.796	55.034	25.538	31.496
8.0	65.842	28.137	37.705	67.115	29.774	37.341
8.5	79.134	34.975	44.159	80.665	36.940	43.725
9.0	93.855	42,706	51.149	95.660	45.020	50.640
9.5	110.01	51.345	58.669	112.10	54.026	58.077
10.0	127.61	60.902	66.710	130.00	63.969	66.029
	$T = 278°$			$T = 288°$		
1.0	$8.06 \cdot 10^{-2}$	$8.60 \cdot 10^{-4}$	$7.97 \cdot 10^{-2}$	$7.99 \cdot 10^{-2}$	$9.68 \cdot 10^{-4}$	$7.90 \cdot 10^{-2}$
1.5	0.283	$9.21 \cdot 10^{-3}$	0.274	0.282	$1.03 \cdot 10^{-3}$	0.271
2.0	0.707	$4.65 \cdot 10^{-2}$	0.661	0.707	$5.18 \cdot 10^{-2}$	0.655
2.5	1.461	0.151	1.310	1.465	0.167	1.298
3.0	2.648	0.372	2.276	2.664	0.408	2.256
3.5	4.407	0.786	3.621	4.445	0.856	3.589
4.0	6.860	1.477	5.383	6.932	1.599	5.333
4.5	10.120	2.534	7.586	10.241	2.728	7.513
5.0	14.292	4.037	10.255	14.478	4.325	10.153
5.5	19.502	6.081	13.421	19.773	6.490	13.283
6.0	25.822	8.726	17.096	26.197	9.281	16.917
6.5	33.325	12.029	21.296	33.823	12.756	21.067
7.0	42.059	16.070	26.029	42.699	19.956	25.743
7.5	54.512	22.862	31.650	55.559	24.224	31.335
8.0	66.477	28.949	37.528	67.758	30.610	37.147
8.5	79.898	35.951	43.947	81.437	37.942	49.495
9.0	94.756	43.856	50.900	96.567	46.197	50.370
9.5	111.06	52.678	58.379	113.15	55.386	57.765
10.0	128.80	62.429	66.376	131.19	65.521	65.671
	$T = 293°$			$T = 298°$		
1.0	$7.96 \cdot 10^{-2}$	$1.03 \cdot 10^{-3}$	$7.86 \cdot 10^{-2}$	$7.92 \cdot 10^{-2}$	$1.08 \cdot 10^{-3}$	$7.81 \cdot 10^{-2}$
1.5	0.281	$1.09 \cdot 10^{-2}$	0.270	0.280	$1.15 \cdot 10^{-2}$	0.269
2.0	0.707	$5.45 \cdot 10^{-2}$	0.652	0.706	$5.74 \cdot 10^{-2}$	0.649
2.5	1.467	0.175	1.292	1.469	0.183	1.286
3.0	2.672	0.427	2.245	2.680	0.447	2.234
3.5	4.464	0.892	3.571	4.483	0.930	3.553
4.0	9.969	1.663	5.306	7.006	1.728	5.278
4.5	10.303	2.829	7.474	10.365	2.933	7.433
5.0	14.573	4.475	10.098	14.669	4.628	10.041
5.5	19.912	6.702	13.210	20.054	6.920	13.139
6.0	26.390	9.568	16.821	26.585	9.862	16.723
6.5	34.078	13.132	20.946	34.338	13.517	20.821
7.0	43.026	17.434	25.591	43.358	17.922	25.436
7.5	56.089	24.921	31.168	56.622	25.626	30.996
8.0	68.405	31.458	36.946	69.056	32.316	36.740
8.5	82.213	38.956	43.257	82.994	39.980	43.013
9.0	97.478	47.385	50.092	98.393	48.585	49.808
9.5	114.20	56.757	57.444	115.25	58.139	57.116
10.0	132.39	87.083	65.303	133.58	68.654	64.928

In one of his papers Stephens (Bibl.31) gives effective cross sections for attenuation, scattering, and absorption for particles of a given size, which are average for the long-wave spectrum in the range of $4 \leq \lambda \leq 90\mu$. The averaging was performed by means of the formula

$$K_{av} = \frac{\int_{4\mu}^{90\mu} B_\lambda(T) K_\alpha(\lambda, a)\, d\lambda}{\int_{4\mu}^{90\mu} B_\lambda(T)\, d\lambda}. \qquad (I.4.5)$$

The computation was carried out for a set of values of radii and temperatures. These data are presented in Table I.4.9.

K.S.Shifrin (Bibl.43) computed the total volumetric attenuation factor $\tilde{D}_\lambda$ for a monodisperse cloud at a = 6.265μ. The value D_λ was determined by means of

$$\tilde{D}_\lambda = \tilde{\alpha}_{v,\lambda} + \tilde{\sigma}_{v,\lambda} + \tilde{\alpha}_{w,\lambda}.$$

The spectral interval ($4 \leq \lambda \leq 36\mu$) was subdivided into segments $\Delta\lambda$ of a width of 4μ. First, the average values of K_s and of K_a and then the values of $\tilde{\alpha}_{v,\lambda} + \tilde{\sigma}_{v,\lambda}$ for various values of liquid-water content $\tilde{\rho}_v$ were computed for each segment. The values $\tilde{\alpha}_{w,\lambda}$ were determined from the mass absorption coefficient of water vapors given in the monograph of K.Ya.Kondrat'yeva (Bibl.25); see Table I.5.2. It was assumed that the relative humidity in the cloud was 100%. Thus, the coefficient $\tilde{\alpha}_{w,\lambda}$ was found to be dependent on the temperature. The results of the computation of D_λ (in km^{-1}) are given in Table I.4.10*. /41

Along with the attenuation factor, the scattering coefficient must be known in solving the transfer equation. Such data, for a droplet with a radius of a = 6.265μ, were obtained by K.S.Shifrin (Bibl.42). His values are given in Table I.4.6 and in Fig.I.4.6. This diagram yielded average values of $K_{s,\lambda}$ from which we computed $\sigma_{v,\lambda}$ for the same 4μ spectral region for which the values of D_λ are given in Table I.4.10. The values of $\sigma_{v,\lambda}$ are shown in Table I.4.11.

The computation of $\tilde{\sigma}_{v,\lambda}$ at given $K_{s,\lambda}$ was performed on the basis of the formula

$$\tilde{\sigma}_{v,\lambda} = \frac{3K_s \rho_v}{4a\tilde{\rho}_v},$$

where $\tilde{\rho}_v$ is the density of water ($\tilde{\rho}_v$ = 1 gm/cm³) and a is the droplet radius.

---

* The misprint discovered in Shifrin's paper (Bibl.43) for the interval (8 - 12μ) was corrected in Table I.4.10. Averaging of the quantities $K_\lambda = K_{s,\lambda} + K_{a,\lambda}$ (Bibl.42) in this region will yield K = 2 instead of K = 1.5 as had been given by Shifrin (Bibl.43).

Average values of $\tilde{\sigma}_{v,\Delta\lambda}$ for the spectral regions shown in Table I.4.11 were determined from the relation

$$\tilde{\sigma}_{v,\Delta\lambda} = \frac{\int_{\lambda_i}^{\lambda_{i+1}} \tilde{\sigma}_{v,\lambda} d\lambda}{\lambda_{i+1} - \lambda_i},$$

where $\lambda_{i+1} - \lambda_i = 4\,\mu$.

In supplementing the enumerated data, we can give the following approximate formula of Van de Hulst (Bibl.30) which makes it possible to compute the cross section for attenuation (without fine structure) in the case when $|m-1| \to 0$, i.e., in the so-called approximation of "soft" particles

$$K(\delta, n) = 2 - 4\frac{\cos z}{\delta} e^{-x} \sin(\delta - z) + 4\left(\frac{\cos z}{\delta}\right)^2 [\cos 2z - e^{-x} \cos(\delta - 2z)], \quad \text{(I.4.6)}$$

where

$$\delta = 2\rho(m-1), \quad \text{(I.4.7)}$$

$$z = \operatorname{arc\,tg} \frac{\varkappa}{m-1}, \quad \text{(I.4.8)}$$

$$x = \delta \frac{\varkappa}{m-1}. \quad \text{(I.4.9)}$$

In comparing the computations performed by means of eq.(I.4.6) with the exact data given in Table I.4.5, Deirmendjian (Bibl.45) came to the conclusion that the former could be utilized when $m \approx 1.3$, i.e., for water droplets, by introducing a correction factor $D_1(\delta, z)$ obtained from the formula

$$K'(\delta, n) = (1 + D_1) K(\delta, n), \quad \text{(I.4.10)}$$

where $K'(\delta, n)$ denotes the corrected attenuation cross section.

Deirmendjian gives the following values D_1 for various intervals of the quantities δ: /43

$$D_1(z, \delta) = \frac{5(m-1)^2}{8{,}16\,m}[f(z) + 1] - \frac{5(m-1) - \delta}{5(m-1) f(z)} \quad \text{(I.4.11)}$$

$$\text{at} \quad \delta \leqslant 5(m-1) < \frac{4{,}08}{1 + 3\operatorname{tg} z},$$

$$D_2(z, \delta) = \frac{m-1}{2m}[f(z) + 1]\frac{\delta}{4{,}08} \quad \text{at} \quad 5(m-1) \leqslant \delta \leqslant \frac{4{,}08}{1 + 3\operatorname{tg} z}, \quad \text{(I.4.12)}$$

$$D_3(z, \delta) = \frac{m-1}{2m}\frac{f(z)+1}{1 + 3\operatorname{tg} z} \quad \text{at} \quad \frac{4{,}08}{1 + 3\operatorname{tg} z} \leqslant \delta \leqslant \frac{4{,}08}{1 + \operatorname{tg} z}, \quad \text{(I.4.13)}$$

TABLE I.4.10

/42

t, °C	ρ_v, g/m³					
	0.05	0.1	0.2	0.5	0.8	1.0
			$\Delta\lambda = 4—8\ \mu$			
—20	25.8	43.0	77.5	181	284	353
—10	36.1	53.8	87.8	191	294	363
—5	44.5	61.7	96.2	199	303	372
0	55.0	73.2	108	211	314	384
5	71.7	88.9	123	227	330	399
10	92.5	110	144	247	351	420
20	156	173	208	311	414	583
			$\Delta\lambda = 8—12\ \mu$			
—20	9.01	24.0	48.0	120.0	192	240
—10	9.02	24.0	48.0	120.0	192	240
—5	9.03	24.0	48.0	120.0	192	240
0	9.05	24.0	48.0	120.0	192	240
0	9.05	24.0	48.0	120.0	192	240
5	9.07	24.1	48.1	120.1	192	240
10	9.09	24.1	48.1	120.1	192	240
20	9.2	24.2	48.2	120.2	192	240
			$\Delta\lambda = 12—16\ \mu$			
—20	13.0	25.9	51.7	129	206	258
—10	13.1	26.0	51.8	129	207	258
—5	13.2	26.1	51.9	129	207	258
0	13.4	26.2	52.1	129	207	258
5	13.6	26.5	52.3	130	207	259
10	13.8	26.7	52.5	130	207	259
20	14.6	27.5	53.3	131	208	260
			$\Delta\lambda = 16—20\ \mu$			
—20	15.7	29.1	56.2	137	218	272
—10	18.2	31.7	58.7	140	221	275
—5	20.3	33.8	60.1	142	223	277
0	24.2	36.7	63.7	145	226	280
5	27.1	40.6	67.6	149	230	284
10	32.3	45.8	72.8	154	232	289
20	48.1	61.6	88.6	170	251	305
			$\Delta\lambda = 20—24\ \mu$			
—20	18.5	31.1	56.3	132	207	258
—10	26.6	38.2	63.4	129	215	265
—5	31.4	44.0	69.2	145	220	271
0	39.3	51.9	77.1	153	228	279
5	50.1	62.7	87.9	164	239	289
10	64.4	77.0	102	178	253	304
20	108	120	146	221	197	347
			$\Delta\lambda = 24—28\ \mu$			
—20	20.2	31.3	53.5	120	187	231
—10	31.2	42.3	64.5	131	198	242

TABLE I.4.10 (end)

/43

t, °C	ρ_v, g/m³					
	0.05	0.1	0.2	0.5	0.8	1.0
−5	40.1	51.2	73.4	140	207	251
0	52.4	63.5	85.7	153	219	263
5	69.0	80.1	102	169	235	280
10	91.9	102	124	191	258	302
20	158	169	192	258	325	369
			$\Delta\lambda = 28$—$32\ \mu$			
−20	27.6	37.8	58.2	119	181	221
−10	48.5	58.7	79.1	140	201	242
−5	65.5	75.7	96.1	157	218	259
0	88.9	99.1	129	181	242	283
5	120	131	151	212	273	314
10	163	173	193	254	316	356
20	291	301	321	383	444	485
			$\Delta\lambda = 32$—$36\ \mu$			
−20	29.7	39.6	59.4	119	178	218
−10	53.4	63.3	83.1	144	202	242
−5	62.7	82.6	102	162	221	261
0	99.3	108	129	188	248	287
5	135	145	165	224	284	323
10	183	193	213	272	332	371
20	329	338	358	418	477	517

TABLE I.4.11

$\Delta\lambda$, μ	K_ε, μ^2	$\sigma_{v,\lambda}$		
		$\rho_v = 0{,}1\ g/m^3$	$\rho_v = 0{,}2\ g/m^3$	$\rho_v = 0{,}5\ g/m^3$
4—8	2.11	25.18	50.36	125.89
8—12	1.39	16.64	33.28	83.20
12—16	0.83	9.92	19.84	49.61
16—20	0.99	11.86	23.72	59.31
20—24	0.94	11.28	22.57	56.43
24—28	0.78	9.34	18.69	46.72

/44

$$D_4(z, \delta) = \frac{m-1}{2m} \frac{f(z)+1}{1+3\,\mathrm{tg}\,z} \frac{4{,}08}{\delta} \quad \text{at} \quad \delta > \frac{4{,}08}{1+\mathrm{tg}\,z}, \qquad \text{(I.4.14)}$$

where

$$f(z) = (1 + \operatorname{tg} z)(1 + 3 \operatorname{tg} z) = 1 + 4\frac{\varkappa}{m-1} + 3\left(\frac{\varkappa}{m-1}\right)^2. \qquad \text{(I.4.15)}$$

Equation (I.4.10) gives an error in the quantity $K(\delta, n)$ in the range of $\pm 4\%$ at $1 \leq m \leq 1.5$ and $0 \leq \varkappa \leq 0.25$.

This brief review demonstrates the obvious insufficiency of data on the optical parameters of water droplets in the absorption region. Specifically, almost no data exist on the scatter indicatrix. The only paper in this respect is that by K.S.Shifrin (Bibl.46) who computed the scattering indicatrix with consideration of absorption, at $\lambda = 10\mu$ and $a = 6.265\mu$.

TABLE I.4.12

λ, μ	α_v, cm²/g			λ, μ	α_v, cm²/g		
	Layer	a = 6.26 μ	a = 12.5 μ		Layer	a = 6.26 μ	a = 12.5 μ
4.0	46.0			14.0	3703.0		
4.5	266.8	597.2		16.0	3703.0		
5.0	250.7			18.0	2921.0	1691.1	825.3
5.5	220.8			20.0	2258.6		
6.0	2806.0	1345.9		22.0	1752.6		
6.5	1872.2			24.0	1363.9		
7.0	402.5	840.8		26.0	1097.1		
7.5	381.8			28.0	947.6		
8.0	363.4	279.5		30.0	784.3		
8.5	358.8			32.0	662.4		
9.0	363.4	752.4	544.6	34.0	614.1		
9.5	381.8			36.0	593.4		
10.0	462.3	686.7	465	38.0	593.4		
12.0	2323.0	1354.3		40.0	549.7		
				42.0	570.4		

Another paper (Bibl.84) gives scattering indicatrices for $\varkappa \neq 0$ and a few values of λ and of a. The indicatrices are presented in graphic form, which is quite inconvenient to use.

Because of the lack of data on absorption in droplets, the absorption coefficients of a continuous water layer (Bibl.44, 47) are often used. Therefore, it might be of interest to give here the values of the absorption coefficient for a layer of water. Such data are given in Table I.4.12, taken from McDonald (Bibl.44) and based on measurements by Plyler and Acquista (Bibl.33). For comparison, columns 3 and 4 of the Table give absorption coefficients of droplet water, computed by the formula

$$\alpha_v = \frac{3}{4}\frac{K_\alpha}{a\rho_v}10^4 \qquad \text{(I.4.16)}$$

for a = 6.26μ and a = 12.53μ at values of K_a taken from Tables I.4.6 and I.4.7, respectively.

The Table shows that the absorptivity of continuous and droplet water may differ by a factor of 2, toward either the plus or minus side.

It must be noted especially that there are almost no data on the optical characteristics of ice. There are only the old computations (for ice spheres) by Blumer (Bibl.48) and by Winer (Bibl.49) which are insufficient for the investigation of radiative transfer in ice clouds. For this reason, in our /45 subsequent investigation on scattering, we consider only water clouds which, in accordance with Fig.I.1.1, means a critical temperature of $t^\circ \geq -10^\circ$.

In concluding this Section, we will briefly discuss the coefficient C_1 for the first term of the scattering function expansion in a series in Legendre polynomials. We have

$$C_1 = \int_0^\pi \gamma(\varphi) P_1(\cos\varphi) \sin\varphi d\varphi \qquad \text{(I.4.17)}$$

or

$$C_1 = \frac{3}{2}\int_0^\pi \gamma(\varphi) \cos\varphi \sin\varphi d\varphi. \qquad \text{(I.4.18)}$$

Hence

$$C_1 < 3,$$

because of [see eq.(I.2.7)]

$$\frac{1}{2}\int_0^\pi \gamma(\varphi) \sin\varphi d\varphi = 1.$$

It is also obvious that the coefficient C_1 is proportional to the resultant flux or to the difference between the fluxes of radiation scattered into the front and back hemispheres (with respect to the direction of incidence of the light). This defines the special role of this coefficient in a number of cases, as will be shown in the following Chapters.

TABLE I.4.13

	ρ										
	1	2	3	4	5	6	10	15	20	25	30
C_1	0.55	2.01	2.35	2.48	2.54	2.41	2.14	2.38	2.31	2.56	2.48
$\gamma(0)/\gamma(\pi)$	2.48	90.4	204.6	227.0	271.6	387.7	254.8	109.4	200.0	242.4	2331.3

Table I.4.13 gives the values of C_1 from (Bibl.40) for n = 1.33 and for various values of ρ. The ratios $\frac{\gamma(0)}{\gamma(\pi)}$ for the same cases are given in the

third row of the Table.

Table I.4.13 shows that the value C_1 varies over a relatively narrow range: $2 \leq C_1 \leq 2.6$ at $2 \leq \rho \leq 30$ and that it is not very sensitive to fluctuations in the elongation of the indicatrix. With an increase in ρ, the quantity C_1 first increases and then varies irregularly, remaining on the whole within the limits of 2.3 - 2.6.

TABLE I.4.14

C_1	0.34	0.71	1.05	1.56	1.97
$\gamma(0)/\gamma(\pi)$	1.9	4.3	10	30	70

The increase in C_1 with an increase in elongation for moderately elongated indicatrices is shown in Table I.4.14. This Table gives values of C_1 corresponding to the scattering indicatrices measured by Foyttsik and Chaek in the atmosphere layer near the ground (Bibl.50).

It follows from Tables I.4.13 and I.4.14 that, in the case of moderately /46 elongated indicatrices, the quantity C_1 increases with an increase in ρ or in elongation, remaining within the range of 0 - 2. Strongly elongated indicatrices are characterized by minor and irregular fluctuations in the quantity C_1 within the range of 2.3 - 2.6.

4.2 Optical Parameters of Real Clouds

The optical properties of real clouds, at present, are very little investigated. Below, we give individual results of computations and measurements.

TABLE I.4.15

a, μ	2—3	3—5	5—6	6—10	10—11	11—15	15—17	17—19
$p(a)$, %	2.7	3.4	10.1	15.4	7.4	2.7	0.7	1.3

The scattering coefficient of a stratus cloud was computed for the visible region of the spectrum in another paper (Bibl.18), based on data by Stratton and Houghton (Fig.I.4.3) for a drop-size distribution p(a) (in percent for an interval of the values of a in 1μ) obtained by Neiburger (Bibl.51) and given in

Table I.4.15.

If n(z) denotes the total number of drops per unit volume at the level z which, for a given liquid-water content $\rho_v(z)$, is determined by means of the formula

$$n(z) = \frac{\rho_v(z)}{4/3\,\pi \approx{\rho}_v \int_0^\infty a^3 p(a)\,da}, \tag{I.4.19}$$

then the number of droplets of a given size per unit volume will be equal to

$$N(a, z) = \frac{\rho_v(z)\,p(a)}{4/3\,\pi \approx{\rho}_v \int_0^\infty a^3 p(a)\,da}. \tag{I.4.20}$$

Obviously,

$$\tilde{\sigma}_{v,\lambda}(z) = \pi \int_0^\infty a^2 K_s(a, \lambda)\, N(a, z)\, dz. \tag{I.4.21}$$

From this and taking into account eq.(I.4.20), we obtain

$$\tilde{\sigma}_{v,\lambda}(z) = \frac{3}{4} \frac{\rho_v(z) \int_0^\infty a^2 K_s(a, \lambda)\, p(a)\,da}{\approx{\rho}_v \int_0^\infty a^3 p(a)\,da}. \tag{I.4.22}$$

According to Neiburger's measurements, the gradient of liquid-water content in the cloud is 0.13 gm/m^3 per 100 m, from the base of the cloud to the top.

The results of the computations of $\tilde{\sigma}_{v,\lambda}$ based on eq.(I.4.22) for such a liquid-water content are shown in Table I.4.16.

TABLE I.4.16

/47

λ, μ	0.4	0.5	0.6	0.7	0.8	0.9	1	1.5	2
$\frac{1}{z}\tilde{\sigma}_{v,\lambda}$, km^{-1}	21	21	21	21	21	21	21	21	22

Here z is the height in hundreds of meters, counted from the lower boundary of the cloud upward.

Deirmendjian (Bibl.52) computed the scattering indicatrix and coefficient on the basis of the drop-size distribution curve given by A.Kh.Khrgian and

I.P.Mazin [see eq.(I.1.1)] with a droplet concentration equal to 100 per cm^3 and a model radius of 4μ.

The results of Deirmendjian's computations are presented in Tables I.4.17 and I.4.18.

TABLE I.4.17

λ, μ	0.45	3.07	5.30	10.00
$\tilde{\sigma}_{v,\lambda}$, km^{-1}	16.33	18.58	24.01	11.18

TABLE I.4.18

λ, μ	φ_0				
	0	10	100	140	180
0.7	267.4	1.398	0.00476	0.03750	0.09940
5.3	7.636	4.282	0.01069	0.01074	0.00882
10.0	3.704	2.993	0.00668	0.00386	0.00472

It can be concluded that the above author (Bibl.52) apparently took the absorption in the long-wave region of the spectrum into consideration. Obviously, Deirmendjian computed $\tilde{\sigma}_{v,\lambda}$ by means of eq.(I.4.22) and determined the effective scattering indicatrix $\gamma_{v,\lambda}(\varphi)$ from the formula

$$\gamma_{v,\lambda}(\varphi) = \frac{\int_0^\infty a^2 K_s(a,\lambda)\,\gamma(a,\lambda)\,N(a)\,da}{\int_0^\infty a^2 K_s(a,\lambda)\,N(a)\,da}. \qquad (I.4.23)$$

Ye.P.Novosel'tsev (Bibl.53), in his calculation of the absorption cross section in the near-infrared region of the spectrum, used the K.S.Shifrin approximate formula of the form of

$$K_s = \pi a^2 (1 - e^{-4\rho x})(1 - R), \qquad (I.4.24)$$

where R is the radiation flux reflected by the droplet

$$R = \int_0^{\pi/2} r(\varphi) \sin 2\varphi d\varphi, \qquad (I.4.25)$$

Here, $r(\varphi)$ is the Fresnel coefficient which parametrically depends on the complex refractive index n.

Equation (I.4.24) was obtained from the methods of geometrical optics and is constructed as an interpolation formula yielding correct values for small and large particles. The same formula was used by K.S.Shifrin in computing $\tilde{D}$ (see above).

The results of calculating of R in the interval $(0.7 \leq \lambda \leq 3.02\mu)$ are shown in Table I.4.19. /48

TABLE I.4.19

λ, μ	R	λ, μ	R	λ, μ	R
0.700	0.0646	1.50	0.0631	2.60	0.0704
0.800	0.0642	1.60	0.0630	2.70	0.0736
0.900	0.0638	1.70	0.0625	2.74	0.0746
1.00	0.0640	1.80	0.0616	2.77	0.0754
1.05	0.0635	1.90	0.0607	2.80	0.0764
1.10	0.0632	2.00	0.0603	2.90	0.0800
1.20	0.0628	2.20	0.0620	2.95	0.0822
1.30	0.0629	2.40	0.0658	3.00	0.0847
1.40	0.0631	2.50	0.0680	3.02	0.0850

With the aid of the Khrgian-Mazin formula [eq.(I.1.1)], Ye.P.Novosel'tsev later derived the following relation which describes the absorption coefficient per unit volume of a polydisperse cloud $\tilde{\alpha}_{v\lambda}$ cm^{-1}:

$$\tilde{\alpha}_{v,\lambda} = 0{,}45 \frac{\rho_v}{\bar{a}} (1 - R) \left[1 - \frac{1}{\left(1 + \frac{2}{3} \tilde{\tilde{\alpha}}_{v,\lambda} \bar{a}\right)^5} \right], \qquad (I.4.26)$$

where ρ_v denotes the water content, in gm/cm^3; $\bar{a}$ is the average droplet radius, in μ; $\tilde{\tilde{\alpha}}_{v,\lambda}$ is the absorption coefficient of the continuous water layer, cm^{-1}.

Since $4\rho\varkappa = 2a\tilde{\tilde{\alpha}}_{v,\lambda} \leq 0.1$ at $\lambda \leq 2.5\mu$, it is possible to assume, in the relation (I.4.24),

$$1 - e^{-4\rho\varkappa} \approx 2a\tilde{\tilde{\alpha}}_v$$

and to obtain a simpler expression for $\tilde{\alpha}_{v,\lambda}$:

$$\tilde{\alpha}_{v,\lambda} = 1.43\tilde{\tilde{\alpha}}_{v,\lambda}\rho_v(1-R). \qquad (I.4.27)$$

Computations with this formula in the indicated region of values of λ lead to results close to those computed by means of eq.(I.4.26).

In calculating with eqs.(I.4.26) or (I.4.27), the absorption coefficient of a continuous water layer $\tilde{\tilde{\alpha}}_{v,\lambda}$ must be known. For $\lambda \leq 2.5\mu$, only the data by Aschkinass which are more than 50 years old (see Fig.I.4.7) and a few more recent individual measurements are available for use.

Table I.4.20 shows that satisfactory agreement exists between the results of measurements by various authors.

TABLE I.4.20

λ, μ	$\alpha_{v,\lambda}, cm^{-1}$		
	Aschkinass, 1895	Collins, 1925	Burchio, 1954
0.97	0.416	0.448	0.46
1.27	1.21	1.28	—
1.44	38.4	29.4	26.0
2.00	123.2	103.0	114.0

On the basis of Fig.I.4.7, the values of $\tilde{\alpha}_{v,\lambda}$ were computed with eq.(I.4.27) for 22 spectrum regions at $\rho_v = 0.2$ gm/m^3. /49

The values for $\tilde{\tilde{\alpha}}_v$ in cm^2/gm taken from Fig.I.4.7, as well as the computed values for $\tilde{\alpha}_v$ in km^{-1} and the mass (α_w) and volume (α_w) absorption coefficients of water vapor are given in Table I.4.21. The latter is determined for the condition of saturation at temperatures of 0 and -15°. Finally, the last column contains the values of the spectral solar constant for each of the selected bands. All these data are compiled here since they will be used in Chapter III in the computation of infrared radiation fluxes.

The spectral regions in Table I.4.21 are so selected that they correspond to the infrared bands of water vapor and to the intervals between the bands. Each band is subdivided into three segments in accordance with the concept of the absorption function described in Section 5. The absorption spectrum of water vapor within the boundaries of the band is characterized by two absorption coefficients: α the average of all large values and β the average of all small values.

Assuming a large coefficient α corresponding to the center of the band, /50

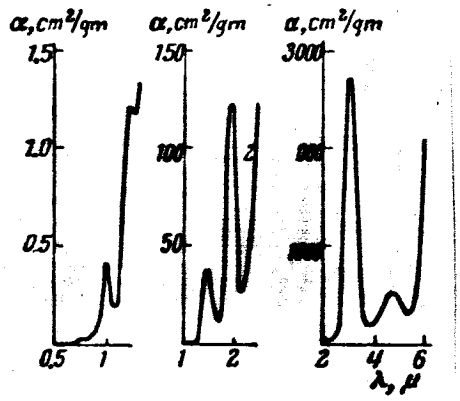

Fig.I.4.7 Absorption Spectrum of Water

each band can be subdivided into three segments

$$\frac{1}{2}(1-\gamma)\Delta\lambda,\ \gamma\Delta\lambda,\ \frac{1}{2}(1-\gamma)\Delta\lambda,$$

TABLE I.4.21

	Δλ	$\tilde{\tilde{\alpha}}_v$, cm²/gm	$\tilde{\alpha}_v$, km⁻¹	α_w, cm²/gm	$\tilde{\alpha}_w$, cm⁻¹		πS, cal/, cm²·min.
					t = 0°	t = −15°	
	0.700—0.719	0.006	0.00017	0.019	0.0093	0.0029	
a	0.719—0.721	0.012	0.0034	0.267	0.13	0.041	0.0806
	0.721—0.740	0.016	0.00046	0.019	0.0093	0.0029	
	0.740—0.790	0.025	0.00072	0	0	0	0.0870
	0.790—0.814	0.030	0.00086	0.020	0.0098	0.0031	
0,8 μ	0.814—0.816	0.030	0.00086	0.479	0.23	0.074	0.0760
	0.816—0.840	0.031	0.00089	0.020	0.0098	0.0031	
	0.840—0.860	0.040	0.0011	0	0	0	0.0277
	0.860—0.915	0.069	0.0020	0.038	0.019	0.0059	
ρστ	0.915—0.935	0.147	0.0042	1.153	0.56	0.18	0.1511
	0.935—0.990	0.400	0.011	0.038	0.019	0.0059	
	0.990—1.030	0.352	0.010	0	0	0	0.0380
	1.030—1.112	0.186	0.0053	0.030	0.015	0.0046	
Φ	1.112—1.148	0.583	0.017	0.107	0.54	0.17	0.1466
	1.148—1.230	1.100	0.031	0.030	0.015	0.0046	
	1.230—1.240	1.206	0.034	0	0	0	0.0054
	1.240—1.321	1.166	0.033	0.047	0.023	0.0073	
Ψ	1.321—1.449	12.7	0.36	3.157	1.55	0.49	0.1239
	1.449—1.530	38.6	1.10	0.047	0.023	0.0073	
	1.530—1.755	15.8	0.45	0.022	0.011	0.0034	
Ω	1.755—1.965	47.8	1.37	4.178	2.05	0.65	0.1036
	1.965—2.190	40.7	1.16	0.022	0.011	0.0034	

where $\Delta\lambda$ is the width of the band and, γ the relative length of the segments that correspond to the coefficient α. The average absorption coefficient of water in each of these parts was determined on the basis of the data by Aschkinass. The values of α, β, γ for the water vapor band in the near-infrared region are contained in Table I.5.5.

The most important of all experimental investigations on the optical parameters of real clouds are the measurements of transparency or the scattering coefficient at $\lambda \leq 1\mu$. Kampe (Bibl.55) determined the transparency of various types of clouds by measuring the attenuation of light of a searchlight installed on the wing of an aircraft flying in the cloud. He presented the results in terms of values of the meteorological visibility range v (MVR), related to the scattering coefficient by a formula of the form of

$$v = \frac{3{,}91}{\tilde{\sigma}_v}. \qquad \text{(I.4.28)}$$

The average values obtained by Kampe for clouds of various forms are presented in Table I.4.22.

TABLE I.4.22

Type of Cloud	v, m	$\tilde{\sigma}_v$, km^{-1}	σ_v, km^{-1} accd. to (Bibl.11)
Sc	100	39.1	38
St	140	28	26
As	150	26	19.5

Here, $\tilde{\sigma}_v$ is computed by means of eq.(I.4.28) for given values of v. Bullrich (Bibl.11) gives values for $\tilde{\sigma}_v$ apparently obtained from the same measurements by Kampe but differing from those computed by eq.(I.4.28). These are given in the last column of Table I.4.22.

Complex investigations of stratus clouds and fogs in the Arctic were carried out by G.M.Zabrodskiy, V.G.Morachevskiy and A.L.Dergach (Bibl.10, 56, 57). Specifically, they made detailed investigations on the transparency, with simultaneous measurements of the water content and the microstructure.

The principal qualitative conclusions from these papers are as follows:

1) Optically, fogs are quite uniform over their entire thickness except for the upper boundary.

2) In the stratocumulus clouds, the transparency decreases rapidly with height in the lower part of the cloud but remains about constant in its middle part.

3) The vertical distribution of transparency in stratus clouds is similar to that observed in fog but is characterized by greater variability.

4) The transparency rapidly increases in all cases at the upper boundary of the cloud or fog layer. However, as indicated above, the latest investigations by G.M.Zabrodskiy (Bibl.7) indicated that the high transparency obtained at the boundary of the clouds is not real but must be considered an experimental error.

5) The behavior of liquid-water content and transparency (or the meteorological visibility range) are in good agreement. /51

TABLE I.4.23

Gradation of MVR, m	Fog		St		Sc		Ns–As	
	No. of Test	%	No. of Test	%	No. of Test	%	No. of Test	%
26	4	2.9	1	1.5	—	—	24	9.4
27—50	7	5.0	2	3.0	—	—	11	4.3
51—100	16	11.5	4	6.1	18	7.4	41	15.9
101—200	53	38.2	22	33.3	78	32.2	81	31.9
201—300	35	25.2	25	37.9	97	40.2	56	22.1
301—400	12	8.6	7	10.6	16	6.6	34	13.4
401—500	5	3.6	4	6.1	12	4.9	—	—
500	7	5.0	1	1.5	21	8.7	2.7	2.7
Total measurements	139	100	66	100	242	100	258	100

Quantitative analyses of the correlation between liquid-water content and visibility, carried out by G.M.Zabrodskiy (Bibl.7) permitted establishing of a connection between these two quantities:

$$vp_v^{0.63} = 34.1 \quad \text{for clouds Sc,}$$
$$vp_v^{0.78} = 42.7 \quad \text{for clouds St;} \qquad (I.4.29)$$

here v is expressed in meters.

For a St cloud, at $\rho_v = 0.2$ gm/m^3 this yields v = 135 m and $\tilde{\sigma}_v = 29$ km^{-1}. The obtained value $\tilde{\sigma}_v$ agrees well with the data by Kampe and with the values of α_v (see Table I.4.16) computed by us for the z = 150 m level where the water content, according to Neiburger, is equal to 0.2 gm/m^3.

The repetitive values of the meteorological visibility range in clouds and fogs according to data of (Bibl.57) are presented in Table I.4.23. The frequency

TABLE I.4.24

Gradation of MVR, m	Recurrence in % by Cloud Form				Gradation of MVR, m	Recurrence in % by Cloud Form			
	St	Sc	Ns—As	Fog		St	Sc	Ns—As	Fog
26	0.1	0.5	8.1	1.0	501—600	4.2	4.9	2.0	6.4
27—50	2.0	2.1	5.4	5.4	601—700	2.7	0.2	1.3	1.0
51—100	21.7	18.0	10.1	10.3	701—800	1.5	1.8	2.7	0.5
101—200	36.1	35.6	33.1	32.9	801—900	0.7	1.1	1.4	1.0
201—300	21.4	21.1	20.3	21.7	901—1000	0.1	0.7	0.7	0.5
301—400	5.6	7.1	12.2	11.3	1000	—	0.9	—	1.0
401—500	4.4	5.3	2.7	6.9					

of meteorological visibility range based on a larger volume of experimental material of the same paper (Bibl.57) is given in Table I.4.24.

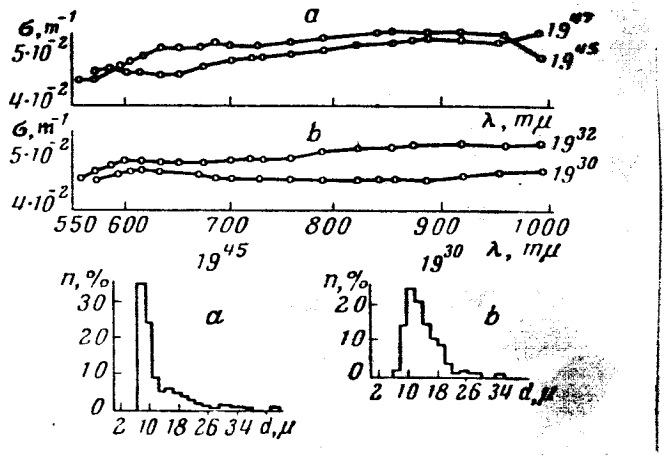

Fig.I.4.8 Spectral Transparency and Microstructure of a Cloud
a - ρ_v = 0.241 gm/m^3, b - ρ_v = 0.146 gm/m^3

Ye.I.Bocharov (Bibl.58) made measurements of the spectral attenuation of radiation of clouds ($0.5 \leq \lambda \leq 1.0\mu$) under high-mountain conditions - on the slopes of Mt.Elbrus. A control check on the microstructure of the investigated cloud was carried out simultaneously. The results of the measurements of the attenuation factor, together with particle-size distribution curves, are plotted in Figs.I.4.8 and I.4.9. The plots indicate that, in accordance with the Mie theory, the attenuation factor in the region ($0.5 - 1\mu$) is practically independent of the wavelength. The water content of clouds computed on the basis of hyperfine structure data, is shown in the same diagrams. Obviously, in a number of cases there is a lack of correspondence between the low water content

/52

and the high attenuation factors, in difference to the above data (shown in Tables I.4.22 - I.4.24).

Ye.I.Bocharov considers 60 km^{-1} to be the mean value of the attenuation

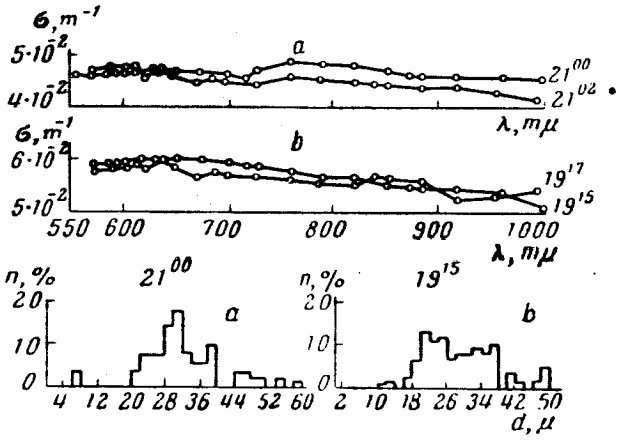

Fig.I.4.9 Spectral Transparency and Microstructure of a Cloud
a - ρ_v = 0.237 gm/m^3, b - ρ_v = 0.286 gm/m^3

factor in Sc clouds with an average water content of 0.26 gm/m^3. Such a value for the water content agrees well with the data presented in Section 1, but the attenuation factor apparently is too high.

TABLE I.4.25

α, μ	λ, μ							
	3.6	4.4	7	8.5	10	11	11.8	12.6
5	0.67	0.95	0.84					
10	0.78	1.0	0.91	0.86	0.63	0.44	0.54	0.64

It is possible that the high values of the attenuation factor obtained elsewhere (Bibl.58) can be attributed to the large drop sizes of mountain clouds which appear in Fig.I.4.9.

Ye.I.Bocharov measured also the spectral attenuation of radiation in artificial fogs (Bibl.59) with a droplet radius from 2.5 to 13μ and with a predominating radius of 3.5 - 4.5μ. The measurements were made at 13 points /53 within the spectrum of wavelength ranges of 2 - 13μ. As a result of the investigations, the author arrived at two conclusions:

The first conclusion was as follows: The ratio of the attenuation factor $D_{\lambda\ opt}$ measured by the optical method to the attenuation factor $D_{\lambda\ micr}$ computed with data of photomicrography of fog, using the formula

$$D_{\lambda\ micr.} = \sum_i \pi a_i^2 K(\rho_i) N(a_i), \qquad \text{(I.4.30)}$$

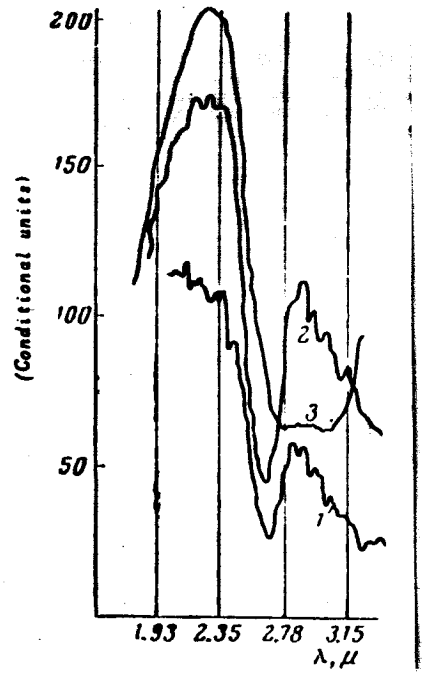

Fig.I.4.10 Transmission Spectrum of an Artificial Fog

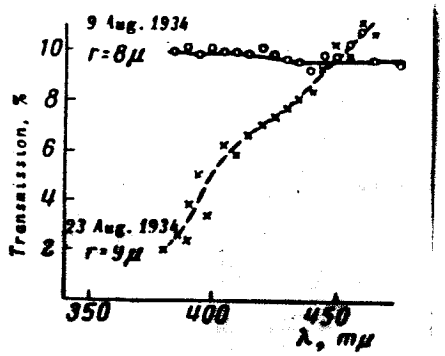

Fig.I.4.11 Spectral Transparency in Fog

is a constant independent of the wavelength. In eq.(I.4.30) $K(\rho_i)$ is the effective attenuation cross section computed by Stratton and Houghton for the true refractive index of n = 1.33 which characterizes the short-wave region of the spectrum ($\lambda \leq 2\mu$; see Sect.4.1). Therefore, this conclusion by Ye.I.Bocharov

can be formulated in the following manner: The attenuation factor in the long-wave region of the spectrum ($2 \leq \lambda \leq 13\mu$) depends on the wavelength as it does in the short-wave region. Apparently, such a conclusion is correct only as to order of magnitude. Table I.4.25 gives the values K/K_c computed with the data of Johnson-Terrel (for K) and of Stratton-Houghton for K_c at $n = 1.33$ for the averages of spectral intervals of Table I.4.5(at $a = 5\mu$ and $a = 10\mu$).

Table I.4.25 indicates that the value K/K_c for a particle of a given diameter is not at all constant. In the case of a polydisperse fog, considered

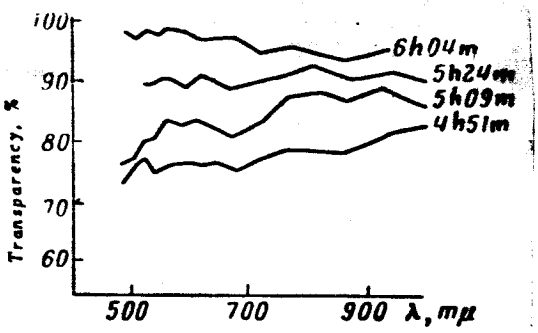

Fig.I.4.12 Spectral Transparency in Fog

by Ye.I.Bocharov, the ratio K/K_c will possibly be less noticeable and the law defined by him (Bibl.59) will, in general, not hold. /54

Ye.I.Bocharov's second conclusion is that, in the attenuation spectrum of fog, only absorption bands of water vapor but no water bands appear. Thus, his

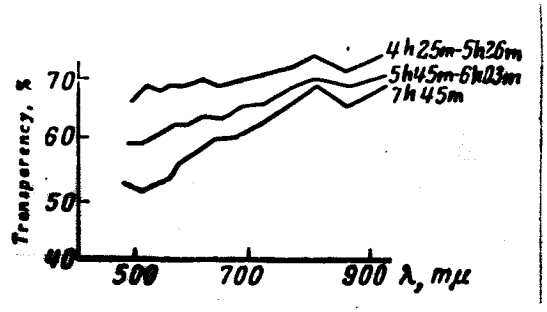

Fig.I.4.13 Spectral Transparency in Fog

curves of radiation transfer by a fog layer (curves 1 and 2 in Fig.I.4.10) show only a band of water vapor with a center of $\lambda = 2.7\mu$ and no water band with a center of 2.94μ, which is clearly seen in the curve of transmission by a water layer (Curve 3).

This effect is discussed elsewhere (Bibl.60, 61). It consists in that, in

the region of resonance absorption bands, the scattering cross section is sharply attenuated. The reduction in scattering compensates the increase in absorption, so that the total attenuation cross section undergoes no appreciable changes.

In addition to the mentioned investigations by Ye.I.Bocharov, several tests were also made of the transparency of artificial and natural fogs. The principal results of the work done, beginning with the Forties, are enumerated below.

Two cases of measuring the transparency of fog by the Elbrus expedition of the Academy of Sciences, USSR (Bibl.17) are given in Fig.I.4.11. Both cases relate to about the same hyperfine structure with average droplet diameters of 8 and 9μ, except that the spectral variation in transparency differs sharply and, in one case, actually contradicts the theory. The same anomaly (increase in transparency with an increase in λ) was obtained by Driving (Bibl.62); see Figs.I.4.12 and I.4.13. I.A.Khvostikov (Bibl.17) explained the anomalous transparency observed in a number of cases by the presence of a large number of submicroscopic ($a < 1\mu$) droplets.

Saito (Bibl.63) measured the integral transparency of artificial fog in the infrared region of the spectrum (2 - 40μ). His results in fogs with various average radii of particles are presented in Figs.I.4.14. Curves 1 - 4 represent the computation of transparency by means of the formula

$$T = \frac{\int B_\lambda \exp\left[-n_i \pi a_i^2 K_i d\right] d\lambda}{\int B_\lambda d\lambda} \qquad \text{(I.4.31)}$$

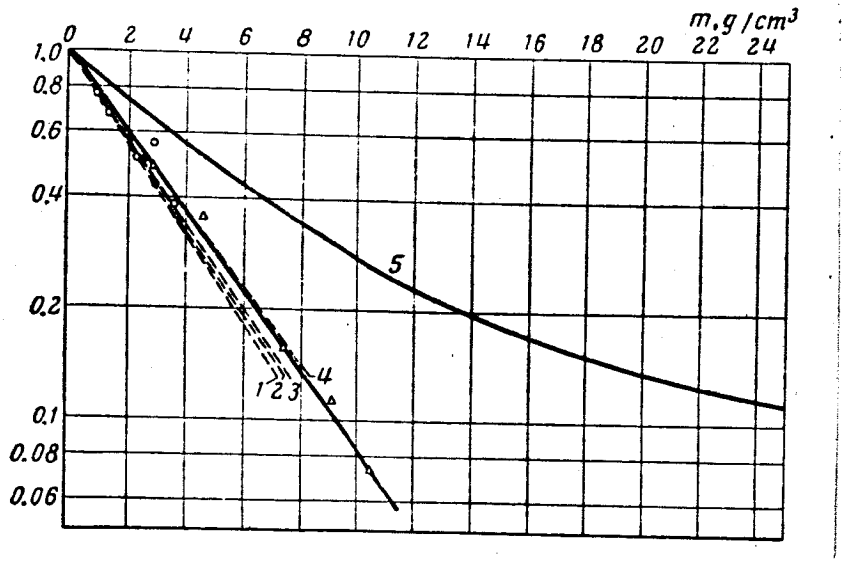

Fig.I.4.14 Integral Transparency of Artificial Fog

for a_i = 3, 4, 4.1, 4.5, 5.1μ. Here K_i is the attenuation cross section of particles with a radius of a_i, whose number per unit volume is equal to n_i; d is the length of the path; and B_λ is Planck's function. The values K_i given in Table I.4.5 were used in the computation. Figure I.4.14 shows that the results of the calculation agree well with the measurements. The transparency /55

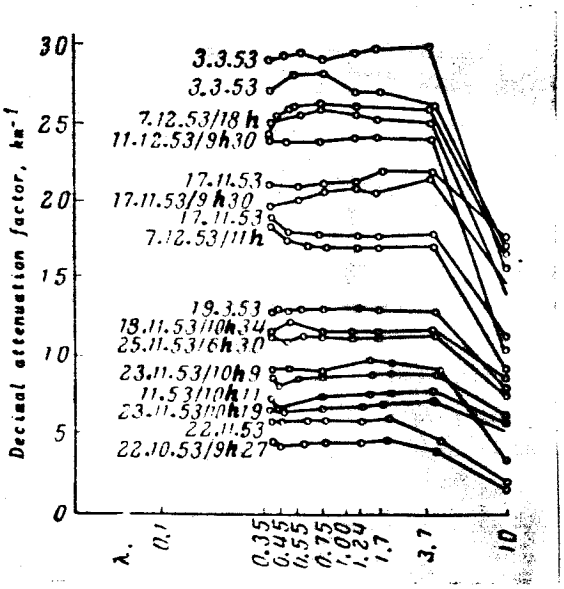

Fig.I.4.15 Variations in Transparency of Fog with Time

was relatively weak but increased rapidly with increasing radius. Curve 5 in Fig.I.4.14 represents results of the computation of transparency in a continuous water layer. The substantially lower values of transparency in the case of curves 1 - 4 as compared with curve 5 are due to the increase in the length of the path of light in the droplet layer due to multiple scattering.

The spectral transparency at $0.3 \leq \lambda \leq 13\mu$ was measured in a natural fog (Bibl.64). An example of the transparency distribution over the spectrum in a stable fog with a mean droplet radius of 3μ is shown in Fig.I.4.15 (each curve corresponds to a separate measurement). The transparency is nonselective up to values of the order of 3μ. /57

In natural fog, measurements were also made of the scattering indicatrix in the visible spectrum region (Bibl.65). The data of these measurements, which correspond to various values of the meteorological visibility range, are presented in Figs.I.4.16 and I.4.17. According to these graphs, the ratio $\delta = \frac{\gamma_\varphi = 20^\circ}{\gamma_\varphi = 120^\circ}$ decreases with decreasing visibility (for v = 38 m, δ = 80 and for v = 100 m, δ = 120), which may indicate a reduction in particle size. The author (Bibl.65), however, sees here the manifestation of multiple scattering. In such a case, the curves plotted in Figs.I.4.16 and I.4.17 cannot be considered

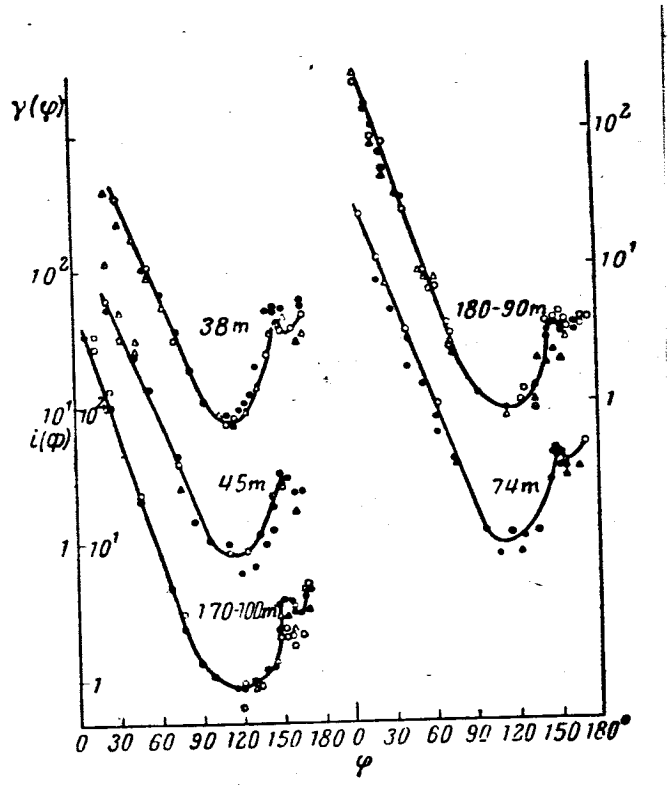

Fig.I.4.16 Scattering Indicatrix in Fog

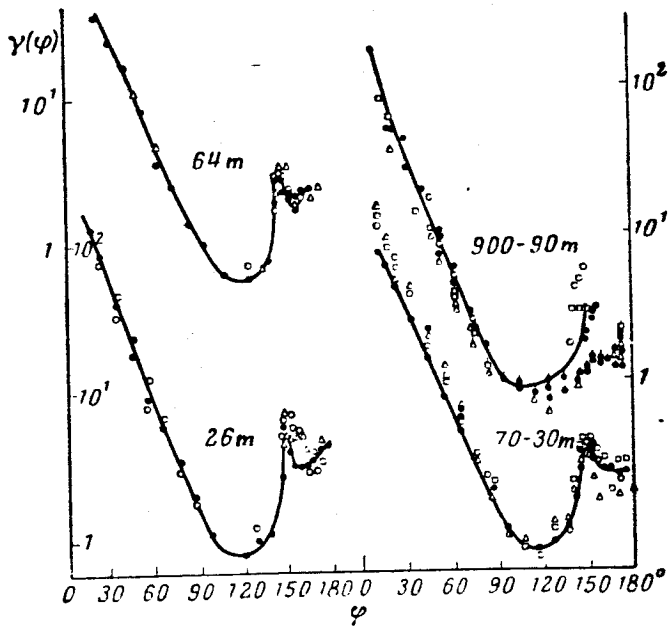

Fig.I.4.17 Scattering Indicatrix in Fog

as true scattering indicatrices.

The fact that the scattering indicatrix is independent of the wavelength within the visible spectrum region, as clearly shown in Figs.I.4.16 and I.4.17 (the circles and triangles indicate experimental data for various wavelengths), is of great interest.

A comparison of three indicatrices is made in Table I.4.26. Here a gives the indicatrix shown in Fig.I.4.16 for v = 170 - 100 m (according to Tables I.4.23 and I.4.24 a meteorological visibility of the order of 100 - 200 m occurs most frequently in St, Sc, Ns-As clouds); b gives the indicatrix calculated by Deirmendjian (see Table I.4.18 for $\lambda = 0.7\mu$); and c gives the indicatrix corresponding to the rigorous calculation with the Mie theory for n = 1.33, $\rho = 30$ [see (Bibl.37)]. The Table indicates that all three indicatrices agree well

TABLE I.4.26

	a	b	c		a	b	c
$\frac{\gamma(0)}{\gamma(\pi)}$	—	2700	2300	$\frac{\gamma(100)}{\gamma(180)}$	—	0.05	0.035
$\frac{\gamma(10)}{\gamma(100)}$	400	300	400	$\frac{\gamma(100)}{\gamma(140)}$	0.7	0.11	0.16

so that each one can be considered a representative (of course, only in general terms) indicatrix for stratus clouds in the visible region of the spectrum.

The data discussed above makes it possible to judge their suitability for computations of the spectral optical conditions of clouds. A summary of the basic information for three regions of the spectrum is given below.

1. Range of visible radiation. There are sufficient data (Bibl.37 - 40) in existence for computing the scattering indicatrix of a polydisperse cloud, similar to that given in Table I.4.18. In accordance with the comparison presented above, the scattering indicatrix calculated on the basis of the Mie theory for $\rho = 30$ (Bibl.37, 40) can also be used. Table I.4.27 gives the coefficient of expansion of this indicatrix in a series of Legendre polynomials (Bibl.40).

It must, however, be pointed out that computation with an indicatrix of an individual particle (see Chapter II, Sect.6) will yield a brightness of reflected light with several unreal maxima and minima, due to the diffraction character of the indicatrix.

The scattering coefficient is determined by means of the formula

$$\tilde{\sigma}_v = 2\pi \int_0^\infty a^2 N(a)\, da. \qquad (I.4.32)$$

If N(a) is prescribed according to Khrgian-Mazin [eq.(I.1.1)] for $a_{av} = 5\mu$ and $\rho = 0.2 \times 10^{-6}$ gm/cm^3 (see Table I.1.15), we will obtain /58

$$\tilde{\sigma}_v = 36\ km^{-1}.$$

According to the experimental data in Table I.4.22, $\tilde{\sigma}_v$ which varies in the range of 25 - 40 km^{-1}, corresponds to clouds of the stratus type in the long-wave region of the spectrum. The frequency of the meteorological visibility

TABLE I.4.27

k	C_k	k	C_k	k	C_k	k	C_k
0	1.0000	21	8.5914	41	11.6481	61	0.2343
1	2.4808	22	8.8260	42	11.6803	62	0.1371
2	3.7005	23	8.9365	43	11.6180	63	0.0390
3	4.1818	24	9.1373	44	11.3395	64	—0.0380
4	4.6059	25	8.3198	45	11.0574	65	—0.0446
5	5.0221	26	9.4504	46	10.3846	66	0.0170
6	5.3963	27	9.6893	47	9.6262	67	0.0030
7	5.8988	28	9.7740	48	8.4612	68	0.0030
8	6.3979	29	10.0078	49	7.3262	69	—0.0055
9	6.7932	30	10.1152	50	5.9052	70	0.0018
10	7.2377	31	10.2799	51	4.5614	71	0.0004
11	7.4772	32	10.4256	52	3.4454	72	0.0000
12	7.7512	33	10.5526	53	2.6292	73	0.0000
13	7.8539	34	10.6629	54	2.4340	74	0.0000
14	7.9614	35	10.8522	55	2.7312	75	0.0000
15	8.0729	36	10.9022	56	2.7320		
16	8.0888	37	11.1601	57	2.7224		
17	8.1954	38	11.2681	58	2.1933		
18	8.2869	39	11.4457	59	1.4118		
19	8.3388	40	11.6264	60	1.0595		
20	8.5358						

range presented in Tables I.4.23 and I.4.24 makes it possible to obtain, on the basis of eq.(I.4.28), values of $\tilde{\sigma}_v$ which vary within the limits of

$$20 \leqslant \sigma_v \leqslant 39\ km^{-1}.$$

Finally, for $\rho_v = 0.2$ gm/m^3 we have $\tilde{\sigma}_v = 30$ km^{-1} according to data in Table I.4.16 and $\tilde{\sigma}_v = 16$ km^{-1} according to data in Table I.4.17. All these

values agree fairly well and determine the range of variations in the values of $\tilde{\sigma}_v$ (15 - 40 km^{-1}). Apparently, $\tilde{\sigma}_v$ = 30 km^{-1} can be taken as a rough average. It should be mentioned that, according to Table I.4.22, the scattering coefficient of Sc clouds differs substantially from the case of St and As clouds. This difference is apparently quite real since it is manifested in the greater reflectivity of Sc clouds (see Chapter II, Sect.1). The data of Table I.1.15 and some other material presented in Section 1 of this Chapter make it possible to explain the high scattering coefficient of Sc clouds by the particle-distribution spectrum elongated to the right and also by the larger mean radius and the liquid-water content of Sc clouds as compared with St clouds.

TABLE I.4.28

k	C_k	k	C_k	k	C_k	k	C_k	k	C_k
0	1.0000	11	5.1361	21	6.9805	31	7.9652	41	0.4457
1	2.3074	12	5.3283	22	7.1620	32	7.2868	42	0.5470
2	3.4942	13	5.2985	23	7.4153	33	6.6917	43	0.1645
3	3.8380	14	5.5323	24	7.5386	34	5.4769	44	0.7538
4	4.4437	15	5.6562	25	7.8988	35	4.1629	45	−0.0310
5	4.6789	16	5.8217	26	7.8994	36	3.0580	46	0.0034
6	4.9652	17	6.1148	27	8.3109	37	2.1214	47	0.0013
7	5.0129	18	6.2260	28	8.2279	38	1.6349	48	0.0005
8	5.2174	19	6.5630	29	8.3934	39	1.4217	49	0.0000
9	5.0559	20	6.7061	30	8.1502	40	1.0143	50	0.0000
10	5.2371								

2. Near-infrared region of the spectrum. In this region, the scattering coefficient maintains the same value as in the visible region. The scattering indicatrix corresponds to $15 \leq \rho \leq 30$ for $a_{av} = 5\mu$. Keeping in mind some /59
shortening of the indicatrix of a real cloud due to the presence of fine droplets, the indicatrix for $\rho = 20$ can be used in the computation. The coefficients of its expansion in a series of Legendre polynomials (Bibl.40) are presented in Table I.4.28.

The absorption coefficients of droplet water together with the absorption coefficient of water vapor are presented in Table I.4.21.

3. Region of thermal radiation ($\lambda > 2.2\mu$). In this region, the computation for a monodisperse cloud for $a_{av} = 6.26\mu$ can be performed by means of K.S.Shifrin's data presented in Tables I.4.6, I.4.10, and I.4.11. On the basis of Tables I.4.8 and I.4.9, it is also possible to compute the absorption coefficient of a polydisperse cloud.

The scattering indicatrix for $\lambda > 2.2\mu$ is determined by the variation range in the parameter ρ.

$$1 \leqslant \rho \leqslant 15.$$

The method of determining the long-wave radiation fluxes, outlined in Chapter IV, does not require assignment of an indicatrix. Here, it is only necessary to know the coefficients for the first term of its expansion in a Legendre polynomial series.

According to Tables I.4.13 and I.4.14, the coefficient C_1 changes within the limits 0.5 - 2.5 for the above indicated changes in ρ.

For pp.59 - 65 of original see translation FTD-MT-65-48 of Air-Force System Command

BIBLIOGRAPHY /66

1. Borovikov, A.M., Gayvoronskiy, I.I., Zak, Ye.G., Kostarev, V.V., Mazin, I.P., Minervin, V.Ye., Khrgian, A.Kh., and Shmeter, S.M.: Physics of Clouds (Fizika oblakov). Gidrometeoizdat, 1961.
2. Meyson, B.Dzh.: Physics of Clouds (Fizika oblakov). Gidrometeoizdat, 1960.
3. Khrgian, A.Kh.: Physics of the Atmosphere (Fizika atmosfery). Fizmatgiz, 1958.
4. - Compendium "Investigation of Clouds, Precipitation, and Lightning Electricity" (Sb. "Issledovaniya oblakov, osadkov i grozovogo elektrichestva"). Izd. Akad. Nauk SSSR, 1961.
5. Murgatroyd, G. and Goldsmith, P.: High Clouds over Southern England. Prof. Notes of Met. Off., Vol.7, No.119, 1956.
6. Matveyev, L.T. and Kozharin, V.S.: The Role of Turbulent Mixing in the Structure Formation of Stratus Clouds (Rol' turbulentnogo peremeshivaniya v formirovanii struktury sloistoobraznykh oblakov). Izv. Akad. Nauk SSSR, ser. geofiz., No.11, 1956.
7. Zabrodskiy, G.M.: Results of Experimental Investigation of the Optical Density of Clouds (Rezul'taty eksperimental'nykh issledovaniy opticheskoy plotnosti oblakov). Transactions of the All-Union Scientific Meteorological Conference, No.6, Gidrometeoizdat, 1963.
8. Minervin, V.Ye.: Seasonal Changes in the Water Content of Clouds (Sezonnyye izmeneniya vodnosti oblakov). Transactions Central Aerological Observatory, No.36, 1961.
9. Voskresenskiy, A.I. and Dergach, A.L.: Microphysical Characteristics of St and Sc Clouds in the Arctic during the Warm Period of the Year. Investigations of Clouds, Precipitation, and Lightning Electricity (Mikrofizicheskiye kharakteristiki oblakov tipa St i Sc v Arktike v teplyy period goda. Issledovaniya oblakov, osadkov i grozovogo elektrichestva). Proceedings of the VIth Inter-Agency Conference Ac. of Sci. USSR Press, 1961.
10. Dergach, A.L., Zabrodskiy, G.M., and Morachevskiy, V.G.: Experience in the Complex Investigation of St-Sc Clouds and of Fogs in the Arctic (Opyt kompleksnogo issledovaniya oblakov St-Sc i tumanov v Arktike). Izv. Akad. Nauk SSSR, ser. geofiz., No.1, 1960.
11. Bullrich, K.: Light Transmissivity of Clouds (Lichtdurchlässigkeit in Wolken). Zs. Met., Vol.2, 1948.
12. Keily, D.P. and Millen, S.C.: An Airborne Cloud-Drop-Size Distribution Meter. J. Met., Vol.17, No.3, 1960.
13. Eldridge, R.G.: Measurement of Cloud-Drop-Size Distributions. J. Met., Vol.14, No.1, 1957.
14. McDonald, J.: Comments on "An Airborne Cloud-Drop-Size Distribution Meter". J. Met., Vol.18, No.3, 1961.
15. Warner, J.: Comments on "An Airborne Cloud-Drop-Size Distribution Meter". J. Met., Vol.18, No.6, 1961.
16. Pendorp, R.: Comments on "Measurements of Cloud-Drop-Size Distributions". J. Met., Vol.14, No.6, p.573, 1957.
17. Khvostikov, I.A.: Some Questions of Optics of Fogs (Nekotoryye voprosy

optiki tumanov). Izv. Akad. Nauk SSSR, ser. geograf. i geofiz., No.3, 1942.
18. Feygel'son, Ye.M: Radiative Properties of St Clouds (Radiatsionnyye svoystva oblakov St). Izv. Akad. Nauk SSSR, ser. geofiz., No.4, 1951.
19. Levin, L.M.: On the Distribution Functions of Cloud Droplets (O funktsiyakh raspredeleniya oblachnykh kapel'). Izv. Akad. Nauk SSSR, ser. geofiz., No.10, 1958.
20. Chandrasekar, S.: Transfer of Radiant Energy (Perenos luchistoy energii). I.L., 1953.
21. Sobolev, V.V.: Transfer of Radiant Energy in the Atmospheres of Stars and Planets (Perenos luchistoy energii v atmosferakh zvezd i planet). Gostekhizdat, 1956.
22. Pagurova, V.I.: Tables of Integral-Exponential Functions. Mathematical Table of the Computer Center (Tablitsy integro-eksponentsial'noy funktsii. Matematicheskiye tablitsy vychislitel'nogo tsentra). Izd. Akad. Nauk SSSR, 1959.
23. Kuznetsov, Ye.S. and Ovchinskiy, B.V.: Results of Numerical Solution of the Integral Equation of the Theory of Scattering of Light in the Atmosphere (Rezul'taty chislennogo resheniya integral'nogo uravneniya teorii rasseyaniya sveta v atmosfere). Trudy Geofiz. Inst., No.4, 1949.
24. Kastrov, V.G.: Measurement of Absorption of Solar Radiation in the Free Atmosphere up to 3 - 5 km (Izmereniye pogloshcheniya solnechnoy radiatsii v svobodnoy atmosfere do 3-5 km). Trudy TsAO, No.8, 1952.
25. Kondrat'yev, K.Ya.: Radiant Heat Exchange in the Atmosphere (Luchistyy teploobmen v atmosfere). Gidrometeoizdat, 1956.
26. Kuhn, P.M., Suomi, V.E., and Darkow, G.Z.: Soundings of Terrestrial Radiation Flux over Wisconsin. Monthly Weather Rev., Vol.87, No.5, 1959.
27. Brewer, A.B. and Houghton, J.T.: Some Measurements of the Flux of Infrared Radiation in the Atmosphere. Proc. Roy. Soc., Vol. A236, No.1205, 1956.
28. Kuznetsov, Ye.S.: On Evaluating the Radiant Exchange in Deriving Conditions for Heat Fluxes at the Interface of Two Media (Ob uchete luchistogo obmena pri vyvode usloviy dlya teplovykh potokov na poverkhnosti razdela dvukh sred). Izv. Akad. Nauk SSSR, ser. geograf. i geofiz., No.5, 1942.
29. Shifrin, K.S.: Scattering of Light in a Turbid Medium (Rasseyaniye sveta v mutnoy srede). Gostekhizdat, 1951.
30. Hulst, Van de: Scattering of Light by Small Particles (Rasseyaniye sveta malymi chastitsami). I.L., 1961.
31. Stephens, J.J.: Spectrally Averaged Total Attenuation, Scattering and Absorption Cross-Sections for Infrared Radiation. J. Met., Vol.18, No.6, 1961.
32. Johnson, J.O. and Terrel, J.R.: Transmission Cross-Sections for Water Spheres Illuminated by Infrared Radiation. J. Opt. Soc. Amer., Vol.45, 1955.
33. Plyler, E.K. and Acquista, N.: Infrared Absorption of Liquid Water from 2 to 42 Microns. J. Opt. Soc. Amer., Vol.44, 1954.
34. Cartwright, C.H.: Extreme Infrared Investigations of Hindered Rotation in Water. Nature, No.135, 1935.
35. Stephens, J.J. and Gerhardt, J.R.: Absorption Cross-Sections of Water Drops for Infrared Radiation. J. Met., Vol.18, No.6, 1961. /67
36. Penndorf, R.: New Tables of Total Mie Scattering Coefficients for Spherical Particles of Real Refractive Indexes. J. Opt. Soc. Amer., Vol.47, No.11, 1957.

37. Walter, H.: Scattered Light Intensity of Large Spherical Particles, Part II (Streulichtintensität grosser sphärischer Partikel, II). Optik, Vol.16, No.7, 1959.
38. Pfleiderer, J.: Scattered Light Intensity of Large Spherical Particles, Part III (Streulichtintensität grosser sphärischer Partikel, III). Optik, Vol.16, No.7, 1959.
39. Giese, R.: Examples of Calculated Scattering Functions of Relatively Large Spherical Particles (Beispiele berechneter Streufunktionen von grösseren kugelförmigen Teilchen). Met. Rundschau, No.2, 1961.
40. Chu, C.M., Clark, G.C., and Churchill, S.W.: Tables of Angular Distribution Coefficients for Light Scattering by Spheres. Engineering Research Inst. Univ. of Michigan, 1957.
41. Shifrin, K.S.: Principal Results of Investigations of Light Scattering on Individual Particles (Osnovnyye rezul'taty issledovaniya rasseyaniya sveta na otdel'nykh chastitsakh). Trans. of the All-Union Scientific Meteorological Conference, Gidrometeoizdat, No.6, 1963.
42. Shifrin, K.S.: Transfer of Thermal Radiation in Clouds (Perenos teplovoy radiatsii v oblakakh). Trans. Main Geophysical Observatory, No.46, 1955.
43. Shifrin, K.S.: Computation of Radiative Characteristics of Clouds (Raschety radiatsionnykh kharakteristik oblakov). Trans. of the Main Geophysical Observatory, No.109, 1961.
44. McDonald, J.: Absorption of Atmospheric Radiation by Water Films and Water Clouds. J. Met., Vol.17, No.2, 1960.
45. Deirmendjian, D.: Atmospheric Extinction of Infrared Radiation. Quart. J. Roy. Met. Soc., Vol.86, No.369, 1960.
46. Shifrin, K.S.: On the Computation of the Radiative Property of Clouds (O vychislenii radiatsionnykh svoystv oblakov). Trudy GGO (Main Geophysical Observatory), No.46, 1955.
47. Feygel'son, Ye.M.: Determination of Liquid-Water Content and Moisture of Clouds from the Absorption of Radiant Energy (Opredeleniye vodnosti i vlazhnosti oblakov po pogloshcheniyu luchistoy energii). Trudy Geofiz. Inst., ser. geofiz., No.23, 1954; No.4, 1951.
48. Blumer, H.: Zs. Phys., Vol.32, p.119, 1925; Vol.38, pp.302, 902, 1926; Vol.39, p.195, 1926.
49. Winer, C.: The Brightness of the Cloudless Sky and Illumination by Sun, Sky, and Reflection (Die Helligkeit des klaren Himmels und die Beleuchtung durch Sonne, Himmel und Rückstrahlung). Abh. Kaiser Leop.-Carol. Deutsch. Akad. Naturforsch., No.73, 1907.
50. Feygel'son, Ye.M., Malkevich, M.S., Kogan, S.Ya., Koronatova, T.D., Glazova, K.S., and Kuznetsova, M.A.: Computation of Brightness of Light in the Atmosphere for Anisotropic Scattering, Part I (Raschet yarkosti sveta v atmosfere pri anizotropnom rasseyanii, Ch.I). Trudy Inst. Fiz. Atmosf., No.1, 1958.
51. Neiburger, M.: Reflection, Absorption, and Transmission of Insolation by Stratus Clouds. J. Met., Vol.6, No.2, 1949.
52. Deirmendjian, D.: The Scattering Coefficient and Scattering Function of Real Clouds. Doctor Thesis Read before the Symposium on Radiation, Vienna, 1961.
53. Novosel'tsev, Ye.P.: On the Water Content of Clouds of the Upper Layer (O vodnosti oblakov verkhnego yarusa). Meteorol. i gidrol., No.8, 1962; Gidrometeoizdat, No.6, 1963.

54. Aschkinass: Ann. d. Phys., Vol.55, 1895.
55. Kampe, Aufm.: Visibility and Liquid Water Contents in Clouds in the Free Atmosphere. J. Met., Vol.7, No.1, 1950.
56. Zabrodskiy, G.M. and Morachevskiy, V.G.: Investigation of Transparency of Clouds and Fogs (Issledovaniye prozrachnosti oblakov i tumanov). Trudy Arkt. i Antarkt. Nauk Inst., Vol.1, No.228, 1959.
57. Zabrodskiy, G.M.: On the Temperature Field and the Transparency of Clouds of the Lower and Middle Layers (O temperaturnom pole i prozrachnosti oblakov nizhnego i srednego yarusov). Trudy Arkt. i Antarkt. Nauk Inst., No.239, 1962.
58. Bocharov, Ye.I.: Spectral Transparency of Clouds (Spektral'naya prozrachnost' oblakov). Izv. Akad. Nauk SSSR, ser. geofiz., No.5, 1958.
59. Bocharov, Ye.I.: Attenuation of the Infrared Radiation by Water Fogs (Oslableniye infrakrasnoy radiatsii vodnymi tumanami). Izv. Akad. Nauk SSSR, ser. geofiz., No.6, 1958.
60. Rozenberg, G.V.: Absorption Spectroscopy of Disperse Media (Absorptsionnaya spektroskopiya dispergirovannykh sred). Uspekh.fiz. nauk, Vol.69, No.1, p.57, 1959.
61. Malyshev, V.A.: Investigation of the Transmission Spectrum of Fog in the Infrared Spectrum Region (Issledovaniye spektra propuskaniya tumana v infrakrasnoy oblasti spektra). Trans. of the Tenth Conference on Spectroscopy, p.121; Izd. L'vov. Inst., 1956.
62. Driving, A.Ya., Mironov, A.V., Morozov, V.M., and Khvostikov, I.A.: Study of Optical and Physical Properties of Natural Fogs (Izucheniye opticheskikh i fizicheskikh svoystv estestvennykh tumanov). Izv. Akad. Nauk SSSR, ser. geograf. i geofiz., No.2, 1943.
63. Saito, T.: Measurement of Transmissivity of Infrared Radiation through Fog. Science Reports of Tohoku Univ. Geophysics, Vol.8, No.1, 1956.
64. Arnulf, A., Bricard, J., Curé, E., and Veret, C.: Research on the Transmission of Light by Mist and Fog (Recherches sur la transmission de la lumière par la brume et par le brouillard). Revue d'Optique, Vol.38, No.1, 1959.
65. Bullrich, K.: Scattered Light Measurements in Mist and Fog (Streulichtmessungen in Dunst und Nebel). Met. Rundschau, Vol.13, No.1, 1960.
66. Pyaskovskaya-Fesenkova,Ye.: Investigations of Scattered Light in the Earth Atmosphere (Issledovaniye rasseyaniya sveta v zemnoy atmosfere). Izd. Akad. Nauk SSSR, 1957. /68
67. Georgiyevskiy, Yu.S., Driving, A.Ya., Zolotavina, N.V., Rozenberg, G.V., Feygel'son, Ye.M., and Khazanov, V.S.: A Searchlight Beam in the Atmosphere (Prozhektornyy luch v atmosfere). Izd. Akad. Nauk SSSR, 1960.
68. Belov, F.F.: Results of the Study of Scattering of Light in the Free Atmosphere (Rezul'taty izucheniya rasseyaniya sveta v svobodnoy atmosfere). Trans. All-Union Scientific Meteorological Conference, Gidrometeoizdat, No.6, 1963.
69. Atroshenko, V.S., Glazova, K.S., Malkevich, M.S., and Feygel'son, Ye.M.: Computation of Brightness of Light in the Atmosphere for Anisotropic Scattering (Raschet yarkosti sveta v atmosfere pri anizotropnom rasseyanii, Ch.II). Trudy Inst. Fiz. Atmosf., No.3, 1962.
70. Feygel'son, Ye.M.: Absorption of Solar Energy in the Atmosphere in the Presence of Clouds (Pogloshcheniye solnechnoy energii v atmosfere pri nalichii oblakov). Trudy Geofiz. Inst., No.23, 1954.

71. Feygel'son, Ye.M.: On the Absorption Properties of Water Vapor and Carbon Dioxide in the Atmosphere (O pogloshchatel'nykh svoystvakh vodyanogo para i uglekislogo gaza v atmosfere). Izv. Akad. Nauk SSSR, ser. geofiz., No.1, 1955
72. Roach, W.T. and Goody, R.M.: Absorption and Emission in the Atmospheric Window from 770 to 1.25 cm^{-1}. Quart. J. Roy. Met. Soc., Vol.84, No.362, 1958.
73. Saedy, F. and Goody, R.M.: The Solar Emission Intensity at 11μ. Monthly Notices of the Roy. Astronomical Soc., Vol.119, No.3, 1959.
74. Kuznetsov, Ye.S.: Computation of the Absorption Coefficient of Water Vapor with Deviations from Bouguer's Law (Vychisleniye koeffitsientov pogloshcheniya vodyanogo para pri otkloneniyakh ot zakona Buge). Trudy Geofiz. Inst., No.23, 1954.
75. Niylisk, Kh.Yu.: On the Question of Computation of Thermal Radiation of the Atmosphere (K voprosu o raschetakh teplovogo izlucheniya atmosfery). Investigations on the Physics of the Atmosphere, Part II, Institute of Physics and Astronomy Estonian SSR, Tartu, 1960.
76. Feygel'son, Ye.M.: Accounting for Selective Absorption in the Theory of Radiant Heat Exchange in the Atmosphere (Uchet izbiratel'nogo pogloshcheniya v teorii luchistogo teploobmena v atmosfere). Izv. Akad. Nauk SSSR, ser. geofiz., No.53, 1955.
77. Howard, J.H., Burch, D.E., and Williams, D.: Near-Infrared Transmission in Synthetic Atmospheres. Geophys. Res. Papers, No.40, 1955.
78. - Handbook of Geophysics, No.1, 1960.
79. Plass, G.N.: The Influence of the 15μ Carbon-Dioxide Band on the Atmospheric Infrared Cooling Rate. Quart. J. Roy. Met. Soc., Vol.82, No.353, 1956.
80. Walshaw, C.D.: Infrared Absorption by the 9.6μ Band Ozone. Quart. J. Roy. Met. Soc., Vol.83, No.357, 1957.
81. Burch, D.E. and Shaw, J.H.: Infrared Emission Spectra of the Atmosphere between 14.5μ and 22.5μ. J. Opt. Soc. Amer., Vol.47, No.3, 1957.
82. Yamamoto, G. and Onishi, G.: Absorption Coefficient of Water Vapor in the Far-Infrared Region. Sci. Rep. Tohoku Univ., Ser.5, No.1, 1949.
83. Dmitriyev, A.A.: On the Rate of Heating of the Atmosphere by Solar Radiation (O skorosti progrevaniya atmosfery solnechnoy radiatsiyey). Trudy Morskogo Gidrofiz. Inst., No.3, 1953.
84. Giese, R.: Scattering of Electromagnetic Waves on Absorbing and Dielectric Spherical Individual Particles and on Mixtures of such Particles (Streuung elektromagnetischer Wellen an absorbierenden und dielektrischen kugelförmigen Einzelteilchen und an Gemischen solcher Teilchen). Zs. Astrophys., Vol.51, No.2, 1961.

For pp.69 - 120 of original, see translation

FTD-MT-65-48 of Air-Force System Command

CHAPTER III

/121

ABSORPTION OF SOLAR RADIATION IN CLOUDS

Section 1. Basic Relations

In clouds, absorption of solar radiation takes place in the near-infrared region of the spectrum ($0.7 \leq \lambda \leq 2.5\mu$). The intensity of radiation in this region is described by an equation of the form (see Chapter I, Sect.3):

$$\cos\theta \frac{\partial I}{\partial \tau} = \frac{\varphi(\tau)}{4\pi}\int I(\tau, r')\gamma_v(r, r')\,d\omega' - I(\tau, r), \tag{III.1.1}$$

where

$$\varphi(\tau) = \frac{\tilde{\sigma}_v}{\tilde{\alpha}_v + \tilde{\alpha}_w + \tilde{\sigma}_u}, \tag{III.1.2}$$

$$\tau = \int_0^z (\tilde{\alpha}_v + \tilde{\alpha}_w + \tilde{\sigma}_v)\,dz. \tag{III.1.3}$$

If $I(\tau, r)$ is determined, the fluxes of infrared radiation $F_i(\tau)$ ($i = 1, 2$) and the amount of solar energy $Q(\tau)$ absorbed per unit volume of the cloud can be computed.

In Chapter I, Sect.2 expressions were given for these quantities:

$$F_1(\tau) = \int_0^{2\pi}\int_0^{\pi/2} I_1(\tau, r)\cos\theta\sin\theta\,d\theta\,d\psi, \tag{III.1.4}$$

$$F_2(\tau) = \int_0^{2\pi}\int_0^{\pi/2} I_2(\tau, r)\cos\theta\sin\theta\,d\theta\,d\psi, \tag{III.1.5}$$

$$Q(\tau) = \int_{\lambda_0}^{\lambda_1} [\tilde{\alpha}^{\circ}_{v,\lambda} + \tilde{\alpha}_{w,\lambda}]\int I_\lambda(\tau, r)\,d\omega d\lambda; \tag{III.1.6}$$

where $\lambda_0 \approx 0.75\mu$, $\lambda_1 \approx 2.5\mu$.

Below we give the solution of eq.(III.1.1) for the condition

$$\varphi(\tau) = k = \text{const}, \tag{III.1.7}$$

which assumes the presence of a relationship between the densities of water and of water vapor of the form

$$\rho_w(z) = c\rho_v(z). \tag{III.1.8}$$

For such a condition, the problem discussed in this Chapter formally in no way differs from the case of pure scattering investigated in Chapter II. Never-

theless, it is difficult to make full use here of the method of solution used in Chapter II in view of the fact that, in the presence of absorption, the condition of conservation of energy assumes the form /122

$$F_1(0) + F_2(\tau_0) = F_1(\tau_0) + F_2(0) + \int_0^{\tau} Q(\tau)\, d\tau, \qquad \text{(III.1.9)}$$

where $F_1(0)$ and $F_2(0)$ are the radiation fluxes arriving at the boundary of the cloud; $F_1(\tau_0)$ and $F_2(\tau_0)$ denote the fluxes leaving the cloud; $\int_0^{\tau_0} Q(\tau)d\tau$ is the total amount of energy absorbed in the cloud.

The relation (III.1.9) considered as the equation for determining the average cosine $\bar{\mu}$ (see Chapter II, Sect.4) is too complicated; therefore, another method of determining the zero approximation of the problem was selected in this Chapter.

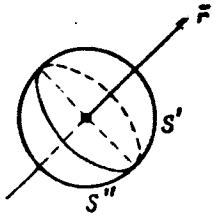

Fig.III.1.1 Hemispheres S' and S''

The basic principle of solution remains as before, meaning that the solution proceeds by the method of successive approximation. By the special selection of the zero approximation method which accounts for the major features of the examined physical process, it is possible to limit the calculation to a small number of approximations.

Let the direction of propagation of radiation r be given. We will then present the spherical integral in eq.(III.1.1) in the form

$$\frac{1}{4\pi}\int I(\tau, r')\,\gamma\left(r', r\right) d\omega' = \frac{1}{4\pi}\int_{S'} I(\tau, r')\,\gamma\left(r', r\right) d\omega' + \frac{1}{4\pi}\int_{S''} I(\tau, r')\,\gamma(r', r)\, d\omega', \qquad \text{(III.1.10)}$$

where S' denotes the front hemisphere and S'' is the back hemisphere with respect to the ray r (Fig.III.1.1). We will subject the elongated scattering indicatrix in the cloud to the following condition:

$$\gamma(r, r') = 4\pi\beta\delta(r - r'), \quad \text{if} \quad \angle(r, r') \leqslant \frac{\pi}{2}. \qquad \text{(III.1.11)}$$

No special conditions are imposed when $\angle(r, r') \geq \frac{\pi}{2}$ but from eq.(III.1.1) it follows that

$$\int_{S''} \gamma(r, r')\, d\omega' = 4\pi(1-\beta). \qquad \text{(III.1.12)}$$

The condition (III.1.11) means that, as a result of the elongation of the radiation indicatrix, the radiation scattered into the front hemisphere is almost all scattered forward.

The relation (III.1.10) can now be presented in the form of /123

$$\frac{1}{4\pi}\int I(\tau, r')\gamma(r, r')\, d\omega' = \beta I(\tau, r) + \frac{1}{4\pi}\int_{S''} I(\tau, r')\gamma(r, r')\, d\omega'. \qquad \text{(III.1.13)}$$

In the investigated case, a small proportion of the energy ($\beta \gg 1-\beta$) is scattered backward; according to Section 4 in Chapter I, it is possible, for instance, to assume $\beta = 0.9$; therefore, in the zero approximation, we will assume that

$$I(\tau, r') = I(\tau, -r) \quad \text{for} \quad \angle(r, r') \geqslant \frac{\pi}{2}.$$

This condition means that, within the limits of the back hemisphere S'', the intensity is isotropic and is equal to the intensity in the direction $-r$ (i.e., in a direction opposite to the direction r).

With the above assumptions, eq.(III.1.1) becomes

$$\cos\theta \frac{\partial I(\tau, r)}{\partial \tau} = -(1-k\beta) I(\tau, r) + k(1-\beta) I(\tau, -r). \qquad \text{(III.1.14)}$$

By separating the intensity of the ascending radiation ($\theta \leq \frac{\pi}{2}$; $0 \leq \varphi \leq 2\pi$) from the descending radiation ($\frac{\pi}{2} \leq \theta \leq \pi$; $0 \leq \varphi \leq 2\pi$) we obtain

$$\cos\theta \frac{\partial I_1(\tau, r)}{\partial \tau} = -(1-k\beta) I_1 + k(1-\beta) I_2. \qquad \text{(III.1.15)}$$

$$-\cos\theta \frac{\partial I_2(\tau, r)}{\partial \tau} = -(1-k\beta) I_2 + k(1-\beta) I_1. \qquad \text{(III.1.16)}$$

It is not difficult to obtain solutions of eqs.(III.1.15) - (III.1.16) in the form of

$$I_1(\tau, r) = c_1 \frac{1-k-g}{1-k} e^{-g\sec\theta(\tau_0-\tau)} + c_2 \frac{1-k+g}{1-k} e^{-g\sec\theta\tau}, \qquad \text{(III.1.17)}$$

$$I_2(\tau, r) = -c_1 \frac{g+1-k}{1-k} e^{-g\sec\theta(\tau_0-\tau)} + c_2 \frac{g-1+k}{1-k} e^{-g\sec\theta\tau}, \qquad \text{(III.1.18)}$$

where

$$g = \sqrt{(1-k)(1+k-2k\beta)}. \qquad \text{(III.1.19)}$$

The constants c_1 and c_2 are determined from the boundary conditions. At the cloud boundary, scattered solar radiation arrives from without, while direct solar radiation of an intensity of

$$I_s = \pi S e^{-\tau_2 \sec\theta}\,\delta(r - r_0). \qquad \text{(III.1.20)}$$

strikes the upper boundary.

Here, τ_2 is the optical thickness of the layer above the clouds.

Observations made at Leningrad University (Bibl.1) and various computations (Bibl.2, 3) show that, at $\zeta < 75^\circ$ the scattered radiation fluxes in the lower layers of the atmosphere are small compared with the direct radiation flux. Therefore, at $\zeta < 75^\circ$ the scattered radiation fluxes can be neglected in the boundary conditions, keeping in mind the unavoidable error in our problem due to the approximately given absorption spectrum and to the approximate method of solution. However, it does not require a special effort to solve the problem even with consideration of scattered fluxes in the boundary conditions, if only single scattering is taken into account outside of the cloud. The necessary solutions are given elsewhere (Bibl.4).

Thus, let

$$I_1(0, r) = 0, \qquad \text{(III.1.21)}$$

$$I_2(\tau_0, r) = \pi S e^{-\sec\theta\tau_2}\,\delta(r - r_0). \qquad \text{(III.1.22)}$$

At sufficiently large τ_0, eqs.(III.1.17) and (III.1.18) will yield /124

$$c_1 = \pi S e^{-\sec\theta\tau_2}\delta(r - r_0)\,\frac{1-k}{k-1-g}\,\frac{1}{1-\varphi_1(\theta)}, \qquad \text{(III.1.23)}$$

$$c_2 = \pi S e^{-\sec\theta\tau_2}\delta(r - r_0)\,\frac{(1-k)(1-k-g)}{(1-k+g)^2}\,\frac{e^{-g\sec\theta\tau_0}}{1-\varphi_1(\theta)}, \qquad \text{(III.1.24)}$$

where

$$\varphi_1(\theta) = \left(\frac{1-k-g}{1-k+g}\right)^2 e^{-2g\sec\theta\tau_0}. \qquad \text{(III.1.25)}$$

Substituting the obtained values c_1 and c_2 in eqs.(III.1.17) and (III.1.18) we will find

$$I_1(\tau, r) = \frac{\pi S e^{-\sec\theta\tau_2}}{1-\varphi_1(\theta)}\,\delta(r - r_0)\,\frac{1-k-g}{k-1-g}\left[e^{-g\sec\theta(\tau_0-\tau)} - e^{-g\sec\theta(\tau_0+\tau)}\right]. \qquad \text{(III.1.26)}$$

$$I_2(\tau, r) = \frac{\pi S e^{-\sec\theta\tau_2}}{1-\varphi_1(\theta)}\,\delta(r - r_0)\left[e^{-g\sec\theta(\tau_0-\tau)} - \frac{1-k-g}{k-1-g}e^{-g\sec\theta(\tau_0-\tau)}\right]. \qquad \text{(III.1.27)}$$

The latter expressions are considered as the zero approximation to the solution of the problem.

Let us return now to the exact equation (III.1.1). By separating the intensity of ascending radiation I_1 from the descending radiation I_2, we obtain expressions for both quantities in integral form, taking conditions (III.1.21) and (III.1.22) into consideration,

$$I_1^{(0)}(\tau, r) = \sec\theta \int_0^{\tau} e^{-(\tau-t)\sec\theta} K_1(t, r)\, dt, \qquad \text{(III.1.28)}$$

$$I_2^{(0)}(\tau, r) = \pi S e^{-\tau_0\sec\theta}\,\delta(r - r_\odot)\, e^{-(\tau_0-\tau)\sec\theta} + \sec\theta \int_{\tau}^{\tau_0} e^{-(t-\tau)\sec\theta} K_2(\tau, r)\, dt, \qquad \text{(III.1.29)}$$

where $K_1(\tau, r)$ and $K_2(\tau, r)$ are determined from the relations (I.2.35) and (I.2.36).

After substituting into the right-hand sides of eqs.(III.1.28) and (III.1.29), the zero approximations of intensity (III.1.26) and (III.1.27), we find

$$I_1(\tau,r)=\frac{kS}{4}-\frac{e^{-\sec\zeta\tau_2}}{1-\varphi_1(\zeta)}\sec\theta\left\{\frac{1-k-r}{k-1-r}\gamma_{1,1}(r, r_\odot)\left[\frac{e^{-g\sec\zeta(\tau_0-\tau)}-e^{-\sec\theta\tau}e^{-g\sec\zeta\tau_0}}{\sec\theta+g\sec\zeta}-\right.\right.$$
$$-\frac{e^{-g\sec\zeta(\tau_0+\tau)}-e^{-\sec\theta\tau}e^{-g\sec\zeta\tau_0}}{\sec\theta-g\sec\zeta}\Big]+\gamma_{1,2}(r, r_\odot)\left[\frac{e^{-g\sec(\tau_0-\tau)}-e^{-\sec\theta\tau}e^{-g\sec\zeta\tau_0}}{\sec\theta+g\sec\zeta}-\right.$$
$$\left.\left.-\frac{e^{-g\sec\zeta(\tau_0+\tau)}-e^{-\sec\theta\tau}e^{-g\sec\zeta\tau_0}}{\sec\theta-g\sec\zeta}\left(\frac{1-k-g}{k-1-g}\right)^2\right\}, \qquad \text{(III.1.30)}$$

$$I_2(\tau, r)=\frac{kS}{4}\frac{e^{-\sec\zeta\tau_2}}{1-\varphi_1(\zeta)}\sec\theta\left\{\gamma_{2,1}(r, r_\odot)\frac{1-k-g}{k-1-g}\left[\frac{e^{-\sec\theta(\tau_0-\tau)}-e^{-g\sec\zeta(\tau_0-\tau)}}{g\sec\zeta-\sec\theta}-\right.\right.$$
$$-\frac{e^{-g\sec\zeta(\tau_0+\tau)}-e^{-\sec\theta(\tau_0-\tau)}e^{-2g\sec\zeta\tau_0}}{\sec\theta+g\sec\zeta}\Big]+$$
$$+\gamma_{2,2}(r, r_\odot)\left[\frac{e^{-\sec\theta(\tau_0-\tau)}-e^{-g\sec\zeta(\tau_0-\tau)}}{g\sec\zeta-\sec\theta}-\right.$$
$$\left.\left.-\left(\frac{1-k-g}{k-1-g}\right)^2\frac{e^{-g\sec\zeta(\tau_0+\tau)}-e^{-\sec\theta(\tau_0-\tau)}e^{-2g\sec\zeta\tau_0}}{\sec\theta+g\sec\zeta}\right]+\right.$$
$$\left.+\pi S e^{-\sec\theta\tau_2}\delta(r - r_\odot)\, e^{-\sec\theta(\tau_0-\tau)}\right\}. \qquad \text{(III.1.31)}$$

In accordance with eqs.(III.1.30) and (III.1.31), the expression for the intensity of radiation emerging from the boundaries of the cloud is presented in the following form: /125

$$I_1(\tau_0, r)=\frac{kS}{4}\frac{e^{-\sec\zeta\tau_2}}{1-\varphi_1(\zeta)}\sec\theta\left\{\frac{1-k-g}{k-1-g}\gamma_{1,1}(r, r_\odot)\times\right.$$
$$\times\left[\frac{1}{\sec\theta+g\sec\zeta}-\frac{e^{-2g\sec\zeta\tau_0}}{\sec\theta-g\sec\zeta}\right]+\gamma_{1,2}(r, r_\odot)\times$$
$$\left.\times\left[\frac{1}{\sec\theta+g\sec\zeta}-\left(\frac{1-k-g}{k-1-g}\right)^2\frac{e^{-2g\sec\zeta\tau_0}}{\sec\theta-g\sec\zeta}\right]\right\}, \qquad \text{(III.1.32)}$$

$$I_2(0, r)=\frac{kS}{4}\frac{e^{-\sec\zeta\tau_2}}{1-\varphi_1(\zeta)}\sec\theta\left[\frac{1}{\sec\theta-g\sec\zeta}-\right.$$
$$\left.-\frac{1}{\sec\theta+g\sec\zeta}\right]+\left[\frac{1-k-g}{k-1-g}\gamma_{2,1}(r, r_0)+\gamma_{1,1}(r, r_\odot)\right]e^{-g\sec\zeta\tau_0}. \qquad \text{(III.1.33)}$$

These relations and Table III.2.1 show that everywhere in the near-infrared region of the spectrum, except in the centers of the broad bands Ψ and Ω, the

clouds differ from semi-infinite.

TABLE III.2.1

$\Delta\lambda_i$, μ	$t = 0°$			$t = -15°$			
	k	g	τ_i	k	g	τ_i	πS_i
0.700—0.719	0.999684	0.0080	0.021	0.999901	0.0044	0.0057	
0.719—0.721	0.995649	0.030	0.029	0.998611	0.017	0.080	0.081
0.721—0.740	0.999674	0.0080	0.021	0.999886	0.0048	0.0057	
0.740—0.790	0.999976	0.0022	0	0.999976	0.0022	0	0.087
0.790—0.814	0.999645	0.0084	0.022	0.999868	0.0051	0.0060	
0.814—0.816	0.992209	0.040	0.053	0.997502	0.022	0.14	0.076
0.816—0.840	0.999644	0.0084	0.022	0.999867	0.0052	0.0060	
0.840—0.860	0.999962	0.0028	0	0.999961	0.0028	0	0.028
0.860—0.915	0.999314	0.012	0.042	0.999737	0.0072	0.011	
0.915—0.935	0.981380	0.063	1.27	0.993940	0.035	0.34	0.15
0.935—0.990	0.998990	0.014	0.042	0.999422	0.011	0.011	
0.990—1.030	0.999664	0.0082	0	0.999664	0.0082	0	0.038
1.030—1.112	0.999333	0.012	0.033	0.999667	0.0082	0.0090	
1.112—1.148	0.981700	0.062	1.22	0.993763	0.036	0.33	0.15
1.148—1.230	0.998464	0.018	0.033	0.998797	0.016	0.0090	
1.230—1.240	0.998852	0.015	0	0.998851	0.015	0	0.0054
1.240—1.321	0.998124	0.019	0.052	0.998647	0.016	0.014	
1.321—1.449	0.940141	0.12	3.47	0.972368	0.078	0.95	0.12
1.449—1.530	0.963792	0.091	0.052	0.964281	0.090	0.014	
1.530—1.755	0.984811	0.057	0.024	0.985049	0.056	0.0066	
1.755—1.965	0.897819	0.17	4.60	0.937069	0.12	1.25	0.10
1.965—2.190	0.962316	0.093	0.024	0.962543	0.093	0.0066	

After computing the intensity, it is possible to determine from eqs. (III.1.4) - (III.1.6) the radiation fluxes and amount of solar energy absorbed at different levels in the clouds. The results of the calculations are given below. Here, we only note that a comparison of the computations made by means of eqs.(III.1.4) - (III.1.5) and (III.1.32) - (III.1.33) with the exact computations by L.M.Romanova (see Chapter II, Sect.1) showed that the above approximate method permits to determine the fluxes of reflected radiation and of radiation transmitted by the cloud, with an error of the order of 5 - 10%. However, this method results in excessive errors in the degree of intensity, for which reason we did not use it in the computation of these quantities. In determining the intensity, it is apparently necessary to carry out a few more successive /126 approximations, which must be done by calculation. Analytical expressions can be obtained only in zero and in first approximation.

Section 2. Spectral Fluxes of Infrared Radiation

We used the relations (III.1.4) - (III.1.6) and (III.1.32) - (III.1.33) in

computing radiation fluxes in the 22 spectral intervals shown in Table I.4.21. All absorption bands of water vapor in the near-infrared region of the spectrum and the intervals between them were considered. The computations were made for thin (H = 0.25 km) and thick (H = 1 km) clouds, with the upper boundary at the level z_2 = 2 km, at a mean cloud temperature of 0°C, and an average liquid-water content of 0.2 gm/m^3.

So-called "high" clouds (as distinguished from "low" clouds indicated above) located in the layer ($4 \le z \le 5$ km) with a temperature of -15° and a water content of 0.2 gm/m^3 were also considered.

The moisture content was determined as a function of the temperature. The density of water vapor in the saturation state at the above temperatures was equal to 4.9 gm/m^3 for a low cloud and 1.55 gm/m^3 for a high cloud. The distribution of moisture with height above the cloud is described by the formula

$$\rho_w(z) = \rho_w(z_2)\ e^{-0.45\,(z-z_2)}, \qquad \text{(III.2.1)}$$

where $\rho_w(z_2)$ = 4.9 gm/m^2 or 1.55 gm/m^3. From this, we determined the optical thickness of the layer above the clouds $\tau_{2,i}$ in the spectrum interval $\Delta\lambda_i$:

$$\tau_{2,i} = \alpha_{w,i}\int_{z_2}^{\infty} \rho_w(z)\,dz = \alpha_{w,i}\,m_2, \qquad \text{(III.2.2)}$$

where m_2 is the water-vapor content in the layer above the clouds which, for the condition (III.2.1), is equal to 1.1 gm/cm^2 for a low cloud and 0.3 gm/cm^2 for a high cloud.

In accordance with the differing moisture content, a low and high cloud differ in their absorptivity. In the computations, the values $\tilde{\alpha}_{w,i}$ from column 5 of Table I.4.21 were used in the first case and the values from column 6 in the second case. The absorption coefficient of water $\tilde{\alpha}_{v,i}$ was taken from column 3 of the same Table and, finally, the scattering coefficient $\tilde{\sigma}_v$ was taken as equal to 30 km^{-1} in accordance with the data of Chapter I, Sect.4. According to Table I.4.22, this value of σ_v refers to St and As clouds and slightly underestimates the scattering coefficient of Sc clouds.

Later, we used the scattering indicatrix of a droplet at ρ = 20. Some justification for the selection of this indicatrix and the numerical values of the coefficient of its expansion in a series of Legendre polynomial are given in Chapter I, Sect.4.

The numerical values for the parameters of eqs.(III.1.32) - (III.1.33), which correspond to the selected values of the physical parameters, are given in Table III.2.1. For convenience, the quantities $\Delta\lambda_i$ and πS_i are repeated here.

Tables III.2.2 and III.2.3 give the results of calculations of the spectral radiation fluxes, those reflected by the cloud $F_{1,i}(\tau_0)$ and those transmitted by it $F_{2,i}(0)$, together with the albedo A_i and the relative transmission P_i. The last two quantities for a separate spectral interval are computed by

$$A_i = \frac{F_{1,i}(\tau_0)}{\pi S_i \cos\zeta e^{-\sec\zeta\tau_{2,i}}}, \qquad \text{(III.2.3)}$$

$$P_i = \frac{F_{2,i}(0)}{\pi S_i \cos\zeta e^{-\sec\zeta\tau_{2,i}}}. \qquad \text{(III.2.4)}$$

The albedo and transmission of an entire band are determined from the relations /127

$$A_j = \frac{\sum_{i=1}^{3} F_{1,i}(\tau_0)}{\cos\zeta \sum_{i=1}^{3} \pi S_i e^{-\sec\zeta\tau_{2,i}}}, \qquad \text{(III.2.5)}$$

$$P_j = \frac{\sum_{i=1}^{3} F_{2,i}(0)}{\cos\zeta \sum_{i=1}^{3} \pi S_i e^{-\sec\zeta\tau_{2,i}}}. \qquad \text{(III.2.6)}$$

TABLE III.2.2

Band	Δλ, μ	Low Clouds				High Clouds
		$F_1(\tau_0)$ cal/cm^2·min	$F_2(0)$ cal/cm^2·min	A, %	P, %	A, %
e	0.700—0.719	0.022	0.0069	66	21	66
	0.719—0.721	0.0011	0.00030	59	16	63
	0.721—0.740	0.022	0.0069	66	21	66
	0.740—0.790	0.045	0.014	65	22	65
0.84 μ	0.790—0.814	0.020	0.0065	66	21	66
	0.814—0.816	0.00073	0.0318	55	13	62
	0.816—0.840	0.020	0.0065	66	21	66
	0.840—0.860	0.016	0.0052	66	22	66
ρσ τ	0.860—0.915	0.035	0.011	65	20	65
	0.915—0.935	0.0021	0.0338	45	8	57
	0.935—0.990	0.034	0.011	65	20	66
	0.990—1.030	0.022	0.0269	66	21	66
Φ	1.030—1.112	0.033	0.010	66	21	66
	1.112—1.148	0.0025	0.0348	46	9	57
	1.148—1.230	0.032	0.0295	62	19	63
	1.230—1.240	0.0030	0.0392	64	20	64
Ψ	1.240—1.321	0.018	0.0252	62	18	63
	1.321—1.449	0.00021	0.0411	25	1	40
	1.449—1.530	0.010	0.0211	37	4	37
Ω	1.530—1.755	0.014	0.0030	46	10	48
	1.755—1.965	0.0425	0.0636	18	0.25	24
	1.965—2.190	0.010	0.0396	34	3	34

Here the summation is made along three spectral intervals which compose the band. With the same formulas, the integral albedo and transmission can be computed if the summation is extended to the entire infrared region.

Table III.2.2 presents all 22 spectral intervals for the case of $\tau_0 = 30$, $\zeta = 30^\circ$. These data are given here to demonstrate the changes in the optical properties of a cloud within the boundaries of an individual band and for clarifying the difference between the center and the fringes of the band.

Since the division of the band on the basis of the scheme by Ye.S.Kuznetsov (see Chapter I, Sect.5) is quite arbitrary and does not correspond to the true

TABLE III.2.3

Band	$\zeta = 30°$				$\zeta = 60°$			
	F_1, cal/cm^2·min	F_2, cal/cm^2·min	A, %	P, %	F_1, cal/cm^2·min	F_2, cal-cm^2·min	A, %	P, %
				Low Cloud, $\tau_0 = 6$				
a	0.022	0.042	33	63	0.020	0.019	50	48
	0.024	0.038	32	61	0.024	0.019	53	42
0.8 μ	0.021	0.039	33	62	0.019	0.018	50	48
	0.0078	0.014	32	58	0.0073	0.0070	50	48
ρστ	0.036	0.062	33	56	0.034	0.017	54	28
	0.011	0.020	33	61	0.010	0.0095	50	47
Φ	0.034	0.059	32	56	0.030	0.029	50	48
	0.0015	0.0026	32	55	0.0014	0.0014	49	47
Ψ	0.014	0.029	24	50	0.014	0.013	42	40
Ω	0.014	0.022	24	37	0.013	0.012	37	36
Σ	0.1853	0.328	31	55	0.173	0.145	50	42
				High Cloud, $\tau_0 = 30$				
a	0.044	0.014	67	21	0.030	0.0057	78	15
	0.045	0.014	65	19	0.033	0.0044	76	10
0,8 μ	0.042	0.013	65	21	0.027	0.0053	77	15
	0.016	0.0052	67	22	0.009	0.0020	78	14
ρστ	0.071	0.022	64	20	0.045	0.0083	75	14
	0.022	0.0069	67	21	0.014	0.0029	76	15
Φ	0.067	0.020	64	19	0.044	0.0075	75	13
	0.0030	0.00092	64	20	0.002	0.00034	72	12
Ψ	0.028	0.0063	48	11	0.017	0.0020	55	6
Ω	0.024	0.0040	41	7	0.015	0.00076	45	2
Σ	0.362	0.1063	60	18	0.23	0.0392	71	12

distribution of the lines in the band, we found it necessary to give detailed values for all computational data. Table III.2.3 therefore gives only information characterizing individual bands. The last rows of each part of the Table contain the integral values F_1, (τ_0), $F_2(0)$, A and P for the entire infrared /128 region of the spectrum.

In studying Tables III.2.2 and III.2.3 the following conclusions can be drawn:

1. With an increase in absorption the reflectivity of the clouds is reduced. In the broad band Ω, the albedo is only 60 - 70% of that of the weakest band a. For $k_{min} = 0.8978$ (N = 21), we have A = 18%, and for $K_{max} = 0.999976$ (N = 4), we have A = 65%. Simultaneously, the transmission is also noticeably decreased.

2. Because of the near-infrared region, the total albedo of the cloud with respect to the total solar radiation is reduced relative to the visible region of the spectrum.

If the total albedo $\tilde{A}$ is computed by means of the equation

$$\tilde{A} = \frac{A_v \pi S_v + A_{i.r} \pi S_{i.r.}}{\pi S_v + \pi S_{i.r.}},$$

where A_v and πS_v are the albedo and the solar constant in the visible region of the spectrum, respectively; $A_{i.r.}$ and $\pi S_{i.r.}$ are the same for the infrared region, then we obtain, in the case of $\tau_0 = 30$, the following

$$A_v = 76\%, \qquad \tilde{A} = 67\% \text{ when } \zeta = 30°,$$
$$A_v = 81\%, \qquad \tilde{A} = 74\% \text{ when } \zeta = 60°.$$

3. In the infrared region, the albedo increases with increasing optical thickness of the cloud and of zenith distance of the sun. This proceeds more rapidly than in the visible spectrum region. /129

4. The albedo of a high cloud is somewhat greater than that of a lower cloud because of a lesser absorption of water vapor in the former case; the difference in albedo is particularly noticeable in the centers of the absorption bands.

5. A thin cloud transmits more radiation than it reflects. However, a relatively small thickness ($\tau = 6$) is sufficient for the reflected radiation to be greater than the transmitted radiation, beginning at some solar zenith distance ($\zeta = 60°$).

In conclusion, we can state that at present no experimental data are available with which to compare the computations made on the spectral radiation fluxes in the infrared region of the spectrum, emitted from the cloud layer.

In discussing various theoretical papers, reference is made first to the bibliography at the end of Chapter II [see (Bibl.2-7, 16, 18, 22)] since, at $\varpi(\tau) = \text{const} = k < 1$, eq.(III.1.1) does not differ in form from eq.(III.2.3) which describes the radiative transfer from the visible region. To this list should be added the paper by Fritz (Bibl.5) in which the case $k < 1$ is considered on the basis of the method of diffusion approximation, described in

Chapter II. In order of magnitude, our values agree with those by Fritz; more exact comparisons are of no use since no error evaluation was made by this author (Bibl.5). The same is true of other papers (Bibl.2 - 7) listed in Chapter II. Therefore, a comparison can be made only with the results of L.M. Romanova [see (Bibl.16) in the bibliography at the end of Chapter II] by means of which the accuracy of our computations could be checked, as shown in Section 1.

Section 3. Total Quantity of Energy Absorbed in a Cloud; Comparison with Calculations by other Authors and with Experiments

If the intensity of radiation $I_\lambda(\tau, r)$ is known, eqs.(III.1.6) will permit computation of the absorption per unit volume $Q(\tau)$ and of the total amount of radiant energy Q absorbed by a given cloud. The quantity Q can also be calculated from the relation

$$Q = F_1(0) + F_2(\tau_0) - F_1(\tau_0) - F_2(0), \qquad \text{(III.3.1)}$$

where $F_1(0)$ and $F_2(\tau_0)$ are the integral radiation fluxes of incoming radiation at the upper and lower boundaries of the cloud, respectively; $F_1(\tau_0)$ and $F_2(0)$ are the fluxes leaving the boundary.

The method and the results of calculating the quantity Q by means of eq.(III.3.1) are given in a paper by Korb, Michalowsky, and Möller (Bibl.6). The authors made use of the two-flux approximation (see Chapter II) and improved it further. It is assumed that in the depths of the cloud layer where the flux of direct solar radiation becomes zero, it is possible to use, in describing the flux of purely scattered or diffused radiation, the so-called Mecke equation

$$\begin{aligned} \frac{dF_1}{dz} &= -\chi a F_1 - \beta'(1-\chi)\, a\,(F_1 - F_2), \\ \frac{dF_2}{dz} &= \chi a F_2 - \beta'(1-\chi)\, a\,(F_1 - F_2), \end{aligned} \qquad \text{(III.3.2)}$$

where a is the coefficient of extinction; χ is the component of absorbed light; β' is the component of back-scattered radiation or the reflection factor.

In discussing any of the levels inside the cloud, up to the upper boundary, the authors replaced β in eq.(III.3.2) by a variable quantity of the type of /130

$$\beta(z) = \beta' - (\beta' - \beta)\frac{F_0}{F_2} e^{-dz}, \qquad \text{(III.3.3)}$$

where F_0 and β are, respectively, the flux and reflection factor of direct insolation. Naturally, the reflection of a parallel beam is different from the reflection of diffuse radiation. It is, however, difficult to say to what extent the solution of the problem is made more precise by accounting for the variability in the reflection factor in the form of eq.(III.3.3), if only be-

cause of the rough determination of the value β used by the author. In addition, it must be kept in mind that also in the depth of a strongly scattering medium, the intensity of scattered radiation is anisotropic in the presence of absorption. For this reason, eq.(III.3.1) is not completely exact.

The second improvement of the two-flux approximation made by Korb (Bibl.6) consists in the introduction of a so-called "inversion factor", i.e., of a

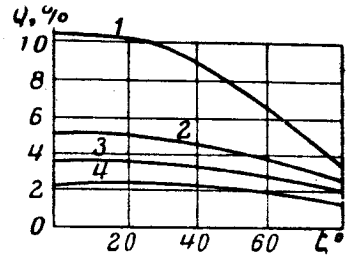

Fig.III.3.1 Relative Absorption According to Data by Korb

variable factor for the absorption coefficient, which is to account for the elongation of the path of light in the cloud due to scattering and for the difference in absorption by droplet water and by a continuous layer.

TABLE III.3.1

Case	Water-Vapor Content, cm	Water Content g/m³	Droplet Radius, μ	Case	Water-Vapor Content, cm	Water Content g/m³	Droplet Radius, μ
1	1.1	0.5	7	3	0.8	0.3	5
2	1.02	0.3	6	4	0.65	0.3	6

Korb et al (Bibl.6) just as Fritz (Bibl.5) give no evaluation of the accuracy of their solutions. The only criterion for reliability of the results in both cases is the fact that they do not contradict the small amount of available observational data. Thus, the computations by Korb et al (Bibl.6) agree better with the results obtained by Neiburger (Bibl.7) than the latter's own computations made on the basis of the solution of eq.(III.3.2) without correction. In view of the small amount of observational data and of the lack of information on the values of the basic parameters of the problem at the instant of measurement, such a method of checking the theory cannot be considered reliable. The relative absorption (in %) according to data by Korb, for four cases described in Table III.3.1, is plotted in Fig.III.3.1.

The few data on infrared radiation Q absorbed by clouds are compiled else-

where (Bibl.7 - 9). Common to the data presented in these papers is the low accuracy of the experimental determination of the quantity Q. By nature, this quantity is small and with the present experimental methodology is obtained as the difference between nearly equal large values, namely, the radiation fluxes entering and leaving the cloud. According to Neiburger (Bibl.7), the average value of Q for St clouds amounts to 7% of the short-wave radiation arriving at the cloud while the scattering of the data already exceeds this value. The data by N.I.Chel'tsov (Bibl.8) reveal some relationship between absorption and thickness of the cloud.

At an average thickness of 360 m for 26 cases, the value of Q was found to be equal to 3.5 ± 0.2%; in another group of measurements with an average thickness of 530 m, Q was equal to 7.2 ± 1.8%. The averaging here was made for /131 clouds of various types with an upper boundary of 3 km.

Data of absorption measurements in very thick clouds (of the order of 6 - 8 km), mostly multi-layer cloud systems with an upper boundary at the 7 - 8 km level, were given by Fritz (Bibl.9). Here, the amount of absorbed radiation constituted about 15 ± 5% (in one case 27 ± 3%).

TABLE III.3.2

Band	Low Cloud			High Cloud	Band	Low Cloud			High Cloud
	$\tau_0 = 6$, $\zeta = 30°$	$\tau_0 = 30°$ $\zeta = 30°$	$\zeta = 60°$	$\tau_0 = 30$, $\zeta = 30°$		$\tau_0 = 6$, $\zeta = 30°$	$\tau_0 = 30°$ $\zeta = 30°$	$\zeta = 60°$	$\tau_0 = 30$, $\zeta = 30°$
α	0.003	0.008	0.0023	0.010	Φ	0.013	0.018	0.0065	0.020
	0.013	0.011	0.0056	0.011		0.0006	0.00078	0.00036	0.00078
0.8 μ	0.003	0.009	0.0037	0.009	Ψ	0.015	0.0237	0.012	0.031
	0.0022	0.0028	0.003	0.0029	Ω	0.023	0.031	0.018	0.036
psr	0.012	0.017	0.0067	0.019	Σ	0.0868	0.1304	0.0603	0.144
	0.002	0.0041	0.0021	0.0041					

We also computed the total amount of absorbed radiation in a cloud on the basis of eq.(III.3.1). The computation error was 20%.

Examples of absolute absorption (in cal/cm^3 · min) of infrared solar radiation in individual bands, showing the difference in the absorption properties of thin and thick, low and high clouds and also the reduction in absorption with increase in the zenith distance of the sun are given in Table III.3.2. At first, the latter appears improbable because of the fact that, with an increase in ζ, the effective thickness of the cloud increases and the radiation path within this thickness lengthens, as a result of which the albedo, for instance, also will increase. However, precisely because of the growth in albedo, the absorptivity of the cloud will decrease.

We will demonstrate later that, as shown in Table III.3.2, a high cloud

absorbs more energy than a low cloud. Therefore, the absorption in the first case takes place mainly in the broad bands Ψ and Ω. In these segments of the spectrum a smaller amount of solar energy arrives at the lower cloud and the role of the weak bands in absorption is increased. The difference in the absorption properties of a "high" and a "low" cloud is partly compensated by the lower temperature of the former and a correspondingly smaller absorption coefficient of water vapor.

The relative integral absorption of infrared radiation q (in %) is presented in Table III.3.3. The quantity q was computed by means of the formula

$$q = 100 \frac{\Sigma Q_i}{\left| \pi S_B e^{-\sec\zeta \tau_2} + \Sigma \pi S_i e^{-\sec\zeta \tau_{2,i}} \right| \cos\zeta} . \qquad \text{(III.3.4)}$$

Here, the denominator is the total amount of solar radiation incident on the upper boundary of the cloud. The first addend in the denominator refers to the visible region of the spectrum; in its determination, it was assumed that

$$\tau_2 = \tau^* e^{-\frac{\sigma(0)}{\tau^*} z_2},$$

where $\tau^* = 0.3$ is the total optical thickness of the atmosphere in the range of wavelengths of visible light; $\sigma(0) = 0.1$ km^{-1} is the scattering coefficient in the layer near the ground; z_2 is the height of the upper boundary of the cloud.

/132

TABLE III.3.3

Cloud Position	τ	ζ°	q
Low	6	30	6.2
		60	2.5
	30	30	9.5
		60	8.1
High	30	30	8.9

It is interesting to note that the laws of variation in relative q and in absolute Q of absorption differ. The reasons involved need no further explanation.

Section 4. Absorption of Solar Radiation in a Cloudy Atmosphere

The appearance of a cloud leads to a change in the amount of absorbed solar energy at all levels of the atmosphere. It is not difficult to predict the

nature of this change: The absorption above the cloud is greater than in a cloudless sky because of the reflection of radiation from the cloud; conversely, in the layer below the cloud, absorption must increase since a smaller portion of the infrared radiation will reach this layer.

The distribution of the quantity Q (τ) [see eq.(III.1.6)] with height in a cloudy atmosphere is given in another paper (Bibl.10). Here, in the layers outside of the clouds, absorption in the water-vapor band and scattering on air molecules and on aerosol particles were taken into consideration; absorption by the water layer in the cloud, scattering by water droplets, and absorption by water vapor were also considered; on the interfaces between clouds and ambient medium, equality of radiation fluxes was assumed. It was also stipulated that the intensity of radiation leaving the cloud does not depend on the direction. A solution is given, taking into account only single scattering outside of cloud. In the cloud layer itself, the solution in the zero approximation is used (see Sect.1).

The obtained relations are not given here since they present nothing new compared to Section 1. We will confine the discussion here to the results of computations performed with the following values of the parameters: $\zeta = 60^\circ$, $H = 1$ km, $z_1 = 1$ km; $z_2 = 2$ km, where z_1 and z_2 are levels of the lower and upper boundaries of the clouds

$$\rho_v^{(0)} = 0.5\ g/m^3;\ \rho_w^{(0)} = 5\ g/m^3;\ \rho_w^{(i)}(z) = \rho^{(i)}(0)\ e^{-z/2.6}\quad (i = 1,\ 2);$$

The numerals 0, 1, and 2 refer to the layers below, within, and above the cloud, respectively. The quantity $\rho^{(i)}(0)$ was so selected that the density of water vapor on the boundaries of the cloud varies continuously.

The scattering properties of a cloud were characterized by the scattering coefficients $\tilde{\sigma}_v = 25\ km^{-1}$ and by two values of the parameter β (see Sect.1) $\beta = 0.6$ and $\beta = 0.9$.

The same spectral intervals as in Section 1 were examined; here, the values of the absorption coefficients of water vapor $\alpha_{w,\lambda}$ and the values of the absorption coefficient of a water layer $\tilde{\alpha}_{v,\lambda}$ given in Table I.4.21 were used.

The results of the computations are presented in Tables III.4.1 - III.4.3 and in Fig.III.4.1. /133

The absorption Q (in 10^{-6} cal/cm^2·min) on three levels in the cloud layers is given: in Table III.4.1 for the layer below the cloud; in Table III.4.2 for the layer within the cloud; and in Table III.4.3 for the layer above the cloud. The solid heavy curves in Fig.III.4.1 show the distribution of Q with height, Q(z), in a cloudless atmosphere according to the data from another paper (Bibl.11). The solid thin curves refer to a cloudy atmosphere with $\beta = 0.6$, while the broken curves indicate the case of $\beta = 0.9$.

A study of these diagrams and Tables shows the following regularities:

1. The absorption at the boundaries shows a discontinuity due to a dis-

continuity in the density of water and in the absorption coefficient.

2. The absorption in the layer below the cloud is sharply reduced compared with the absorption at corresponding heights in a cloudless atmosphere. Thus,

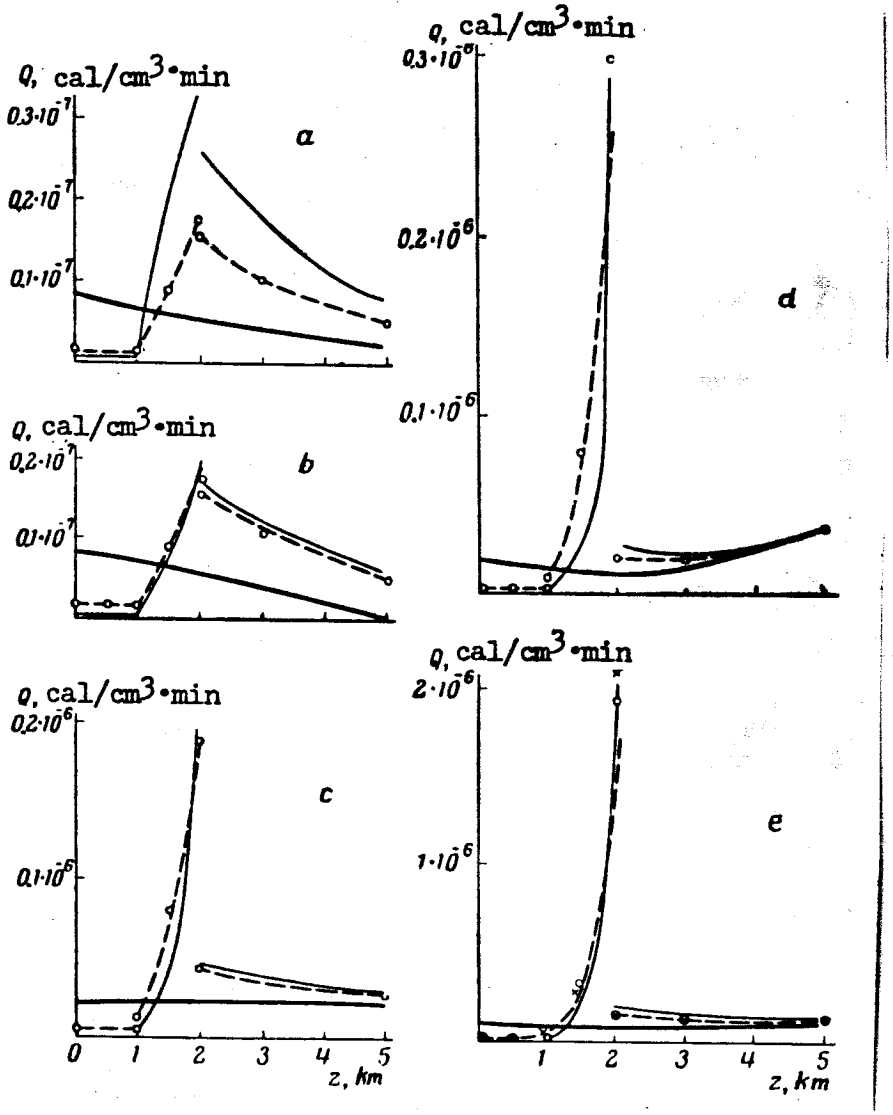

Fig.III.4.1 Distribution of Absorbed Energy with Height
a - In the band a; b - In the band 0.8μ; c - In the band Φ;
d - In the band Ψ; e - Composite curve

at the same water-vapor content in the entire thickness of the atmosphere, the data by Ye.S.Kuznetsov (Bibl.11) yield $Q(0) = 0.1 \times 10^{-6}$ cal/cm³·min. Our /134 computations (Table III.4.1) give $Q^{(1)}(0) = 0.0029 \times 10^{-6}$ cal/cm³·min for $\beta = 0.6$ and $Q^{(1)}(0) = 0.01 \times 10^{-6}$ cal/cm³·min for $\beta = 0.9$. Here, $Q(0)$ and $Q^{(1)}(0)$ are the amount of absorbed radiation near the surface of the earth in cloudless and cloudy skies, respectively. /135

TABLE III.4.1

Band	β = 0.6			β = 0.9		
	z, km					
	0	0.5	1.0	0	0.5	1.0
a	$0.0^{3}97$	$0.0^{3}85$	$0.0^{3}72$	$0.0^{2}15$	$0.0^{2}13$	$0.0^{2}11$
0.8 μ	$0.0^{3}42$	$0.0^{3}37$	$0.0^{3}32$	$0.0^{2}17$	$0.0^{2}15$	$0.0^{2}13$
ρστ	$0.0^{3}96$	$0.0^{3}85$	$0.0^{3}75$	$0.0^{2}36$	$0.0^{2}33$	$0.0^{2}31$
Φ	$0.0^{3}43$	$0.0^{3}41$	$0.0^{3}39$	$0.0^{2}29$	$0.0^{2}28$	$0.0^{2}27$
Ψ	$0.0^{4}92$	$0.0^{4}80$	$0.0^{4}67$	$0.0^{2}12$	$0.0^{2}10$	$0.0^{3}88$
Ω	$0.0^{6}32$	$0.0^{6}27$	$0.0^{6}22$	$0.0^{4}33$	$0.0^{4}28$	$0.0^{4}23$
0.70—2.19 μ	$0.0^{2}29$	$0.0^{2}25$	$0.0^{2}22$	0.011	0.0101	$0.0^{2}92$

TABLE III.4.2

Полоса	β=0,6			β=0,9		
	z, km					
	1	1.5	2	1	1.5	2
a	$0.0^{3}92$	$0.0^{2}19$	0.320	$0.0^{2}14$	$0.0^{2}84$	0.017
0.72—0.79 μ	$0.0^{4}74$	$0.0^{2}15$	$0.0^{2}25$	$0.0^{4}18$	$0.0^{2}10$	$0.0^{2}19$
0,8 μ	$0.0^{3}36$	$0.0^{3}79$	0.020	$0.0^{2}16$	$0.0^{2}96$	0.019
0.84—0.86 μ	$0.0^{4}24$	$0.0^{3}48$	$0.0^{2}10$	$0.0^{3}85$	$0.0^{3}49$	$0.0^{3}95$
ρστ	$0.0^{2}12$	0.027	0.095	$0.0^{3}54$	0.034	0.079
0.99—1.03 μ	$0.0^{3}25$	$0.0^{2}53$	0.013	$0.0^{2}10$	$0.0^{2}61$	0.012
Φ	$0.0^{2}15$	0.043	0.20	0.011	0.073	0.18
1.23—1.24 μ	$0.0^{4}72$	$0.0^{2}17$	$0.0^{2}61$	$0.0^{3}41$	$0.0^{2}25$	$0.0^{2}5$
Ψ	$0.0^{3}61$	0.025	0.29	$0.0^{2}87$	0.069	0.26
Ω	$0.0^{4}28$	$0.0^{2}54$	1.38	$0.0^{2}22$	0.065	1.13
0.70—2.19 μ	$0.0^{2}52$	0.13	2.05	0.032	0.27	1.78

TABLE III.4.3

Band	β = 0,6			β = 0,9		
	z, km					
	2	3	5	2	3	5
a	0.026	0.018	0.082	0.015	0.010	0.049
0.8 μ	0.17	0.012	0.059	0.016	0.011	0.056
ρστ	0.054	0.042	0.029	0.049	0.038	0.028
Φ	0.046	0.037	0.028	0.043	0.035	0.027
Ψ	0.026	0.020	0.028	0.024	0.018	0.027
Ω	0.011	0.084	0.010	$0.0^{2}99$	$0.0^{2}72$	0.010
0.70—2.19 μ	0.18	0.138	0.11	0.15	0.12	0.10

3. Directly above the clouds, the absorption increases more than two-fold compared with the cloudless case.

4. The more elongated indicatrix ($\beta = 0.9$) gives a lower absorption above the cloud also in its upper portion (sometimes almost to the lowest boundary of the cloud); over the greater part of the cloud (as a rule) and below it, absorption is greater at $\beta = 0.9$ than at $\beta = 0.6$.

5. The absorption within a cloud assumes the greatest value in its upper layer. The broader the band under consideration the narrower will be the layer at whose boundary the absorption is concentrated.

TABLE III.4.4

	Below the Cloud $0 < z < 1$ km	Within the Cloud $1 < z < 2$ km	Above the Cloud $2 < z < 5$ km	Upper Layer $z > 5$ km
$\beta = 0.6$	0.0003	0.039	0.041	0.061
$\beta = 0.9$	0.001	0.060	0.035	
Korb (Bibl. 6)	0.001	0.053	0.087	

Composite data (total absorbed energy in an individual layer) are given in Table III.4.4.

The last row in Table III.4.4 presents the data by Korb et al (Bibl.6) for a cloud of 1 km thickness, with an upper boundary at a height of 2 km for $\zeta = 60^\circ$ and $\rho_v = 0.3$ gm/m^3. The Table shows agreement of our data with the calculations by Korb.

Here, we used the absorption data for $z > 5$ km from the computation by Ye.S.Kuznetsov (Bibl.11), which are valid for the case of a cloudless atmosphere. As shown in Fig.III.4.1, the absorption at heights of $z > 5$ km in a cloudless and cloudy atmosphere are nearly equal.

The most interesting conclusion from Table III.4.4 is that the total amount of absorbed energy in a cloudy atmosphere is 0.155 cal/cm^2·min, i.e., 55% more than in a cloudless atmosphere whereas, according to Ye.S.Kuznetsov's computation, 0.1 cal/cm^2·min is absorbed at the same water-vapor content.

The absorbed energy is distributed by layers in the following manner: Below the clouds, about as much is absorbed as in the entire cloudless atmosphere; furthermore, 55% of this amount is absorbed by the cloud. The absorption in the layer below the cloud can be considered roughly to be equal to zero.

BIBLIOGRAPHY

1. Kondrat'yev, K.Ya., Burgova, M.P., and Gol'm, T.S.: Distribution of Energy in the Spectrum of Total and Scattered Radiation (Raspredeleniye energii v spektre summarnoy i rasseyannoy radiatsii). Compendium on Scattering and Polarization of Light in the Earth's Atmosphere. Izd. Akad. Kaz. SSR, 1962.
2. Feygel'son, Ye.M., Malkevich, M.S., Kogan, S.Ya., Glazova, K.S., and Kuznetsova, A.M.: Computation of Brightness of Light in the Atmosphere for Anisotropic Scattering (Raschet yarkosti sveta v atmosfere pri anizotropnom rasseyanii). Trudy Inst. Fiz. Atmosf., No.1, 1958; No.3, 1962.
3. Feygel'son, Ye.M.: Interaction between Scattered Light and Light Reflected from the Earth's Surface (Vzaimodeystviye mezhdu rasseyannym i otrazhennym ot zemnoy poverkhnosti svetom). Transactions of the Conference on the Optics of the Atmosphere. Alma - Ata, 1963.
4. Feygel'son, Ye.M.: Absorption of Solar Energy in the Atmosphere in the Presence of Clouds (Pogloshcheniye solnechnoy energii v atmosfere pri nalichii oblakov). Trudy Geofiz. Inst., No.23, 1954.
5. Fritz, S.: Absorption and Scattering of Solar Energy in Clouds of "Large /136 Water Drops" II, J. Met., Vol.15, No.1, 1958.
6. Korb, G., Michalowsky, J., and Möller, F.: Absorption of Insolation in Cloudless and Cloudfree Atmosphere (Die Absorption der Sonnenstrahlung in der wolkenfreien und bewölkten Atmosphäre). Beiträge zur Phys. der Atmosphäre, Vol.30, No.1, 1957.
7. Neiburger: Reflection, Absorption and Transmission of Insolation by Stratus Clouds. J. Met., Vol.6, No.2, 1949.
8. Chel'tsov, N.I.: Investigation of Reflection, Transmission and Absorption of Insolation by Clouds of any Form (Issledovaniye otrazheniya, propuskaniya i pogloshcheniya solnechnoy radiatsii oblakami nekotorykh form). Transactions Trudy TsAO (Central Aerological Observatory), No.8, 1952.
9. Fritz, S. and Macdonald, T.H.: Measurements of Absorption of Solar Radiation by Clouds. Bull. Amer. Met. Soc., Vol.32, No.6, 1951.
10. Feygel'son, Ye.M.: Absorption of Solar Energy in the Atmosphere in the Presence of Clouds (Pogloshcheniye solnechnoy energii v atmosfere pri nalichii oblakov). Trudy Geofiz. Inst., No.23, 1954.
11. Kuznetsov, Ye.S.: On the Absorption of Solar Radiation by the Earth's Atmosphere (O pogloshchenii radiatsii solntsa zemnoy atmosferoy). Trudy Geofiz. Inst., No.23, 1954.

CHAPTER IV

SPECTRAL FLUXES OF LONG-WAVE RADIATION

Section 1. Approximation Formulas for the Fluxes

In the long-wave region of the spectrum, the equations of transfer of ascending and descending radiation in a cloud can be written in the following form [see eq.(I.3.23)]:

$$\cos\theta\frac{\partial I_1}{\partial\tau}=(1-k)B(\tau)+\frac{k}{4\pi}\int_{+}I_\lambda(\tau,r')\,\gamma_{11}(r,r')\,d\omega'+$$
$$+\frac{k}{4\pi}\int_{+}I_2(\tau,r')\,\gamma_{12}(r,r')\,d\omega'-I_1(\tau,r), \tag{IV.1.1}$$

$$-\cos\theta\frac{\partial I_2}{\partial\tau}=(1-k)B(\tau)+\frac{k}{4\pi}\int_{+}I_\lambda(\tau,r')\,\gamma_{21}(r,r')\,d\omega'+$$
$$+\frac{k}{4\pi}\int_{+}I_2(\tau,r')\,\gamma_{22}(r,r')\,d\omega'-I_2(\tau,r), \tag{IV.1.2}$$

where

$$k=\frac{\tilde{\sigma}_v}{\tilde{\alpha}_v+\tilde{\sigma}_v+\tilde{\alpha}_w}. \tag{IV.1.3}$$

Assuming k = const

$$\tau=\int_0^z(\tilde{\alpha}_v+\tilde{\alpha}_w+\tilde{\sigma}_v)\,dz. \tag{IV.1.4}$$

Integrating each term of eqs.(IV.1.1) and (IV.1.2) with respect to r within the boundaries of the hemisphere, we obtain

$$\frac{dF_1}{d\tau}=2\pi(1-k)B(\tau)+k\int_{+}I_1(\tau,r')\,\Gamma_1(r')\,d\omega'+$$
$$+k\int_{+}I_2(\tau,r')\,\Gamma_2(r')\,d\omega'-\int_{+}I_1(\tau,r)\,d\omega \tag{IV.1.5}$$

$$-\frac{dF_2}{d\tau}=2\pi(1-k)B(\tau)+k\int_{+}I_1(\tau,r')\Gamma_2(r')\,d\omega'+$$
$$+k\int I_2(\tau,r')\,\Gamma_1(r')\,d\omega'-\int_{+}I_2(\tau,r)\,d\omega; \tag{IV.1.6}$$

Here

$$\Gamma_1(r')=\frac{1}{4\pi}\int_{+}\gamma_{11}(r,r')\,d\omega=\frac{1}{4\pi}\int_{+}\gamma_{22}(r,r')\,d\omega, \tag{IV.1.7}$$

$$\Gamma_2(r')=\frac{1}{4\pi}\int_{+}\gamma_{12}(r,r')\,d\omega=\frac{1}{4\pi}\int_{+}\gamma_{21}(r,r')\,d\omega. \tag{IV.1.8}$$

We can then present the scattering function $\gamma(r, r')$ in the form of

$$\gamma(r, r') = \sum_{k=0}^{\infty} c_k \left[P_k(\mu) P_k(\mu') + 2 \sum_{\nu=1}^{k} \frac{(k-\nu)!}{(k+\nu)!} P_k^{\nu}(\mu) P_k^{\nu}(\mu') \cos \nu(\psi - \psi') \right].$$

In this case,

$$\Gamma_1(r') = \frac{1}{2} \sum_{k=0}^{\infty} c_k P_k(\mu') \int_0^1 P_k(\mu)\, d\mu, \tag{IV.1.9}$$

$$\Gamma_2(r') = \frac{1}{2} \sum_{k=0}^{\infty} (-1)^k c_k P_k(\mu') \int_0^1 P_k(\mu)\, d\mu. \tag{IV.1.10}$$

Let us check the sums and differences of eqs.(IV.1.5) and (IV.1.6):

$$\frac{d(F_1 - F_2)}{d\tau} = 4\pi(1-k) B(\tau) + k \int_+ (I_1 + I_2)(\Gamma_1 + \Gamma_2)\, d\omega' - \int_+ (I_1 + I_2)\, d\omega', \tag{IV.1.11}$$

$$\frac{d(F_1 + F_2)}{d\tau} = k \int_+ (I_1 - I_2)(\Gamma_1 - \Gamma_2)\, d\omega' - \int_+ (I_1 - I_2)\, d\omega'. \tag{IV.1.12}$$

It follows from eqs.(IV.1.9) and (IV.1.10) that

$$\Gamma_1 + \Gamma_2 = \sum_k' c_k P_k(\mu') \int_0^1 P_k(\mu)\, d\mu, \tag{IV.1.13}$$

$$\Gamma_1 - \Gamma_2 = \sum_r'' c_k P_k(\mu') \int_0^1 P_k(\mu)\, d\mu, \tag{IV.1.14}$$

where $\sum_k'$ and $\sum_k''$ are the sums of even and odd values of k, respectively. It is known (see Chapter II) that

$$\int_0^1 P_k(\mu)\, d\mu = \begin{cases} 1 & \text{if } k = 0, \\ 0 & \text{if } k = 2, 4, \ldots 2m. \end{cases}$$

Hence,

$$\Gamma_1 + \Gamma_2 = 1$$

and eq.(IV.1.11) will become

$$\frac{d(F_1 - F_2)}{d\tau} = 4\pi(1-k) B(\tau) - (1-k) \int_+ (I_1 + I_2)\, d\omega. \tag{IV.1.15}$$

Let us next examine the quantity $\Gamma_1(\mu) - \Gamma_2(\mu)$. It is easy to show /139 that irrespective of the form of the indicatrix, this value has the following properties:

1. $0 \leq \Gamma_1(\mu) - \Gamma_2(\mu) < 1$ for $0 \leq \mu \leq 1$

2. $\Gamma_1 - \Gamma_2 \to 0$ for $\mu \to 0$.

In the long-wave region of the spectrum ($3\mu \leq \lambda \leq 40\mu$) the parameter ρ varies within the limits of

$$1 \leqslant \rho \leqslant 10,$$

i.e., the scattering indicatrix is represented by a Legendre polynomial series with two to twenty terms. Examples of the expansion factor C_k of such indicatrices (Bibl.1) are given in Table IV.1.1. Only the odd k contained in eq.(IV.1.14) are given.

TABLE IV.1.1

		k											
		1	3	5	7	9	11	13	15	17	19	21	23
C_k	$\rho = 10$	2.14	2.83	2.63	2.61	2.94	3.47	4.13	4.74	4.34	2.23	0.18	0.03
	$\rho = 2$	0.55	0.11	0									

The relation of $\Gamma_1 - \Gamma_2$ to μ in both cases is plotted in Fig.IV.1.1. We see that $\Gamma_1 - \Gamma_2$ depends relatively little on the degree of elongation of the

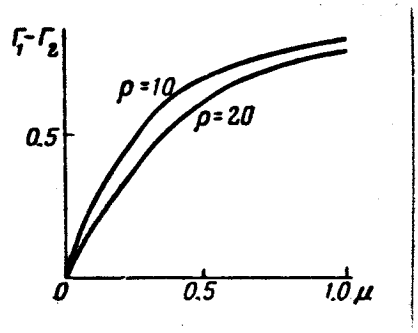

Fig.IV.1.1 $\Gamma_1 - \Gamma_2$ for Different Elongations of the Indicatrix

indicatrix and is everywhere less than unity. If we also note that $k < 1$, it becomes clear that the first addend on the right-hand side of eq.(IV.1.12) is small compared with the second. In some cases, for instance, at $k \ll 1$, i.e., for values of λ for which $\tilde{\sigma}_{v,\lambda} \ll \tilde{\alpha}_{w,\lambda} + \tilde{\alpha}_{v,\lambda} + \tilde{\sigma}_{v,\lambda}$, this addend can be neglected. However, if the first addend is retained, an approximate calculation is sufficient in view of the relative smallness of this addend. Thus, the calculations made with various indicatrices show that, with an error not exceeding 25%, it can be assumed that

$$\Gamma_1 - \Gamma_2 = C_1 P_1(\mu) \int_0^1 P_1(\mu)\, d\mu = \frac{1}{2} C_1 \mu.$$

Outside the vicinity of the point $\mu = 1$, the error is much less than 25%.

From the last expression it follows that

$$\int_+ (I_1 - I_2)(\Gamma_1 - \Gamma_2)\, d\omega' = \frac{C_1}{2} \int_+ (I_1 - I_2)\, \mu d\omega = \frac{c_1}{2} (F_1 - F_2)$$

and eq.(IV.1.12) assumes the form

$$\frac{d(F_1 + F_2)}{d\tau} = \frac{1}{2} k C_1 (F_1 - F_2) - \int_+ (I_1 - I_2)\, d\omega. \qquad \text{(IV.1.16)}$$

For further simplification of the system of equations (IV.1.15) and (IV.1.16) we will assume that /140

$$\bar{\mu} \int_+ (I_1 + I_2)\, d\omega = \int_+ (I_1 + I_2)\, \mu d\omega, \qquad \text{(IV.1.17)}$$

$$\bar{\mu} \int_+ (I_1 - I_2)\, d\omega = \int_+ (I_1 - I_2)\, \mu d\omega. \qquad \text{(IV.1.18)}$$

For $\bar{\mu} = \frac{1}{2}$, this assumption corresponds to Schwarzschild's approximation.

Other values of $\bar{\mu}$ give different variations of the two-flux approximation.

Strictly speaking, $\bar{\mu}$ in eqs.(IV.1.17) - (IV.1.18) is a variable quantity. Methods of determining this variable and of evaluating the error introduced on replacing $\bar{\mu}$ by a constant, are proposed in a number of papers [see for instance, (Bibl.2 - 4)]. We hold the view that $\bar{\mu}$ = const; however, unlike in other variants of the two-flux approximation - here as well as in Chapter II - $\bar{\mu}$ is not assigned beforehand but is determined from the physical condition. In addition, with our method of obtaining the approximate equation for fluxes, only one parameter $\bar{\mu}$ is introduced whereas, in the usual approach, a second parameter is required which generally is a variable parameter connected with averaging of the indicatrix [see, for instance (Bibl.4)].

For the conditions (IV.1.17) and (IV.1.18), eqs.(IV.1.5) and (IV.2.16) become

$$\frac{d(F_1 - F_2)}{d\tau} = 4\pi (1 - k) B(\tau) - \frac{1 - k}{\bar{\mu}} (F_1 + F_2), \qquad \text{(IV.1.19)}$$

$$\frac{d(F_1 + F_2)}{d\tau} = \left(k \frac{C_1}{2} - \frac{1}{\bar{\mu}} \right) (F_1 - F_2). \qquad \text{(IV.1.20)}$$

After solving these equations, we obtain

$$F_1 = \bar{c}_1 R_1 e^{-p(\tau_0-\tau)} + \bar{c}_2 R_2 e^{-p\tau} + \pi P_2 \int_0^{\tau} B(t)\, e^{-p(\tau-t)}\, dt + \pi P_1 \int_{\tau}^{\tau_0} B(t)\, e^{-p(t-\tau)} dt, \quad \text{(IV.1.21)}$$

$$F_2 = \bar{c}_1 R_2 e^{-p(\tau_0-\tau)} + \bar{c}_2 R_1 e^{-p\tau} + \pi P_1 \int_0^{\tau} B(t)\, e^{-p(\tau-t)} dt + \pi P_2 \int_{\tau}^{\tau_0} B(t)\, e^{-p(t-\tau)} dt, \quad \text{(IV.1.22)}$$

where

$$R_1 = 1 - \frac{1-k}{\bar{\mu}p}; \qquad R_2 = 1 + \frac{1-k}{\bar{\mu}p};$$

$$P_1 = \bar{\mu}p - (1-k); \; P_2 = \bar{\mu}p + (1-k);$$

$$p^2 = \frac{1-k}{\bar{\mu}}\left(\frac{1}{\bar{\mu}} - k\,\frac{C_1}{2}\right). \quad \text{(IV.1.23)}$$

From eq.(IV.1.23) it follows that the value $\bar{\mu}$ must satisfy the inequality

$$\bar{\mu} < \frac{2}{kc_1}.$$

The constants $\bar{c}_1$ and $\bar{c}_2$ in eqs.(IV.1.21) and (IV.1.22) are determined from the boundary conditions. Let there be given: the flux of long-wave radiation $F_1(0)$ that reaches the lower boundary of the cloud from below and the radiation flux $F_2(\tau_0)$ arriving at the upper boundary; then,

/141

$$\bar{c}_1 = \frac{1}{R_2}\left\{F_2(\tau_0) - \pi P_1 \int_0^{\tau_0} B(t)\, e^{-p(\tau_0-t)}\, dt\right\}, \quad \text{(IV.1.24)}$$

$$\bar{c}_2 = \frac{1}{R_2}\left\{F_1(0) - \pi P_1 \int_0^{\tau} B(t)\, e^{-pt} dt\right\}. \quad \text{(IV.1.25)}$$

The last expressions were obtained for the condition:

$$e^{-p\tau_0} \ll 1,$$

which, obviously, always exists in the case of real clouds because p is not small (see Table IV.3.1).

Section 2. Determination of the Mean Cosine and of the Fluxes on the Boundaries

We will determine the numerical value of $\bar{\mu}$ from the following considerations. In the inner layers of sufficiently dense clouds the derivative $dB/d\tau$ is small so that, at $p \approx 1$, the following relations are valid with a higher degree of accuracy:

$$\int_0^{\tau} B(t)\, e^{-p(\tau-t)}\, dt = \frac{1}{p} B(\tau), \quad \text{(IV.2.1)}$$

$$\int_{\tau}^{\tau_0} B(t)\, e^{-p(t-\tau)}\, dt = \frac{1}{p} B(\tau). \qquad \text{(IV.2.2)}$$

The possibility of using eqs.(IV.2.1) and (IV.2.2) is discussed in detail in Chapter VI, Sect.5. With the aid of these equalities, the relations (IV.1.21) and (IV.1.22) give for $\tau \approx \tau_0/2$

$$F_1(\tau) = \frac{\pi}{p}(P_1 + P_2) B(\tau) = F_2(\tau)$$

or [see eq.(IV.1.23)]

$$F_1(\tau) = 2\pi\bar{\mu} B(\tau) = F_2(\tau). \qquad \text{(IV.2.3)}$$

Therefore, in the inner layers of sufficiently dense clouds the ascending radiation flux is equal to the descending and the resultant flux $F_1 - F_2$ becomes zero. Measurements of radiation fluxes in a cloud made by V.L.Gayevskiy (Bibl.5) also showed that $F_1 - F_2 = 0$ at some distance from the edges. This means that the inner layers of the clouds are in a state of thermal dynamic equilibrium and that here the thermal radiation must be equal to the radiation of a black body for the given temperature. Hence,

$$F_1(\tau) = F_2(\tau) = \pi B(\tau) \quad \text{for} \qquad \text{(IV.2.4)}$$

and, therefore, $\bar{\mu} = \frac{1}{2}$.

We note that, according to eqs.(IV.1.17) and (IV.1.18), the value $\bar{\mu}$ is the average cosine of the polar angle of the direction of propagation of the long-wave radiation.

We will compute the radiation flux leaving the boundaries of the cloud. Equations (IV.1.21) - (IV.1.22) and (IV.1.24) - (IV.1.25) will then yield

$$F_1(\tau_0) = F_2(\tau_0)\frac{R_1}{R_2} + \pi\left[P_2 - P_1\frac{R_1}{R_2}\right]\int_0^{\tau_0} B(t)\, e^{-p(\tau_0 - t)}\, dt, \qquad \text{(IV.2.5)}$$

/142

$$F_2(0) = F_1(0)\frac{R_1}{R_2} + \pi\left[P_2 - P_1\frac{R_1}{R_2}\right]\int_0^{\tau_0} B(t)\, e^{-pt}\, dt. \qquad \text{(IV.2.6)}$$

The ratio R_1/R_2 obviously represents the wave albedo A of the cloud which is equal to

$$A = \frac{R_1}{R_2} = \frac{\bar{\mu}p - (1-k)}{\bar{\mu}p + (1-k)}. \qquad \text{(IV.2.7)}$$

The last formula together with eq.(IV.1.23) show that A depends on c_1, i.e., on the scattering indicatrix and on the ratio of scattering to absorption. It is obvious that A = 0 for pure absorption and A = 1 for pure scattering.

Equation (IV.2.7) can be applied to spectroscopic problems. In fact, knowing the wavelength and having assigned the mean droplet radius, the quanti-

ty C_1 can be determined from Table I.4.13 after which, from measurements of A, the quantity k can be computed, i.e., the ratio of scattering to absorption. If, conversely, k and A are known, then C_1 can be computed by means of eqs. (IV.2.7) and (IV.1.23) and the mean radius can be determined on the basis of Tables I.4.13 and I.4.14.

According to eq.(IV.2.7) the albedo does not depend on the optical thickness of the cloud and reflection from each boundary proceeds as if there had been no second boundary, i.e., as from an infinite medium. We recall that for visible radiation all real clouds that transmit light are finite. In the near-infrared region, clouds are infinite only in the middle portion of the widest absorption bands Ψ and Ω. Because of the strong absorption in the region of thermal radiation, all real clouds that are not too thin are semi-infinite, i.e., they do not transmit the radiation of the layer above the cloud to the layer below the cloud and vice versa.

Making use of the relations (IV.2.1) and (IV.2.2), eqs.(IV.2.5) and (IV.2.6) can be reduced to the form of

$$F_1(\tau_0) = AF_2(\tau_0) + 2\pi(1-A)\bar{\mu}B(\tau_0), \qquad \text{(IV.2.8)}$$

$$F_2(0) = AF_1(\tau_0) + 2\pi(1-A)\bar{\mu}B(0), \qquad \text{(IV.2.9)}$$

where $2\pi\bar{\mu}B(\tau)$ according to eq.(IV.2.3) represents the radiation flux of the cloud itself at arbitrary $\bar{\mu}$.

At $\bar{\mu} = \frac{1}{2}$, the radiation from the boundary obeys Kirchhoff's law with an accuracy satisfied by the equalities (IV.2.1) and (IV.2.2) at $\tau = 0$ and $\tau = \tau_0$. On the lower boundary, the equality (IV.2.2) may not hold because of the slow increase in τ with height (slow increase in liquid-water content), as a result of which the derivative $\frac{dB}{d\tau}$ may be great. As shown in Chapter VI, the temperature gradients are high on the upper boundary and $\frac{dB}{d\tau}$, generally speaking, may also be considerable. However, the evaluation made in Chapter VI shows that eq.(IV.2.1) holds in the vicinity of the upper boundary with satisfactory accuracy when the temperature gradients are of the order of not more than 10^0 per 100 m if the liquid-water content of the cloud is not less than 0.1 gm/m^3.

From eqs.(IV.2.8) and (IV.2.9) and from previous remarks it follows that the radiative heat exchange in both boundary layers of a sufficiently dense cloud proceeds independently and is determined only by the properties of these layers and of the adjoining portions of the atmosphere outside the cloud. Inside the cloud, there is no radiative long-wave heat exchange - the inflow of heat is equal to zero [see eq.(IV.2.3)]. If the non-radiative forms of heat exchange are excluded from consideration, it will be found that the cloud divides the atmosphere into two unconnected parts in each of which the thermal /143 state is determined by their own energy sources. In the layer below the clouds, such an "external source" is represented by the radiation of the Earth and to a

lesser extent by the inflow of heat from the sun in the near-infrared region. In the atmosphere above the clouds, there are no other radiative sources of heat aside from solar radiation, if the weak inflow of radiation from the stratosphere, discussed in Section 3 of Chapter I, is disregarded. Therefore, at night under conditions of radiation equilibrium, the atmosphere below the clouds should necessarily have a temperature almost equal to absolute zero. Actually, this does not occur because of the non-radiative forms of heat exchange.

Section 3. Spectral Albedo of Clouds in the Long-Wave Region

The calculation of the spectral albedo was based on the optical characteristics of clouds computed by K.S.Shifrin and is presented in Section 4 of Chapter I. Table I.4.10 gave the values of the attenuation factor in a cloud

$$\tilde{D}_{\Delta\lambda} = \tilde{\alpha}_{w,\,\Delta\lambda} + \tilde{\alpha}_{v,\,\Delta\lambda} + \tilde{\sigma}_{v,\,\Delta\lambda}, \qquad \text{(IV.3.1)}$$

as the mean for spectral intervals 4μ in the region ($4 \leq \lambda \leq 36\mu$), for a droplet radius of $a = 6.265\mu$ at various values of ρ_v and t°, while Table I.4.11 showed the values of the scattering coefficient $\sigma_{v,\Delta\lambda}$ for the same conditions. Knowing $\tilde{D}_{\Delta\lambda}$ and $\sigma_{v,\Delta\lambda}$ it is possible to compute first k and then the basic parameter of the problem, namely, the value of p which is determined from eq.(IV.1.23). Table IV.3.1 gives the results of computations of the spectral values p for $\bar{\mu} = \frac{1}{2}$; ρ_v = 0.1, 0.2, and 0.5 gm/m^3; t° = 0, -5, -10, and C_1 = 0.5, 3 (which, according to Table I.4.13 represents the extreme values of C_1). The Table shows that p does not assume values less than 0.7. At the same time, the quantity $\tilde{D}_{\Delta\lambda}$ in Table I.4.10 shows that τ_0 is greater than 9 at $\rho_v \geq 0.1$ gm/m^3, $H \geq 0.5$ km, where H is the thickness of the cloud layer. Therefore, the assumption $e^{-p\tau_0} \ll 1$ holds for real, sufficiently developed clouds. Table IV.3.1 indicates that, outside the spectral interval (8 - 12μ), the inequality $e^{-p\tau} \ll 1$ holds also for very thin clouds.

The results of computing the albedo A by means of eq.(IV.2.7) with the above input parameter are presented in Table IV.3.2* and in Fig.IV.3.1, which makes it possible to establish the following characteristics of the behavior of A as a function of λ, c_1, ρ_v, and t°.

1. The albedo depends largely on the shape of the indicatrix or, more precisely, on the quantity C_1. As shown by Tables I.4.13 and I.4.14, the value of C_1 fluctuates within the limits of 0.5 - 3. Table IV.3.2 indicates that, in this case, A is reduced two-fold. We note that, within the limits of the long-wave region of the spectrum, C_1 varies from 0.5 to 2.5.

2. It follows from Fig.IV.3.1 that A_λ depends on the wavelengths and

---

* The errors in the value of $D_{\Delta\lambda}$ (Bibl.6, see remark on p.42) were corrected in Tables IV.3.2 and IV.3.1.

increases greatly in the atmospheric "transparent window" (8 - 12μ).

The interval (8 - 12μ) is distinguished also by the peculiarity that the albedo here does not depend on the temperature or on the liquid-water content.

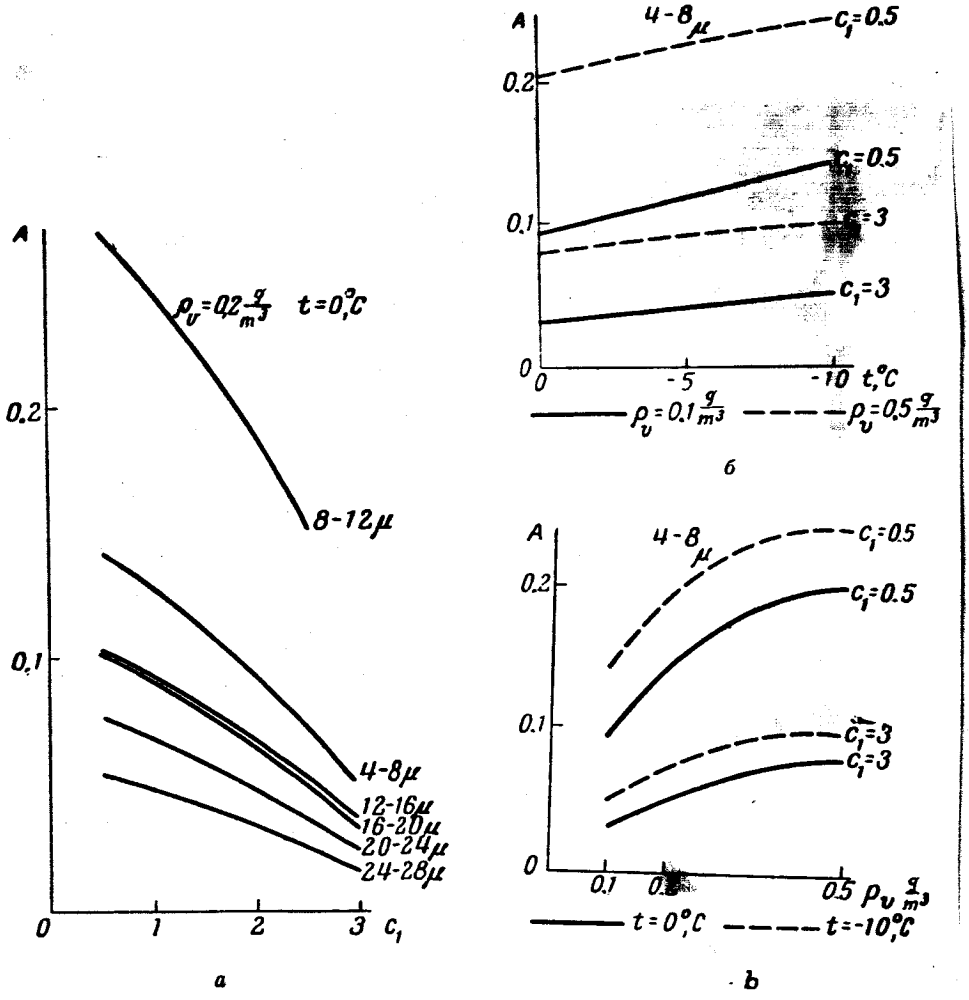

Fig.IV.3.1 Albedo as a Function of the Type of Indicatrix (a), of the Temperature (b), and of the Water Content (c)

Both these facts can be attributed to the smallness of $\tilde{\alpha}_v$ at ($8 \leq \lambda \leq 12\mu$). Here, the quantity k is determined by means of the formula

$$k = \frac{\tilde{\sigma}_v}{\tilde{\alpha}_v + \tilde{\sigma}_v} = \frac{\sigma_v}{\alpha_v + \sigma_v}$$

and hence, does not depend on t° and ρ_v. Moreover, the absorption of droplet /144 water in the transparent interval is relatively small; therefore, k increases

TABLE IV.3.1

/145

t, °C	ρ_v, g/m³			ρ_v, g/m³		
	0.1	0.2	0.5	0,1	0.2	0.5
			$c_1 = 0,5$			
	4—8 μ			16—20 μ		
0	1.58	1.42	1.22	1.61	1.55	1.50
—5	1.50	1.33	1.16	1.58	1.52	1.49
—10	1.41	1.26	1.12	1.55	1.50	1.48
	8—12 μ			20—24 μ		
0	1.06	1.06	1.06	1.75	1.65	1.55
—5	1.06	1.06	1.06	1.70	1.61	1.52
—10	1.06	1.06	1.06	1.65	1.57	1.46
	12—16 μ			24—28 μ		
0	1.54	1.54	1.55	1.83	1.74	1.67
—5	1.53	1.53	1.53	1.79	1.70	1.60
—10	1.53	1.53	1.53	1.74	1.66	1.57
			$c_1 = 3$			
	4—8 μ			16—20 μ		
0	1.40	1.18	0.94	1.43	1.35	1.28
—5	1.28	1.08	0.88	1.38	1.31	1.27
—10	1.18	0.99	0.83	1.34	1.29	1.25
	8—12 μ			20—24 μ		
0	0.70	0.70	0.70	1.62	1.49	1.35
—5	0.70	0.70	0.70	1.55	1.43	1.32
—10	0.70	0.70	0.70	1.48	1.37	1.23
	12—16 μ			24—28 μ		
0	1.33	1.33	1.32	1.74	1.62	1.46
—5	1.33	1.33	1.32	1.68	1.55	1.41
—10	1.33	1.33	1.32	1.61	1.49	1.37

TABLE IV.3.2

t, °C	ρ_v, g/m³			ρ_v, g/m³		
	0.1	0.2	0.5	0.1	0.2	0.5
			$c_1 = 0,5$			
	4—8 μ			16—20 μ		
0	0.09	0.14	0.2041	0.09	0.10	0.12
—5	0.12	0.17	0.2252	0.10	0.11	0.12
—10	0.14	0.19	0.2424	0.10	0.12	0.12

TABLE IV.3.2 (cont'd)

/146

t, °C	ρ_v, g/m³			ρ_v, g/m³		
	0.1	0.2	0.5	0.1	0.2	0.5
	8—12 μ			20—24 μ		
0	0.27	0.27	0.27	0.05	0.08	0.10
—5	0.27	0.27	0.27	0.07	0.09	0.11
—10	0.27	0.27	0.27	0.08	0.10	0.13
	12—16 μ			24—28 μ		
0	0.11	0.11	0.11	0.03	0.05	0.08
—5	0.11	0.11	0.11	0.04	0.06	0.09
—10	0.11	0.11	0.11	0.06	0.08	0.10
	$c_1 = 1$					
	4—8 μ			16—20 μ		
0	0.08	0.12	0.18	0.08	0.09	0.10
—5	0.10	0.14	0.20	0.08	0.10	0.11
—10	0.13	0.17	0.22	0.09	0.10	0.11
	8—12 μ			20—24 μ		
0	0.24	0.24	0.24	0.05	0.07	0.10
—5	0.24	0.24	0.24	0.06	0.08	0.10
—10	0.24	0.24	0.24	0.07	0.09	0.11
	12—16 μ			24—28 μ		
0	0.09	0.09	0.10	0.03	0.05	0.07
—5	0.09	0.09	0.10	0.04	0.06	0.08
—10	0.09	0.09	0.10	0.05	0.07	0.09
	$c_1 = 2$					
	4—8 μ			16—20 μ		
0	0.06	0.09	0.14	0.05	0.06	0.07
—5	0.07	0.11	0.15	0.06	0.07	0.08
—10	0.09	0.13	0.17	0.06	0.07	0.08
	8—12 μ			20—24 μ		
0	0.19	0.19	0.19	0.03	0.05	0.06
—5	0.19	0.19	0.19	0.04	0.05	0.07
—10	0.19	0.19	0.19	0.05	0.06	0.08
	12—16 μ			24—28 μ		
0	0.07	0.07	0.07	0.02	0.03	0.05
—5	0.07	0.07	0.07	0.03	0.04	0.06
—10	0.07	0.07	0.07	0.03	0.05	0.06

TABLE IV.3.2 (end)

t, °C	ρ_v, g/m³			ρ_v, g/m³		
	0.1	0.2	0.5	0.1	0.2	0.5
			$c_1 = 2.5$			
	4—8 μ			16—20 μ		
0	0.04	0.06	0.11	0.04	0.04	0.06
—5	0.06	0.08	0.12	0.04	0.06	0.06
—10	0.07	0.10	0.14	0.04	0.06	0.06
	8—12 μ			20—24 μ		
0	0.15	0.15	0.15	0.02	0.04	0.04
—5	0.15	0.15	0.15	0.03	0.04	0.06
—10	0.15	0.15	0.15	0.04	0.04	0.06
	12—16 μ			24—28 μ		
0	0.06	0.06	0.06	0.02	0.02	0.04
—5	0.06	0.06	0.06	0.02	0.03	0.04
—10	0.06	0.06	0.06	0.02	0.04	0.04

and thus also A.

4. In the other spectral intervals, as shown, for instance, in Fig.IV.3.1, the albedo increases with increasing liquid-water content and with decreasing temperature.

5. Outside the transparent window, the albedo seldom exceeds 15% if $t^\circ \geq -10^\circ$. Therefore, with an error not exceeding the indicated value, the cloud in the entire long-wave range, except for the segment 8 - 12μ, can be considered a black body if the water content is $\rho_v \geq 0.1$ gm/m³ and the temperature is $t^\circ \geq -10^\circ$.

Averaging the albedo by spectral intervals of 4μ yields too rough an estimate for a number of problems.

Table IV.3.3 gives the spectral albedo of clouds in the interval 8 - 12μ while Table IV.3.4 gives the interval 3 - 4μ for various temperatures and for a water content of 0.2 gm/m³. The computations of the albedo shown in Tables IV.3.3 and IV.3.4 were made with the data by K.S.Shifrin (Bibl.6). The two selected spectral intervals are of substantial interest in the problems of identifying clouds and of determining their temperature when observed from above. Because of the transparency of these intervals the radiation reaching /147 the observer is here determined principally by the temperature of the underlying surface, i.e., of the clouds or of the surface of the ground.

Having measured the radiation for $\lambda \approx 11 - 12\mu$ it is obviously possible to compute the temperature of the underlying surface by means of Planck's formula. A simultaneous measurement at $\lambda \approx 8\mu$ will permit to determine the nature of the underlying surface also in the case of low clouds, i.e., to separate the cloud according to the substantially smaller (by about 40%) radiation in this case.

Summarizing the above statements, we will first answer the question formulated by Gergen (Bibl.7): "What must be the thickness of the cloud for it to be considered a black body?" Our evaluations show that, strictly speaking, real

TABLE IV.3.3

λ, μ	8	9	10	11	12
A, %	41	18	12	5	5

TABLE IV.3.4

λ, μ	t, °C		
	−15	−5	+15
3	9	6	5
3.4	12	12	11
4	24	22	21

clouds are not black bodies anywhere in the long-wave region of the spectrum. Yet, clouds containing no less than 50μ of liquid-water*, i.e., essentially all real clouds, radiate according to Kirchhoff's law if the temperature gradient at the boundary does not exceed $10^{\circ}/100\mu$ (see Chapter VI).

The albedo of a cloud reaches a high value only in the region of the "atmospheric window" (8 - 12μ) and at $\lambda \approx 4\mu$. Outside of this region, the albedo fluctuates within the limits of 5 - 15% at a temperature of $t^{\circ} \geq -10^{\circ}$. Subject to such an error, we can thus consider a cloud to be a black body in the wavelength intervals of (4 - 8μ) and $\lambda \gg 11\mu$. /148

An evaluation of the "degree of blackness" of clouds was given by MacDonald (Bibl.8). The paper poses the problem of improving and developing, on the basis of recent data, the views of Brent (Bibl.9) who considered a cloud to be "black" in the entire long-wave region of the spectrum. It seems to us, however, that the work was not done on an up-to-date level and contains erroneous premises. Primarily, the author does not take into account the basic difference of absorption in a scattering medium as compared with a non-scattering medium. Actually, at the same absorption coefficient, the absorption in the second case approaches 100% with an increase in content of matter or in optical

* We call the value $\frac{\rho_0 H}{\rho_0}$ the liquid-water content.

thickness. In the presence of scattering, the absorptivity of the medium never reaches 100% and approaches, at the limit, the value 1 - A, where A is the albedo of the semi-infinite layer. Further, in the same paper (Bibl.8), the absorption coefficients of a continuous water layer are used, which was unnecessary (at $\lambda \gg 4\mu$) since the data by K.S.Shifrin for droplets were available, a fact apparently not known to the author (Bibl.8). Finally, on the basis of several computational data by Kaugen on the absorption of droplets [see (Bibl.8) and Chapter I, Sect.4] MacDonald made an attempt to establish the degree of blackness of a droplet cloud as compared with the blackness of the layer. He arrived at the erroneous conclusion that the absorptivity of a cloud in both cases would be greater only because of the difference in the value of the absorption coefficients. Since, in the latter case, the absorption increases also because of the elongation of the radiation path as a result of scattering, the author draws the following incorrect conclusion: Inasmuch as a continuous water layer of 100μ absorbs all of the incident radiation, a real cloud which, as a rule, contains such a quantity of water will certainly have this property, i.e., will radiate like a black body. This conclusion is incorrect both because of the above-shown difference between the absorption processes in scattering and non-scattering media and also because of the fact that, according to Table I.4.12, the absorption coefficient of droplet water for different wavelengths can be both greater and smaller than in the case of a continuous volume.

BIBLIOGRAPHY

1. Chu, C.M., Clark, F.C., and Churchill, S.M.: Tables of Angular Distribution Coefficients for Light Scattering by Spheres. Engineering Research Inst. University of Michigan, 1957.
2. Kuznetsov, Ye.S.: On the Question of Approximate Equations of Radiant Energy Transfer in a Scattering and Absorbing Medium (K voprosu o priblizhennykh uravneniyakh perenosa luchistoy energii v rasseivayushchey i pogloshchayushchey srede). Dokl. Akad. Nauk SSSR, Nos.7-8, 1942.
3. Yudin, M.I. and Kogan, N.R.: Approximate Solutions of the Equation of Scattering of Light (Priblizhennoye resheniye uravneniya rasseyaniya sveta). Izv. Akad. Nauk SSSR, ser. geofiz., No.8, 1956.
4. Atroshenko, V.S., Glazova, K.S., Malkevich, M.S., and Feygel'son, Ye.M.: Computations of Brightness of Light in Anisotropic Scattering, Part II (Raschet yarkosti sveta pri anizotropnom rasseyanii, Ch.II). Trudy Inst. Fiz. Atmosf., No.3, 1962.
5. Gayevskiy, V.L.: The Profile of Fluxes of Long-Wave Radiation in Clouds (Profil' potokov dlinnovolnovoy radiatsii v oblakakh). Compendium "Investigation of Clouds, Precipitation, and Lightning Electricity". Izd. Akad. Nauk SSSR, 1961.
6. Shifrin, K.S.: Transfer of Thermal Radiation in Clouds (Perenos teplovoy radiatsii v oblakakh). Trudy GGO (Main Geophysical Observatory), No.46, 1955.
7. Gergen, J.L.: Black-Ball Observations and the Radiation Chart. J. Met., Vol.15, 1958.
8. MacDonald, J.E.: Absorption of Atmospheric Radiation by Water Films and Water Clouds. J. Met., Vol.17, No.2, 1960.

9. Brent, D.: Physical and Dynamic Meteorology (Fizicheskaya i dinamicheskaya meteorologiya). Gidrometeoizdat, 1938.

CHAPTER V

/149

RADIATIVE EQUILIBRIUM IN AN ATMOSPHERE CONTAINING A CLOUD LAYER

In this Chapter, we investigate the thermal behavior of the atmosphere containing a cloud layer. Unlike in the other Chapters, the subject here is not the cloud but the ambient space and the changes introduced by the cloud in the thermal state of the latter. Only radiative heat exchange is discussed here since the principal thermal effect of the cloud is determined by its radiation properties.

Section 1. Basic Relations

An infinite homogeneous horizontal cloud layer of finite thickness divides the atmosphere into two layers, in each of which the heat exchange under conditions of radiative equilibrium is determined by the following equation (see Chapter I, Sect.2):

$$Q_s^*(z)+\int_{\lambda_1}^{\lambda_2}\tilde{\alpha}_\lambda(z)\int I_\lambda(z,r)\,d\omega\,d\lambda=4\pi\int_{\lambda_1}^{\lambda_2}\tilde{\alpha}_\lambda(z)\,B_\lambda(T)\,d\lambda, \qquad (V.1.1)$$

where $Q_s(z)$ is the inflow of heat due to absorption of solar radiation. According to the rough model of the absorption spectrum of a cloudless atmosphere constructed in Chapter I, Section 5, we will here divide the spectral intervals ($\lambda_1 = 3\mu$, $\lambda_2 = 40\mu$) into three parts: (R_1, R_2, R_3) to which correspond small, medium, and large absorption coefficients.

It is known [see for instance (Bibl.1)] that, in the region of large absorption coefficients, the long-wave transfer exerts no influence on the temperature; the absorbed energy is equal to the radiant energy:

$$\int_{R_3}\tilde{\alpha}_\lambda\int I_\lambda d\omega\,d_\lambda=4\pi\int_{R_3}\tilde{\alpha}_\lambda B_\lambda(T)\,d\lambda. \qquad (V.1.2)$$

This latter relation will not exist near the upper boundary of the atmosphere since a medium of zero absorption is located on the other side of the boundary. Near the cloud, eq.(V.1.2) is valid because of the large absorptivity of the latter.

In accordance with eq.(V.1.2), the integration along the wavelength in eq.(V.1.1) extends only over the interval $R_1 + R_2$.

As seen in Chapter I, Section 5, the interval R_1 consists basically of the wavelength region (8 - 12μ), the absorption coefficient α_1 is here equal to 0.2 cm^2/gm, the interval R_2 can be considered to be approximately equal to

(12 - 14μ) and (16 - 17μ) and can be given an absorption coefficient of α_2 = /150
= 4 cm^2/gm. If we introduce

$$I_{1,j} = \int_{R_j} I_\lambda(z, r)\, d\lambda \quad \text{at} \quad 0 \leqslant \theta \leqslant \frac{\pi}{2},$$

$$I_{2,j} = \int_{R_j} I_\lambda(z, r)\, d\lambda \quad \text{at} \quad \frac{\pi}{2} \leqslant \theta \leqslant \pi,$$

$$B_j = \int_{R_j} B_\lambda(T)\, d\lambda,$$

$$\tau_j = \alpha_j \int_0^z \rho_w(z)\, dz = \alpha_j m, \qquad j = 1, 2,$$

then eq.(V.1.1) can be written in the form of

$$Q_s(z) + \sum_{j=1}^{2} \tilde{\alpha}_j \left[\int_+ I_{1,j}(\tau_j, r)\, d\omega + \int_+ I_{2,j}(\tau_j, r)\, d\omega \right] = 4\pi \sum_{j=1}^{2} \tilde{\alpha}_j B_j(T). \qquad \text{(V.1.3)}$$

The radiation intensities $I_{1,j}$ and $I_{2,j}$ are determined from transfer equations of the following form [see eq.(I.3.15)]:

$$\cos\theta \frac{\partial I_{1,j}}{\partial \tau_j} = B_j(\tau_j) - I_{1,j}(\tau_j, r), \qquad \text{(V.1.4)}$$

$$-\cos\theta \frac{\partial I_{2,j}}{\partial \tau_j} = B_j(\tau_j) - I_{2,j}(\tau_j, r). \qquad \text{(V.1.5)}$$

Considering separately the layer below the cloud, the cloud layer itself, and the layer above the cloud, we will denote the quantities referring to the layer below the cloud by the subscript 1; those referring to the layer above the cloud, by the subscript 2; and those referring to the cloud layer proper, by the subscript 0.

With the given boundary conditions, eqs.(V.1.4) and (V.1.5) can be solved for $I_{1,j}(\tau_j, r)$ and $I_{2,j}(\tau_j, r)$. If the intensity of the ascending radiation on the lower boundary of the layer $I_{1,j}^{(i)}(0, r)$ and the intensity of the descending radiation on the upper boundary of the layer $I_{2,j}^{(i)}(\tau_{i,j}, r)$ [here $\tau_{i,j}$ is the total optical thickness of the i^{th} layer in the j^{th} spectral interval; below, we will not use the subscripts j in the quantities $\tau_{i,j}$] are known in each layer, then the solution of eqs.(V.1.4) and (V.1.5) in the i^{th} layer would be represented in the following form [see eqs.(I.2.37) - (I.2.38)]:

$$I_{1,j}^{(i)}(\tau, r) = I_{1,j}^{(i)}(0, r)\, e^{-\tau \sec\theta} + \sec\theta \int_0^\tau B_j^{(i)}(t)\, e^{-\sec\theta(\tau - t)} dt, \qquad \text{(V.1.6)}$$

$$I_{2,j}^{(i)}(\tau, r) = I_{2,j}^{(i)}(\tau_i, r)\, e^{-\sec\theta(\tau_i-\tau)} + \sec\theta \int_{\tau}^{\tau_i} B_j^{(i)}(t)\, e^{-\sec\theta(t-\tau)} dt. \qquad (V.1.7)$$

We will prescribe the following boundary conditions:

1) for z = 0

$$I_{1,j}^{(1)}(0, r) = B_{e,j}, \qquad (V.1.8)$$

where $B_{e,j}$ is the radiation of the underlying surface proper in the j^{th} wave- /151
length interval, which is assumed to be known and equal to the radiation of a black body at the temperatures of the lower boundary of the atmosphere;

2) for $z = z_1 (\tau = \tau_1)$

$$I_{2,j}^{(1)}(\tau_1, r) = I_{2,j}^{(0)}(0, r); \qquad (V.1.9)$$

3) for $z = z_2 (\tau = \tau_0)$

$$\sum_{j=1}^{2} F_{1,j}^{(2)}(0) = \sum_{j=1}^{2} F_{1,j}^{(0)}(\tau_0) + \pi q, \qquad (V.1.10)$$

where πq is heat flow from the cloud due to non-radiation factors. In view of the fact that the cloud isolates the layer below it from the layer above it, as shown in Chapter IV, Section 2, it is not permissible to assume a condition of radiative equilibrium in the cloud. In this case, at a sufficient optical thickness of this cloud, a temperature of absolute zero will prevail in the atmosphere above the clouds at night.

Condition (V.1.10), with the additional assumption

$$I_{1,j}^{(2)}(0, r) = \frac{1}{\pi} F_{1,j}^{(2)}(0) \qquad (V.1.11)$$

will yield

$$\sum_{j=1}^{2} I_{1,j}^{(2)}(0) = \frac{1}{\pi} \sum_{j=1}^{2} F_{1,j}^{(0)}(\tau_0) + q. \qquad (V.1.12)$$

For simplicity, we assume on the upper boundary of the atmosphere $z = \infty$ $(\tau = \tau_2)$ the following condition:

$$I_{2,j}^{(2)}(\tau_2, r) = 0. \qquad (V.1.13)$$

In eqs.(V.1.8) - (V.1.13) z is counted from the Earth's surface; z_1 and z_2 correspond to the lower and upper boundaries of the cloud; τ_i in each layer is counted from its lower boundary.

Substituting the boundary conditions in eqs.(V.1.6) and (V.1.7) we obtain

$$I_{1,j}^{(1)}(\tau, r) = B_{e,j} e^{-\sec\theta\tau} + \sec\theta \int_{0}^{\tau} B_j^{(1)}(t)\, e^{\sec\theta(\tau-t)} dt, \qquad (V.1.14)$$

$$I_{2,j}^{(1)}(\tau, r) = I_{2,j}^{(0)}(0, r)\, e^{-\sec\theta(\tau_1-\tau)} + \sec\theta \int_{\tau}^{\tau_1} B_j^{(1)}(t)\, e^{-\sec\theta(t-\tau)}\, dt, \tag{V.1.15}$$

$$I_{1,j}^{(2)}(\tau, r) = I_{1,j}^{(2)}(0, r)\, e^{-\sec\theta\tau} + \sec\theta \int_{0}^{\tau} B_j^{(2)}(t)\, e^{-\sec\theta(\tau-t)}\, dt, \tag{V.1.16}$$

$$I_{2,j}^{(2)}(\tau, r) = \sec\theta \int_{\tau}^{\tau_2} B_j^{(2)}(t)\, e^{-\sec\theta(t-\tau)}\, dt. \tag{V.1.17}$$

The relations (V.1.14) - (V.1.17), together with eq.(V.1.12) show that the influence of the cloud on the radiation balance of the medium outside the cloud is produced by $F_{1,j}^{(0)}(\tau_0)$, $I_{2,j}^{(0)}(0, r)$ and q. In determining these quantities (except q), we make use of the results of Chapter IV with the additional assumption

$$I_{2,j}^{(0)}(0, r) = \frac{1}{\pi} F_{2,j}^{(0)}(0). \tag{V.1.18}$$

We note that the relation (V.1.18) as well as eq.(V.1.11) indicate isotropy /152 of the radiation leaving the boundaries of the cloud.

According to eqs.(IV.2.7) and (IV.2.8), we obtain for $\bar{\mu} = 1/2$

$$F_{1,j}^{(0)}(\tau_0) = A_j F_{2,j}^{(2)}(0) + \pi(1 - A_j) B_j^{(0)}(\tau_0), \tag{V.1.19}$$

$$F_{2,j}^{(0)}(0, r) = A_j F_{1,j}^{(1)}(\tau_1) + \pi(1 - A_j) B_j^{(0)}(0). \tag{V.1.20}$$

The values of $F_{1,j}^{(1)}(\tau_1)$ and $F_{2,j}^{(2)}(0)$ in the last equation can be found from eqs.(V.1.14) and (V.1.17). Multiplying both sides of eqs.(V.1.14) and (V.1.17) by the cosine θ and integrating for r over the boundaries of the hemisphere, we obtain

$$F_{1,j}^{(1)}(\tau_1) = 2\pi \left[B_{e,j} E_3(\tau_1) + \int_0^{\tau_1} B_j^{(1)}(t)\, E_2(\tau_1 - t)\, dt \right], \tag{V.1.21}$$

$$F_{2,j}^{(2)}(0) = 2\pi \int_0^{\tau_2} B_j^{(2)}(t)\, E_2(t)\, dt. \tag{V.1.22}$$

Substituting these expressions of flux in eqs.(V.1.19) and (V.1.20), we find

$$F_{1,j}^{(0)}(\tau_0) = 2\pi A_j \int_0^{\tau_2} B_j^{(2)}(t)\, E_2(t)\, dt + \pi(1 - A_j) B_j^{(0)}(\tau_0), \tag{V.1.23}$$

$$F_{2,j}^{(0)}(0) = 2\pi A_j \left[B_{e,j} E_3(\tau_1) + \int_0^{\tau_1} B_j^{(1)}(t)\, E_2(\tau_1 - t)\, dt \right] + \pi(1 - A_j) B_j^{(0)}(0). \tag{V.1.24}$$

The equality (V.1.23) together with eq.(V.1.12) yields

$$\sum_{j=1}^{2} I_{1,j}^{(2)}(0) = q + \sum_{j=1}^{2} \left\{ 2A_j \int_0^{\tau_2} B_j^{(2)}(t) E_2(t)\, dt + (1 - A_j) B_j^{(0)}(\tau_2) \right\}. \quad \text{(V.1.25)}$$

Here, $I_{2,j}^{(0)}(0, r)$ is determined from eq.(V.1.24) together with eq.(V.1.18).

We shall now turn to the equation of the heat balance (V.1.3) and will transform it by utilizing (V.1.15) - (V.1.17). Having made the usual transformation (see Chapter, Sect.2) we shall obtain the following expressions of the radiation balance in the atmosphere under and above the cloud.

$$Q_e^{(1)}(\tau) + 2\pi \sum_{j=1}^{2} \tilde{\alpha}_j \left\{ B_{e,j} E_2(\tau) + \int_0^{\tau_1} B_j^{(1)}(t) E_1(|\tau - 1|)\, dt + \right.$$
$$\left. + X_j E_2(\tau_1 - \tau) \right\} = 4\pi \sum_{j=1}^{2} \tilde{\alpha}_j B_j^{(1)}(\tau), \quad \text{(V.1.26)}$$

$$Q_e^{(2)}(\tau) + 2\pi \sum_{j=1}^{2} \tilde{\alpha}_j \left\{ Y_j E_2(\tau) + \int_0^{\tau_2} B_j^{(2)}(t) E_1(|\tau - t|)\, dt \right\} = 4\pi \sum_{j=1}^{2} \tilde{\alpha}_j B_j^{(2)}(\tau); \quad \text{(V.1.27)}$$

Here X_j and Y_j are constants equal to $I_{2,j}^{(1)}(0, r)$ and $I_{1,j}^{(2)}(0, r)$, respectively, which are determined by means of eqs.(V.1.25) and (V.1.24), taking into account eq.(V.1.18). Equations (V.1.26) and (V.1.27) make it possible to determine the radiation temperature of the atmosphere, taking account of the following factors: /153

1) presence of a cloud which absorbs and scatters long-wave radiation;
2) interaction between long-wave heat exchange and heating due to absorption of solar radiation;
3) presence, in the absorption spectrum of the air, of regions with weak, medium, and strong absorption.

We will solve several model problems, to clarify the effect of each factor.

Section 2. Night Conditions; the "Gray" Atmosphere

First, we will consider the night conditions ($Q_e = 0$) but disregard for the moment the so-called "selectivity" of absorption, i.e., we will introduce in the interval $R_1 + R_2$, the mean absorption coefficient equal to $\tilde{\alpha}_{av} = 1$ cm^2/gm [see (Bibl.2)].

In this case, eqs.(V.1.26) and (V.1.27) will readily yield

$$B^{(1)}(\tau) = \frac{1}{2} B_e E_2(\tau) + \frac{1}{2} \int_0^{\tau_1} B^{(1)}(t) E_1(|\tau - t|)\, dt + \frac{1}{2} X E_2(\tau_1 - \tau), \quad \text{(V.2.1)}$$

$$B^{(2)}(\tau) = \frac{1}{2} Y E_2(\tau) + \frac{1}{2} \int_0^{\tau_2} B^{(2)}(t) E_1(|\tau - t|)\, dt; \quad \text{(V.2.2)}$$

where $B^{(i)}(\tau)$, X, and Y are integrals of the corresponding spectral quantities for the interval $R_1 + R_2$.

For solving eq.(V.2.1), we will introduce the unknown functions $\overline{B}^{(1)}(\tau)$ and $\overline{\overline{B}}^{(1)}(\tau)$ which satisfy the equations

$$\overline{B}^{(1)}(\tau) = \frac{1}{2}E_2(\tau) + \frac{1}{2}\int_0^{\tau_1} \overline{B}^{(1)}(t)\, E_1(|\tau - t|)\, dt, \tag{V.2.3}$$

$$\overline{\overline{B}}^{(1)}(\tau) = \frac{1}{2}E_2(\tau_1 - \tau) + \frac{1}{2}\int_0^{\tau_1} \overline{\overline{B}}^{(1)}(t)\, E_1(|\tau - t|)\, dt. \tag{V.2.4}$$

Let us assume that eqs.(V.2.3) and (V.2.4) are solved. The function

$$B^{(1)}(\tau) = B_e\overline{B}^{(1)}(\tau) + X\overline{\overline{B}}^{(1)}(\tau) \tag{V.2.5}$$

apparently satisfies the initial equation (V.2.1). This leaves the unknown constant X to be determined by means of eq.(V.1.24). If the temperature on the lower boundary of the cloud is considered to be continuous, i.e.,

$$B^{(0)}(0) = B^{(1)}(\tau_1) = B_e\overline{B}^{(1)}(\tau_1) + X\overline{\overline{B}}^{(1)}(\tau_1),$$

then we shall obtain from eq.(V.1.24)

$$X = 2A\left[B_eE_3(\tau_1) + B_e\int_0^{\tau_1} B^{(1)}(t)\, E_2(\tau_1 - t)\, dt + \right.$$

$$\left. + X\int_0^{\tau_1} \overline{\overline{B}}^{(1)}(t)\, E_2(\tau_1 - t)\, dt\right] + (1 - A)\left[B_e\overline{B}^{(1)}(\tau_1) + X\overline{\overline{B}}^{(1)}(\tau_1)\right]$$

or

/154

$$X = B_e\,\frac{2AE_3(\tau_1) + 2A\int_0^{\tau_1} B^{(1)}(t)\, E_2(\tau_1 - t)\, dt + (1 - A)\,\overline{B}^{(1)}(\tau_1)}{1 - 2A\int_0^{\tau_1} \overline{\overline{B}}^{(1)}(t)\, E_2|\tau_1 - t)\, dt - (1 - A)\,\overline{\overline{B}}^{(1)}(\tau_1)}. \tag{V.2.6}$$

These relations yield the sought function $B^{(1)}(\tau)$ without difficulty. Next, let us add eqs.(V.2.3) and (V.2.4) termwise. It is easy to verify that $\overline{B}^{(1)}(\tau) + \overline{\overline{B}}^{(1)}(\tau) = 1$ is the solution of the obtained equation and also is the unique solution, as follows from the general theory of Fredholm integral equations of the second kind.

By substituting, in eq.(V.2.6),

$$\overline{\overline{B}}^{(1)}(\tau) = 1 - \overline{B}^{(1)}(\tau), \tag{V.2.7}$$

we will find that, for any A,

$$X = B_e, \tag{V.2.8}$$

after which eq.(V.2.5) will yield

$$B^{(1)}(\tau) = B_e. \qquad \text{(V.2.9)}$$

Therefore, if the cloud layer is of sufficient thickness so that its upper boundary radiates according to Kirchhoff's law, a constant temperature equal to the temperature of the Earth's surface sets up at night in the atmosphere above the cloud, for the condition of radiative equilibrium.

The problem of determining the radiation temperature of the layer above the cloud, according to eqs.(V.2.2) and (V.1.25), reduces to a solution of the equation

$$\bar{B}^{(2)}(\tau) = \frac{1}{2} E_2(\tau) + \frac{1}{2}\int_0^{\tau_2} \bar{B}^{(2)}(t)\, E_1(|\tau - t|)\, dt \qquad \text{(V.2.10)}$$

and to a determination of Y from the relation

$$Y = \frac{q}{1 - 2A\int_0^{\tau_2} \bar{B}^{(2)}(t)\, E_2(t)\, dt - (1-A)\,\bar{B}^{(2)}(0)}. \qquad \text{(V.2.11)}$$

If $\bar{B}^{(2)}(\tau)$ and Y are known, the sought function $\bar{B}^{(2)}(\tau)$ will have the form

$$B^{(2)}(\tau) = Y\bar{B}^{(2)}(\tau). \qquad \text{(V.2.12)}$$

We note that, in deriving the relation (V.2.11), the condition of temperature continuity on the upper boundary of the cloud was used:

$$B^{(0)}(\tau_0) = B^{(2)}(0) = Y\bar{B}^{(2)}(0).$$

At A = 0, the equality (V.2.11) becomes

$$Y = \frac{q}{1 - \bar{B}^{(2)}(0)}. \qquad \text{(V.2.13)}$$

Equations (V.2.11) or (V.2.13) show that in the case of radiative equilibrium in the clouds, at q = 0, we obtain Y = 0 and $B^{(2)}(\tau) \equiv 0$, i.e., absolute zero temperature is established above the cloud. /155

An approximate solution of eq.(V.2.10) can be obtained on replacing it by an algebraic system of the form

$$\bar{B}_k^{(2)} = \frac{1}{2} E_2(\tau_k) + \frac{1}{2}\sum_{j=1}^{n} B_j^{(2)} \int_{\tau_{j-1}}^{\tau_j} E_1(|\tau_k - t|)\, dt \qquad k;\ j = 1, \ldots, n; \qquad \text{(V.2.14)}$$

Here

$$\bar{B}_k^{(2)} = \bar{B}^{(2)}(\tau_k);\ \tau_0 = 0; \qquad \tau_n = \tau_2.$$

If we compute the integrals

$$\int_{\tau_{j-1}}^{\tau_j} E_1(|\tau_k - t|)\,dt,$$

then the system (V.2.14) will become

$$2\bar{B}_k^{(2)} = E_2(\tau_k) + \sum_{j=1}^{k} \bar{B}_j^{(2)} [E_2(\tau_k - \tau_j) - E_2(\tau_k - \tau_{j-1})] + \\ + \sum_{j=k+1}^{n} \bar{B}_j^{(2)} [E_2(\tau_{j-1} - \tau_k) - E_2(\tau_j - \tau_k)]. \qquad (V.2.15)$$

The solution of eq.(V.2.15) was obtained with the following values of the problem parameters. The distribution of moisture with height is given by

$$\rho_w(z) = \rho_w(0) e^{-az}, \qquad (V.2.16)$$

where $a = 0.45\ km^{-1}$.

For $\rho_w(0) = 6\ gm/m^3$, we have $z_1 = 1$ km, $z_2 = 1.5$ km. From this, we obtain $m_1 = 0.5\ gm/cm^2$ and $m_2 = 0.65\ gm/cm^2$, where m_1 and m_2 are the water-vapor content in the atmosphere above and below the cloud, respectively. For $\alpha = 1\ cm^2/gm$, we obtain further: $\tau_1 = 0.5$ and $\tau_2 = 0.65$. The conversion of the radiation function of a black body B(T) from the integral over the interval $R_1 + R_2$ to the temperature was made by means of the following formula:

$$B(T) = 0.146\,[\bar{B}_1(T) + \bar{B}_2(T)] \qquad (V.2.17)$$

with $\bar{B}_1(T)$ and $\bar{B}_2(T)$ taken from the graph in Fig.I.5.3; here B(T) is expressed in $cal/cm^2 \cdot min$. The value of the non-radiative inflow of heat πq from the cloud upward, and the albedo A of the cloud are also given. Let us assume that πq is the thermal flux due to turbulent mixing, i.e.,

$$\pi q = C_p \rho k \frac{d\theta}{dz},$$

where θ is the potential temperature. It is known (see Chapters VI or VII) that

$$\frac{d\theta}{dz} = \gamma_a + \frac{dT}{dz},$$

where $\gamma_a = 10$ deg/km. Hence, at the usual temperature gradient in the clouds, we have $\frac{d\theta}{dz} \approx 5$ deg/km. Let us assume that $k = 10^5\ cm^2/sec$, $\rho = 1.3 \times 10^{-3}$

gm/cm^3 and C_p = 0.24 cal/deg · gm. This will yield πq = 0.1 cal/cm^2 · min. /156

The integral albedo of the cloud in the spectral interval $R_1 + R_2$ was determined as the means of the albedo in the intervals (8 - 12μ) and (12 - 16μ), computed in Chapter IV. At a water content of the cloud of ρ_v = 0.2 gm/m^3 and at a temperature of 0°C, the mean albedo, according to Table IV.3.2, was 0.15. We mention that, after solving eq.(V.2.10), it is possible to determine the functions $B^{(2)}(\tau)$ and thus also the temperature distribution in the atmosphere below the cloud, for any values of A and q. The situation is different when a moisture of $\rho_w(z)$ is prescribed. The problem is solved for the prescribed form of the function $\rho_w(z)$; as soon as this value changes, eq.(V.2.10) or - more accurately - the system of equations (V.2.15) must be solved anew.

Section 3. Radiative Equilibrium by Day

The equations of the radiation balance [eqs.(V.1.26) and (V.1.27)] which were written for day conditions contain addends $Q_s^{(i)}$ (i = 1; 2) that represent the influx of heat from the sun to the atmosphere below and above the cloud, respectively.

In Chapter III we showed that $Q_s^{(1)}$ is small; the atmosphere below the cloud is in about the same condition as at night, with respect to the transfer of infrared solar radiation. Therefore, only eq.(V.1.27), i.e., the above-cloud layer under daytime conditions, need be considered.

The insolation per unit volume is represented in the form of

$$Q_s(z) = \rho_w(z) \int_{\lambda_0}^{\lambda_1} \alpha_{\lambda, w} \int I_{s, \lambda} \, d\omega \, d\lambda, \qquad (V.3.1)$$

where $\lambda_0 \approx 0.7\mu$, $\lambda_1 = 2.5\mu$, $I_{s,\lambda}$ represents the infrared solar radiation (direct and scattered). The value Q_s was determined by Ye.S.Kuznetsov (Bibl.3), taking into account all water-vapor bands in the near-infrared region of the spectrum (see Chapter I, Sect.5). This author (Bibl.3) gives the values of $Q_{\Delta\lambda}$ for absorption in a separate band. We will confine our calculation to the relatively rough formula proposed by Ye.S.Kuznetsov, which determines the total inflow of heat due to all absorption bands. Namely,

$$\begin{aligned}\frac{1}{\pi S} Q_s(m) \doteq \rho_w \{ & \gamma\alpha e^{-(\alpha+\sigma)\sec\zeta\,(m^*-m)} + (1-\gamma)\beta e^{-(\beta+\sigma)\sec\zeta\,(m^*-m)} + \\ & + 2A\cos\zeta\gamma\alpha e^{-(\alpha+\sigma)\sec\zeta m^*} E_2[(\alpha+\sigma)m] + \\ & + 2A\cos\zeta(1-\gamma)\beta e^{-(\beta+\sigma)\sec\zeta m^*} E_2[(\beta+\sigma)m]\}. \end{aligned} \qquad (V.3.2)$$

Here α, β, γ are the parameters of the interpolation formula, of the following form (see Chapter I, Sect.5):

$$P(m) = \gamma e^{-\alpha m} + (1-\gamma) e^{-\beta m}, \qquad (V.3.3)$$

which describes the transmission function of the entire infrared region of the water-vapor spectrum P(m), where m is the water-vapor content (in gm/cm^2). According to Kuznetsov (Bibl.3) $\alpha = 2.48$; $\beta = 0.36$, $\gamma = 0.192$; and σ is the scattering coefficient integrated for the infrared region of the spectrum which, according to Ye.S.Kuznetsov's data, is equal to 0.5 - 0.6 cm^2/gm; $\pi S = 0.83$ cal/cm^2·min is the solar constant for the infrared region of the spectrum; A is the albedo of the underlying surface. In our case where only the atmosphere below the cloud is considered, A represents the infrared albedo of the cloud layer.

According to the data in Chapter III, within the limits of the infrared absorption band A_e is 0.6 - 0.7 for $\zeta = 30 - 60^\circ$, $\tau_0 = 30$.

Equation (V.3.2) is not too accurate, but, in general terms, correctly reproduces the behavior of the quantity $Q_s(m)$ and leads to errors not exceeding about 20%. The main error source is the rough presentation of the integral absorption function by eq.(V.3.3). Moreover, the relation (V.3.2) does not take account of the absorption of scattered radiation; however, the resultant error is not great. /157

The result of computation of $Q_s^{(2)}(m)$ by means of eq.(V.3.2), at the above moisture distribution, is presented in Table V.3.1. Here it is assumed that $A = 0.4$, $\sigma = 0.5$ cm^2/gm, and $\zeta = 60^\circ$.

TABLE V.3.1

z, km	m, g/cm^2	$\frac{1}{4\pi\rho_w} Q^{(2)}(m)$	z, km	m, g/cm^2	$\frac{1}{4\pi\rho_w} Q^{(2)}(m)$
1.5	0	0.00184	3.6	0.39	0.00680
2.0	0.13	0.00238	5.1	0.52	0.0214
2.7	0.26	0.00420		0.65	0.0275

Retaining the "gray" model of the spectrum in the long-wave region, eq.(V.1.27) reduces under daytime conditions to the form of

$$\frac{1}{4\pi\rho_w} Q_s^{(2)}(\tau) + \frac{1}{2} Y E_2(\tau) + \frac{1}{2}\int_0^{\tau_1} B^{(2)}(t)\, E_1(|\tau - t|)\, dt = B^{(2)}(\tau). \qquad (V.3.4)$$

We will again introduce the auxiliary functions $\bar{B}^{(2)}(\tau)$ and $\bar{\bar{B}}^{(2)}(\tau)$ which, respectively, satisfy the equations

$$\frac{1}{4\pi\rho_w} Q_\lambda^{(2)}(\tau) + \frac{1}{2}\int_0^{\tau_1} \bar{B}^{(2)}(t)\, E_1(|\tau - t|)\, dt = \bar{B}^{(2)}(\tau) \qquad (V.3.5)$$

and

$$\frac{1}{2}E_2(\tau)+\frac{1}{2}\int_0^{\tau_2}\overline{\overline{B}}^{(2)}(t)\,E_1(|\tau-t|)\,dt=\overline{\overline{B}}^{(2)}(\tau). \tag{V.3.6}$$

Then, the function $B^{(2)}(\tau)$ which is equal to

$$B^{(2)}(\tau)=\overline{B}^{(2)}(\tau)+Y\overline{\overline{B}}^{(2)}(\tau), \tag{V.3.7}$$

satisfies eq.(V.3.4). The constant Y is determined from the relation

$$Y=\frac{q+2A\int_0^{\tau_2}\overline{B}^{(2)}(t)\,E_2(t)\,dt+(1-A)\,\overline{B}^{(2)}(0)}{1-2A\int_0^{\tau_2}\overline{\overline{B}}^{(2)}(t)\,E_2(t)dt-(1-A)\,\overline{\overline{B}}^{(2)}(0)}. \tag{V.3.8}$$

Section 4. Allowing for the Absorption "Selectivity"

Neglecting the stipulation of "grayness" and introducing two absorption coefficients $\alpha_1 = 0.2$ cm^2/gm and $\alpha_2 = 4$ cm^2/gm, then the following fundamental fact will be taken into consideration, in first approximation: the existence, /158 in the new spectrum of atmospheric absorption, of segments in which the black radiation of the earth's surface and of the cloud passes through the atmosphere without appreciable inhibition. It is understood that in the layer below the cloud nothing will change, so that the radiation of the Earth, together with the back-radiation of the cloud will lead to an equalization of temperature along the vertical. Therefore, only the atmosphere above the clouds, where the temperature must obviously be reduced, need be investigated. Under night conditions, the fundamental equation of the problem, in accordance with eq.(V.1.27), can be presented in the form of

$$\sum_{j=1}^{2}\widetilde{\alpha}_j B_j^{(2)}(m)=\frac{1}{2}\sum_{j=1}^{2}\alpha_j\{Y_j E_2(\alpha_j m)+\alpha_j\int_0^{m_2}B_j^{(2)}(m')\,E_1(\alpha_j|m-m'|)\,dm'; \tag{V.4.1}$$

where $\alpha_1 = 0.2$ cm^2/gm, $\alpha_2 = 4$ cm^2/gm,

$$m=\int_{z_2}^{z}\rho_w(z)\,dz.$$

We recall that the constants Y_j are equal to $I_{1,j}^{(2)}$ and are determined from the conditions (V.1.25). Here we are faced with a new difficulty as compared with the case of a "gray" atmosphere. The relation (V.1.25) permits determining the sum of the values of Y_j but not each separately. The latter fact is responsible for the general difficulty of formulating the boundary condition of the problems of radiation transfer in a two-layer zone. This problem is discussed in greater detail in Chapter VI.

For this reason, it became necessary in this Chapter to introduce the additional assumptions (V.1.11) and (V.1.18). Here, we will introduce still another

condition:

$$I^{(2)}_{1,j}(0) = k_j I^{(2)}_1(0), \tag{V.4.2}$$

where

$$I^{(2)}_1(0) = \sum_{j=1}^{2} I^{(2)}_{1,j}(0).$$

It is logical to determine the weights k_j from the equalities [see eq.(V.2.17)]

$$k_j = \frac{\bar{B}_j(T)}{\bar{B}(T)}$$

for a temperature of the order of that observed in clouds of the lower and middle layers. At $T = 270^\circ$, we obtain

$$k_1 = \frac{3}{4}, k_2 = \frac{1}{4}.$$

As shown by Table I.5.11 about the same values of the quantity k_j are maintained at any T in the interval $220^\circ \leq T \leq 280^\circ$. The condition (V.4.2), together with eq.(V.1.25), permits to establish that

$$Y_j = I^{(2)}_{1,j}(0) = k_j \{q + [2A_j \alpha_j \int_0^{m_2} B^{(2)}_j(m') E_2(\alpha_j m')\, dm' + (1 - A_j) B^{(0)}_j(\tau_0)]\}. \tag{V.4.3}$$

Equation (V.4.1) contains two unknown functions $B^{(2)}_j(m)$. This can be considered an equation relative to one unknown T(m), but in this case the equation will be nonlinear. It is more convenient to consider eq.(V.4.1) as a linear equation with respect to $B_j(m)$ and to use it for determining T(m), since the form of the function $B_j(T)$ is known. In the solution, we will make use of the method proposed elsewhere (Bibl.2, 4), with slightly changed numerical values of the parameters in accordance with the corrections introduced into the computation of the quantities $B_j(T)$. Table I.5.9 shows that, in the range of temperature variations $220^\circ \leq T < 280^\circ$, the following relation holds with satisfactory accuracy: /159

$$B_1(T) = 3B_2(T). \tag{V.4.4}$$

By substituting in eq.(V.4.1)$3B_2(T)$ for $B_1(T)$ on the basis of this correlation, we obtain

$$B^{(2)}_2(m)(3\alpha_1 + \alpha_2) = \frac{1}{2}\sum_{j=1}^{2} \alpha_j Y_j E_2(\alpha_j m) + \frac{1}{2}\int_0^{m_2} B^{(2)}_2(m')[3\alpha_1^2 E_1(\alpha_1 |m - m'|) + \alpha_2^2 E_1(\alpha_2 |m - m'|)]\, dm'. \tag{V.4.5}$$

Let us denote

$$K(m, m') = \frac{3\alpha_1^2 E_1(\alpha_1^2 | m - m' |) + \alpha_2^2 E_1(\alpha_2 | m - m' |)}{3\alpha_1 + \alpha_2}, \quad \text{(V.4.6)}$$

$$\bar{a} = \frac{\alpha_1}{3\alpha_1 + \alpha_2}, \quad \bar{\bar{a}} = \frac{\alpha_2}{3\alpha_1 + \alpha_2} \quad \text{(V.4.7)}$$

and then solve the equations

$$\bar{B}_2^{(2)}(m) = \frac{\bar{a}}{2} E_2(\alpha_1, m) + \frac{1}{2} \int_0^{m_2} \bar{B}_2^{(2)}(m') K(m, m') dm', \quad \text{(V.4.8)}$$

$$\bar{\bar{B}}_2^{(2)}(m) = \frac{\bar{\bar{a}}}{2} E_2(\alpha_2, m) + \frac{1}{2} \int_0^{m_2} \bar{\bar{B}}_2^{(2)}(m') K(m, m') dm'. \quad \text{(V.4.9)}$$

Then, the function

$$B_2^{(2)}(m) = Y_1 \bar{B}_2^{(2)}(m) + Y_2 \bar{\bar{B}}_2^{(2)}(m) \quad \text{(V.4.10)}$$

will represent the solution of eq.(V.4.5)

The constants Y_1 and Y_2 were determined from the system of equations (V.4.11) which is readily obtained by substituting eqs.(V.4.6) and (V.4.10) into eq.(V.4.5):

$$Y_j = k_j \{q + \int_0^{m_2} [Y_1 \bar{B}_2^{(2)}(m') + Y_2 \bar{\bar{B}}_2(m')] [6 d_1 A_1 E_2(\alpha_1 m') + 2\alpha_2 A_2 E_2(\alpha_2 m')] dm' + [Y_1 \bar{B}_2^{(2)}(0) + Y_2 \bar{\bar{B}}_2^{(2)}(0)] \times [3(1 - A_1) + (1 - A_2)]\}. \quad \text{(V.4.11)}$$

In the solution of eqs.(V.4.11) new parameters appear, namely, the spectral albedo of the cloud A_1 and A_2. In accordance with the data of Chapter IV (see Table IV.4.1) we assumed $A_1 = 0.2$ and $A_2 = 0.07$ which correspond to the spectral intervals (8 - 12μ) and (12 - 16μ) for $\rho_v = 0.2$ gm/m^3 and t = 0° and t = 10°.

Section 5. Vertical Temperature Distribution /160

The temperature profiles for all cases described in Sections 2 - 4 are presented in Fig.V.5.1. We will first discuss some general laws which follow from the computations and from the analyses performed.

As demonstrated above, at a sufficient thickness of the cloud the temperature in the layer below the cloud becomes constant with height and is equal to the temperature at the surface of the ground. In this connection, in the presence of a mechanism that transports heat from the lower boundary to the upper (we introduce turbulent mixing as such a mechanism) the temperature above the cloud will become higher than it would be at the same level in the absence of a cloud. This determines the temperature conditions of the atmosphere above the clouds. If scattering is disregarded, one could imagine the ground surface as extending to the height of the top of the cloud and radiating like a black body

at about the same temperature as before.

When scattering is considered, the temperature of each level in the atmosphere above the clouds must obviously be reduced as compared with the case of pure absorption. Actually, the radiation absorbed per unit volume in the atmosphere above the clouds comes partly from the cloud and partly from the cold

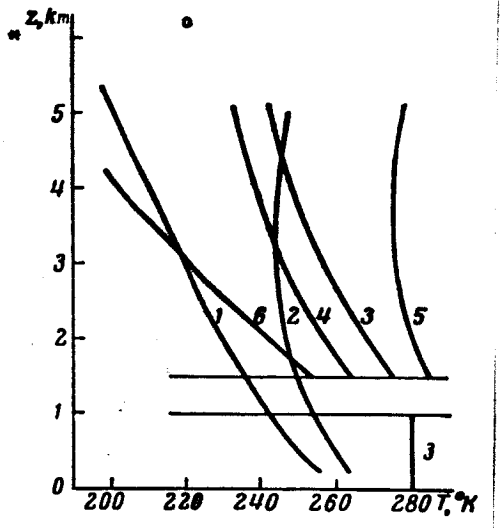

Fig.V.5.1 Vertical Temperature Distribution for Different Models
1 and 2 - Cloudless atmosphere, night and day; 3 and 4 - Cloud, night, with and without account of scattering; 5 - Cloud, day; 6 - Cloud, night, selective absorption (differing from curves 1 - 5, where the absorption spectrum of water vapor is assumed to be "gray")

layers above the cloud. The greater the reflection (which represents scattering in our statement of the problem) the less will be the role played in absorption by the "warm" radiation coming from the cloud.

We note further that the temperature profile in the atmosphere above the clouds is determined by the nature of the absorption spectrum (in our case by the correlation between the coefficients α_1 and α_2) and by the distribution of moisture with height.

The absolute temperature values depend on external heat sources: πq under night conditions and πq and $Q_s(z)$ in the daytime.

Finally, it is obvious that in calculating the transparent interval (8 - 12μ), the temperature in the atmosphere above the cloud will be lower than in the case of a gray atmosphere.

The above statements on the temperature distribution mean that they all describe the state of radiative equilibrium. The condition of radiative equilibrium is far from representing the true nature of heat exchange in the atmosphere, so that the results of our computations are not applicable to reality. The purpose of these computations was merely to reveal the role of the cloud layer in establishing the radiation conditions of the atmosphere and to clarify the correlation between the various factors in the overall process of radiative heat exchange.

The computed temperature distributions with height for various cases are given in Fig.V.5.1. Obviously, compared with the case of a cloudless atmosphere, the temperature in the layer above the cloud increases sharply (see curves 1 and 3). However, this fact cannot be given excessive importance. According /161 to eqs.(V.2.11) and (V.2.12), the temperature is proportional to the nonradiative flow of heat πq which is prescribed independently. By varying πq it is generally speaking possible to obtain any correlation between the temperatures on the prescribed level, in a cloudy and a cloudless atmosphere. Nevertheless,

TABLE V.5.1

	z, km					
	0	0,5	1,0	2,5	3,5	5
$\frac{1}{4\pi\rho_w} Q_e(z)$	0.00087	0.00095	0.0010	0.0019	0.0038	0.0093
$\frac{B_e}{2} E_R(\tau)$	0.031	0.0145	0.0100	0.0053	0.0043	0.0034

there are reasons to consider the obtained relation (curves 1 and 3) valid, since the value of πq selected for the computation corresponds to the real values of the coefficient of turbulent mixing in stratus clouds (see Chapter VI, Sect.9). Other conditions being equal (see Sect.2), a comparison of the temperature profiles represented by Curves 1 and 3 in Fig.V.4.1 and also a comparison of Curves 3 and 4 which represent the cases $A \neq 0$ (Curve 4) and $A = 0$ (Curve 3) show excellent agreement. Above the cloud, in its immediate vicinity, the temperature varies with height in the same manner in cloudy and in cloudless atmospheres. Then, toward greater heights the temperature difference begins to increase (the cross and the circle in Fig.V.5.1 represent the temperature values at $z = \infty$, for Curves 1 and 3 respectively) due to the variation in the temperature profile with the change in water-vapor content m over the entire thickness of the atmosphere. In the case of a cloudless atmosphere, it was assumed that $m = 1.35$. In the case of a cloud, the computation was made for $m_2 = 0.65$.

The temperatures below a cloud and at the same height but in the absence of a cloud show a different behavior. The reasons for the difference in this case were explained above. A comparison of Curves 3 and 4, as shown previously, indicates that the neglecting of scattering leads to a noticeable increase in

temperature.

The effect of scattering, revealed by a comparison of Curves 4 and 3, constitutes 25% of the total effect of the cloud (see Curves 3 and 1). Such an estimate of the percentage of scattering agrees with the results of Chapter VI (see Sect.7).

A comparison of Curves 5 and 4 (obtained with consideration of scattering) also shows the extremely important role of infrared insolation in the development of the radiation temperature in daytime. This role, as indicated in Fig.2 as compared with Fig.1, is considerable under conditions of a cloudless atmosphere. The point here is that, under conditions of radiative equilibrium, the inflow of heat from the sun is one of two available sources of heat. The second source is the radiation of the earth proper B_e in a cloudless atmosphere or the nonradiative inflow πq in the cloud in a cloudy atmosphere.

In order to determine the role of each of these factors, the quantities $\frac{1}{4\pi\rho_w} Q_s(z)$ and $\frac{B_e}{2} E_2(\tau)$ which represent both heat sources in a cloudless atmosphere are compared in Table V.5.1. In the Table the values $Q_s(z)$ computed by Ye.S.Kuznetsov (Bibl.3) are used, and it is assumed that $\rho_w = 9 \times 10^{-0.45z}$ gm/m^3 and that $B_e = 0.063$ cal/cm^2·min which corresponds to a temperature of 280° in the interval $R_1 + R_2$. Obviously, the insolation at a height of 1 km con- /162 stitutes 10% of the terrestrial radiation proper, then becoming equal to the latter and finally exceeding it at the 5-km level. The same occurs with a shift in height, in a cloudy atmosphere.

Figure V.5.1 also defines the role of the "selectivity" of the absorption spectrum of water vapor. Accounting for the selectivity or, more exactly, for the "transparent window" (8 - 12μ) leads to a strong drop in temperature on all levels (cf. Curves 3 and 6), especially at great heights.

It should be noted that the model of the water-vapor spectrum used in this work is least suitable for solution of the problem discussed in this Chapter. In view of the fact that here the heat exchange outside of clouds is considered, it is obviously necessary to account more accurately for the absorption spectrum of a cloudless atmosphere. The calculation of "selectivity" gives only a quantitative idea on the variations in the thermal conditions introduced by this factor.

The general conclusion to be drawn from Fig.V.5.1 is that a thick cloud layer introduces a sharp change in the distribution of radiation temperature with height. The atmosphere in its entirety becomes warmer in the presence of a cloud, and a temperature constant with height is established between the lower boundary of the cloud and the earth's surface. In computing the radiation temperature in the layer above the cloud, the selectivity of absorption of water vapor and of insolation must necessarily be taken into consideration. With respect to these factors, the scattering of long-wave radiation in the cloud can be neglected, with an error of the order of 25%.

The problem posed in this Chapter was solved by us previously (Bibl.5)

where we used a different, more complicated and less substantiated method for the approximate calculation of the radiation leaving the cloud and also a different method for prescribing the nonradiative heat source. In both cases, we obtain qualitatively similar relations between the temperature profiles in a cloudless and a cloudy atmosphere. The equalization of temperature in the layer below the cloud and the secondary role of scattering as compared with the radiation of the cloud proper were likewise revealed there. In this former paper, the temperature above the cloud was found to be less than on a corresponding level without the presence of a cloud. This was due to the selection of the nonradiative heat source.

Thus, the previous conclusions as to the highly important role played by solar radiation in the development of the radiation temperature in daytime were confirmed, and a greater importance of the selectivity than had previously been believed was revealed. Complete disagreement with our previous results was shown with respect to the role of scattering; our calculation (Bibl.5) revealed an increase in the temperature above the clouds. This result (Bibl.5) is apparently in error.

BIBLIOGRAPHY

1. Feygel'son, Ye.M.: Distribution of Temperature of the Earth Atmosphere with Height in the Presence of Radiative and Vertical Turbulent Heat Exchange (Raspredeleniye temperatury zemnoy atmosfery po vysote pri nalichii luchistogo i vertikal'nogo turbulentnogo teploobmena). Izv. Akad. Nauk SSSR, ser. geograf. i geofiz., No.4, 1950.
2. Feygel'son, Ye.M.: On the Absorption Properties of Water Vapor and Carbon Dioxide in the Atmosphere (O pogloshchatel'nykh svoystvakh vodyanogo para i uglekislogo gaza v atmosfere). Izv. Akad. Nauk SSSR, ser. geofiz., No.1, 1955.
3. Kuznetsov, Ye.S.: On the Absorption of Solar Radiation by the Earth's Atmosphere (O pogloshchenii radiatsii solntsa zemnoy atmosferoy). Trudy Geofiz. Inst., No.23, 1954.
4. Feygel'son, Ye.M.: Accounting for Selective Absorption in the Theory of Radiative Heat Exchange in the Atmosphere (Uchet izbiratel'nogo pogloshcheniya v teorii luchistogo teploobmena v atmosfere). Izv. Akad. Nauk, ser. geofiz., No.3, 1955.
5. Feygel'son, Ye.M.: Effect of Clouds on the Thermal Conditions of the Atmosphere (Vliyaniye oblakov na teplovoy rezhim atmosfery). Trudy Geofiz. Inst., No.37, 1956.

CHAPTER VI

/163

RADIATIVE COOLING OF CLOUDS

Section 1. Formulation of the Problem

The transfer of radiant energy in a cloud leads to its heating due to absorption of infrared solar radiation and to cooling as a result of radiation from the boundaries. In this Chapter, the process of variation in temperature in the upper part of the cloud layer under the influence of both factors is studied. The lower part of the cloud is not considered since the basic features of the thermal regime are here determined by interaction with the earth's surface and are described in Chapter V.

Qualitative considerations of radiative cooling of clouds, of haze, and fog are discussed elsewhere (Bibl.1 - 5). As early as 1931 Mal (Bibl.1) drew attention to the possibility of temperature inversions in the atmosphere due to radiation from haze layers. In other papers (Bibl.2, 3) it is also shown that a stratus cloud (haze, fog) having formed under the layer of temperature inversion itself actively affects the development and increase of the latter. Urfer (Bibl.4), in observing the temperature variation in persistent layers of fog attributed this to radiative cooling. In Urfer's opinion, intensive radiation from the upper boundary of a fog leads to the formation of an unstable cold belt. Thermal convection takes place, leading to reconstruction of the temperature profile. Investigations of radiation fogs led A.L.Dergach (Bibl.5) to the following conclusion: The ground radiation fog produced below the layer of temperature inversion exerts a direct influence on the process of evolution of inversions; the fog intensifies the inversion both by lowering the minimum temperatures at the base of the inversion and by slightly increasing the temperature at the upper boundary of the inversion.

All these qualitative considerations indicate the need for investigating radiative cooling of cloud layers. In this Chapter, a quantitative evaluation of the above process and of its extension into the atmosphere above the cloud is attempted.

Let us investigate a cloud layer which is infinite and uniform along the horizontal. The temperature variations in this layer, taking the inflow of heat due to transfer of long-wave radiation from phase transformations of water into consideration, are described by the equation [see eq.(I.2.40)]:

$$C_p \rho \frac{\partial T^{(0)}}{\partial t} = \int_{\lambda_1}^{\lambda_2} [a_{v,\lambda} \rho_v^{(0)} + a_{w,\lambda} \rho_w^{(0)}] \cdot [I_\lambda(z, r, t)\, d\omega - A_\lambda B_\lambda (T^{(0)})]\, d\lambda - L \frac{\partial \rho_w^{(0)}}{\partial t}, \qquad \text{(VI.1.1)}$$

where λ_1 is the lower boundary of the interval of thermal radiation; λ_2 is its upper boundary; L is the latent heat of condensation. The remaining notations retain their previous meaning. /164

The corresponding equation for the layer above the clouds has the form

$$C_p\rho \frac{\partial T^{(1)}}{\partial t} = \rho_w^{(1)}(z, t) \int_{\lambda_1}^{\lambda_2} \alpha_{w,\lambda} \left[\int_{\omega} I_\lambda^{(1)} d\omega - 4\pi B_\lambda (T^{(1)})\right] d\lambda. \qquad \text{(VI.1.2)}$$

The superscript 1 applies to the characteristics of the atmosphere above the clouds and the superscript 0, to the characteristics of the cloud itself.

Equations (VI.1.1) and (VI.1.2) contain the unknowns $T^{(0)}(z, t), T^{(1)}(z, t)$, $I^{(0)}(z, r, t)$, $I^{(1)}(z, r, t)$ and must be supplemented by two transfer equations:

$$\cos\theta \frac{\partial I_\lambda^{(0)}}{\partial z} = (\alpha_{v,\lambda}\rho_v^{(0)} + \alpha_{w,\lambda}\rho_w^{(0)})[B_\lambda(T^{(0)}) - I_\lambda^{(0)}(z, r, t)], \qquad \text{(VI.1.3)}$$

$$\cos\theta \frac{\partial I_\lambda^{(1)}}{\partial z} = \alpha_{w,\lambda}\rho_w^{(1)}[B_\lambda(T^{(1)}) - I_\lambda^{(1)}(z, r, t)]. \qquad \text{(VI.1.4)}$$

Equations (VI.1.3) and (VI.1.4) neglect the scattering, which is indisputable for the atmosphere above the clouds. Within the cloud, the scattering of long-wave radiation is extensive and the scattering coefficient is of the same order of magnitude as the absorption coefficient. Nevertheless, because of the complexity of its calculation, we will disregard here the scattering of long-wave radiation within the cloud. The resultant errors are discussed in Sections 2 and 7.

If the quantities $\alpha_{w\lambda}$, $\alpha_{v\lambda}$, $\rho_w^{(j)}(z, t)$ and $\rho_v^{(o)}(j = 0, 1)$ are given, then the system of equations (VI.1.1) - (VI.1.4) makes it possible to determine the unknown temperature in both layers.

The boundary and initial conditions necessary for the solution are given below.

Initial conditions:

Given are the quantities $T^{(j)}(z, 0)(j = 0, 1)\rho_w^{(1)}(z, 0)$ and $\rho_v(z, 0)$.

Boundary conditions:

1. $I_\lambda^{(o)}(0, r, t) = I_\lambda^{(1)}(0, r, t)$ (the height in each layer is counted from the common boundary),

2. $I_\lambda^{(1)}(z, r, t)_{z=\infty} = 0$ at $0 > \pi/2$.

The conditions on the lower boundary of the cloud are not determined since only optically dense clouds are considered in which radiation of the lower layers does not reach the upper layers.

The water vapor within the clouds is assumed to be saturated, as a result of which each instant of time $\rho_w^{(0)}(z, t)$ is treated as a known function of temperature determined by Magnus' formula

$$\rho_w^{(0)}(z, t) = 0.1 \frac{E_0 \cdot 10^{\frac{at^\circ}{b+t^\circ}}}{R_w T}, \qquad \text{(VI.1.5)}$$

where $E_0 = 6.1$ mb is the saturation pressure of water vapor at 0°C; $a = 7.5$; $b = 237^\circ$; $R_w = 460$ m²/sec²·deg is the gas constant of water vapor; t° is the temperature in °C; $\rho_w^{(0)}$ is expressed in gm/cm³.

Below, relatively narrow time intervals are treated over which the distribution of moisture above the clouds is considered constant:

$$\varrho_w^{(1)}(z, t) = \varrho_w^{(1)}(z, 0).$$

The liquid-water content of the cloud $\rho_v(z, 0)$ is also given at the initial instant. Subsequent changes in the water content are controlled by the variations in moisture and are determined by the formula /165

$$\varrho_v(z, t) = \varrho_w^{(0)}(z, 0) - \varrho_w[T^{(0)}(z, t)], \qquad \text{(VI.1.6)}$$

where $\rho_w(T)$ is the density of the vapor saturating the volume at a temperature T.

Thus, in our formulation of the problem, the exchange of moisture of the cloud with the ambient medium is disregarded. Variations in liquid-water content and in moisture occur only due to phase transformations of water, connected with the radiative temperature variation.

Section 2. Simplifications Introduced

The solution of the system of equations (VI.1.1) - (VI.1.4) was carried out in other papers (Bibl.6 - 9) with simplifying assumptions as to the absorption spectra of water vapor and of droplet water and also with neglecting the scattering of long-wave radiation in the cloud. Below, we give some justifications for the simplification introduced.

2.1 Schematization of the Spectrum of Water Vapor

We will describe the spectrum of water vapor (see Chapter I, Sect.5) by three absorption coefficients:

$$\alpha_1 = 0.2 \text{ cm}^2/g, \ \alpha_2 = 4 \text{ cm}^2/g, \ \alpha_3 = 10 \text{ cm}^2/g.$$

The coefficients α_1, α_2, and α_3 apply to the sum total of individual segments

of all absorption bands of water vapor. Integrals from Planck's functions along the same spectrum intervals are presented in Fig.I.5.6 and in eq.(I.5.11).

In the present investigation, we are fully justified to use the indicated spectrum model since, in the rather complex problem involved here, a detailed consideration of the true structure of the water-vapor spectrum is quite impossible. In fact, this may not even be necessary. Thus, absorption of water vapor in the cloud can be neglected. The layer above the cloud is here considered principally from the viewpoint of its effect on the cloud. Therefore, the main problem is to define, in the spectrum of the atmosphere above the clouds, regions with weak, strong, and average absorption, which interact differently with the radiation of the cloud. The selected spectrum model is well suited for this purpose.

2.2 Neglect of the Scattering

As mentioned above, scattering of long-wave radiation in the cloud is disregarded in this Chapter although, according to the data in Chapter I, Sect.4, the coefficients of scattering and of absorption of droplet water in the long-wave region of the spectrum are equal in order of magnitude.

The problem of radiative heat exchange, taking scattering into account, is quite difficult and has never been solved in full. Below in Section 7 and in Chapters II and V, attempts have been made to account for scattering or, more accurately, to circumvent the difficulties connected with this. The computations made there give some idea as to the nature of the effect of the scattering process on the thermal regime and indicate the subordinate but still considerable influence of this factor.

Ye.S.Kuznetsov (Bibl.10) gave a detailed treatment of the role of scattered radiation in the heat exchange, for the simplest case of radiation equilibrium of a gray atmosphere and of a spherical scattering indicatrix. He also gave /166 approximate computations for slightly elongated indicatrices. The principal conclusions of this paper (Bibl.10) are presented below.

In the case of radiation equilibrium in a gray atmosphere, the following relation [see eq.(I.2.39)] exists:

$$B(\tau) = \frac{1}{4\pi}\int I(\tau, r)\, d\omega. \qquad \text{(VI.2.1)}$$

Hence eq.(I.3.23) can be presented in the form:

$$\cos\theta \frac{\partial I}{\partial \tau} = \frac{1}{4\pi}\int I(\tau, r)\,[(1-k) + k\gamma(r, r')]\, d\omega' - I(\tau, r), \qquad \text{(VI.2.2)}$$

where

$$k = \frac{\sigma}{\alpha+\sigma},$$

$$\tau = \int_0^z (\tilde{\alpha} + \tilde{\sigma})\, dz.$$

For $\gamma = 1$, we obtain the equation

$$\cos\theta \frac{\partial I}{\partial \tau} = \frac{1}{4\pi}\int I d\omega - I, \qquad \text{(VI.2.3)}$$

which differs from the transfer equation in the problem of pure scattering [see eq.(I.3.1)] only by the determination of the optical thickness τ which now depends not only on the scattering coefficient $\tilde{\sigma}$ but also on the absorption coefficient $\tilde{\alpha}$.

Thus, the question as to the role of scattering reduces to the problem of the dependence on the solution of the integral equation which is equivalent to eq.(VI.2.3) on any variation in τ^*.

If the value of the function $B(\tau)$ for an atmosphere with an optical thickness $\tau^* + \Delta\tau^*$ is designated by $\tilde{B}(\tau)$, then we obtain the following integral equations [see eq.(I.2.45)] for the determination of the functions $B(\tau)$ and $\tilde{B}(\tau)$:

$$B(\tau) = \frac{1}{2} B(0) E_2(\tau) + \frac{1}{2}\int_0^{\tau^*} B(t) E_1(|\tau - t|)\, dt, \qquad \text{(VI.2.4)}$$

$$B(\tau) = \frac{1}{2} B(0) E_2(\tau) + \frac{1}{2}\int_0^{\tau^*+\Delta\tau^*} B(t) E_1(|\tau - t|)\, dt. \qquad \text{(VI.2.5)}$$

Hence,

$$\tilde{B}(\tau) - B(\tau) = \frac{1}{2}\int_{\tau^*}^{\tau^*+\Delta\tau^*} \tilde{B}(t) E_1(|\tau - t|)\, dt + \frac{1}{2}\int_0^{\tau^*} [\tilde{B}(t) - B(t)] E_1(|\tau - t|)\, dt. \qquad \text{(VI.2.6)}$$

Because the kernel and the three terms of the last equation are positive, its solution, i.e., $\tilde{B}(\tau) - B(\tau)$, will be positive in the interval $(0, \tau^*)$. Above the level $\tau = \tau^*$, the function $\tilde{B}(\tau)$ decreases on decreasing temperature T with height and may reach values smaller than $B(\tau^*)$.

In another paper (Bibl.10), it is shown that if

$$\Delta\tau^* > \tau^* + 2, \qquad \text{(VI.2.7)}$$

the following inequality will exist in each case:

$$\tilde{B}(\tau^* + \Delta\tau^*) < B(\tau^*). \qquad \text{(VI.2.8)}$$

The inequation (VI.2.7) is valid in clouds since here α is about equal to σ and is large; in addition this inequality has deliberately been made too large. /167

Thus, scattering increases the temperature in the lower layers of the cloud and apparently reduces it in the upper.

Ye.S.Kuznetsov, in Schwarzschild's approximation, calculated the temperature at the lower (T_0) and at the upper (T^*) boundaries of a scattering and absorbing layer under conditions of radiative equilibrium, for a scattering indicatrix of the form $\gamma(\varpi) = 1 + g \cos \varpi$ and for $g = 0, 1$. The results of the computation are presented in Table VI.2.1.

TABLE VI.2.1

k	$g=0$		$g=1$	
	T_0	T^*	T_0	T^*
0.00	293.8	161.3	293.8	161.3
0.5	296.4	138.5	296.1	143.7
0.75	298.2	117.8	297.9	124.6
0.90	299.3	94.4	298.9	101.7

It follows from the Table that the scattering of radiant energy somewhat increases the temperature in the lower parts of the layer and substantially reduces it at the upper boundary. The asymmetry of the indicatrix (in the weak form in which it is considered here) somewhat compensates this effect. The results of our computations given in Section 7 of this Chapter confirm Ye.S. Kuznetsov's conclusion and also prove the temperature drop due to scattering of radiant energy in the upper part of the cloud.

Therefore, the estimates of radiative cooling obtained below, neglecting the scattering of long-wave radiation refer only to the lower boundary of this phenomenon.

2.3 Neglect of Water Vapor in the Cloud and Averaging the Absorption Coefficient of Water

If scattering is neglected, the inflow of heat per unit volume of the cloud, i.e., the first term on the right-hand side of expression (VI.1.1) will have the following form [see eq.(I.2.44)]:

$$Q(\tau) = \int_{\lambda_1}^{\lambda_2} [\tilde{\alpha}_{v,\lambda} + \tilde{\alpha}_{w,\lambda}] \left\{ \int I_{1,\lambda}(0, r)\, e^{-\sec\theta\tau}\, d\omega + \int I_{2,\lambda}(\tau_0, r)\, e^{-\sec\theta(\tau_0-\tau)}\, d\omega + \right.$$
$$\left. + 2\pi \int_0^{\tau_0} B_\lambda(t)\, E_1(|\tau - t|)\, dt - 4\pi B_\lambda(T) \right\} d\lambda. \qquad \text{(VI.2.9)}$$

Let us evaluate the possible errors in the quantity $Q(\tau)$ due to neglecting the water vapor in the cloud and also due to replacing the spectral absorption coefficient of droplet water $\tilde{\alpha}_{v,\lambda}$ by its mean value α_v. The evaluation was made for sufficiently dense clouds ($\tau_0 \geq 10$) and in the vicinity of the upper boundary of the cloud ($\tau \approx \tau_0$).

Under these conditions, it can be assumed that, in eq.(VI.2.9), we have $I_1(0, r) = 0$, since the effect of the lower boundary does not extend to the upper layers of the cloud.

It is natural to present the radiation incident on the upper boundary of the cloud from the outside in the following form [see for instance eq.(V.1.17)]:

$$I_{2,\lambda}(\tau_0, r) = \sec\theta \int_0^{\tau_{1,\lambda}} B_\lambda^{(1)}(t)\, e^{-\sec\theta\, t}\, dt,$$

after which the expression $Q(\tau)$ is transformed into

/168

$$Q(\tau) = 2\pi \int_{\lambda_1}^{\lambda_2} [\tilde{\alpha}_{v,\lambda} + \tilde{\alpha}_{w,\lambda}] \left\{ \int_0^{\tau_0} B_\lambda(t)\, E_1(|\tau - t|)\, dt - \right.$$
$$\left. - 2B_\lambda(T) + \int_0^{\tau_1} B_\lambda^{(1)}(t)\, E_1(\tau + t)\, dt. \right. \qquad \text{(VI.2.10)}$$

The calculation on the basis of eq.(VI.2.10) was made for $\tau = \tau_0$ under the assumption that

$$B_\lambda^{(1)}(t) = \text{const}$$

for the quantities $\alpha_{w,\lambda}$ taken from Table I.5.2 and for the quantities $\alpha_{v,\lambda}$ calculated by means of the formula (see Chapter I):

$$\tilde{\alpha}_{v,\lambda} = \frac{3K_{a,\lambda}\rho_v}{4a\tilde{\rho}}$$

at $a = 6.26\mu$ and for the quantities $K_{a,\lambda}$ taken from Table I.4.6.

The computational data showed that, at an error not exceeding 1%, it can be assumed that

$$\tilde{\alpha}_{w,\lambda} + \tilde{\alpha}_{v,\lambda} = \tilde{\alpha}_{v,\lambda}.$$

Substituting $\alpha_{v,\lambda}$ by the arithmetic mean of this quantity α_v in the interval ($4 - 20\mu$) leads to an error of the order of 30%. If, however, the arithmetic mean of the absorption coefficient of water in the narrow interval of wavelengths ($8 - 12\mu$) is taken as α_v, the error due to this assumption

$$\alpha_{v,\lambda} = \text{const} = \alpha_v$$

will not exceed 10%. The value of α_v will then be equal to about 1000 cm^2/gm. The reduction in the error in the last case is explained by the major role played by the (8 - 12μ) interval in forming the value of $Q(\tau)$ at $\tau \approx \tau_0$. Outside of this interval, the absorption of water vapor is extensive as a result of which the radiation of the cloud is compensated by back-radiation of the atmosphere above the cloud. For the same reason, in calculating $Q(\tau)$, the water vapor could be neglected with respect to water, without loss of accuracy.

Another point of importance is the differing role played by water vapor in the solution of various problems. Thus, in Chapter IV it was shown that the attenuation factor in a cloud is largely determined by the absorption properties of water vapor. As a consequence, the role of the latter is substantial in computing the albedo and the radiation fluxes (we recall the increase in albedo in the transparent interval). In this Section, however, we show that, in computing the influx of radiation in a cloud, water vapor can be neglected.

Section 3. Method of Solution

Let us make some transformations of eqs.(VI.1.1) and (VI.1.2). First, on the basis of the above considerations, we replace $\alpha_{w,\lambda}$ and $\alpha_{v,\lambda}$ by their mean values. Then, with the aid of eqs.(VI.1.3) and (VI.1.4), we express the radiation intensity $I_\lambda^{(j)}(z, r, t)(j = 0, 1)$ by the corresponding temperatures $T^{(j)}(z, t)$ [see eq.(I.3.7)] and substitute the obtained expressions in eqs. (VI.1.1) and (VI.1.2). Finally, we introduce the optical thickness of the cloud:

$$\tau = \alpha_v \int_0^z \rho_v(z)\, dz \qquad \text{(VI.3.1)}$$

and the mass of the vertical vapor column in the atmosphere above the cloud /169

$$m = \int_0^z \rho_w^{(1)}(z)\, dz. \qquad \text{(VI.3.2)}$$

With regard to the last relations, the following statements must be made:

a) The optical thickness of the entire cloud is equal to

$$\tau_0 = \alpha_v \int_0^H \rho_v(z)\, dz, \qquad \text{(VI.3.3)}$$

where H is the thickness of the cloud layer.

b) The mass of water vapor in the entire layer below the cloud is

$$m_1 = \int_0^\infty \rho_w^{(1)}(z)\, dz; \qquad \text{(VI.3.4)}$$

c) The quantity τ depends on the time.

After transformation, eqs.(VI.1.1) and (VI.1.2) reduce to the form

$$C_p \rho \frac{\partial T^{(0)}}{\partial t} = 2\pi\alpha_v \rho_v(z, t) \left\{ \sum_{i=1}^{3} \alpha_i \int_0^{m_1} B_i^{(1)}(\xi, t) E_1(\alpha_i \xi + \tau)\, d\xi + \right.$$

$$\left. + \int_0^{\tau_0} B^{(0)}(\xi, t) E_1(|\xi - \tau|)\, d\xi - 2B^{(0)}(\tau, t) \right\} - L \frac{\partial \rho_w^{(0)}}{\partial t}, \qquad \text{(VI.3.5)}$$

$$C_p \rho \frac{\partial T^{(1)}}{\partial t} = 2\pi\rho_w^{(1)}(z, t) \left\{ \sum_{i=1}^{3} \alpha_i \int_0^{\tau_0} B_i^{(0)}(\xi, t) E_1(\xi + \alpha_i m)\, d\xi + \right.$$

$$\left. + \sum_{i=1}^{3} \alpha_i^2 \int_0^{m_1} B_i^{(1)}(\xi, t) E_1(\alpha_i |m - \xi|)\, d\xi - 2 \sum_{i=1}^{3} \alpha_i B_i^{(1)}(m, t) \right\}; \qquad \text{(VI.3.6)}$$

where $E_1(x)$ is Gold's function [see Chapter I, eq.(I.2.43)].

We then introduce the dimensionless quantities

$$\bar{t} = \frac{t}{t_0}, \quad \bar{T}^{(j)} = \frac{T^{(j)}}{T_0}, \quad \bar{B}_i = \frac{B_i}{B_0}, \quad \bar{\rho}_v = \frac{\rho_v}{\rho_{v,0}}, \quad \bar{\rho}_w^{(j)} = \frac{\rho_w^{(j)}}{\rho_{w,0}}$$

and the dimensionless parameters

$$a^{(0)} = \frac{C_p \rho T_0}{2\pi\alpha_v \rho_{v,0} t_0 B_0}, \quad a^{(1)} = \frac{C_p \rho T_0}{2\pi\alpha_w \rho_{w,0} t_0 B_0}, \quad b = \frac{L\rho_{w,0}}{2\pi\alpha_v t_0 B_0 \rho_{v,0}}. \qquad \text{(VI.3.7)}$$

If we assume T = 273°, then $B_0 = 0.146$ cal/cm²·min = $\frac{\sigma}{\pi} T_0^4$; $\rho_{w\rho} = 4.9 \times$ $\times 10^{-6}$ gm/cm³ = $\rho_w(T_0)$.

We will assume that the air density ρ is constant, which will not lead to appreciable errors in our problem since we are considering a layer which is not great in height. Let us assume $\rho = 1.3 \times 10^{-3}$ gm/cm³; $C_p = 0.24$ cal/gm·deg. For the remaining characteristic quantities we will assume the following values: $t_0 = 24$ hr, $\alpha_v = 1100$ cm²/gm, $\alpha_w = 1$ cm²/gm; $\rho_{v,0} = 0.5 \times 10^{-6}$ gm/cm³.

The calculation by means of eqs.(VI.3.7), in this case, will yield /170

$$a^{(0)} = 0.117, \quad a^{(1)} = 13.1, \quad b = 0.398 \cdot 10^{-3}.$$

In calculating b, it is assumed that L = 590 cal/gm.

In the transition to dimensionless quantities, eqs.(VI.3.5) and (VI.3.6) are replaced by

$$a_0^{(0)} \frac{\partial \bar{T}^{(0)}}{\partial \bar{t}} = \bar{R}^{(0)}(\tau, \bar{t}) - b \frac{\partial \bar{\rho}_w^{(0)}}{\partial \bar{t}}, \tag{VI.3.8}$$

$$\alpha^{(1)} \frac{\partial \bar{T}^{(1)}}{\partial \bar{t}} = \bar{R}^{(1)}(\tau, \bar{t}). \tag{VI.3.9}$$

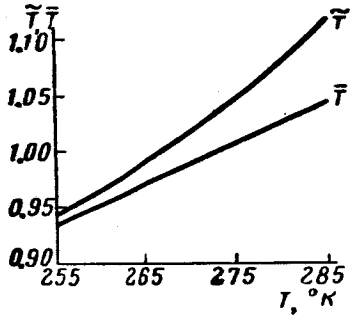

Fig.VI.3.1 Effective $\tilde{T}$ and Dimensionless $\bar{T}$ Temperatures as a Function of T

The amounts $\bar{R}^{(0)}(\tau,\bar{t})$ and $\bar{R}^{(1)}(\tau,\bar{t})$ represent the radiative inflow of heat:

$$\bar{R}^{(0)}(\tau, \bar{t}) = \bar{\rho}_v(\tau, \bar{t}) \left\{ \sum_{i=1}^{3} \alpha_i \int_0^{m_1} \bar{B}_i^{(1)}(\xi, \bar{t}) E_1(\alpha_i \xi + \tau)\, d\xi + \right.$$
$$\left. + \int_0^{\tau_0} \bar{B}^{(0)}(\xi, \bar{t}) E_1(|\tau - \xi|)\, d\xi - 2\bar{B}^{(0)}(\tau, \bar{t}), \right\}, \tag{VI.3.10}$$

$$\bar{R}^{(1)}(m, \bar{t}) = \bar{\rho}_w^{(1)}(m, \bar{t}) \left\{ \sum_{i=1}^{3} \frac{\alpha_i}{\alpha_w} \int_0^{\tau_0} B_i^{(0)}(\xi, \bar{t}) E_1(\xi + \alpha_i m)\, d\xi + \right.$$
$$\left. + \sum_{i=1}^{3} \frac{\alpha_i^2}{\alpha_w} \int_0^{m_1} \bar{B}_i^{(1)}(\xi, \bar{t}) E_1(\alpha_i |m - \xi|)\, d\xi - 2 \sum_{i=1}^{3} \frac{\alpha_i}{\alpha_w} \bar{B}_i^{(1)}(\tau, \bar{t}) \right\}. \tag{VI.3.11}$$

In what follows, the vinculum denoting dimensionless quantities is omitted.

It is easy to obtain the algorithm of an approximate solution of eqs. (VI.3.8) and (VI.3.9). If both sides of these equations are integrated (under the assumption that a solution exists) with respect to time within the limits from the instant t_{k-1} to the instant t_k, then eq.(VI.3.8) will yield

$$a^{(0)} [T^{(0)}(\tau, t_k) - T^{(0)}(\tau, t_{k-1})] = \int_{t_{k-1}}^{t_k} R^{(0)}(\tau, t)\, dt -$$
$$- b\, [\rho_w^{(0)}(\tau, t_k) - \rho_w^{(0)}(\tau, t_{k-1})] \tag{VI.3.12}$$

and a corresponding expression from (VI.3.9). Let us assume that /171

$$\int_{t_{k-1}}^{t_k} R^{(j)}(\tau, t)\, dt = \Delta t R^{(j)}(\tau, t_{k-1}) \qquad j = 1, 0 \tag{VI.3.13}$$

and introduce the notation

$$\tilde{T}(\tau, t) = T^{(0)}(\tau, t) + \frac{b}{a^{(0)}} \rho_w^{(0)}(\tau, t). \tag{VI.3.14}$$

Since ρ_w is a known function of the temperature [see eq.(VI.1.5)], it is obvious that $\tilde{T}$ also represents a known function of the temperature, whose curve is plotted in Fig.VI.3.1 (the straight line in the diagram represents $\tilde{T} = \frac{T}{T_0}$).

If the phase transformation of water is neglected in the equation of heat inflow, then $\tilde{T}(\tau, t)$ will coincide with the temperature. In our case, $\tilde{T}(\tau, t)$ plays the role of the effective temperature which includes corrections for moisture condensation.

The final formula, taking eqs.(VI.3.13) and (VI.3.14) into consideration, can be written in the form of

$$\tilde{T}(\tau, t_k) = \tilde{T}(\tau, t_{k-1}) + \frac{\Delta t}{a^{(0)}} R^{(0)}(\tau, t_{k-1}), \tag{VI.3.15}$$

$$T^{(1)}(\tau, t_k) = T^{(1)}(\tau, t_{k-1}) + \frac{\Delta t}{a^{(1)}} R^{(1)}(\tau, t_{k-1}). \tag{VI.3.16}$$

If $\tilde{T}(\tau, t_{k-1})$ and $T^{(1)}(\tau, t_{k-1})$ are known, then it is possible to compute $R^{(j)}(t_{k-1})$ from eqs.(VI.3.10) and (VI.3.11), to read off $\tilde{T}(t_{k-1})$ from the graph, then to compute $T^{(1)}(t_k)$ and $\tilde{T}(t_k)$ and finally, with the aid of the same graph, to determine $T(t_k)$.

Section 4. A Few Laws

Some qualitative idea as to the temperature variations in a cloud with time can be obtained by examining $R^{(0)}(\tau, t)$.

In Section 5, it will be shown that, in the case of sufficiently dense clouds ($\tau_0 \geq 10$), it can be assumed with a large degree of accuracy, for any $0 \leq \tau \leq \tau_0$, that

$$\int_0^{\tau_0} B^{(0)}(\xi, t)\, E_1(|\tau - t|)\, dt \approx B^{(0)}(\tau, t)\,[2 - E_2(\tau) - E_2(\tau_0 - \tau)]. \tag{VI.4.1}$$

In this case, eq.(VI.3.10) will yield

$$R^{(0)}(\tau, t) = \rho_v(\tau, t)\left\{\sum_{i=1}^{3}\alpha_i\int_0^{m_1} B_i^{(1)}(\xi, t)\,E_1(\alpha_i\xi + \tau)\,d\xi - \right.$$
$$\left. - B^{(0)}(\tau)\,[E_2(\tau) + E_2(\tau_0 - \tau)]\right\}. \qquad \text{(VI.4.2)}$$

Since the optical thickness of a cloud in the long-wave region of the spectrum is great (of the order of several tens) it follows that, in the depth of the cloud layer, $R^{(0)}(\tau, t) = 0$ (see also Chapters IV and V).

At the upper boundary, i.e., at $\tau \approx 0$, we obtain

$$R^{(0)}(\tau, t) = \rho_v(\tau, t)\left\{\sum_{i=1}^{3}\alpha_i\int_0^{m_1} B_i^{(1)}(\xi, t)\,E_1(\alpha_i\xi + \tau)\,d\xi - B^{(0)}(\tau)\,E_2(\tau)\right\}. \qquad \text{(VI.4.3)}$$

From this it follows that fluctuations in the liquid-water content of the cloud as a whole or variations in its geometric dimensions or its optical thickness τ_0 will not lead to changes in the radiation conditions at the level τ if the water content $\rho_v(\tau, t)$ remains constant. In the level under consideration, the radiative influx of heat is proportional to the liquid-water content. /172

In eq.(VI.4.3), the first term on the right-hand side represents back-radiation in the atmosphere above the clouds. The second term expresses the radiation balance of the cloud proper, i.e., the difference between the amount of absorbed and radiated energy per unit volume of the cloud.

The expression (VI.4.3) shows that, due to its natural radiation balance, the upper layer of the cloud can only be cooled.

The influence of the layer above the cloud is dependent on the temperature distribution in this layer.

Let

$$B_i^{(1)}(\xi, t) = B_i^{(1)}(0, t) + \xi b_i(t).$$

Then,

$$\sum_{i=1}^{3}\alpha_i\int_0^{m_1} B_i^{(1)}(\xi, t)\,E_1(\alpha_i\xi)\,d\xi =$$
$$= \sum_{i=1}^{3}\left\{B_i^{(1)}(0, t)\,[1 - E_2(\tau)] + b_i(t)\left[\frac{1}{2} - \tau_i E_2(\tau_i) - E_3(\tau_i)\right]\right\},$$

where τ_i is the optical thicknesses of the atmosphere above the cloud, corresponding to the three selected segments of the spectrum ($\tau_i = \alpha_i m$).

The radiative heat influx in this case is expressed in the form (for simplicity, we assume $\tau = 0$):

$$R^{(0)}(0,t) = \rho_v(0,t)\left\{\sum_{i=1}^{3} B_i^{(1)}(0,t)\,[1 - E_2(\tau_i)] + \right.$$

$$\left. + \sum_{i=1}^{3} b_i\left[\frac{1}{2} - \tau_i E_2(\tau_i) - E_3(\tau_i)\right] - B^{(0)}(0,t)\right\}. \qquad \text{(VI.4.4)}$$

If the temperature in the layer above the cloud remains constant with height ($b_1 = 0$) and equal to the temperature in the upper part of the cloud, then eq.(VI.4.4) will yield

$$R^{(0)}(0,t) = -\rho_v(0,t)\sum_{i=1}^{3} B_i^{(1)}(0,t)\,E_2(\tau_i). \qquad \text{(VI.4.5)}$$

In this case, the cloud undergoes cooling, which proceeds less rapidly the higher the water vapor content above it, i.e., the greater τ_1. At an average water vapor content in the atmosphere above the cloud of($m = 1.5$ gm/cm^2) we have

$$E_i(\tau_i) = 0 \qquad (i = 2;\ 3)$$

and

$$R^{(0)}(0,t) = -\rho_v(0,t)\,B_1^{(1)}(0,t)\,E_2(\tau_1). \qquad \text{(VI.4.6)}$$

From this it follows that the region of small absorption coefficients plays the principal role in radiation.

The corresponding expression for a "gray" atmosphere ($\alpha_1 = \text{const} = 1$ cm^2/gm; $\tau_1 = \tau^* = m \cdot 1$ cm^2/gm $= 1.5$) has the form

$$R^{(0)}_{gray}(0,t) = -\rho_v(0,t)B^{(1)}(0,t)E_2(\tau^*). \qquad \text{(VI.4.7)}$$

It is easy to calculate $R^{(0)}_{gray} \ll R^{(0)}$. It is thus very important to take /173 the selective nature of water-vapor absorption into consideration.

We will now study the case of a temperature varying with height in the layer above the clouds. It is not difficult to verify that

$$\frac{1}{2} - \tau_i E_2(\tau_i) - E_3(\tau_i) > 0. \qquad \text{(VI.4.8)}$$

Therefore, if the temperature above the cloud decreases with height ($b_1 < 0$), then according to eq.(VI.4.4) the cooling of the cloud will be even more extensive than in the above case of $b_1 = 0$. For a temperature inversion above the cloud, the condition of the sign reversal $R^{(0)}$ assumes the following form [for $T^{(1)}(0, t) = T_0(0, t)$]:

$$\sum_{i=1}^{3} b_i \left[\frac{1}{2} - \tau_i E_2(\tau_i) - E_3(\tau_i)\right] \geqslant \sum_{i=1}^{3} E_2(\tau_i)\, B_i^{(1)}(0, t). \qquad \text{(VI.4.9)}$$

It can be approximately assumed that $b_1 = 0.3\ b$ where $b = \sum_{i=1}^{3} b_i$. Then, considering that $E_2(\tau_i) = 0$ $(i = 2, 3)$, the condition (VI.4.9) can be replaced by

$$0.3b\left\{\frac{1}{2} - \tau_1 E_2(\tau_1) - E_3(\tau_1)\right\} \geqslant E_2(\tau_1)\, B_1^{(1)}(0, t). \qquad \text{(VI.4.10)}$$

Calculation on the basis of eq.(VI.4.10) at $\tau_1 = 0.3$ yields $b \geq 0.3$, which corresponds to a temperature inversion of the order of $10 - 12^{\circ}$ in a layer of 0.1 km thickness above the cloud.

The above statement on eq.(VI.4.3) means that the value of $R^{(0)}(\tau, t)$ decreases extremely rapidly with increasing τ because of the decrease in $E_j(\tau)$ $(j = 1; 2)$. For $\tau = 5$ which corresponds to about 100 m from the top of the cloud, we have $R^{(0)}(\tau, t) = 0$ so that the radiative cooling does not extend into the deeper layers.

The results of computations with eqs.(VI.3.15) and (VI.3.16), in the simplest case of a constant initial temperature along the height of the cloud and above it, are given below. These data confirm the obtained qualitative laws and, to some extent, extend them and make them more accurate.

Let there exist, at the initial instant t_0,

$$T^{(1)}(z, t_0) = T^{(0)}(z, t_0) = T_0,$$

i.e.,

$$B_i^{(1)}(z, t_0) = B_i^{(0)}(z, t_0) = B_{i,0}.$$

The relations (VI.3.15) and (VI.3.16), together with eqs.(VI.3.10) and (VI.3.11), then will yield

$$\widetilde{T}(\tau, t_1) = \widetilde{T}(\tau, t_0) - \frac{\Delta t}{a^{(0)}} \rho_v(\tau, t_0)\{B_{1,0}E_2(\alpha_1 m_1 + \tau) + B_0 E_2(\tau_0 - \tau)\}, \qquad \text{(VI.4.11)}$$

$$T^{(1)}(m, t_1) = T^{(1)}(m, t_0) - \frac{\Delta t}{a^{(1)}} \rho_w^{(1)}(m) \sum \frac{\alpha_i}{\alpha_w} B_{i,0} E_2[\alpha_i (m_i - m)]. \qquad \text{(VI.4.12)}$$

Specifically, at $\tau = 0$, $m = 0$ the following relations exist:

$$\widetilde{T}(0, t_1) = \widetilde{T}(0, t_0) - \rho_v(0, t_0) \frac{\Delta t}{a^{(0)}} B_{1,0} E_2(\alpha_1, m_1), \qquad \text{(VI.4.13)}$$

/174

$$T^{(1)}(0, t_1) = T^{(1)}(0, t_0) - \rho_w^{(1)}(0) \frac{\Delta t}{a^{(1)}} \frac{\alpha_1}{\alpha_w} B_{1,0} E_2(\alpha_1, m_1). \qquad \text{(VI.4.14)}$$

It is obvious from eqs.(VI.4.11) and (VI.4.12) that cooling in the cloud does not extend to a great depth: $E_2(\tau_0 - \tau) = 0$ in the upper layer, while $E_2(\alpha_1 m_1 + \tau)$ rapidly decreases with increasing τ. Conversely, above the cloud the cooling extends to great heights since $E_2(\alpha_1 |m_1 - m|)$ varies slowly.

It is also evident that the cooling within the clouds proceeds at greater speed than above the cloud, because of the relation

$$\frac{\rho_0}{\rho_m} \approx 10 \frac{\rho_0}{\rho_{00}}.$$

For the same reason, the absolute value of cooling at the upper boundary of the cloud is considerably greater than directly above it.

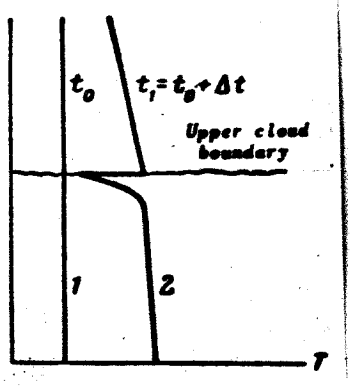

Fig.VI.4.1 Qualitative Nature of the Temperature Profile in the Vicinity of the Upper Cloud Boundary

We encounter here the phenomenon of a discontinuity of radiation temperatures on the interface of two media with different optical properties. It is known [see (Bibl.10)] that the problem of radiative transfer of heat is characterized by a temperature discontinuity at the boundary in the case of continuous intensity. In the case of constant temperature at the initial moment, this discontinuity appears in analytical form.

Thus, if the following equality exists at the initial instant:

$$T^{(0)}(z, 0) = T^{(1)}(z, 0) = \text{const},$$

then, after a certain, not excessively long, interval of time a temperature profile is established whose qualitative features are represented by Curve 2 in Fig.VI.4.1.

The obtained temperature discontinuity must be considered as a mathematical idealization of the real effect of formation of a sharp temperature inversion at the upper boundary of a stratus cloud, since the concept of the boundary, in itself, is an idealization of the transitional layer between the cloud and the

medium above the cloud. Theoretical considerations permit to determine the thickness of the inversion $\Delta T = T^{(1)}(0, t) - T^{(0)}(0, t)$ as a function of time but do not give a quantitative estimate on the thickness of the inversion layer.

Judging by the fact that the cooling extends only slightly into the depth of the cloud (to within 50 - 100 m), it can be assumed only that the thickness of this layer is small - of the same order as the thickness of the interface between the cloud and the medium above the cloud.

It should be mentioned that this temperature inversion is the result of radiative cooling of the cloud. In fact, the same phenomenon is involved in a study of radiative temperature inversion or radiative cooling and both these terms can be used in the same sense.

To conclude our statements, we give the computational results on radiative cooling for the case that

$$T^{(0)}(z, t_0) = T^{(1)}(z, t_0) = 273°.$$

Assuming that $\rho_v(z, t_0) = 0.5$ gm/m^3, eq.(VI.4.11) will furnish the distribution of temperature, moisture, and liquid-water content with depth in the cloud at the instant $t_1 = t_0 + \Delta t(\Delta t = 0.5$ hr), presented in Table VI.4.1. Here the initial temperature above the cloud is retained. /175

TABLE VI.4.1

z, km	$T^{(0)}(z, t_1)$	$\rho_w^{(0)}(z, t_1)$, g/m^3	$\rho_v^{(0)}(z, t_1)$, g/m^3	$\hat{T}^{(0)}(z, t_1)$	z, km	$T^{(0)}(z, t_1)$	$\rho_w^{(0)}(z, t_1)$, g/m^3	$\rho_v^{(0)}(z, t_1)$, g/m^3	$\hat{T}^{(0)}(z, t_1)$
0	269.2	3.72	1.19	272.3	0.055	272.9	4.88	0.03	273.0
0.018	272.2	4.65	0.26	272.8	0.073	272.9	4.88	0.03	273.0
0.036	272.8	4.84	0.07	272.95	0.091	273.0	4 91	0.0	273.0

Table VI.4.1 shows that, during the first half-hour, the upper part of the cloud cools rapidly. No doubt, this is a manifestation of the small absorption coefficients ($\alpha_1 = 0.2$ cm^2/gm) participating in the process of radiant heat exchange. For comparison purposes, the temperature $T^{(0)}(z, t_1)$, calculated from eq.(VI.4.11) for a rougher spectrum model in accordance with which the interval ($4 - 40\mu$) is divided into two parts with the absorption coefficients $\alpha_1 = 1$ cm^2/gm and $\alpha_2 = 10$ cm^2/gm, is given in Column 5 of Table VI.4.1.

The calculations of the temperature on the upper boundary of the cloud $T^{(0)}(0, t)$ at successive instants of time, shown in the first row of Table VI.4.2, characterizes the time rate of cooling.

TABLE VI.4.2

	t_0	t_1	t_2	t_3	t_4	t_5
1. $T^{(0)}(0, t)$, deg	273	269.2	267.0	266.1	265.3	265.0
2. $\rho_w^{(0)}(0, t)$, gm/m^3	4.91	3.72	3.20	3.00	2.81	2.76
3. $\rho_v^{(0)}(0, t)$, gm/m^3	0.5	1.19	1.71	1.91	2.10	2.15
4. $T^{(0)}(0, t)$, deg ($\Delta t = 0{,}254$ hr)	273	269.6	267.5	266.3	265.6	
5. $T_c^{(0)}(0, t)$, deg	273	—	271.6	—	270.8	
6. $T^{(0)}(0, t)$, deg (at variable $\rho_v(0, t)$)	273	269.2	262.0			

The Table shows that the rate of cooling decreases rapidly. An investigation of the above quantity $R^{(0)}(\tau, t)$ yields an explanation for this phenomenon: As a result of intensive cooling, at the initial instant, a strong temperature inversion takes place in the boundary layer, which prevents further cooling of the cloud.

The time interval Δt, in our calculation, is equal to 0.5 hr. To demonstrate the reliability of the computation, the values of $T^{(0)}(0, t)$ at the same instants of time and computed for $\Delta t = 0.25$ hr are given in the fourth row of Table VI.4.2. The fifth row shows the values of $T^{(0)}(0, t)$ for the case of a "gray" atmosphere - $T_{gr}(0, t)(\alpha_w = 1$ cm^2/gm). Here the cooling of the cloud is considerably less.

The second and third rows of Table VI.4.2 give the time rate of change in moisture in the upper part of the cloud and the corresponding variations in its liquid-water content. Clouds of the stratus type, in accordance with the data given in Table I.1.6, are characterized by liquid-water contents of the order of 0.2 - 0.3 gm/m^3. It is obvious that, for stratus clouds, the presence of liquid water in amounts of the order of 1.5 - 2.5 gm/m^3 is not typical. Therefore, we assume in our calculations that all the condensed water either drops out of the cloud or is redistributed so that the geometric dimensions of the /176 cloud and its optical thickness increase while the liquid-water content on each level in the upper layer remains as before. As shown above, the radiation balance on a given level is retained in this case. If all the condensed moisture is retained in the upper part of the cloud, its radiative cooling will increase strongly. A corresponding example for variations in $T^{(0)}(0, t)$ is given in the sixth row of Table VI.4.2.

As distinguished from the cloud itself, the layer above the cloud cools extremely slowly. Calculations show that, for the selective model of the water-vapor spectrum, this layer will cool by 0.3° during the first two hours. Further cooling will proceed at about the same rate. Therefore, a temperature inversion of the order of 7 - 8° is established in the boundary layer, with a thickness of nearly 100 m, approximately two hours after the initial instant, characterized by a temperature which is constant with height in the cloud and

above it.

In conclusion, we will discuss the effect of moisture condensation on the temperature of the cloud. Using the straight line $\overline{T}$ instead of the curve $\tilde{T}$ in the graph of Fig.VI.3.1 and neglecting condensation, we can compute the temperature for each step Δt, which will naturally be lower than the previous temperature. Corrections for condensation $\Delta T^{(0)}(0, t)$ for the four time steps (Δt = = 0.5 hr) are given in Table VI.4.3 where, in computing $\Delta T^{(0)}(0, t_k)$, we used

TABLE VI.4.3

t_k	t_1	t_2	t_3	t_4
$\Delta T^{(0)}(0, t_k)$	1.9	2.75	2.85	3

the "true" temperature, i.e., the temperature obtained when taking the condensation in the (k-1)-th step into consideration. The Table shows that, due to the heat of condensation liberated during radiative cooling of the cloud, the temperature at the given instant increases by about $2 - 3^{\circ}$.

Section 5. Calculation of the Radiative Heat Influx

In determining the values of $T^{(j)}(z, t_k)$ by means of eqs.(VI.3.15) and (VI.3.16), the most difficult point is calculating the radiative heat influx $R^{(j)}(z, t_{k-1})$ from the given temperature, moisture, and liquid-water content at the instant t_{k-1}.

First, we will discuss the calculation of $R^{(0)}(0, t)$ since a determination of the radiation temperature of the upper portion of the cloud layer is of the greatest interest.

For $\tau = 0$,

$$R^{(0)}(0, t) = \rho_v(0, t)\left\{\sum_{i=1}^{3} a_i \int_0^{m_1} B_i^{(1)}(\xi, t) E_1(a_i \xi)\, d\xi + \right.$$
$$\left. + \int_0^{\tau_0} B^{(0)}(\xi, t) E_1(\xi)\, d\xi - 2B^{(0)}(0, t)\right\}. \qquad \text{(VI.5.1)}$$

We will consider the quantity

$$X(0, t) = \int_0^{\tau_0} B^{(0)}(\xi, t) E_1(\xi)\, d\xi. \qquad \text{(VI.5.2)}$$

Let /177

$$B^{(0)}(\tau, t) = B^{(0)}(0, t) + \tau \left.\frac{dB^{(0)}}{d\tau}\right|_{\tau=0} \quad \text{at} \quad \tau \approx 0 \qquad \text{(VI.5.3)}$$

Then,

$$X(0, t) = B^{(0)}(0, t)\,[1 - E_2(\tau_0)] + \left.\frac{dB^{(0)}}{d\tau}\right|_{\tau=0} \left[\frac{1}{2} - \tau_0 E_2(\tau_0) - E_3(\tau_0)\right],$$

or

$$X(0, t) = B^{(0)}(0, t)\,[1 - E_2(\tau_0)] \left\{1 + \frac{\varphi(\tau_0)}{B^{(0)}(0, t)} \left.\frac{dB^{(0)}}{d\tau}\right|_{\tau=0}\right\}, \qquad \text{(VI.5.4)}$$

where

$$\varphi(\tau_0) = \frac{\frac{1}{2} - \tau_0 E_2(\tau_0) - E_3(\tau_0)}{1 - E_2(\tau_2)}.$$

It is easy to demonstrate that $\varphi(0) = 0$ $\frac{d\varphi}{d\tau_0} > 0$ for any τ_0, $\lim_{\tau_0 \to \infty} \varphi(\tau_0) = \frac{1}{2}$.

Here,

$$\varphi(\tau_0) \approx \frac{1}{2}, \qquad E_2(\tau_0) \approx 0,$$

if $\tau_0 > 3$.

Therefore, for all real clouds, even for very thin ones, there exists the relation

$$X(0, t) = B^{(0)}(0, t) \left\{1 + \frac{1}{2B^{(0)}(0, t)} \left.\frac{dB^{(0)}}{d\tau}\right|_{\tau=0}\right\}. \qquad \text{(VI.5.5)}$$

We recall that

$$\frac{dB}{d\tau} = \frac{1}{\alpha_v \rho_v} \frac{dB}{dT} \frac{dT}{dz}, \qquad B(T) = \frac{\sigma T^4}{\pi B_0}, \qquad \frac{dB}{dT} = \frac{4\sigma}{\pi B_0} T^3.$$

Hence

$$X(0, t) = B^{(0)}(0, t) \left\{1 + \frac{\cdot 2}{\alpha_v \rho_v T(0, t)} \left.\frac{dT^{(0)}}{dz}\right|_{z=0}\right\}. \qquad \text{(VI.5.6)}$$

For $\alpha_v = 1000$ cm^2/gm, $\rho_v = 0.5$ gm/m^3, $T(0, t) = 273^\circ$ we obtain

$$X(0, t) = B^{(0)}(0, t) \left\{1 + 0.00015 \left.\frac{dT}{dz}\right|_{z=0}\right\}, \qquad \text{(VI.5.7)}$$

where $\frac{dT^{(0)}}{dz}$ is expressed in deg/km.

The expression (VI.5.7) shows that, for any values of $\left.\frac{dT^{(0)}}{dz}\right|_{z=0}$ all the way to gradients of the order of 100 deg/km it can be practically assumed that

$$X(0) = B^{(0)}(0, t) \tag{VI.5.8}$$

for clouds with a liquid-water content of $\rho_v \geq 0.1$ gm/m^3.

/178

Since no large temperature gradients occur inside the cloud it can, with even greater justification, be assumed that

$$X(\tau, t) = \int_0^{\tau_0} B^{(0)}(\xi, t) E_1(|\tau - \xi|) d\xi = B^{(0)}(\tau, t)[2 - E_2(\tau) - E_2(\tau_0 - \tau)]. \tag{VI.5.9}$$

The physical meaning of eqs.(VI.5.8) and (VI.5.9) becomes obvious when examining the sum of the second and third terms in the braces of eq.(VI.5.1):

$$Z(\tau, t) = \int_0^{\tau_0} B^{(0)}(\xi, t) E_1(\xi) d\xi - 2B^{(0)}(\tau, t) - X(\tau, t) - 2B^{(0)}(\tau, t). \tag{VI.5.10}$$

As shown above, $Z(\tau, t)$ represents the radiation balance of the cloud proper (difference between inflow and outflow of energy), neglecting radiation coming from the outside. The equality (VI.5.10) together with eq.(VI.5.8) will give

$$Z(0, t) = -B^{(0)}(0, t), \tag{VI.5.11}$$

and, at a sufficient depth inside the cloud, eq.(VI.5.9) will yield

$$Z(\tau, t) = -B^{(0)}(\tau, t)\{E_2(\tau) + E_2(\tau_0 - \tau)\} \approx 0. \tag{VI.5.12}$$

The last two expressions show that, with respect to long-wave radiation, an optically dense cloud is a black body and its inner layers are in a state of thermodynamic equilibrium (within the frame of radiant heat exchange).

The conclusion as to the inner layers agrees with the results of Chapter IV. It was shown there that radiation from the boundaries of the cloud is subject to Kirchhoff's law and, strictly speaking, is not equal to the radiation of a black body. In our case, the cloud behaved like a black body because radiation was neglected. We recall that the difference from black-body radiation, according to the data in Chapter IV, is about 10% everywhere except in the transparent interval (8 - 12μ) where it is equal to 20%. It makes sense to take such a difference into consideration when determining the spectral radiative fluxes. In this Chapter, only the radiative influx of heat is of interest and the error of 10 - 20% in its determination is negligible. At any rate, this error is less than the errors due to other factors.

Next, we will derive the quantity

$$Y(0, t) = \sum_{i=1}^{3} \alpha_i \int_0^{m_i} B_i^{(1)}(\xi, t) E_1(\alpha_i \xi) d\xi, \tag{VI.5.13}$$

which determines the influx of energy to the cloud from layers above the cloud. Generally speaking, $Y(0, t)$ varies in time with variations in the temperature and moisture in the layer above the cloud. However, in computing $R^{(o)}(0, t)$ for time intervals which are not too great, it can be considered that $Y(0, t)$ is not a time-dependent quantity since $T^{(1)}$ and $\rho_w^{(1)}$ vary much slower than $T^{(o)}$ and $\rho_v^{(o)}$. Table VI.5.1 gives the values of $Y(0, t_k)$ for five time steps (Δt = = 0.5 hr) accounting for the changes in $T^{(1)}$ and $m^{(1)}$ in each step according to the data of example 1.

If, in computing $R^{(o)}(0, t_k)$, the quantity $Y(0, t_k)$ from Table VI.5.1 is replaced by a constant value of $Y(0, t_1) = 0.69816$ we will obtain the temperature values of $\hat{T}^{(o)}(0, t_k)$ given in Table VI.5.2 along with "exact" values of $T^{(o)}(0, t_k)$ computed from $Y(0, t_k)$.

TABLE VI.5.1 /179

	k				
	1	2	3	4	5
$Y(0, t_k)$	0.69816	0.69786	0.69654	0.69515	0.69422

TABLE VI.5.2

	k				
	1	2	3	4	5
$\hat{T}^{(0)}(0, t_k)$	261.3	258.2	255.7	253.9	252.8
$T^{(0)}(0, t_k)$	261.3	258.2	255.7	253.9	252.7

Obviously, the assumption $Y(0, t)$ = const ensures a greater accuracy and is justified at least for time intervals of the order of three hours.

The following examples show that, in the computation with eq.(VI.5.13), the quantities $T^{(1)}(z, 0)$ and $\rho_w^{(1)}(z, 0)$ must be known only in the layers of a thickness of 1 - 3 km above the upper boundary of the cloud.

We will select here the layer of a thickness of z_0 above the clouds. To this layer, there corresponds a mass of water vapor m_0.

We will present $Y(0)$ in the form of

$$Y(0) = \sum_{i=1}^{3} \alpha_i \int_0^{m_0} B_i^{(1)}(\xi) E_1(\alpha_i \xi)\, d\xi + \sum_{i=1}^{3} \alpha_i \int_{m_0}^{m_1} B_i^{(1)}(\xi) E_1(\alpha_i \xi)\, d\xi$$

or

$$Y(0) = \sum_{i=1}^{3} \left\{ \tilde{B}_i [1 - E_2(\alpha_i m_0)] + \tilde{\tilde{B}}_i [E_2(\alpha_i m_0) - E_2(\alpha_i m_1)] \right\}, \qquad \text{(VI.5.14)}$$

where $\tilde{B}_i$ and $\tilde{\tilde{B}}_i$ are mean values of the function $B_i^{(1)}(\xi)$ on the intervals $(0, m_0)$ and (m_0, m_1), respectively. If the temperature decreases with height, then

$$\tilde{B}_i > \tilde{\tilde{B}}_i. \qquad \text{(VI.5.15)}$$

TABLE VI.5.3

i	α_i, cm²/g	z_0, km							
		1		2		3		4	
		m_0, g/cm²							
		0.40		0.68		0.87		1.0	
		a	b	a	b	a	b	a	b
1	0.2	0.240	0.250	0.340	0.150	0.390	0.100	0.430	0.070
2	4	0.936	0.063	0.985	0.014	0.994	0.001	0.997	0.003
3	10	0.997	0.003	0.999	0	1	0	1	0

In Table VI.5.3, the values of the quantities $a = 1 = E_1(\alpha_1 m_0)$ and $b = E_2(\alpha_1 m_0) - E_2(\alpha_1 m_1)$ are given for $z_0 = 1, 2, 3, 4$ km; $i = 1, 2, 3$; $\alpha_1 = 0, 2, 4, 10$ cm²/gm. In the computations it was assumed that /180

$$^{1}(0)\, e^{-zk}, \qquad k = 0{,}45\ km^{-1}, \qquad m_0 = \int_0^{\infty} \rho_w^{(1)}(z)\, dz.$$

The selected distribution of moisture with height corresponds approximately to Hann's formula.

The computation showed that for $i = 1, 2, 3$ it is actually sufficient to integrate over ξ in eq.(VI.5.13) with respect to the interval $(0, m_0)$ which corresponds to a layer about 4 km in thickness above the cloud. Here we disregarded the inequality (VI.5.15) and also the fact that B_1 and B_2 are smaller than B_3.

Table VI.5.4 gives the actual upper limit of integration in eq.(VI.5.13) for the real distribution of temperature and moisture with height. In each example, we give the individual terms ($i = 1, 2, 3$) in the expression (VI.5.13) and their sums $\Delta Y(0)$ for the atmosphere layers Δz shown in the first column; δ are the errors in the quantity $Y(0)$ due to neglecting, in eq.(VI.5.13), the thickness of the atmosphere higher than 1 km and higher than 3 km above the upper boundary of the cloud.

Thus, in determining Y(0) the integration in eq.(VI.5.13) must be carried out only in the interval $(0, m_0)$ where m_0 corresponds to the height 1 - 3 km above the cloud. The same statement also holds for $Y(\tau)$.

TABLE VI.5.4

Δz, km	i			ΔY (0)	δ, %	i			ΔY (0)	δ, %
	1	2	3			1	2	3		
	Example 1					*Example 2*				
0—1	0.080	0.082	0.532	0.694	7.0	0.108	0.106	0.556	0.770	1.1
1—3	0.012	0.012	0.020	0.044	0.86	0.010	0	0	0.010	0.24
3—10	0.004	0.002	0	0.006	—	0.009	0	0	0.009	—
	Example 3					*Example 4*				
0—1	0.134	0.110	0.582	0.826	2.5	0.041	0.092	0.559	0.692	5.0
1—3	0.007	0	0	0.007	1.18	0.013	0.008	0.008	0.029	0.98
3—10	0.002	0	0	0.002	—	0.005	0.002	0	0.007	—

* In examples 1, 2, and 3, the experimental data are given only for heights of $z \approx 1$ km. Above this level, a linear temperature distribution is assumed and $\rho_w^{(1)}(z)$ is assigned according to Hann's formula.

The expression for the radiative heat influx in the cloud $R^{(0)}(\tau, t)$ taking the above evaluations and eq.(VI.5.12) into consideration, can then be written as

$$R^{(0)}(\tau, t) = \rho_v(\tau, t)\left\{\sum_{i=1}^{3}\alpha_i\int_0^{m_0} B_i^{(1)}(\xi, t_0)\,E_1(\alpha_i\xi + \tau)\,d\xi - B^{(0)}(\tau, t)\,[E_2(\tau) + E_2(\tau_0 - \tau)]\right. \quad \text{(VI.5.16)}$$

Making use of the identity

$$B_i^{(1)}(\xi, t_0) = B_i^{(1)}(\xi, t_0) - B_i^{(1)}(0, t_0) + B_i^{(1)}(0, t_0),$$

it is easy to reduce eq.(VI.5.16) to the form of /181

$$R^{(0)}(\tau, t) = \rho_v(\tau, t)\left\{\sum_{i=1}^{3}\alpha_i\int_0^{m_0}[B_i^{(1)}(\xi, t_0) - B_i^{(1)}(0, t_0)]\,E_1(\alpha_i\xi + \tau)\,d\xi + \right.$$
$$\left. + \sum_{i=1}^{3} B_i^{(1)}(0, t_0)\,[E_2(\tau) - E_2(\alpha_i m_0 + \tau)] - B^{(0)}(\tau, t)\,[E_2(\tau) + E_2(\tau_0 - \tau)]\right\}. \quad \text{(VI.5.17)}$$

A calculation on the basis of eq.(VI.5.17) is more accurate than based on eq.(VI.5.16) because of the reduction in the order of magnitude of the integral term whose approximate computation is the principal source of errors. Furthermore, $E_1(\alpha_i \xi)|_{\xi=0} = \infty$ at $\tau = 0$, and the accuracy of calculation is considerably increased by equating the factor at $E_1(\alpha_i \xi)$ under the integral sign to zero.

Limitation of the calculation to the layer $(0, m_0)$ in the determination of $Y(\tau)$ leads to the possibility of a further simplification in eq.(VI.5.17). In fact, in the interval $(0, m_0)$ it is possible to approximate $\Delta B_i^{(1)}(\xi)$ by the linear function

$$\Delta B^{(1)}(\xi) = B_i^{(1)}(\xi, t_0) - B_i^{(1)}(0, t_0) = b_i \xi \qquad \text{(VI.5.18)}$$

or to assume

$$\Delta B_i^{(1)}(\xi) = \Delta \tilde{B}_i^{(1)} = \text{const} \qquad \text{(VI.5.19)}$$

and to determine $\Delta \tilde{B}_i^{(1)}$ for instance as the arithmetic mean of the values of $\Delta B_i(\xi)$ in the interval $(0, m_0)$. The selection of the method of approximation is suggested by the nature of the experimental data.

Table VI.5.5 gives the errors in computing the quantity

$$\tilde{Y}(0) = \sum \alpha_i \int_0^{m_0} B_i^{(1)}(\xi) E_1(\alpha_i \xi) d\xi \qquad \text{(VI.5.20)}$$

making use of eq.(VI.5.18) (δ_1) and eq.(VI.5.19) (δ_2) in the same four examples. Here the values obtained by numerical integration with eq.(VI.5.20) are taken to be the exact values of Y(0).

TABLE VI.5.5

	Example			
	1	2	3	4
δ_1, %	2.0	5.8	5.3	1.6
δ_2, %	2.8	3.8	2.3	1.9

The expression of $R^{(0)}(0, t)$ for the condition (VI.5.19), which is recommended for approximate estimates of the value of radiative cooling of the cloud at its upper boundary, is given below:

$$R^{(0)}(0, t) = \rho_v(0, t) \left\{ \sum_{i=1}^{3} \Delta \tilde{B}_i [1 - E_2(\alpha_i m_0)] + \right.$$

$$+ [B^{(1)}(0, t_0) - B^{(0)}(0, t)] - \sum_{i=1}^{3} B_i^{(1)}(0, t_0) E_2(\alpha_i m_0). \qquad \text{(VI.5.21)}$$

For computations by means of eq.(VI.5.21), the following factors must be known: /182

1) Liquid-water content of the upper part of the cloud.
2) Distribution of moisture above the cloud at the initial instant in a layer of 1 - 3 km thickness, for deriving m_0 from the formula

$$m_0 = \int_0^{z_2} \rho_w^{(1)}(z)\, dz;$$

where the height is counted from the top of the cloud upward.
3) Distribution of temperature in the same layer at the same time for deriving

$$\Delta B_i^{(1)}(\xi) = B_i^{(1)}(\xi, t_0) - B_i^{(1)}(0, t_0)$$

and for determining the mean value of $\widetilde{\Delta B_i}$.
4) The function $B_i(T)$ for the determination of $B_i^{(1)}(\xi, t_0)$ and $B_i^{(0)}(0, t)$; graphs of these functions are given in Chapter I, Sect.5.
5) Tables of functions $E_2(x)$ (see Bibliography at end of Chapter I).

In conclusion we note the following:

1. If a temperature inversion, concentrated in a narrow layer, exists at the upper boundary of the cloud, then it is logical, in calculations based on eq.(VI.5.21) or on a similar relation, to take $B^{(1)}(0, t_0)$ as the value of this function for temperatures at the upper boundary of the inversion layer and to compute $B^{(0)}(0, t_0)$ from the temperature at its base.

2. From all above computations (see also Sect.4), it follows that the most suitable time step in the computation of $T^{(0)}(z, t_k)$ is 0.5 hr ($\Delta t = \frac{1}{48}$). The step width should be increased for the layer above the cloud.

3. The approximate computational formulas (VI.5.17) and (VI.5.18) given above are correct only for sufficiently dense clouds. In the case of optically thin clouds the relations (VI.5.8) or (VI.5.9) cannot be used and $X(\tau)$ is determined by numerical integration.

4. From physical considerations and based on the assumption as to the time-invariance of $Y(\tau, t)$, the calculations of radiative cooling with the above approximate formula must be limited to time intervals of the order of 3 - 6 hrs.

5. The assumption of $Y(\tau, t) = \varphi(\tau)$ leads to a separation of the problem of determining the temperature within the cloud from the corresponding problem

for the layer above the cloud. Thus, the simultaneous computation with eqs. (VI.3.15) and (VI.3.16) must be replaced by calculation with eq.(VI.3.15) and corresponding approximate expressions. Specifically, it is possible to determine directly the value of inversion

$$\Delta T = T^{(0)}(0, t_0) - T^{(0)}(0, t) \qquad \text{(VI.5.22)}$$

with the aid of eqs.(VI.3.15) and (VI.5.17) or eqs.(VI.3.15) and (VI.5.21).

6. After determining $R^{(0)}(\tau, t_k)$ from eq.(VI.5.17) and $T^{(0)}(\tau, t_k)$ from eq.(VI.3.15), $\rho_w^{(0)}(\tau, t_k)$ is computed by means of Magnus' formula [eq.(VI.1.5)] and then $\rho_v(\tau, t_k)$ by means of eq.(VI.1.6).

Section 6. Comparison with Observation

The above-described methodology was applied to calculating the radiative cooling of clouds under real atmospheric conditions. Data obtained with aerostats and radiosondes by the Central Aerological Observatory were used.

TABLE VI.6.1

	z, km									
	0.2	0.7	1.5	3.1	4.6	5.2	5.7	7.4	9.4	12.1
t, °C	21.5	21.2	15.5	3.5	−7.5	−9.2	−13.2	−24.2	−39.2	−59.8
u, %	64	62	60	70	68	66	65	60	60	—

Four examples of stratus cloudiness were investigated*.

Example 1. Table VI.6.1 gives the distribution of temperature and of relative humidity u with height, according to radiosonde data obtained over 21 hours on 22 July 1957 in the vicinity of Moscow. /183

Visual observations from the earth's surface attest to the presence, at the time of sounding, of altocumulus and cirrus cloudiness of force 8**.

---

* The sounding data were selected for these cases and given to us by scientists of the Central Institute of Forecasts, Ye.I.Gogoleva and M.I.Gorodova, to whom the author expresses his sincere appreciation.

** The low relative humidity shown in Table VI.6.1 does not agree with the cloudiness. Apparently the radiosonde happened to enter a break between clouds.

At 2 hr 40 m on 23 July 1957, a thunderstorm developed. An attempt was made to estimate the possible radiative cooling of the clouds under these conditions and to determine the extent to which this cooling could explain the occurrence of the observed thunderstorm. The synoptic analysis made by M.I. Gorodova did not reveal other reasons for the storm at this time.

It is obvious that the data presented in Table VI.6.1 are insufficient for a quantitative analysis: the thickness of the cloud, the level of its position, and its liquid-water content are unknown factors.

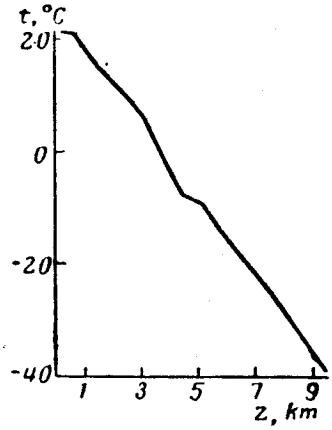

Fig.VI.6.1 Temperature Profile for 22 July 1957 at 21:00

Figure VI.6.1, plotted on the basis of data from Table VI.6.1, gives a layer of $4.6 \leq z \leq 5.2$ km with a reduced temperature gradient.

Let us assume that an Ac cloud is located below this layer, that its thickness is 0.6 km, and its liquid-water content 0.3 gm/cm^3. Under these conditions and with the temperature and moisture distributions presented in Table VI.6.1, the radiative cooling and the variations in liquid-water content were computed; the results are shown in Table VI.6.2. Here k characterizes the instant t_k, so that $t_k = t_{k-1} = 0.5$ hr; the height z in each layer was counted from the general boundary towards the depth of the layer.

Within 4 hours (eight time steps), the temperature of the uppermost part of the clouds was reduced by 14.5°. This led to the laws, discussed in Section 4: a) the time rate of cooling decreases rapidly; b) the cooling extends only negligibly into the depth of the cloud; c) the atmosphere above the cloud cools at a considerably slower rate than the cloud itself.

Thus, within four hours, a hyperadiabatic gradient was established in a narrow layer at the upper boundary of the cloud and the water content increased by a factor of 8. It is possible that, under certain conditions, such an unstable state may result in a thunderstorm.

The basic factors determining such extensive cooling in the considered /184

case are the large temperature gradient and the small optical thickness (m_1 = = 0.4 gm/cm^2) of the atmosphere above the cloud (see below). It must be remembered that the calculation was made almost without real information on the

TABLE VI.6.2

z, m	k								
	0	1	2	3	4	5	6	7	8
Temperature Variation in the Cloud									
0	265.5	261.3	258.2	255.7	253.9	252.7	252.0	251.4	251.0
60	265.9	265.7	265.5	265.3	265.1	264.9	264.7	264.6	264.5
120	266.3	266.3	266.3	266.3	266.3	266.3	266.2	266.2	266
Variation in Water Content									
0	0.3	1.12	1.57	1.85	2.14	2.25	2.32	2.35	2.38
60	0.3	0.35	0.40	0.44	0.48	0.52	0.56	0.58	0.63
120	0.3	0.3	0.3	0.3	0.3	0.3	0.32	0.32	0.32
Temperature Distribution in Above-Cloud Layer									
0	265.5	265.4	265.2	265.0	264.8	264.6	—	—	—
300	265.1	265.0	264.9	264.0	264.8	264.7	—	—	—
700	264.0	264.0	263.9	263.9	263.8	263.7	—	—	—

observed cloudiness, which means that the computational results are only tentative. Apparently, the value of liquid-water content, namely, 0.3 gm/m^3 used in the computation was too large. The data collected in Chapter I indicate that the average liquid-water content of Ac clouds is equal to about 0.1 - 0.2 gm/m^3. With such water content, the cooling at a given instant will be about 1.5 - 3.0 times smaller.

We will discuss three examples based on data obtained in aerostatic soundings.

As opposed to the first example, where a large Ac cloud located quite /185 high in the atmosphere was considered, we will here deal with more or less developed low-lying St clouds. In each case data are given on the temperature and moisture distribution with height and some information (largely descriptive) on the cloudiness. Data on the liquid-water content of the cloud are lacking. The soundings were repeated every three hours so that it was possible to compare the theoretical calculations with observational data.

Example 2. This example is based on temperature-distribution data obtained in three soundings (Curves I, II, III) and on moisture distribution obtained in the first sounding (broken curve), presented in Fig.VI.6.2. A Stratus region with an upper boundary at a height of 500 m is clearly expressed in the curves of the first and the remaining times of sounding. The positions of the upper boundary at each sounding time are indicated by crosses. In Curve II, the

upper cross corresponds to the boundary at the ascent and the lower, to the boundary at the descent. This example represents a typical case of a radiative inversion above a stratus cloud. The magnitude of the temperature inversion

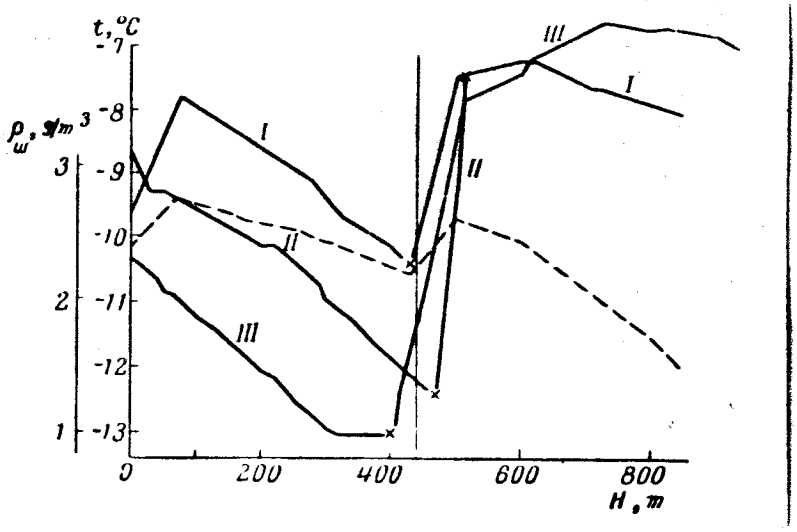

Fig.VI.6.2 Temperature Distribution with Height, 10 March 1962
I - 00.7 - 02.3 hr; II - 03.8 - 05.3 hr; III - 06.7 - 08.4 hr;
(the moisture distribution within 00.7 hr is shown as a broken line)

(up to 5° at the third sounding) and the thickness of its layer (nearly 100 m) agree well with the conclusions in Section 4.

TABLE VI.6.3

TIME RATE OF CHANGE OF TEMPERATURE AT THE UPPER BOUNDARY OF THE CLOUD

$\rho_r, g/m^3$	k									
	0	1	2	3	4	5	6	7	8	9
0.1	262.6	261.8	261.3	260.9	260.7	260.5	260.3	260.1	260.0	259.9
0.2	262.6	261.6	260.9	260.5	260.1	259.8	259.5	259.3	259.2	259.1
0.3	262.6	261.3	260.1	260.1	259.6	259.1	259.2	259.0	258.1	258.7

The development of the inversion during the period between the first and third soundings was computed with the above formula and was then compared with observations. The results of the computations of $T^{(0)}(0, t_k)$ are presented in Table VI.6.3.

The experimental material contained no information on the liquid-water content of the investigated cloud. The calculations were made for three values of water content: ρ_v: 0.1, 0.2, and 0.3 gm/m^3.

In Fig.VI.6.3, Curve 1 represents the time rate of change of the minimum temperature. If the level on which the temperature assumes its lowest value is

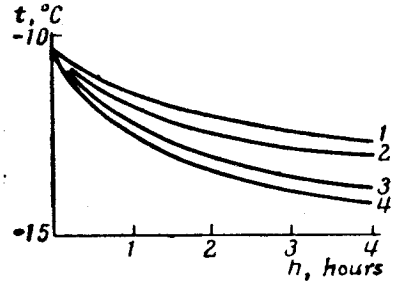

Fig.VI.6.3 Time Rate of Change of Minimum Temperature
1 - Actual data; 2, 3, and 4 - Calculation for ρ_v = 0.1, 0.2, and 0.3 gm/m^3

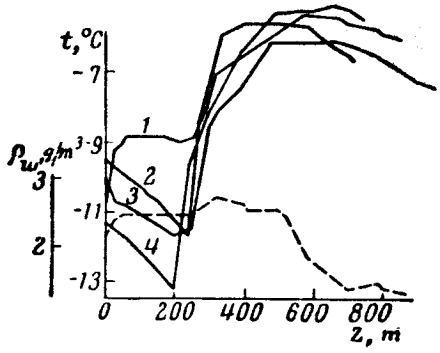

Fig.VI.6.4 Temperature Distribution with Height, 10 - 11 March 1956
1 - 19.0 - 20.9 hr; 2 - 22.1 - 23.9 hr; 3 - 01.3 - 03.2 hr; 4 - 04.2 - 05.7 hr; the distribution of moisture in 9 hrs on 10 March 1956 is shown by the broken line

considered to coincide with the upper boundary of the cloud, which approximately corresponds to the observational data, it is logical to compare the measured minimum temperatures with the value of $T^{(0)}(0, t_k)$. Curves 2, 3, and 4 represent the results of calculating the quantity $T^{(0)}(0, t_k)$ for a mean liquid-water content of the clouds equal to 0.1, 0.2, and 0.3 gm/m^3, respectively. The calculated cooling was obtained as more intensive than the true cooling which, to some extent, is due to the fact that we neglected turbulent mixing in our formulation of the problem (see Sect.9). The lack of measured data on $T^{(1)}(z, t_0)$ and of $\rho_w^{(1)}(z, t_0)$ above the level of z = 1 km also prevents satis-

factory agreement of calculated and measured temperatures.

It is interesting to compare the values of cooling in the first and second examples. At the same liquid-water content $\rho_v = 0.3$ gm/m^3, the cloud in the first example was cooled by 13.5° within three hours and in the second, it was cooled by 4°. The considerably less extensive cooling in the second example is explained by the presence, at the initial instant, of a temperature inversion above the cloud (as distinguished from the gradient of 6°/km in the first example) and of a large optical thickness of the atmosphere above the cloud ($m_1 = 1.4$ gm/cm^2 in the second example and $m_1 = 0.4$ gm/cm^2 in the first).

TABLE VI.6.4

VARIATION IN TEMPERATURE

z*, km	k					
	0	2	4	6	8	10
0.1	264.1	264.1	263.9	263.8	263.7	263.7
0.2	264.0	263.8	263.4	262.9	262.6	262.2
0.25	264.0	263.0	262.1	261.2	260.3	259.6

* z is counted from the earth's surface; z = 0.25 km is the upper boundary of the haze.

TABLE VI.6.5

z, km	k						
	0	1	2	3	4	5	6
0.1	0.05	0.05	0.07	0.09	0.11	0.13	0.13
0.2	0.05	0.07	0.09	0.15	0.19	0.24	0.29
0.25	0.05	0.15	0.27	0.29	0.43	0.55	0.59

Example 3. This example is based on the temperature and moisture distribution plotted in Fig.VI.6.4. The temperature is given for four observation times (solid curves), while the moisture is given for one reading (broken curve). At the initial instant, a ground layer of wet haze with an upper boundary at a height of 250 m was observed. In the next readings, the haze became denser and turned into fog. In the computation, the liquid-water content of the haze at the initial instant was assumed to be equal to 0.05 gm/m^3, for which reason an accumulation of liquid moisture up to 0.2 gm/m^3 was taken into

/186

account. The increase in liquid-water content above a value of 0.2 gm/cm^3 was disregarded in computing the temperature, i.e., it was assumed that all the excess water was redistributed (see Sect.4). The results of the calculation $T^{(0)}(z, t_k)$ and $\rho_v(z, t_k)$ are presented in Tables VI.6.4 and VI.6.5. The time rate of change in minimum temperature is plotted in Fig.VI.6.5.

Example 4. The data of the soundings on 9 March in 21.5 - 23.1 hr /187 are used as the initial instant. The corresponding temperature and dew-point

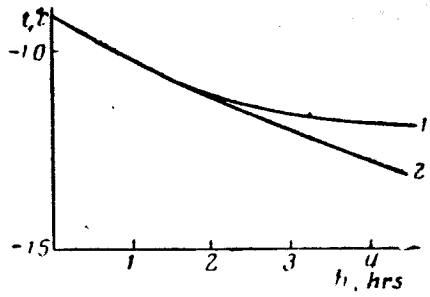

Fig.VI.6.5 Time Rate of Change in Minimum Temperature
1 - Actual data; 2 - Computed data

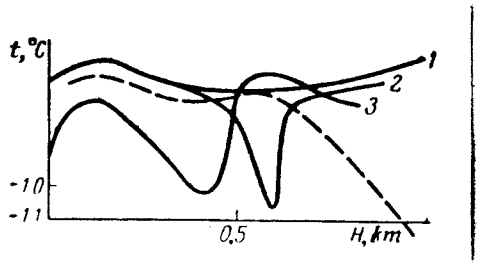

Fig.VI.6.6 Temperature Distribution with Height, 9 March 1965
1 - In 21.5 hr (measured); 2 - In 24 hr computed for the initial temperature distribution; (Curve 1) and dew-point temperature (broken curve);
3 - In 24 hrs (measured)

distribution t_d is plotted in Fig.VI.6.6 (Curve 1 and broken line, respectively). No cloudiness was as yet observed at this time. After three hours, the sounding showed the presence of Stratus cloud and of a clearly expressed temperature inversion, as plotted in Fig.VI.6.6 (Curve 2).

An attempt was made to determine whether cloud formation, in this case, could have been due to radiation processes alone. For this, the calculation method had to be changed. Instead of a two-layer medium, a one-layer medium was used as basis and the radiative cooling was computed by means of eq.(VI.3.16) where $R(z, t_k)$ was determined from the relation [see eq.(I.2.45)]:

$$R(z, t_k) = \sum_{i=1}^{3} [\bar{\alpha}_{r,i}\rho_r + \bar{\alpha}_{w,i}\bar{\rho}_w] \left\{ \bar{B}_i(0, t_k) E_2(\tau_i) + \right.$$
$$\left. + \int_0^{\tau_i^*} \bar{B}_i(\xi, t_k) E_1(|\tau_i - \xi|)\, d\xi - 2\bar{B}_i(\tau_i, t_k); \right. \qquad \text{(VI.6.1)}$$

Here,

$$\tau_i = \int_0^z [\alpha_r \rho_r(\xi) + \alpha_{w,i}\rho_w(\xi)]\, d\xi.$$

At the initial instant $\rho_v = 0$, the radiative cooling is determined only by the water vapor and therefore is small. However, in computing the liquid-water content at each stage on the basis of eq.(VI.1.6), already the second step shows an accumulation of liquid-water content near the point $t^\circ = t_d$, after which the rate of cooling increases. The considerable acceleration of the process in this case is partly due to the sharp reduction in moisture above the level $t^\circ = t_d$, as shown in Fig.VI.6.6.

The theoretical temperature distribution three hours after the initial instant is represented by Curve 3 in Fig.VI.6.6. The diagram shows that the extent and thickness of the inversion layer, formed three hours after the initial instant, agrees well with the observational data. The locus of the inversion is shifted by almost 200 m with respect to the true location, a fact which can be explained by the inaccuracy in the experimental determination of the layer of zero moisture deficit. The cooling of the entire subinversion /188 layer, which actually occurred, is not confirmed by theory for the reasons given in Sections 4 and 10. Within three hours, a water content averaging 0.26 gm/m^3 accumulated in the 100 m layer.

The last example is of methodological interest, because of the fact that we did not introduce the cloud boundary with all the attendant difficulties in formulating the boundary conditions. Here, the thickness of the inversion layer can be determined accurately and was found to be 50 m, which confirms the above estimates.

Section 7. The Role of Reflection

As a result of the scattering process, part of the radiation incident on the cloud from the outside is reflected back into the atmosphere above the cloud while part of the ascending radiation within the cloud is reflected back into its depth. Therefore, there is some justification for replacing the scattering of long-wave radiation by its reflection from the boundary of the cloud. The formulation of the problem remains as before, except that the conditions on the interface between the cloud and the medium above the cloud assume the form (see Chapter I, Sect.3):

$$F_2^{(0)}(0) = A^{(0)} F_1^{(0)}(0) + (1 - A^{(1)}) F_2^{(1)}(0), \qquad \text{(VI.7.1)}$$
$$F_1^{(1)}(0) = A^{(1)} F_2^{(1)}(0) + (1 - A^{(0)}) F_1^{(0)}(0), \qquad \text{(VI.7.2)}$$

where $F_j^{(i)}(0)$ are the fluxes of ascending ($j = 1$) and descending ($j = 2$) radiation at the boundary of the cloud, contributed by the medium above the cloud ($i = 1$) and by the cloud itself ($i = 0$); $A^{(i)}$ is the albedo at the boundary, contributed by the corresponding medium.

The new boundary conditions lead to some change in the expression for the radiation balance in each of the media. Specifically, the radiation balance of the cloud $R^{(0)}(\tau, t)$ with the additional condition

$$I_2^{(0)}(0, r) = \text{const} = \frac{1}{\pi} F_2^{(0)}(0), \tag{VI.7.3}$$

where $I^{(0)}(0, r)$ is the intensity of descending radiation on the upper boundary of the cloud, is expressed in the form of

$$\begin{aligned} R^{(0)}(\tau, t) = \rho_v(\tau, t) \Big\{ & 2A^{(0)} E_2(\tau) \int_0^{\tau_0} B^{(0)}(\xi, t) E_2(\xi)\, d\xi + \\ & + 2(1 - A^{(1)}) E_2(\tau) \sum_{i=1}^{3} \alpha_i \int_0^{m_i} B_i^{(1)}(\xi, t) E_2(\alpha_i \xi)\, d\xi + \\ & + \int_0^{\tau_0} B^{(0)}(\xi, t) E_1(|\tau - t|)\, d\xi - 2B^{(0)}(\tau, t) \Big\}. \end{aligned} \tag{VI.7.4}$$

At $A = 0$, we have

$$\begin{aligned} R^{(0)}(\tau, t) = \rho_v(\tau, t) \Big\{ & 2E_2(\tau) \sum_{i=1}^{3} \alpha_i \int_0^{m_i} B_i^{(1)}(\xi, t) E_2(\alpha_i \xi)\, d\xi + \\ & + \int_0^{\tau_0} B^{(0)}(\xi, t) E_1(|\tau - \xi|)\, d\xi - 2B^{(0)}(\tau, t) \Big\}. \end{aligned} \tag{VI.7.5}$$

The last expression differs from eq.(VI.3.10) by the first term on the right-hand side, which is due to replacing the condition of equality of the intensities at the boundary by the more general condition of equality of the fluxes which is assumed in this Section.

It is difficult to define the advantage of one of the indicated conditions over the other. Strictly speaking, the equality of the intensities makes /189 sense only in the case of radiative equilibrium. The condition of equality of the fluxes follows directly from the expression of the heat balance at the interface of two media (see Chapter I, Sect.2) and is therefore more general. However, even this condition must be supplemented by the assumption (VI.7.3), which strongly limits the generality of the obtained results. Incidentally, it is not difficult to calculate that, on substitution of eq.(VI.3.10) by eq. (VI.7.5), the magnitude of radiative cooling changes negligibly, increasing by 10 - 15%.

Returning to the relation (VI.7.4), it will be noted that the radiation balance at the given levels varies linearly with the albedo $A^{(i)}$. Thus, this also holds for the degree of radiative cooling $\Delta T_k^{(0)}$ which, according to eq. (VI.3.15), is represented in the form of

$$\Delta T_k^{(0)}(\tau) = T^{(0)}(\tau, t_k) - T^{(0)}(\tau, t_{k-1}) = cR^{(0)}(\tau, t_{k-1}) \qquad \text{(VI.7.6)}$$

(the latter expression is written without taking account of the heat of condensation).

Figure VI.7.1 gives the correlation of $\Delta T_1^0(0)$ with $A^{(1)}$ in the following cases: $A^{(0)} = A^{(1)}$ (Curve 1); $A^{(0)} = \frac{3}{4} A^{(1)}$ (Curve 2); $A^{(0)} = \frac{1}{2} A^{(1)}$ (Curve 3); $A^{(0)} = 0$ (Curve 4); the case $A^{(0)} = A^{(1)} = 0$ is shown by the broken line.

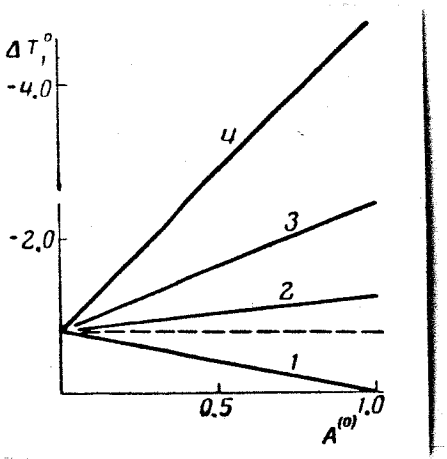

Fig.VI.7.1 Cooling as a Function of Albedo

The quantity $\Delta T_1^{(0)}(0)$ is determined by means of eq.(VI.7.6) at $\tau = 0$ and the initial data

$$T^{(0)}(z, t_0) = T^{(1)}(z, t_0) = \text{const.}$$

The time step Δt is assumed to be equal to 0.5 hr. The different variants of the ratio of $A^{(0)}$ to $A^{(1)}$ are due to the absence of scattering in the long-wave radiation above the cloud, which makes it logical to assume

$$A^{(0)} \leqslant A^{(1)}.$$

However, in our opinion, $A^{(0)}$ is only slightly smaller than $A^{(1)}$ (even the sign of the equality makes sense), in view of the fact that the optical thickness of the cloud is considerable and the reflection of the fluxes $F_2^{(1)}(0)$ and $F_1^{(0)}(0)$ to an almost equal degree is due to scattering in the upper part of the cloud.

In Chapter IV, estimates were made on the spectral albedo of stratus clouds in accordance with which, at $\rho_v = 0.2$ gm/m^3 and $t = 0^\circ$, the albedo will be $A^{(1)} \leq 10\%$ if $\lambda \leq 8\mu$ and $\lambda \geq 12\mu$. In the spectral interval ($8 \leq \lambda \leq 12\mu$), the value of $A^{(1)}$ is of the order of 20%. Figure VI.7.1 shows that, for such values of the albedo, the corrections to be made for cooling due to reflection

are small (except for the non-real case $A^{(0)} = 0$) everywhere except for the interval (8 - 12μ). At ($8 \leq \lambda \leq 12\mu$), in the closest to real case

$$\frac{3}{4} A^{(1)} < A^{(0)} < A^{(1)}$$

the correction due to reflection may be as high as 20 - 30%. This result represents some argument in favor of the assumption made in Section 2 as to the relatively unimportant influence of long-wave radiation scattering in clouds on the temperature of such clouds.

It is also of interest that, in accordance with Fig.VI.7.1, the cooling generally increases with an increase in $A^{(1)}$, i.e., with an increase in re- /190
flection of the radiation arriving at the cloud from the outside. This consideration is in itself trivial; however, as shown in Fig.VI.7.1, if $A^{(0)} \approx A^{(1)}$, i.e., if an approximately equal part of the radiation of the cloud proper is reflected back into its inner layer, the role played of this radiation will become extensive and the cooling will decrease with increasing $A^{(1)}$.

Section 8. Radiative Cooling by Day

In studying the literature on interaction between heating of clouds by absorption of solar radiation and their cooling by natural radiation, contradictions in the statements by various authors will be encountered. For instance in one paper (Bibl.3), it is shown that during the day clouds are heated by insolation; in another paper (Bibl.11) it is asserted that this heating can be neglected with respect to radiative cooling; in still another report (Bibl.12) it is assumed that heating and cooling due to the two above factors compensate each other to some extent; finally, in one paper (Bibl.13) arguments are derived in favor of cooling in the upper layers of clouds and heating in the deeper layers, under daytime conditions. Not one of these authors gave a quantitative analysis of both aspects of the process under consideration; at most, they calculated one of the two factors involved here and more often stayed within the limits of qualitative considerations.

In order to solve this problem completely, the equation of heat exchange in the cloud, the right-hand side of eq.(VI.1.1) must be supplemented by a term that represents the influx of heat due to absorption of infrared solar radiation. This term has the form of (see Chapter III)

$$Q_{\lambda}^{(0)}(z, t) = \int_{\lambda_0}^{\lambda_1} [\alpha_{r,\lambda} \rho_r + \alpha_{w,\lambda} \rho_w^{(0)}] \int I_{\lambda}^{(0)}(z, r, t)\, d\omega\, dt, \qquad \text{(VI.8.1)}$$

where $\lambda_0 \approx 0.75\mu$, $\lambda_1 \approx 2.5\mu$.

However, in view of the linearity of eq.(VI.1.1) and the fact that $Q_{\lambda}^{(0)}(z, t)$ is independent of temperature, the influence of heating and cooling can also be treated separately. Below, we present the results of Chapter III where the heating was investigated and the results of this Chapter where the cooling is

analyzed.

First, let us recall that radiative cooling rapidly decreases with time as the above-cloud inversion develops. In the simplest model which we discussed in Section 4 [initial conditions: $T^{(0)}(z, t_0) = T^{(1)}(z, t_0) = \text{const}$] the rate of cooling dropped from 8°/hr to zero, within three hours. The same result is obtained in using the actual observational data presented in Section 6. In examples 1 and 2, the cooling, within four hours from the initial instant, also decreased almost to zero.

For the same time intervals around noon, the insolation does not change quite so extensively. This makes it obvious that its influence will differ in different stages of development of the cloud and of the above-cloud inversion. In other words, the absorption does not depend on the temperature distribution within the cloud and above it. Cooling is largely determined by temperature. Therefore, the interaction of both factors, while maintaining ρ_v, ρ_w, and ζ, may yield substantially different results on change in the temperature profile.

Thus, according to data in Chapter III, a low cloud as a whole, depending on its thickness, absorbs 0.015 - 0.03 cal/cm^2·min at a zenith distance of the sun of $\zeta = 60^\circ$ and a water content of $\rho_v = 0.2$ gm/m^3. At $\zeta = 30^\circ$, other conditions being equal, the absorption is 0.09 - 0.13 cal/cm^2·min. From the computations performed in Section 4 it follows that as a consequence of radiation, such a cloud loses 0.05 cal/cm^2·min in the first half hour after the initial instant, characterized by a temperature which is constant with height and a /191 liquid-water content of $\rho_v = 0.25$ gm/m^3. By averaging the rate of cooling for three hours we obtain, for the same condition, a radiation equal to a value of 0.02 cal/cm^2·min.

In Example 3 of Section 6, the radiation in the first half hour is 0.04 cal/cm^2·min and, after three hours, becomes equal to 0.02 cal/cm^2·min. According to data in Section 6 (Example 1), a high cloud loses 0.26 cal/cm^2·min in the first half hour; according to the average rate of cooling, such a cloud will cool by 0.15 cal/cm^2·min within three hours. Finally, after three hours this cloud loses only 0.025 cal/cm^2·min. According to data in Chapter III, such a cloud receives 0.14 cal/cm^2·min of solar energy at $\zeta = 30^\circ$.

We see that, as a result of interaction of absorption and radiation, the cloud taken as a whole can be both cooled and heated. Prior to the development of inversion, the cloud will generally cool followed later by heating. Clouds of the middle layer (Example 1) will be cooled at least at the initial instants of time; low clouds (Example 3) may start heating immediately. When the sun is at the zenith, heating may predominate.

However, it does not make much sense to consider the cloud "as a whole".

The following examples show how radiative heating and cooling are distributed with cloud depth. In Fig.VI.8.1, Curve 1 represents the heat influx $Q_\lambda^{(0)}(z)$ per unit volume of the cloud, according to the data in Chapter III, while Curves 2 - 4 represent the heat loss in the case of $T^{(0)}(z, t_0) = T^{(1)}(z, t_0)$ in accordance with the data of Examples 1 and 3, respectively. Curves 2 - 4

correspond to the rate of cooling in the first hour after the initial instant.

The following two facts are clearly revealed: 1) The uppermost part of the cloud of 50 - 100 m thickness cools much more intensively than it heats; 2) heating penetrates into the cloud considerably deeper than does cooling. Therefore, the narrow upper layer of the cloud, during the day, will be in about the

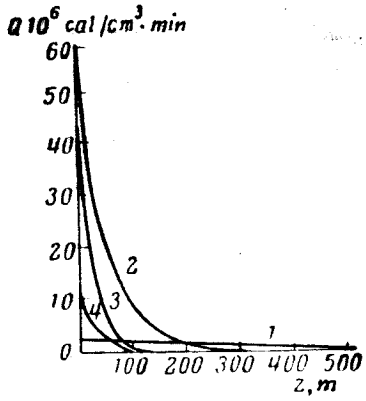

Fig.VI.8.1 Distribution of Heating (1) and of Cooling (2-4) in a Cloud

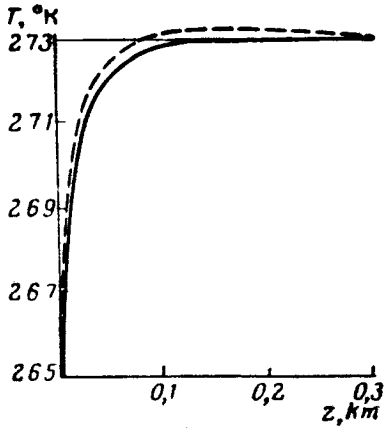

Fig.VI.8.2 Temperature Variation with Height under Night (Solid Curve) and Daytime (Broken Curve) Conditions

same condition with respect to radiative cooling as at night. Below this layer there is a considerably wider one which is heated by absorption of solar radiation. However, the rate of heating here is considerably less than that of cooling in the upper part of the cloud.

Figure VI.8.2 gives an example $\Delta T^{(0)}(z, t_1)$ computed for $T^{(0)}(z, t_0) = T^{(1)}(z, t_0) = 273^0$ (solid line - night conditions, broken line - daytime con-

ditions). At a distance of 85 m from the upper boundary of the cloud, cooling is replaced by heating which extends to a depth greater than 300 m. Maximum /192 heating occurs at z = 200 m and reaches 0.5°/hr.

The above comparisons reveal the basic differences of the processes of heating of a cloud by absorption of solar radiation and of its cooling due to long-wave radiation:

1) Heating varies much more slowly with time than does cooling.

2) Cooling of the uppermost part of the cloud reaches a higher order of magnitude than heating if the liquid-water content is the same.

3) Heating varies more smoothly along the vertical than does cooling and penetrates into greater depths of the cloud.

4) Heating does not depend on the temperature distribution in the upper part of the cloud and above it, whereas cooling decidedly depends on these quantities.

5) Heating is to a much greater extent dependent on the moisture of the cloud than is cooling.

The possibility of neglecting water vapor in the case of cooling is considered in Section 2 of this Chapter. The role of moisture in heating is discussed in Chapter I, Sect.4 where it is shown that in the near-infrared region of the spectrum the absorptivity of water vapor is greater than that of water.

In conclusion, we would like to mention that V.L.Gayevskiy (Bibl.21), in measuring fluxes of long-wave radiation in a cloudy atmosphere, also came to the conclusion that the radiative temperature change in the upper part of a cloud is about the same in daytime and at night: At night the rate of cooling is equal to 9.3°/day, and in the daytime it is 7.5°/day.

Section 9. Allowance for Turbulent Mixing

Radiative cooling of clouds takes place in a narrow boundary layer. It can therefore be expected that even weak turbulent mixing will substantially diminish the effect of cooling.

Simultaneous accounting for turbulent and radiative heat exchange considerably complicates the problem so that, in this Section, we will confine ourselves to an approximate solution for small time intervals.

9.1 Experimental Data

An even greater difficulty is created by the lack of data on the nature of turbulent exchange in clouds. Experimental determinations of the characteristics of turbulence in a free atmosphere are in their very beginnings. In addi-

tion, there is no instrumentation suitable for such investigations in clouds*. Therefore, the few available data are principally qualitative in nature and are based on investigations of indirect characteristics or else represent the results of not fully substantiated computations.

With the available data (Bibl.3, 14 - 17), the following facts can be established: 1) In passing from the cloud into the medium above the cloud, turbulent mixing decays; 2) more extensive turbulent exchange takes place in clouds than in a cloudless atmosphere.

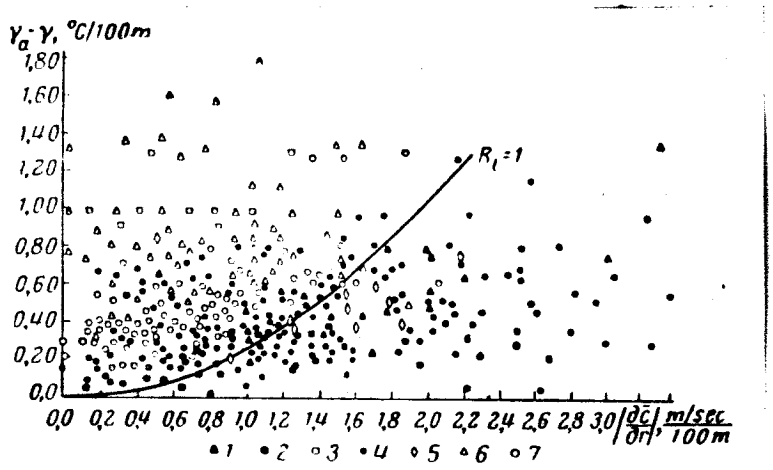

Fig.VI.9.1 Estimating the Richardson Number in the Atmosphere
1 - Friction layer; 2 - Below the tropopause; 3 - Tropopause; 4 - Clouds; 5 - Below the clouds; 6 - Above the clouds; 7 - "Pure" troposphere

Figure VI.9.1, taken from the paper by L.T.Matveyev and V.S.Kozharin (Bibl.14), gives the ratio of the difference $\gamma_a - \gamma$ to the vertical gradient /193 of wind velocity $\frac{du}{dz}$ under various conditions. This ratio determines the Richardson number, equal to

$$\mathrm{Ri} = \frac{g}{T} \frac{\gamma_a - \gamma}{\left(\frac{du}{dz}\right)^2}, \qquad \text{(VI.9.1)}$$

which, in turn, characterizes the rate of turbulent mixing. The smaller the

* In clouds the buffeting of aircraft can be measured. The turbulence in a given frequency range is estimated quantitatively. However, it is not known whether this same spectral interval can be considered responsible for the turbulent exchange of heat and moisture.

value of R_i the stronger will be the turbulent exchange. Figure VI.9.1 shows that turbulence is more developed within the cloud than below it and is much greater than in the layer above the cloud.

An analysis of the experimental data presented in Fig.VI.9.1 induced the authors of another paper (Bibl.14) to compute values of R_i at different levels. Their results are given in Table VI.9.1.

TABLE VI.9.1

Type of Cloud	No. of Cases	Height, m		Ri		
		Lower Boundary	Upper Boundary	Below Cloud	In Cloud	Above Cloud
St	14	420	900	0.6	1.0	19.7
Sc	16	1400	1800	1.4	1.4	62.7
Ns	12	850	1900	1.8	1.6	10.3
As — Ac	10	3100	3700	3.8	3.1	35.5
As	16	3050	3750	4.9	4.3	13.9

TABLE VI.9.2

Type of Cloud	k_t, m^2/sec	
	Cold Half of Year	Warm Half of Year
St	21.2; 2.8	28.2; 25.0
Sc	20.9; 11.1	
Ns	19.3; 43.0	

Readings of the accelerometer carried aboard an aircraft flying within and above a cloud (Bibl.3) are given in Fig.VI.9.2. The diagram shows that the originally nearly continuous buffeting of the aircraft within the cloud rapidly reduced to zero above the cloud, in a layer of about 100 m thickness where a temperature inversion existed in this particular case.

The nature of the available data does not permit to establish where the decay of turbulent exchange begins - in the upper part of the cloud or above it. From general considerations, it appears that the decay of turbulence takes place in the inversion layer which often encompasses also the upper part of the cloud (see Sect.10).

Some estimates of the coefficients of turbulent exchange k_t in stratus cloudiness are given in the paper by M.P.Churinova (Bibl.17). Table VI.9.2 shows the values of k_t based on data by this author (Bibl.17). The data in Table VI.9.2 represent calculations of the quantities k_t with D.L.Laykhtman's formula: /194

$$k_t = c \frac{2l}{\frac{d}{dz} \lg [(u_g - u)^2 + v^2]^2}, \qquad \text{(VI.9.2)}$$

where l is the Coriolis parameter; c is a constant, u_g is the velocity of the geostrophic wind; u and v are the horizontal wind velocity components. The

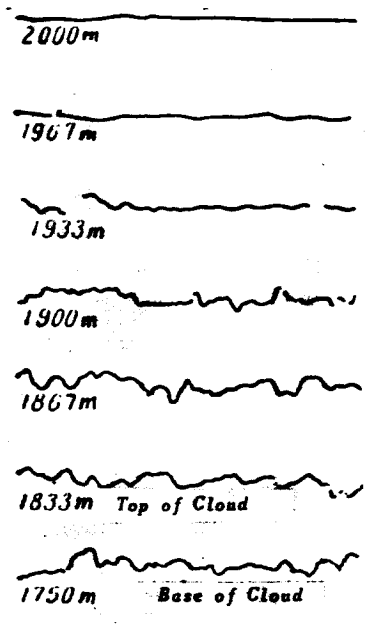

Fig.VI.9.2 Record of Buffeting of an Aircraft within and above a Cloud

computation was made on the basis of a large amount of data collected in aircraft and pilot-balloon measurements. The Table shows that the value of k_t fluctuates within the limits

$$3 \leqslant k_t \leqslant 43 \ m^2/sec,$$

being in the majority of cases of the order of 20 - 25 m^2/sec.

9.2 Method of Solution

Let there be in the cloud, along with radiative influx of heat, also turbulent mixing which is characterized by a constant kinematic exchange factor k_t.

For the sake of simplicity, the heat influx due to phase transformations of water will be disregarded in this Section. This quantity can be computed by the same method as that given in Section 3. Above the cloud, as before, we will consider only radiant heat exchange on the basis of considerations given above.

The equation of the problem, after the same transformations as in Section 3 and with the same notations, will assume the following form*:

$$\frac{\partial T^{(0)}(z, t)}{\partial t} = \frac{1}{a^{(0)}} R^{(0)}(z, t) + D^2 \frac{\partial^2 T^{(0)}}{\partial z^2}, \qquad \text{(VI.9.3)}$$

$$\frac{\partial T^{(1)}(z, t)}{\partial t} = \frac{1}{a^{(1)}} R^{(1)}(z, t). \qquad \text{(VI.9.4)}$$

Equation (VI.9.3) contains the constant $D^2 = k_t \frac{t_0}{z_0^2}$ where z_0 is the dimension of length. If $k_t = 10^4$ cm^2/sec, $t_0 = 1$ day, and $z_0 = 1$ km, then $D^2 = 0.086$; $R^{(0)}(z, t)$ and $R^{(1)}(z, t)$ are the sum total of the terms of the equation that characterize the radiative heat influx in the cloud and above the cloud, respectively. /195

A simultaneous accounting of both turbulent and radiative heat exchange for selective absorption of water vapor introduces basic difficulties in the formulation of the marginal conditions of the investigated problem. First of all, the number of conditions must be increased by two as compared with the purely radiative case because of the presence of the last term in eq.(VI.9.3). In investigating the upper layers of sufficiently dense clouds, we will consider them as semi-infinite. In this case, it is sufficient to assign only one additional condition which can naturally be taken as the equality of temperatures at the interface between the cloud and the medium above the cloud.

---

* The equation of the heat balance reduces to eq.(VI.9.3) if the turbulent heat flow q is presented in the form of

$$q = -C_p \rho k_t \frac{\partial T}{\partial z}.$$

A physically more substantiated relation is

$$q = -C_p \rho k_t \frac{\partial \theta}{\partial z},$$

where θ is the potential temperature. It is known that $\frac{\partial \theta}{\partial z} = \frac{\partial T}{dz} + \gamma_a$ where γ_a is the adiabatic temperature gradient. It is therefore obvious that eq. (VI.9.3) will maintain its form when T is replaced by θ, but that on the left-hand side of the boundary condition (VI.9.6) the term $C_p \rho k_t \gamma_a$ will be added. As demonstrated below, this will not substantially affect the conclusions in this paper.

$$T^{(0)}(0, t) = T^{(1)}(0, t). \tag{VI.9.5}$$

In deriving the expressions $R^{(0)}(z, t)$ and $R^{(1)}(z, t)$ in Section 3, the condition of equality of radiation intensity at the interface of two media was used. Here, this condition must be replaced by a more general condition of heat balance on the boundary (see also Sect.7):

$$F^{(0)}(0) + C_p \rho k_t \frac{\partial T^{(0)}}{\partial z} = F^{(1)}(0) \tag{VI.9.6}$$

together with the condition

$$F_2^{(0)}(0) = A^{(0)} F_1^{(0)}(0) + (1 - A^{(1)}) F_2^{(1)}(0) \tag{VI.9.7}$$

or with the condition

$$F_1^{(1)}(0) = A^{(1)} F_2^{(1)}(0) + (1 - A^{(0)}) F_1^{(0)}(0) + C_p \rho k_t \frac{\partial T^{(0)}}{\partial z}. \tag{VI.9.8}$$

The expressions of radiative heat influx $R^{(0)}$ and $R^{(1)}$ directly contain the radiation intensity on the boundaries [see eq.(I.2.44)] rather than the fluxes determined from conditions (VI.9.6) - (VI.9.8).

In the investigated case of a two-layer medium, we have

$$R^{(0)}(z, t) = \frac{\rho_v}{2\pi \alpha_v \rho_{w,0} B_0} \left\{ \int_+ I_2^{(0)}(0, r) e^{-\sec\theta \tau} d\omega + \right.$$

$$\left. + 2\pi \int_0^{\tau_0} B^{(0)}(\xi) E_1(|\tau - \xi|) d\xi - 4\pi B(T^{(0)}) \right\}, \tag{VI.9.9}$$

$$R^{(1)}(z, t) = \frac{\rho_w}{2\pi \alpha_0 \rho_{w,0} B_0} \sum_{i=1}^{3} \alpha_i \left[\int_+ I_{1,i}^{(1)}(0, r) e^{-\alpha_i m \sec\theta} d\omega + \right.$$

$$\left. + 2\pi \alpha_i \int_0^{m_1} B_i^{(1)}(\xi) E_1(|\alpha_i| m - \xi|) d\xi - 4\pi B_i^{(1)} \right]. \tag{VI.9.10}$$

In Section 7 it was already found that the assigning of fluxes on the boundaries is not sufficient for determining the intensities $I_2^{(0)}(0, r)$ and $I_1^{(1)}(0, r)$ without auxiliary conditions. There, as such a condition it was sufficient to assume that the radiation intensity, leaving the boundaries of the cloud, was independent of direction.

Here, we will also assume that /196

$$I_2^{(0)}(0, r) = \frac{1}{\pi} F_2^{(0)}(0). \tag{VI.9.11}$$

However, an analogous condition is not sufficient for determining the value of $I_{1,i}^{(1)}(0, r)$ in view of the fact that the boundary conditions (VI.9.6)

to (VI.9.8) include radiation fluxes integral to the long-wave spectrum. Therefore, in addition to the assumption as to the diffusivity of the radiation leaving the upper boundary of the cloud

$$I_{1,i}^{(1)}(0, r) = \frac{1}{\pi} F_{1,i}^{(1)}(0), \tag{VI.9.12}$$

it is necessary to introduce still another troublesome assumption, namely, that this radiation is independent of the wavelength:

$$F_{1,i}^{(1)}(0) = \delta\lambda_i F_1^{(1)}(0), \tag{VI.9.13}$$

where $\delta\lambda_i$ is the relative length of the interval $\Delta\lambda_i$.

In this manner, three rather serious limitations are introduced [eqs. (VI.9.11) - (VI.9.13)] which, generally speaking, greatly distort the physical meaning of the problem.

At present, no decision has been reached as to a suitable replacement or supplement of the boundary conditions (VI.9.6) - (VI.9.8). We are convinced that the difficulties connected with the boundary conditions can be completely or largely eliminated if the stationary problem is solved or if the exact equations of transfer are replaced by approximate equations for the radiation flux or, finally, if the selectivity of the absorption spectrum in both media as well as in the case of a purely radiative problem, is disregarded. In our case, the above-mentioned difficulties cannot be eliminated, so that we will confine our calculation to a determination of the temperature for small time intervals in the cloud layer. As shown below, in this case only the first of the three auxiliary assumptions [eqs.(VI.9.11) - (VI.9.13)] is used.

To compare the results of this Section with the case of the pure radiation model given in Section 3, two additional assumptions are introduced, which are of no basic importance:

$$A^{(j)} = 0, \tag{VI.9.14}$$

$$F_2^{(1)}(0) = \pi I_2^{(1)}(0). \tag{VI.9.15}$$

Under these conditions, the expression $R^{(0)}$ will not change with respect to the pure radiation case [see eq.(VI.3.10)]:

$$R^{(0)}(\tau, t) = \bar{\rho}_0 \left\{ \sum_{i=1}^{3} a_i \int_0^{m_0} \bar{B}_i^{(1)}(\xi) E_1(a_i\xi + \tau) + \right.$$
$$\left. + \int_0^{\tau_0} \bar{B}^{(0)}(\xi) E_1(|\xi - \tau|)\, d\xi - 2\bar{B}^{(0)}(\tau) \right\}. \tag{VI.9.16}$$

We will now return to the solution of eqs.(VI.9.3) and (VI.9.4).

Let us formally consider eq.(VI.9.3) as being an inhomogeneous equation of heat conduction in a semi-infinite medium. The free term of the equation equals

$$f(z, t) = \frac{1}{a^{(0)}} R^{(0)} [T^{(0)}(z, t); \quad T^{(1)}(z, t)]. \tag{VI.9.17}$$

The solution of this equation for the boundary condition (VI.9.5) has the form of /197

$$T^{(0)}(z, t) = \frac{1}{2\sqrt{\pi}} \int_0^\infty \frac{1}{\sqrt{D^2 t}} \left\{ e^{-\frac{(z-\xi)^2}{4D^2 t}} - e^{-\frac{(z+\xi)^2}{4D^2 t}} \right\} \times$$
$$\times T^{(0)}(\xi, t_0)\, d\xi + \frac{D^2}{2\sqrt{\pi}} \int_{t_0}^{t} \frac{z}{[D^2(t-\tau)]^{3/2}} e^{-\frac{z^2}{4D^2(t-\tilde{t})}} T^{(1)}(0, \tilde{t})\, d\tilde{t} +$$
$$+ \frac{1}{2\sqrt{\pi}} \int_0^\infty \int_{t_0}^{t} \frac{1}{D^2(t-\tilde{t})} \left\{ e^{-\frac{(z-\xi)^2}{4D^2(t-\tilde{t})}} - e^{-\frac{(z+\xi)^2}{4D^2(t-\tilde{t})}} \right\} f(\xi, \tilde{t})\, dt d\xi. \tag{VI.9.18}$$

The calculation with eq.(VI.9.18) is made numerically. In order to determine $T^{(0)}(z, t)$ at the instant t_k, we will assume a sufficiently close instant t_{k-1} as the initial instant and stipulate that, in the narrow interval (t_{k-1}, t_k), the following relations exist:

$$f(\xi, \tilde{t}) = f(\xi, t_{k-1}),$$
$$T^{(1)}(0, \tilde{t}) = T^{(1)}(0, t_{k-1}).$$

Using such assumptions in eq.(VI.9.18), an integration with respect to time can be made. If, in addition, the right-hand side of eq.(VI.9.18) is presented in the form of the sum of the integrals of the individual terms and if in each integral a replacement of the variable of the type

$$\frac{z \pm \xi}{2\Delta t^{1/2} D} = u,$$

is made, we will obtain the following expression for the temperature of the cloud at the k^{th} instant of time:

$$T(z, t_k) = T^{(1)}(0, t_{k-1}) \left[1 - \Phi\left(\frac{z}{c}\right) \right] +$$
$$+ \frac{1}{\sqrt{\pi}} \int_0^{z/c} e^{-u^2} T^{(0)}[z - cu, t_{k-1}]\, du - \frac{1}{\sqrt{\pi}} \int_{z/c}^\infty e^{-u^2} T^{(0)}[cu - z, t_{k-1}]\, du +$$
$$+ \frac{1}{\sqrt{\pi}} \int_0^\infty e^{-u^2} T^{(0)}[z + cu, t_{k-1}] + \frac{2\Delta t}{\sqrt{\pi}} \int_0^{z/c} f[z - cu, t_{k-1}]\, R(u)\, du +$$

$$+ 2\frac{\Delta t}{\sqrt{\pi}}\int_0^{\infty} f\,[z + cu,\ t_{k-1}]\,R\,(u)\,du - 2\frac{\Delta t}{\sqrt{\pi}}\int_{z/c}^{\infty} f\,[cu - z,\ t_{k-1}]\,R\,(u)\,du. \qquad \text{(VI.9.19)}$$

Here,

$$\Phi\,(u) = \frac{2}{\sqrt{\pi}}\int_0^{u} e^{-t^2}dt, \qquad \text{(VI.9.20)}$$

$$R\,(u) = e^{-u^2} - u\,[1 - \Phi\,(u)], \qquad \text{(VI.9.21)}$$

$$c = 2D\,\Delta t^{1/2}. \qquad \text{(VI.9.22)}$$

At the same time, the formula

$$T^{(1)}\,(z,\ t_k) = T^{(1)}\,(z,\ t_{k-1}) + \frac{\Delta t}{a^{(1)}}\,R^{(1)}\,(z,\ t_{k-1}) \qquad \text{(VI.9.23)}$$

is used for calculating the temperature in the layer above the cloud.

9.3 Study of the Solution

/198

It is easy to verify that

$$\int_0^{\infty} R\,(u)\,du = \frac{\sqrt{\pi}}{4}.$$

In addition,

$$\int_0^{\infty} e^{-u^2}du = \frac{\sqrt{\pi}}{2}.$$

Therefore, at $c \to 0$*, eq.(VI.9.19) is transformed into

$$T^{(0)}\,(z,\ t_k) = T^{(0)}\,(z,\ t_{k-1}) + \Delta t f\,(z,\ t_{k-1}),$$

i.e., into the expression $T^{(0)}(z, t_k)$ for a pure radiation model.

The sum of the first four terms on the right-hand side of eq.(VI.9.19), denoted here by X(z, t), represents the purely turbulent effect, namely, the temperature distribution due to the influence of turbulent mixing at the

---

* Below, the quantity

$$c = 2D\Delta t^{\frac{1}{2}} = 2\Delta t^{\frac{1}{2}}\frac{\sqrt{k_t k_0}}{z_0}$$

is considered as the characteristic of turbulent mixing for a constant Δt.

boundary and to the initial temperature conditions. If, at $t = t_{k-1}$,

$$T^{(0)}(z, t_{k-1}) = T^{(1)}(z, t_{k-1}) = \text{const},$$

then

$$X(z, t_k) = T^{(1)}(z, t_{k-1}) = \text{const}.$$

Generally speaking, X(z, t) depends only on the temperature distribution within the cloud at the instant t_{k-1} and on the characteristic of turbulent mixing k_t (or c). At the same time, it was shown in Section 4 that, in optically dense clouds, the radiation effect does not depend on the temperature distribution inside the clouds but is determined by the initial temperature and moisture above the clouds and by the liquid-water content in the investigated layer within the clouds. Therefore, both effects are separate and, at given k_t, one or the other may prevail depending on the initial conditions.

Although produced by different causes, turbulence and radiation are later subject to interaction. In our formulation of the problem, the influence of radiation on turbulence is neglected. Some qualitative considerations on this point are given in Section 10.

The sum of the fifth to seventh terms in eq.(VI.9.19), denoted by Y(z, t) represents the influence of turbulence on the radiation regime of the cloud:

$$Y(z, t) = \frac{2\Delta t}{\sqrt{\pi}} \int_0^{z/c} f(z - cu, t_{k-1}) R(u)\, du - \frac{2\Delta t}{\sqrt{\pi}} \int_{z/c}^{\infty} f(cu - z, t_{k-1}) R(u)\, du + \frac{2\Delta t}{\sqrt{\pi}} \int_0^{\infty} f(z + cu, t_{k-1}) R(u)\, du. \quad \text{(VI.9.24)}$$

The analysis of eq.(VI.9.16) made in Section 4 suggests that, at a water content in the cloud increasing with height and with the real temperature /199
and humidity distribution above the cloud, the function $f(z, t, \tau_0) = \frac{1}{a^{(0)}} R^{(0)}[T^{(0)}, T^{(1)}]$ has the following properties in the vicinity of the upper boundary:

I. $f(z, t, \tau_0) < 0$ at $z \approx 0$;

II. $\max |f(z, t, \tau_0)| = |f(0, t, \tau_0)| = \text{const}$, irrespective of the value of τ_0;

III. $\frac{d|f|}{dz} \ll 0$ at $z \geq 0$;

IV. $\frac{d|f|}{d\tau_0} < 0$ at $z > 0$.

These properties exist in any case in which

$$\rho_v(z) = a + bz, \qquad b \geqslant 0,$$

if

$$B_i^{(1)}(z) = a_i + b_i z, \qquad b_i \leqslant 0,$$

and also at

$$B^{(1)}(0) - B^{(0)}(0) \leqslant \tilde{a} > 0,$$

where $\tilde{a}$ is determined by the limiting value of the above-cloud inversion, during which cooling takes place; a is greater the smaller the optical thickness of the layer above the cloud. In the last inequality, $B^{(1)}(0)$ is determined from the temperature at the upper boundary of the above-cloud inversion while $B^{(0)}(0)$ is determined from the temperature at its lower boundary.

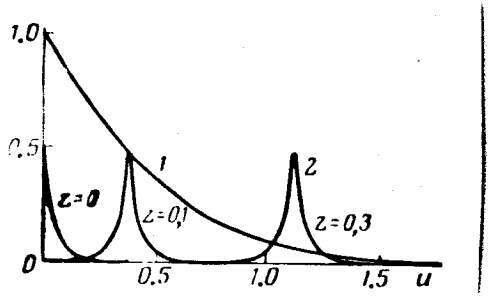

Fig.VI.9.3 Graphs of the Functions R(u) (Curve 1) and $E_2\left(\alpha_1 m_1 + \tau_0 \frac{\xi}{H}\right)$, $\xi = z - cu$ (Curve 2)

If, for instance, at the initial instant

$$\rho_v(z) = \text{const}, \qquad T^{(0)}(z) = T^{(1)}(z) = \text{const},$$

then, during a certain time, the following relation will exist:

$$f(z, t) \approx -cE_2\left(\alpha_1 m_1 + \tau_0 \frac{z}{H}\right),$$

where m_1 is the mass of water vapor in the atmosphere above the cloud; $\alpha_1 = 0.2$ cm^2/gm; c is a constant.

It follows from condition III that, at increasing z, the third term in Y(z, t) rapidly becomes zero. In the first and second terms, f(ξ, t) retains a constant value along the characteristic

$$\xi = |z - cu|$$

so that the curve f(ξ, t) moves along the axis u at any change in z. In Fig.VI.9.3, Curve 1 represents R(u) and Curves 2 represent $|f(\xi, t)| = cE_2(\alpha_1 m_1 + \tau_0 \frac{\xi}{H})$ for z = 0, 0.1, and 0.3 at $k_t = 10^5$ cm^2/sec, $m_1 = 2$ gm/cm^2 and $\tau_0 =$

= 50. The maximum value of $f(\xi, t)$ is reached at $\xi = 0$, i.e., at

$$u = \frac{z}{c} = \frac{z}{2D\Delta t^{1/2}}. \qquad \text{(VI.9.25)}$$

The last relationship, together with eq.(VI.9.3), shows that at increasing z the product $f(\xi, t)\, R(u)$ and thus also $Y(z, t)$ decrease. Therefore, the radiative cooling decreases with increasing z, but considerably slower than in /200 the case of pure radiation. For instance, if $f(z, t) = -cE_{\text{в}}\left(\alpha_1 m_1 + \tau_0 \frac{z}{H}\right)$ at $z = 0.1$ and $\tau_0 = 50$, the purely radiative effect is equal to zero (see Sect.4). As shown in Fig.VI.9.2, the radiative cooling in our case is by no means equal to zero at $z = 0.1$.

At $z \to \infty$, $Y(z, t) \to 0$. From the determination of $Y(z, t)$ it also follows that

$$Y(z,t)_{z=0} = 0,$$

which differentiates the investigated problem from the pure radiation case, where the maximum cooling was reached at the point $z = 0$. In our problem, the following condition is retained at the boundary

$$T^{(0)}(0, t) = T^{(1)}(0, t)$$

and the temperature conditions at $z = 0$ are determined by the cooling of the layer above the cloud, which cannot be extensive in any case (see Sect.5). Maximum cooling takes place inside the cloud (near its upper boundary) at the point z_0, determined from the condition

$$\frac{dY}{dz}\Big|_{z=z_0} = 0.$$

The expression $\frac{dY}{dz}$ is readily reduced to the form

$$\left.\begin{aligned} \frac{dY}{dz} = \frac{2\Delta t}{c\sqrt{\pi}} \int_0^{z/c} f\,[z - cu, t_{k-1}] \frac{dR}{du}\, du - \frac{2\Delta t}{c\sqrt{\pi}} \times \\ \times \int_0^{\infty} f\,[z + cu, t_{k-1}] \frac{dR}{du}\, du - \frac{2\Delta t}{c\sqrt{\pi}} \int_{z/c}^{\infty} f\,[cu - z, t_{k-1}] \frac{dR}{du}\, du, \end{aligned}\right| \qquad \text{(VI.9.26)}$$

where, according to eq.(VI.9.21)

$$\frac{dR}{du} = -\sqrt{\pi}\,[1 - \Phi(u)]. \qquad \text{(VI.9.27)}$$

It follows from eq.(VI.9.26) that

$$\frac{dY}{du}\Big|_{z=0} = -4\frac{\Delta t}{c\sqrt{\pi}}\int_0^\infty f(cu)\frac{dR}{du}\,du < 0. \qquad \text{(VI.9.28)}$$

Since Y(0, t) = 0, the last expression proves that Y(z, t) increases in absolute value near the point z = 0; simultaneously, both radiation and cooling increase.

It is obvious that

$$\lim_{c\to\infty}\frac{dY}{dz}\Big|_{z=0} = 0, \qquad \lim_{c\to 0}\frac{dY}{dz}\Big|_{z=0} = -\infty.$$

Therefore, cooling in the neighborhood of the point z = 0 increases more strongly the less extensive the turbulent mixing becomes and approaches, at the limit, the pure radiation case of maximum cooling on the boundary.

By expanding $\frac{dY}{dz}$ in a series according to powers of z, and limiting the calculation to the first two terms of the series, we obtain the following expression for the determination of the point z_0 where the cooling reaches its maximum value:

$$z_0 = \frac{c}{f(0)}\int_0^\infty f(cu)\,[1-\Phi(u)]\,du. \qquad \text{(VI.9.29)}$$

From this it follows that /201

$$\lim_{c\to 0} z_0 = 0.$$

At the same time it cannot be asserted that z_0 increases with increasing c, since it is easy to demonstrate that the value of

$$\psi(c) = \int_0^\infty f(cu)\,[1-\Phi(u)]\,du$$

decreases with increasing c [see the property III of the functions f(ξ, t)].

Examples for calculating the quantity z_0 will be given below.

Above, we investigated the variation in radiative cooling Y(z, t) with height. Let us now define the behavior of this quantity when other parameters are changed. We recall that

$$\lim_{c\to 0} Y(z, t) = \frac{1}{a^{(0)}}\bar{R}^{(0)}(z, t),$$

i.e., at a lessening in turbulence, the temperature conditions approach the conditions of pure radiation. At given z and at increasing c, the curve

$f(|cu - z|)$, in accordance with eq.(VI.9.25), shifts toward the side of smaller u, as a result of which Y(z, t) increases. However, this causes an increase in the derivative

$$\frac{df}{du} = c\frac{df}{d\xi},$$

and, since

$$\frac{df}{d\xi} < 0,$$

Y(z, t) will decrease. It follows from this that, on increase in c, the variation in Y(z, t) may be non-monotonic.

The sum total of conditions II and IV leads to an - at first sight - unexpected effect: On increase in the optical thickness of the cloud τ_0, the radiative cooling at the given point z decreases in the presence of turbulent mixing. This effect, however, becomes physically understandable when considering that, in accordance with conditions II and IV, the rate of radiative cooling does not increase with increasing τ_0 and that its influence is concentrated in a progressively narrowing layer at the boundary of the cloud. Therefore, in accordance with eq.(VI.9.24), the absolute value of Y(z, t) decreases. This latter consideration applies, of course, only to optically dense clouds.

9.4 Results of the Calculations

Below, we give some results of calculations based on eq.(VI.9.19). The following initial conditions were assumed:

$$T^{(0)}(z,t_0) = T^{(1)}(z,t_0) = 273°,\ \rho_{(r)}(z,t_0) = 0.5\cdot 10^{-6}\ g/cm^3.$$

With this,

$$f(z, t_0) = -cE_2\left(\alpha_1 m_1 + \tau_0\frac{z}{H}\right),$$

where

$$c = \frac{B_1(273°)}{B_0 a^{(0)}}\rho_r.$$

The first time step was computed and the variation in the quantity $\Delta T^{(0)} = -[T^{(0)}(z, t_1) - T^{(0)}(z, t_0)]$ was defined individually for variations in each of the quantities k_t, z, and τ_0, while the other two remained constant. The value of the time step was equal to $\Delta t = \frac{1}{48}$, which corresponds to 0.5 hr.

An interpretation of the calculation results shows that, in determining /202 the temperature inside the cloud at the initial instant of time, only the first of the three conditions (VI.9.11) - (VI.9.13) was used. For computing $\Delta T^{(0)}$ at the subsequent instants of time it is necessary to determine $T^{(1)}(z, t)$, i.e., to make use of the conditions (VI.9.12) and (VI.9.13). However, $T^{(1)}(z, t)$ enters eq.(VI.9.16) only through the expression

$$Y = \Sigma\alpha_i\int_0^{m_1} B_i^{(1)}(\xi)\,E_1(\alpha_i\xi + \tau)\,d\xi.$$

In Section 5, we showed that the quantity Y in a pure radiation model remains practically constant over several steps of time since the variations in $T^{(1)}(z, t)$ are small. Therefore, it can be expected that the calculation of the

TABLE VI.9.3

τ	k_t, cm²/sec	z, m					
		10	25	50	100	200	300
25	10^3	1.95	2.06	0.99	0.19	0.06	—
25	10^4	0.44	0.74	0.55	0.31	0.02	—
15	10^3	2.44	2.97	1.80	0.66	0.10	0.02
8	10^3	2.91	3.93	3.11	1.70	0.55	0.20
δ_μ, %		100	36	15	3	—	—
δ_t, %		95	100	50	10	3	—

temperature within a cloud, based on eq.(VI.9.19), will contain no substantial errors due to the conditions (VI.9.12) and (VI.9.13), if the time interval is not too great.

TABLE VI.9.4

H, km	τ_0	z, km	
		0.05	0.1
0.240	8	3.11	1.70
0.460	15	1.89	0.66
0.760	25	0.98	0.19

TABLE VI.9.5

τ_0	z, km	k_t, cm²/sec			
		10^3	10^4	10^5	10^6
25	0.025	2.057	0.74	0.09	0.01
25	0.050	0.985	0.550	0.148	0.0191
8	0.025	3.93	1.70	0.38	0.05

The results of computation of the quantity $\Delta T^{(o)}$ are presented in Tables VI.9.3 - VI.9.5

Table VI.9.3 shows the variations in $\Delta T^{(o)}$ on penetration into the depth of the cloud, for different values of the coefficient of turbulent mixing k_t and of the optical thickness of the clouds τ_o. In addition, in Table VI.9.3 we give the extent of variation in cooling with depth, for the pure radiation case δ_p (in percent of maximum cooling) and the variations in cooling δ at k_t = $= 10^3$ cm^2/sec. According to Table VI.9.3, the maximum cooling for $k_t = 10^3$ and 10^4 cm^2/sec takes place at the point z = 10 m. For this case, the calculation with eq.(VI.9.29) yields z_o = 10 m at $k_t = 10^3$ cm^2/sec and z_o = 20 m at k_t = 10 cm^2/sec. Therefore, eq.(VI.9.29) gives an approximately correct position of the point of maximum cooling. The agreement between the values of z_o based on data in Table VI.9.3 and on eq.(VI.9.29) would probably have been better if the variation in $\Delta T^{(o)}$ cz had been presented in greater detail in this Table. /203

Table VI.9.4 shows the decrease in cooling at a given point at increasing τ_o for ρ_v = 0.3 gm/cm^3 and for different thicknesses of the cloud H (assuming that $k_t = 10^3$ cm^2/sec).

Finally, Table VI.9.5 gives the variation in ΔT^o with increasing k_t for different values of τ_o and of z. The Table shows that an increase in k_t leads to a noticeable decrease in radiative cooling. According to the data in Table VI.9.1, the value of $k_t = 10^3$ cm^2/sec represents a case in which the turbulent mixing in the cloud is practically zero. Nevertheless, even at such a small k_t, radiative cooling decreases with respect to the pure radiation model by a factor of 1.5 - 3.0. Incidentally, some underestimation of cooling may occur in Table VI.9.5 if z_o is not included in the selected quantities. Nevertheless, radiative cooling remains considerable from the viewpoint of the energy of atmospheric processes and at relatively intensive mixing, if k_t is of the order of 10^5 cm^2/sec. In this case, the cooling, according to Table VI.9.5, is 0.3 - 0.8°/hr. In addition, turbulent mixing leads to a greater penetration of cooling into the depth of the cloud and apparently to a prolongation of the period of this process.

Conclusions

The above-described results yield the principal features of radiative heat exchange in clouds and make it possible to define the nature of its influence on the development of cloudiness. The following conclusions can be drawn:

1. Long-wave radiant heat exchange in a formed, sufficiently dense cloud, when disregarding the smoothing effect on turbulent mixing and heat influx due to phase transformation of water, leads to a sharp cooling of the upper part of the cloud.

The cooling process has the following properties:

a) The rate of cooling at a given level depends on the liquid-water content

and the temperature at this level as well as on the temperature and moisture distribution above the clouds in the layer having a thickness of the order of 2 - 4 km.

b) The cooling remains practically constant on variations in the temperature profile and in the optical thickness of the cloud as a whole.

c) The intensity and rate of cooling is largely determined by the initial conditions in the layer above the cloud, i.e., by the quantities $T^{(1)}(z, t_0)$ and $\rho_w^{(1)}(z, t_0)$; on formation of an above-cloud inversion the rate of cooling decreases.

d) The cooling decreases rapidly in direction of the depth of the cloud and takes place within a narrow layer of the order of 50 - 100 m.

e) If the liquid-water content does not decrease in direction of the upper cloud boundary, then the maximum cooling will take place at its upper boundary.

3. Clouds of the middle layer are cooled much more extensively by natural radiation than clouds in the lower layer, due to the more intense back-scattering in the second case.

4. Interaction between radiative cooling and heating by absorption of infrared solar radiation leads to differing effects at different levels and at different instants of time.

In the absence of a temperature inversion or at moderate thickness of the latter, the uppermost layer of the cloud, 20 - 50 m in thickness, will be in the same condition by day or by night, - meaning that the heating is small with respect to the cooling; this is followed by a zone of heating which is quite weak in intensity compared with the cooling at the boundary but which penetrates considerably deeper into the cloud.

5. Due to the heat of condensation, the radiative cooling is weakened /204 by 20 - 30%.

6. Strongly developed turbulence sharply reduces the rate of cooling in the initial instant of time, making this process more protracted and penetrating more deeply into the cloud.

7. Scattering of long-wave radiation on water droplets, generally speaking, leads to an intensification of the cooling process. However, if the effect of scattering is presented in the form of reflection from the boundary, cases of attenuation of cooling may become possible (at strong reflection of radiation inside the cloud).

8. The inverse of this or another manifestation of the radiative cooling process consists in the formation of a radiative temperature inversion above the clouds: The temperature increases sharply on transition from the cooled layer of the cloud to the layer above the cloud with a slowly varying temperature.

9. In the pure radiation case, the inversion layer is compressed into the surface of temperature discontinuity, which coincides with the upper boundary of the clouds.

10. Since cooling takes place entirely within the cloud layer, it must be assumed that the above-cloud temperature inversion originates from radiation penetrating into the cloud. In considering turbulent exchange, the vertical development of the inversion must be determined. This also takes place primarily in the upper part of the cloud and to a lesser degree below it.

11. The above investigations yield the principal features of radiative temperature inversion. This inversion takes place in a narrow layer (of the order of 100 m) and is characterized by its high intensity, of the order of 10°.

12. The time required for establishing an inversion of radiative origin is 3 - 5 hrs.

13. When the upper layer of a cloud is cool, condensation of water vapor and accumulation of liquid moisture take place. The intensity of the process is such that, within three hours, an amount of 0.1 - 0.2 gm/m^3 and more is accumulated in the 100-m layer at the upper boundary of the cloud.

14. The formation of an inversion of radiative origin and the development of a cloud by radiant transfer is promoted by the rapid drop in moisture above the level of condensation. If the moisture deficit becomes zero at some level and a sharp decrease in the moisture above this level takes place, a cloud can form only by radiative heat exchange.

Next, we will investigate the correlation between the above features of radiative heat exchange in clouds with the actually observed processes.

We note first that, according to measurements made by V.L.Gayevskiy (Bibl.21) the ascending flow of long-wave radiation at the upper boundary of a cloud layer is much greater than the descending flow. As a result, a radiative cooling of the order of 9°/day occurs. This value is small with respect to the computational data given in Sections 4 and 5. It must, however, be considered that V.L.Gayevskiy's data were averaged for layers having a thickness of 200 - 300 m.

We further demonstrate that the temperature inversions observed above stratus clouds quite often resemble the above-described purely radiative types: They take place in a narrow layer of the order of 100 m and have an intensity of 5° or more.

Examples of such inversions are shown in Section 6 and also in the curves of Fig.VI.10.1 plotted with data of aircraft soundings taken by TsAO (Central Aerological Observatory). We note that in almost all of these graphs another inversion layer of greater thickness occurs above the inversion of the radiative type, with a significantly smaller temperature gradient. The same phe- /206
nomenon was discovered by A.M.Borovikov (Bibl.18) who studied 1435 cases of temperature distribution in St, Sc, and Ns cloud layers; another description is

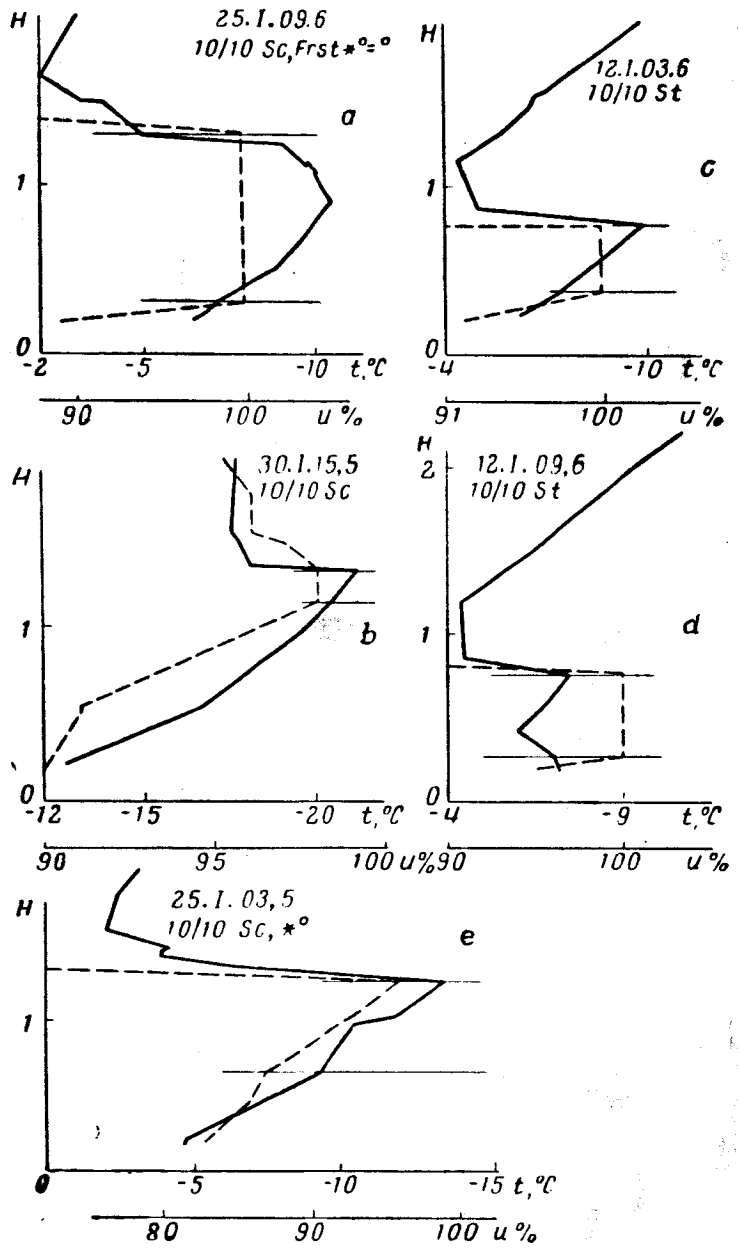

Fig.VI.10.1 Examples of Temperature Data of Above-Cloud Inversions
Solid curves - temperature; Broken curves - relative humidity

given by another author (Bibl.2) based on observations of 500 cases of the same cloudiness. The Table from the latter paper was given in Chapter I. Here, we are obviously dealing with two inversions of different nature which not infrequently occur simultaneously: one of them, known as the sinking inversion, is the principal cause of cloud formation and the second, known as radiative inversion, is produced by the cloud layer itself in the course of its development. As shown in the diagrams, the latter may wedge into the cloud.

A.L.Dergach (Bibl.5) obtained interesting data in investigating radiation fogs in the Arctic. He mentioned that, over a comparatively uniform underlying surface, fogs are sometimes formed in spots and do not coalesce into a continuous cover. The result of temperature soundings in one such case is plotted in Fig.VI.10.2. This shows the considerable difference in the nature of the temperature inversion in the region of fog cover (solid line) and in the region free of fog (broken line). The inversion above the fog has a clearly expressed radiation character.

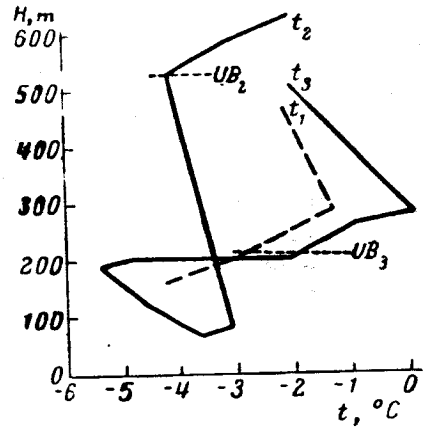

Fig.VI.10.2 Temperature Profile in Fog (Solid Curves) and in a Region Free of Fog (Broken Curve)
UB_2 and UB_3 are the positions of the upper boundary of the fog, corresponding to the temperatures t_2 and t_3

Further, according to measurements made by A.L.Dergach, the temperature within the fog is lower than at the same level outside the fog (see Fig.VI.10.2).

The important role played by radiation in the formation of an above-cloud inversion is confirmed by the absence of an inversion in the lower layers of the cloud in the case of two-layer cloudiness, a fact established by many authors [see for instance (Bibl.2)].

We analyzed the material of large-scale standard aircraft soundings taken by the Central Aerological Observatory at Vnukovo. Work-up of the data permitted the following conclusions:

1) If there is no second cloud layer above them, St and Sc clouds of the

lower layer generally exhibit a temperature inversion which often resembles a radiative inversion in nature but which is less extensive.

2) Almost no inversions were observed above the As, Ac clouds of the middle layer.

3) The data of aircraft soundings also reveal no narrow cold layer in the upper part of the cloud.

We will start with the explanation of the last fact: Apparently, there are two reasons for the difficulty in detecting the layer of radiative cooling. The first reason is of a methodological nature. A low-inertia thermometer having a high resolving power with height is required for detecting the narrow cold layer. The standard aircraft meteorograph does not meet these requirements. In addition, the flight intended to establish the microeffects in the temperature distribution with height must be performed in accordance with a special procedure which differs from that of standard vertical soundings. Therefore, a special investigation procedure must be developed. The first attempt at such an investigation, undertaken at our request by A.M.Borovikov and I.P.Mazin /207 (to whom the author expresses his deep appreciation) with a special electrical meteorograph having a height resolution of the order of 20 m, did not detect a cooling layer.

It is well possible that here the second reason for the difficulty in detecting such a layer, physical in nature, was involved. The narrow boundary layer with the superadiabatic temperature gradient is unstable and cannot exist for prolonged period of time. Apparently this is one of the principal consequences of radiative cooling of clouds. The resolution of the instability of the cold upper layer of a cloud leads to convection one of whose manifestations is the wave-like character of the surface of a stratus cloud. As shown elsewhere (Bibl.19, 20) in the presence of a two-layer cloud cover, the upper boundary of the lower layer is often flat, a finding that confirms our conclusion.

A second manifestation and consequence of convection is the reconstruction of the temperature profile up to establishment of an approximately constant gradient in the cloud. As mentioned at the beginning of this Chapter, these considerations were used by Urfer (Bibl.4) for explaining the evolution of a vertical temperature distribution in a layer of fog many days old. This also explains the disagreement between the calculated and actual temperature profile, shown by Curves 2 and 3 in Fig.VI.6.6. Convection must be taken into consideration in the theory in order that the layer of radiative cooling obtained by computation would lead to a redistribution of temperature in the entire cloud; the stable layer of the inversion is maintained here.

However, on the basis of the above consideration it is not permissible to draw any conclusions as to the impossibility of detecting or, expressed more accurately, as to the short-lived existence of the layer of radiative cooling. Actually, some observational data point toward the existence of such a layer.

First of all, this is shown by the temperature drop in the fog as compared

with the adjoining region not covered by fog, which was discovered by A.L. Dergach (see above). In addition, G.M.Zabrodskiy (Bibl.19) investigated the temperature field in stratus clouds by means of a highly sensitive and accurate thermometer. He found that, in the absence of an upper cloud layer, temperature pulsations occur and the upper boundary of the cloud shows a wavy convective character. For this reason, an aircraft in horizontal flight along the upper boundary will dip in and out of the cloud. The temperature in the cloud crest is found to be 2° lower than at the same level outside of the cloud, i.e., in the trough of the wave, in the absence of an above-cloud inversion and 3° lower in the presence of an inversion. Obviously, the first figure represents only the effect of radiative cooling.

The absence of inversions above the clouds of the middle layer established by us, generally speaking, contradicts the theory according to which the procees of radiative cooling is greater the higher the cloud (see above). Apparently, what is happening here is an increase in turbulent mixing with height. According to the few experimental data available, the coefficient of turbulent mixing in the middle troposphere can be considered equal to $10^6 - 10^7$ cm^2/sec while, according to the data in Table VI.9.1, it is equal to 10^5 cm^2/sec in clouds of the lower layer.

Table VI.9.5 shows that, at $k_t = 10^6 - 10^7$ cm^2/sec, the radiative cooling cannot be appreciable. At the same time, it might well be that our conclusion as to the absence of conversion above the clouds of the middle layer is not sufficiently substantiated.

It is known from the literature that temperature inversions frequently take place also above As and Ac clouds; however, to detect such inversions, a much larger number of cases than done by us must be investigated.

The above statements prove the role played by long-wave radiation in the development of a stratus cloud cover. The process of radiation determines:

1) Formation and intensification of the above-cloud inversion.

2) Creation of convection in the upper part of the cloud, which leads /208
to reconstruction of the temperature profile and to establishment of the wavy nature of the upper boundary.

3) Accumulation of droplet moisture in the upper part of the cloud.

It can therefore be considered that radiant heat exchange is a factor in the self-propagation and self-maintenance of stratus clouds.

BIBLIOGRAPHY

1. Mal, S.: Forms of Stratified Clouds. Beitr. z. Phys. d. Freien Atm., Vol.17, 1931.
2. Borovikov, A.M., Gayvoronskiy, I.I., Zak, Ye.G., Kostarev, V.V., Mazin, I.P.,

Minervin, V.Ye., Khrgian, A.Kh., and Shmeter, S.M.: Physics of Clouds (Fizika oblakov). Gidrometeoizdat, 1961.
3. James, D.G.: Observations from Aircraft of Temperature and Humidities near Stratocumulus Clouds. Quart. J. Roy. Met. Soc., Vol.85, No.364, 1959.
4. Urfer, A.: On the Variations of the Vertical Temperature Gradient in Fog (Sur les changements du gradient vertical de température dans le brouillard). Geophysica pura e applicata, Vol.34, 1956.
5. Dergach, A.A.: The Effect of Radiation Fog on the Development of Temperature Inversion (O vliyanii radiatsionnogo tumana na razvitiye temperaturnoy inversii). Trudy GGO (Main Geophysical Observatory), No.94, 1959.
6. Feygel'son, Ye.M.: Radiative Cooling of Stratus Clouds (Radiatsionnoye vykholazhivaniye sloistykh oblakov). Izv. Akad. Nauk SSSR, ser. geofiz., No.6, 1959.
7. Feygel'son, Ye.M.: The Role of Turbulence in the Process of Radiative Cooling of Clouds (Rol' turbulentnosti v protsesse radiatsionnogo vykholazhivaniya oblakov). Izv. Akad. Nauk SSSR, ser. geofiz., No.2, 1960.
8. Feygel'son, Ye.M.: Calculation of Radiative Cooling of Clouds (Raschet radiatsionnogo vykholazhivaniya oblakov). Izv. Akad. Nauk SSSR, ser. geofiz., No.7, 1960.
9. Feygel'son, Ye.M.: Some Questions of Radiative Heat Exchange in Stratus Clouds (Nekotoryye voprosy radiatsionnogo teploobmena v sloistykh oblakakh). Izv. Akad. Nauk SSSR, ser. geofiz., No.8, 1960.
10. Kuznetsov, Ye.S.: Temperature Distribution in the Atmosphere along the Vertical in the Case of Radiative Equilibrium (Raspredeleniye temperatury atmosfery po vertikali pri luchistom ravnovesii). Trudy Inst. Teor. Geofiz. (Institute of Theoretical Geophysics), Vol.1, 1946.
11. Möller, F.: The Patterns of Radiative Heating and Cooling in the Troposphere and Lower Stratosphere. Proc. Roy. Soc., A 236, No.205, 1956.
12. Kogan, R.L.: The Effect of Condensation Heat Influxes on the Time Rate of Change of Pressure (Vliyaniye kondensatsionnykh pritokov tepla na izmeneniye davleniya vo vremeni). Meteorol. i gidrol., No.2, 1959.
13. Fritz, S.: Absorption and Scattering of Solar Energy in Clouds of "Large Water Drops". J. Met., Vol.15, No.1, 1958.
14. Matveyev, L.T.; and Kozharin, V.S.: The Role of Turbulent Mixing in the Structure Formation of Stratus Clouds (Rol'turbulentnogo peremeshivaniya v formirovanii struktury sloistoobraznykh oblakov). Izv. Akad. Nauk SSSR, ser. geofiz., No.11, 1956.
15. - Meteorological Office Discussion. Stratocumulus Clouds. Meteor. Mag., Vol.86, No.1022, 1958.
16. Ambramovich, K.G.: The Characteristic of Turbulence of the Atmosphere in Days with Low Cloudiness (Kharakteristika turbulentnosti atmosfery v dni s nizkoy oblachnost'yu). Meteorol. i gidrol., No.9, 1958.
17. Churinova, M.P.: Some Characteristics of Turbulence on Days with Stratus Clouds (Nekotoryye kharakteristiki turbulentnosti v dni so sloistymi oblakami). Trudy GGO (Main Geophysical Observatory), No.54, 1955.
18. Borovikov, A.M.: The Characteristics of Cloud Layers Above Moscow (Kharakteristika oblachnykh sloyev nad Moskvoy). Trans. Central Aerological Observatory (TsAO), No.2, 1948.
19. Zabrodskiy, V.K.: On the Temperature Field and Transparency of Clouds of the Lower and Middle Layers (O temperaturnom pole i prozrachnosti oblakov

nizhnego i srednego yarusov). Trudy Arkt. i Antarkt. Inst., No.239, 1962.
20. Nepovitova, A.F.: Shapes of the Upper Surface of Cloud Layers and their Correlation with Vertical Temperature Gradients in Clouds (Formy verkhney poverkhnosti oblachnykh sloyev i ikh svyaz' s vertikal'nym gradiyentom temperatury v oblakakh). Trudy TsAO (Central Aerological Observatory), No.28, 1960.
21. Gayevskiy, V.L.: The Profile of Fluxes of Long-Wave Radiation in Clouds; Collection "Investigation of Clouds, Precipitation, and Thunderstorm Electricity" (Profil' potokov dlinnovolnovoy radiatsii v oblakakh; Sb. "Issledovaniye oblakov, osadkov i grozovogo elektrichestva"). Izd. Akad. Nauk SSSR, 1961.

CHAPTER VII

ROLE OF RADIATION IN THE FORMATION OF THE STRATUS CLOUD /209

Section 1. Formulation of the Problem

In the preceding Chapter, the influence of radiation on a formed sufficiently dense cloud was discussed. However, some of the presented results (see, for instance, Fig.VI.6.6) show that long-wave radiation may play an important role in the establishing of the thermal and water regime of the cloud and in the initial stages of its development. In addition, the problem was simplified: not all forms of heat exchange were fully considered, moisture exchange was neglected, and simplifying assumptions connected with the difficulty of formulating the boundary condition in a two-layer medium were introduced. In the present Chapter, the more general problem of investigating the process of formation and the initial stages of development of a stratus cloud, taking into account moisture exchange and the basic forms of heat exchange (including radiative exchange), is treated. The main purpose of the investigation is a clarification of the role played by radiation in the above process. For this reason, it is advisable from a methodological viewpoint to solve the problem first without and then with consideration of radiative heat exchange and then to compare the obtained solution.

1.1 Fundamental Equations

Let the density of water vapor or the humidity of the air $\rho_w(z, t)$ and the temperature $T(z, t)$ be given. Let $\rho_w[T(z, t)]$ be the density of the vapor, saturating the space at temperature $T(z, t)$. If, at $0 \leq z \leq 10$ km and $t < t_0$, the inequality

$$\rho_w(z,t) < \rho_w[T(z,t)],$$

holds and if, for $t = t_0$, there exists such a value $0 \leq z_0 \leq 10$ that

$$\rho_w(z_0,t_0) = \rho_w[T(z_0, t_0)],$$

then we can define the instant t_0 and the level z_0 as the time and place of incipient formation of the cloud. In this manner, no rigid boundaries of the cloud are introduced here.

The entire atmosphere ($0 \leq Z \leq 10$ km), with a humidity and liquid-water content continuously varying with height is considered. The layer occupied by the cloud is determined at each instant of time t from the relation

$$\rho_v(z_1, t) = 0, \qquad \rho_v(z_2, t) = 0,$$
$$\rho_v(z, t) \neq 0 \text{ and } z_1 < z < z_2.$$

In the case of stratus clouds, the moisture saturation takes place by /210
turbulent transfer of heat and moisture, by vertical currents, by advection, by condensation, and by radiative transfer. The equations of heat and moisture exchange which take all these factors into consideration can be written in the form of (Bibl.2)

$$\rho \frac{dq}{dt} = \frac{\partial}{\partial z}\left(k_t \rho \frac{\partial q}{\partial z}\right) - m, \qquad \text{(VII.1.1)}$$

$$c_p \rho \frac{dT}{dt} = A \frac{dp}{dt} + \frac{\partial}{\partial z}\left(C_p k_t \rho \frac{\partial \theta}{\partial z}\right) + R(T) + Lm, \qquad \text{(VII.1.2)}$$

where ρ is the air density; q the specific humidity; k_t the kinematic coefficient of turbulent heat conduction; p the air pressure; A the thermal work equivalent; θ the potential temperature; m the mass of water vapor condensed per unit volume in unit time; L the latent heat of vaporization; R(T) the influx of heat per unit volume in unit time, due to radiative heat exchange.

If we consider that

$$\frac{d\theta}{dt} = \frac{dT}{dt} - \frac{A}{c_p \rho}\frac{dp}{dt} \qquad \text{(VII.1.3)}$$

and neglect the variations in $\rho(z)$ with respect to $\theta(z)$ and q(z), i.e., if we assume that

$$\frac{\partial}{\partial z}\left(\rho k_t \frac{\partial \theta}{\partial z}\right) = \rho \frac{\partial}{\partial z}\left(k_t \frac{\partial \theta}{\partial z}\right)$$

and

$$\frac{\partial}{\partial z}\left(\rho k_t \frac{\partial q}{\partial z}\right) = \rho \frac{\partial}{\partial z}\left(k_t \frac{\partial q}{\partial z}\right),$$

then eqs.(VII.I.I) and (VII.1.2) will assume the form

$$\frac{dq}{dt} = \frac{\partial}{\partial z}\left(k_t \frac{\partial q}{\partial t}\right) - \frac{m}{\rho}, \qquad \text{(VII.1.4)}$$

$$\frac{d\theta}{dt} = \frac{\partial}{\partial z}\left(c_p k_t \frac{\partial \theta}{\partial z}\right) + \frac{1}{c_p \rho} R(T) + \frac{Lm}{C_p \rho}; \qquad \text{(VII.1.5)}$$

Here,

$$\frac{df}{dt} = \frac{\partial f}{\partial t} + u \frac{\partial f}{\partial x} + w \frac{\partial f}{\partial z},$$

f = θ or q with the x-axis directed along the horizontal flux, u and w are the horizontal and vertical velocity components which are assumed to be known and constant.

In the system of coordinates connected with the horizontal flux, i.e., when substituting

$$x_1 = x - tu$$

we obtain

$$\frac{df}{dt} = \frac{\partial f}{\partial t} + w\frac{\partial f}{\partial z}$$

and eqs.(VII.1.4) and (VII.1.5) are transformed into

$$\frac{\partial q}{\partial t} + w\frac{\partial q}{\partial z} = \frac{\partial}{\partial z}\left(k_t \frac{\partial q}{\partial z}\right) - \frac{m}{\rho}, \qquad \text{(VII.1.6)}$$

$$\frac{\partial \theta}{\partial t} + w\frac{\partial \theta}{\partial z} = \frac{\partial}{\partial z}\left(k_t \frac{\partial \theta}{\partial z}\right) + \frac{1}{C_p\rho}R(T) + \frac{Lm}{C_p\rho}. \qquad \text{(VII.1.7)}$$

We will introduce the characteristic quantities: $T_0 = 273^0$, $t_0 = 1$ day /211 $\rho_{w\rho} = \rho_w(T_0) = 4.9$ gm/m^3, $z_0 = 1$ km; $\rho_0 = 1.3 \times 10^3$ gm/m^3, $w_0 = 1$ cm/sec; the dimensionless variables: $\bar{z} = \frac{z}{z_0}$, $\bar{t} = \frac{t}{t_0}$, $\bar{m} = \frac{mt_0}{\rho_{w\rho}}$, $\bar{\rho} = \frac{\rho}{\rho_0}$, $\bar{\rho}_w = \frac{\rho_w}{\rho_{w\rho}}$, $\bar{q} = \frac{q\rho_0}{\rho_{w\rho}}$ or $\bar{q} = \frac{\bar{\rho}_w}{\bar{\rho}}$ and the designations:

$$c = \frac{w_0 t_0}{z_0} = 0.86, \qquad b = \frac{\alpha \rho_{w,\theta}}{c_p \rho_0 T_0} = 0.034, \qquad D = \frac{t_0}{z_0^2}k_t = 0.086k_t$$

(k_t = const expressed in m^2/sec). Then, eq.(VII.1.6) - (VII.117) will assume the form

$$\frac{\partial \bar{q}}{\partial t} + c\bar{w}\frac{\partial \bar{q}}{\partial z} = D\frac{\partial^2 \bar{q}}{\partial z^2} - \frac{\bar{m}}{\bar{\rho}}, \qquad \text{(VII.1.8)}$$

$$\frac{\partial \bar{\theta}}{\partial t} + c\bar{w}\frac{\partial \bar{\theta}}{\partial z} = D\frac{\partial^2 \bar{\theta}}{\partial z^2} + b\frac{\bar{m}}{\bar{\rho}} + \frac{t_0 R(T)}{T_0 \rho_0 c_p \bar{\rho}}. \qquad \text{(VII.1.9)}$$

Below, the vinculum(denoting dimensionless quantities) is omitted.

1.2 Boundary and Initial Conditions

In discussing heat exchange (correspondingly, moisture exchange) in a limited medium, the conditions of equality of the heat (moisture) flux on both sides of the boundary are physically substantiated.

In this book, heat exchange (moisture exchange) at the level above z = = H = 10 km is disregarded. Therefore, the flow of heat (moisture) through the upper boundary of the investigated layer must be assumed as given. This is justified by the fact that it is logical to assume the level z = H to be the height of the tropopause or the retarding layer and to stipulate that the fluxes of heat and moisture are zero at z = H.

At the lower boundary of the atmosphere we assign the sought quantities T

and q which can be measured at the earth's surface. Thus, eqs.(VII.1.8 and VII.1.9) are solved with the following boundary and initial conditions:

1. At the lower boundary of the atmosphere (z = 0), the temperature T(0, t) and the humidity $\rho_w(0, t)$ and thus also q(0, t) are given, since the air density $\rho(z)$ is assumed to be known.

2. At the upper boundary (z = H), the fluxes of heat and of moisture are given:

$$k_t \frac{\partial \theta}{\partial z} \quad \text{and} \quad k_t \frac{\partial q}{\partial z}.$$

Here the coefficient of turbulent mixing is assumed to be constant and known, so that the following derivatives are given at the upper boundary:

$$\frac{\partial \theta}{\partial z} \quad \text{and} \quad \frac{\partial q}{\partial z}.$$

3. At the initial instant of time, the temperature T(z, 0), the humidity $\rho_w(z, 0)$, and the liquid-water content $\rho_v(z, 0)$ are known.

The conditions at the boundary are assumed to be stationary and coupled with the initial conditions:

$$T(0, t) = T(0, 0), \qquad \frac{\partial T}{\partial z}\Big|_{z=H} = \frac{\partial T}{\partial z}\Big|_{z=H,\ t=0},$$
$$q(0, t) = q(0, 0), \qquad \frac{\partial q}{\partial z}\Big|_{z=H} = \frac{\partial T}{\partial z}\Big|_{z=H,\ t=0},$$

In addition, we also consider the case of /212

$$\frac{\partial T}{\partial z}\Big|_{z=H} = 0; \quad \frac{\partial q}{\partial z}\Big|_{z=H} = 0.$$

After computing T(z, t) and $\rho_w(z, t)$ the liquid-water content $\rho_v(z, t)$ is determined from the condition

$$\rho_v(z, t) = \begin{cases} 0 & \text{or} \quad \rho_w(z, t) \leqslant \rho_s[T(z, t)], \\ \rho_s(z, t) - \rho_s[T(z, t)] & \text{or} \quad \rho_s(z, t) > \rho_s[T(z, t)]. \end{cases}$$

Section 2. The Problem without Allowing for Radiation

The investigation and solution of eqs.(VII.1.1) and (VII.1.2) - at R(T) = = 0 - were covered by M.Ye.Shvets (Bibl.2 - 5) and L.T.Matveyev (Bibl.6 - 8).

The problem is discussed more fully elsewhere (Bibl.2 - 5). Relations are introduced which make it possible to determine m, T, and $\rho_w(T)$ and other values

directly. The interaction between various forms of heat exchange is investigated. Conclusions are drawn as to the rate of shift of the cloud boundaries. However, M.Ye.Shvets and coworkers obtained no concrete numerical results. Such results can be obtained more readily by making use of the method developed by L.T.Matveyev, which is outlined in detail below. In this Chapter, the method is applied to the case of $R(T) \neq 0$.

Thus, in accordance with L.T.Matveyev we introduce the new wanted functions

$$\pi(z, t) = \frac{1}{b}\theta + q, \tag{VII.2.1}$$

$$S(z, t) = q(z, t) + \frac{\rho_n(z, t)}{\rho(z)}. \tag{VII.2.2}$$

Let us assume that the specific total moisture content $S(z, t)$ is dissipated by turbulent exchange as is the specific humidity $q(z, t)$, i.e., that $S(z, t)$ is governed by the equation

$$\frac{\partial S}{\partial t} + cw\frac{\partial S}{\partial z} = D\frac{\partial^2 S}{\partial z^2}. \tag{VII.213}$$

From eqs.(VII.1.8) and (VII.1.9), at $R(T) = 0$, it is easy to obtain an analogous equation for the function $\pi(z, t)$:

$$\frac{\partial \pi}{\partial t} + cw\frac{\partial \pi}{\partial z} = D\frac{\partial^2 \pi}{\partial z^2}. \tag{VII.2.4}$$

If $\pi(z, t)$ and $S(z, t)$ are computed, then the sought values $T(z, t)$, $\rho_w(z, t)$ and $\rho_v(z, t)$ can be determined by the method given in another paper (Bibl.6). Here, we will assume that, at the point z at an instant of time t, the cloud has already formed; then, $\rho_w(z, t) = \rho_w[T(z, t)]$. The last function can be determined, for example, by means of Magnus' formula

$$\rho_w(T) = 0.1\frac{E_0 10^{\frac{at^\circ}{b+t^\circ}}}{R_w T}, \tag{VII.2.5}$$

where $E_0 = 6.1$ mb is the vapor pressure of water vapor, at 0°C; $a = 7.5$; $b = 237^\circ$; $R_w = 460$ m^2/sec^2 · deg is the gas constant of water vapor; $\rho_w(T)$ is determined in gm/cm^3.

If $\rho(z)$ is a known value and $\pi(z, t)$ is computed, then the expression (VII.2.1) taking eq.(VII.2.5) into consideration represents a transcendental equation for determining the temperature $T(z, t)$. /213

Along with the graphical method of solving this equation, proposed by

Matveyev (Bibl.6), a numerical method for determining the temperature can be developed which permits higher accuracy and is more convenient when using high-speed computers.

It is readily demonstrated that the second term in eq.(VII.2.1) constitutes no more than 5 - 10% of the first term. Therefore, using, as zeroth approximation,

$$\theta_0(z,t) = b\,\pi(z,t), \tag{VII.2.6}$$

the quantity $\theta(z, t)$ can be determined by the method of successive approximation, based on the formulas

$$\theta_k(z,t) = b\,\pi(z,t) - bq(T_{k-1}), \tag{VII.2.7}$$

$$q(T_k) = 0{,}1\,\frac{E_0\,10^{\frac{at^\circ}{b+t_k^\circ}}}{R_w T_k \rho(z)}. \tag{VII.2.8}$$

Knowing $\theta(z, t)$ it is easy to compute $T(z, t)$ by means of the following formula [see (Bibl.1)]:

$$T(z,t) = \theta(z,t) - 10\,z. \tag{VII.2.9}$$

After computing $T(z, t)$ from eq.(VII.2.5), $\rho_w(T)$ is determined after which, at given $S(z, t)$, the quantity $\rho_v(z, t)$ is obtained from eq.(VII.2.2).

This completes the computation if, as a result of the solution, the following is obtained:

$$\rho_v(z,t) \geqslant 0.$$

If this is not the case ($\rho_v < 0$), then the point z and the instant t do not correspond to the formation of the cloud and it must be assumed that

$$\rho_v(z,t) = 0, \tag{VII.2.10}$$

$$S(z,t) = q(z,t), \tag{VII.2.11}$$

$$\theta(z,t) = b[\pi(z,t) - q(z,t)]. \tag{VII.2.12}$$

Section 3. Solution

According to eqs.(VII.2.3) and (VII.2.4), the problem reduces to the solution of two equations of the type

$$\frac{\partial \pi_i}{\partial t} + cw\,\frac{\pi_i}{\partial z} = D\,\frac{\partial^2 \pi_i}{\partial z^2}, \quad i = 1, 2, \tag{VII.3.1}$$

where

$$\pi_1(z,t) = \pi(z,t), \qquad \pi_2(z,t) = S(z,t).$$

Let us determine the boundary and initial conditions of eq.(VII.3.1) for i = 1, 2.

Let

$$T(z,0) = T(0,0) - \gamma z, \tag{VII.3.2}$$

$$\rho_w(z,0) = \rho_w(0,0)\, e^{-az} \tag{VII.3.3}$$

for a = 0.45 km^{-1}, which corresponds to Hann's formula (Bibl.1),

$$\rho(z) = 1.3 \cdot 10^{-3} e^{-\frac{a}{3} z}\ g/cm^3, \tag{VII.3.4}$$

/214

$$T(0,t) = \theta(0,t) = \text{const} = T(0,0), \tag{VII.3.5}$$

$$q(0,t) = \rho(0,t) = \text{const} = \frac{\rho_w(0,0)}{\rho(0)}, \tag{VII.3.6}$$

$$\left.\frac{\partial \theta}{\partial z}\right|_{z=H} = \left.\frac{\partial T}{\partial z}\right|_{z=H} + 10 = \gamma_a - \gamma, \tag{VII.3.7}$$

$$\left.\frac{\partial S}{\partial z}\right|_{z=H} = \left.\frac{\partial q}{\partial z}\right|_{z=H} = -\frac{2}{3} a \frac{\rho_w(0,0)}{\rho(0)} e^{-\frac{2}{3} aH}. \tag{VII.3.8}$$

Then,

$$\pi_1(0,t) = \frac{T(0,0)}{T_0 b} + \frac{\rho_w(0,0)}{\rho_{w,0}} = \mu_1, \tag{VII.3.9}$$

$$\pi_2(0,t) = \frac{\rho_w(0,0)}{\rho_{w,0}} = \mu_2, \tag{VII.3.10}$$

$$\left.\frac{\partial \pi_1}{\partial z}\right|_{z=H} = \frac{\gamma_a - \gamma}{T_0 b} - \frac{2}{3} a \frac{\rho_w(0,0)}{\rho_{w,0}} e^{-\frac{2}{3} aH} = \nu_1, \tag{VII.3.11}$$

$$\left.\frac{\partial \pi_2}{\partial z}\right|_{z=H} = -\frac{2}{3} a \frac{\rho_w(0,0)}{\rho_{w,0}} e^{-\frac{2}{3} aH} = \nu_2. \tag{VII.3.12}$$

The initial conditions can be presented in the form:

$$\pi_1(z,0) = \frac{T(0,0)}{T_0 b} + \frac{\gamma_a - \gamma}{T_0 b} z + \frac{\rho_w(0,0)}{\rho_{w,0}} e^{-\frac{2}{3} az} = \varphi_1(z), \tag{VII.3.13}$$

$$\pi_2(z,0) = \frac{\rho_w(0,0)}{\rho_{w,0}} e^{-\frac{2}{3} az} = \varphi_2(z). \tag{VII.3.14}$$

We introduce the substitution

$$\psi_i(z,t) = \pi_i(z,t)\, e^{-\frac{cw}{2D} z + \frac{c^2 w^2}{4D} t}. \tag{VII.3.15}$$

The function $\psi_i(z, t)$ satisfies an equation of the type

$$\frac{\partial \psi_i}{\partial t} = D \frac{\partial^2 \psi_i}{\partial z^2} \qquad \text{(VII.3.16)}$$

for the boundary conditions

$$\psi_i(0, t) = \mu_i e^{\frac{c^2 w^2}{4D} t}, \qquad \text{(VII.3.17)}$$

$$\left[\frac{\partial \psi_i}{\partial z} + \frac{cw}{2D} \psi_i(z, t)\right]_{z=H} = \nu_i e^{-\frac{cw}{2D} H + \frac{c^2 w^2}{4D} t} \qquad \text{(VII.3.18)}$$

and for the initial condition

$$\psi_i(z, 0) = \varphi_i(z)\, e^{-\frac{cw}{2D} z}. \qquad \text{(VII.3.19)}$$

It is convenient to seek the solution of this equation in the form of a sum

$$\psi_i(z, t) = \psi_i^{(1)}(z, t) + \psi_i^{(2)}(z, t), \qquad \text{(VII.3.20)}$$

where

$$\psi_i^{(1)}(z, t) = \chi_i(z)\, e^{kt}, \qquad \text{(VII.3.21)}$$

$$k = \frac{c^2 w^2}{4D}. \qquad \text{(VII.3.22)}$$

Let $\psi_i^{(1)}(z, t)$ satisfy eq.(VII.3.16) for the boundary conditions (VII.3.17) - (VII.3.18).

Then, $\chi_i(z)$ is the solution of the equation /215

$$k\chi_i(z) = D \frac{d^2 \chi_i}{dz^2} \qquad \text{(VII.3.23)}$$

for the boundary conditions

$$\chi_i(0) = \mu_i, \qquad \text{(VII.3.24)}$$

$$\left[\frac{\partial \chi_i}{\partial z} + \frac{cw}{2D} \chi_i\right]_{z=H} = \nu_i e^{-\frac{cw}{2D} H}. \qquad \text{(VII.3.25)}$$

This solution has the form of

$$\chi_i(z) = \frac{\nu_i D}{cw} e^{-\frac{cw}{2D}(2H - z)} + e^{-\frac{cw}{2D} z}\left[\mu_i - \frac{\nu_i D}{cw} e^{-\frac{cw}{D} H}\right] e^{-\frac{cw}{2D} z}. \qquad \text{(VII.3.26)}$$

The function $\psi_i^{(2)}(z, t)$ is the solution of eq.(VII.3.16) for the boundary

conditions

$$\psi_i^{(2)}(0, t) = 0, \tag{VII.3.27}$$

$$\left[\frac{\partial \psi_i^{(2)}}{\partial z} + \frac{cw}{2D}\psi_i^{(2)}\right]_{z=H=0} = 0 \tag{VII.3.28}$$

and for the initial condition

$$\psi_i^{(2)}(z, 0) = \varphi_i(z)\, e^{-\frac{cw}{2D}z} - \chi_i(z). \tag{VII.3.29}$$

Fourier's method makes it possible to present $\psi_i^{(2)}(z, t)$ in the form of

$$\psi_i^{(2)}(z, t) = \sum_{n=0}^{D} \frac{\sin \sqrt{\lambda_n}\, z}{N_n}\, e^{-\lambda_n D t} \int_0^H [\varphi_i(\xi)\, e^{-\frac{cw}{2D}\xi} - \chi_i(\xi)] \sin \sqrt{\lambda_n}\, \xi d\xi, \tag{VII.3.30}$$

where λ_n is the eigenvalue of the problem, determined from the characteristic equation

$$\tan X = -Ax \tag{VII.3.31}$$

for

$$X = H\sqrt{\lambda_n}, \quad A = \frac{2D}{Hcw}. \tag{VII.3.32}$$

The roots of eq.(VII.3.31) are equal to

$$X_n = (2n + 1)\frac{\pi}{2} + Y_n, \tag{VII.3.33}$$

where $Y_n \to 0$ at $n \to \infty$; Y_n is determined from the equation

$$\cot Y_n = A\left[(2n + 1)\frac{\pi}{2} + Y_n\right]. \tag{VII.3.34}$$

A rough solution of this equation can be obtained by expanding cot Y_n in a series according to the exponents of Y_n, and limiting the calculation to the first two terms of this series. Then the obtained values of Y_n are made more accurate by Newton's method which consists in the following: If here the equation

$$f(x) = 0$$

is given and if its rough solution x_0 is known, the solution can be made more exact by the method of successive approximations, using the formula

$$x^n = x^{n-1} - \frac{f(x^{n-1})}{f'(x^{n-1})}. \tag{VII.3.35}$$

In our case, /216

$$f(x) = \operatorname{tg} x + Ax.$$

For the values of A shown in Table VII.3.1 (for H = 10 km), the eigenvalues λ_n (n = 0, 1, 2, ..., 20) were computed which are shown in Table VII.3.2. The computational error does not exceed five units of the last place.

TABLE VII.3.1

w, cm/sec	k_t, cm²/sec		
	10^4	10^5	10^6
1	0.02	0.2	2
2	0.01	0.1	1

In eq.(VII.3.30) the quantity N_n represents the normal of the eigenfunctions, calculated on the basis of

$$N_n = \int_0^H \sin^2 \sqrt{\lambda_n}\, z\, dz = \frac{H}{2} + \frac{\sin 2Y_n}{4\sqrt{\lambda_n}}. \qquad \text{(VII.3.36)}$$

The result of the calculation of N_n, for the cases shown in Table VII.3.1, is presented in Table VII.3.3.

The solution of eq.(VII.3.16) for the conditions (VII.3.17) - (VII.3.18) is presented in the form of

$$\psi_i(z, t) = e^{\frac{c^2w^2}{4D}t} e^{-\frac{cw}{2D}z} \bar{\chi}_i(z) + \sum_{n=0}^{\infty} \frac{\sin \sqrt{\lambda_n}\, z}{N_n} e^{-\lambda_n D t} \times$$
$$\times \int_0^H [\varphi_i(\xi) - \bar{\chi}_i(\xi)]\, e^{-\frac{cw}{2D}\xi} \sin \sqrt{\lambda_n}\, \xi\, d\xi, \qquad \text{(VII.3.37)}$$

where

$$\bar{\chi}_i(z) = \mu_i \frac{\nu_i D}{cw} e^{-\frac{cw}{D}H} + \frac{\nu_i D}{cw} e^{-\frac{cw}{D}(H-z)}. \qquad \text{(VII.3.38)}$$

The relation (VII.3.15) further yields

$$\pi_i(z, t) = \bar{\chi}_i(z) + e^{\frac{cw}{2D}z} \sum_{n=0}^{\infty} \frac{\sin \sqrt{\lambda_n}\, z}{N_n} e^{-\left(\lambda_n D + \frac{c^2n^2}{4D}\right)t} \times$$
$$\times \int_0^H [\varphi_i(\xi) - \bar{\chi}(\xi)]\, e^{-\frac{cw}{2D}\xi} \sin \sqrt{\lambda_n}\, \xi\, d\xi. \qquad \text{(VII.3.39)}$$

Section 4. Analysis of the Numerical Results

The results of the computation of $T(z, t)$, $\rho_w(z, t)$ and $\rho_v(z, t)$ are compiled in another paper (Bibl.7). Below, we give Tables and graphs of the distribution of liquid-water content with time and with height for $w = 1$ cm/sec, $k_t = 10^5$ cm^2/sec, $T(0, t) = 278^\circ$ in three cases:

1) $\rho_w(0, t) = 7$ gm/m^3, i.e., $u(0, t) = 100\%$ (Table VII.4.1, Fig.4.1, a,b);
2) $\rho_w(0, t) = 5$ gm/m^3, i.e., $u(0, t) = 70\%$ (Table VII.4.2, Fig.VII.4.1,c);
3) $\rho_w(0, t) = 3.5$ gm/m^3, i.e., $u(0, t) = 50\%$ (Table VII.4.3,Fig.VII.4.1,d).

In addition, Table VII.4.4 and Fig.VII.4.1,e give an example of the computation for the case of $w = 2$ cm/sec, $k_t = 10^5$ cm^2/sec, $T(0, t) = 278^\circ$, $\rho_w(0,t) = 3.5$ gm/m^3.

In Fig.VII.4.1,f the distributions of liquid-water content are compared /219 for $t = 2$, 3, and 5 days at $w = 1$ cm/sec (solid curves) and $w = 2$ cm/sec (broken curves).

The diagrams and Tables show that, in all cases, cloudiness begins to develop simultaneously in the lower part of the atmosphere and at the upper boundary of the layer. The upper cloudiness is negligible and is weaker the smaller $\rho_w(0, 0)$. The lower cloudiness which is more pronounced is the one that qualitatively determines the process. After five days, this cloudiness approaches the limiting case, and the final stationary conditions are established after about 20 days if $w = 1$ cm/sec and considerably faster (after 10 days) if $w = 2$ cm/sec. The maximum water content is accumulated at heights of 2 - 4 km; the greater the humidity at the earth's surface the lower will be this height. This demonstrates the decisive role played by vertical currents in the development of a cloud.

It could be assumed that the formation of the upper clouds is the result of the possibility that the fluxes of heat and moisture ($\nu_1 = 0$) are equal to zero at the upper boundary of the layer. A comparison of the calculation at $\nu_1 = 0$ and $\nu_1 \neq 0$[$\nu_1 > 0$ and $\nu_2 < 0$ according to eqs.(VII.3.11) and (VII.3.12)] shows, however, that this is not a fact. In the second case, the conditions for cloud formation become worse due to the fact than an inflow of heat and an outflow of moisture take place through the upper boundary. Nevertheless, the solution is about equal in both cases because of the negligible role played by the upper boundary conditions. The formation of the upper cloud is due to the existing initial conditions. Figure VII.4.2 gives the distribution along the vertical of the initial temperature (Curve 1) at $\gamma = 5^\circ$/km and of the dew point, corresponding to the initial distribution of moisture. In the same diagram, Curve 2 corresponds to the case of $\rho(0, 0) = 7$ gm/m^3 and Curve 3 to the case of $\rho(0, 0) = 5$ gm/m^3. Obviously, the moisture deficit reaches a maximum at the innermost portion of the investigated layer and then decreases in the direction toward the upper boundary, where conditions favorable for the formation of a cloud are thus created.

If the initial conditions assumed by us are considered close to reality (we note that, for $\gamma = 6^\circ$/km the above effect increases), then it is apparently pos-

TABLE VII.3.2

n	A					
	0,01	0,02	0,1	0,2	1,0	2,0
0	0.3111	0.3080	0.2863	0.2654	0.2029	0.1836
1	0.6222	0.6161	0.5760	0.5454	0.4913	0.4816
2	0.9333	0.9242	0.8712	0.8392	0.7079	0.7914
3	1.244	1.232	1.170	1.1409	1.109	1.104
4	1.555	1.541	1.473	1.4470	1.421	1.417
5	1.867	1.850	1.779	1.7556	1.734	1.731
6	2.178	2.158	2.087	2.0658	2.047	2.044
7	2.489	2.467	2.396	2.3770	2.360	2.360
8	2.800	2.777	2.706	2.6897	2.6704	2.6704
9	3.111	3.086	3.016	3.0010	2.9845	2.9845
10	3.423	3.396	3.328	3.3137	3.2987	3.2987
11	3.734	3.706	3.640	3.6265	3.5128	3.6128
12	4.045	4.016	3.952	3.9386	3.9270	3.9270
13	4.357	4.327	4.264	4.2529	4.2412	4.2412
14	4.669	4.638	4.577	4.5662	4.5553	4.5553
15	4.980	4.949	4.890	4.8797	4.8695	4.8695
16	5.292	5.260	5.203	5.1932	5.1836	5.1836
17	5.604	5.571	5.516	5.5068	5.4978	5.4978
18	5.916	5.882	5.829	5.8205	5.8120	5.8120
19	6.227	6.194	6.142	6.1342	6.1261	6.1261
20	6.539	6.506	6.456	6.4480	6.4403	6.4403

TABLE VII.3.3

n	A					
	0,01	0,02	0,1	0,2	1,0	2,0
0	5.0491	5.0998	5.4617	5.7798	5.9775	5.6889
1	5.0490	5.0981	5.3756	5.4765	5.1988	5.1069
2	5.0493	5.0965	5.2840	5.2622	5.0776	5.0398
3	5.0501	5.0959	5.2109	5.1616	5.0424	5.0202
4	5.0498	5.0909	5.1573	5.1068	5.0257	5.0117
5	5.0470	5.0868	5.1200	5.0761	5.0178	5.0092
6	5.0469	5.0847	5.0939	5.0559	5.0122	5.0049
7	5.0467	5.0808	5.0745	5.0426	5.0082	5.0000
8	5.0465	5.0761	5.0605	5.0340	5.0000	
9	5.0461	5.0726	5.0489	5.0271		
10	5.0444	5.0684	5.0417	5.0229		
11	5.0440	5.0646	5.0356	5.0181		
12	5.0434	5.0609	5.0305	5.0165		
13	5.0421	5.0572	5.0260	5.0139		
14	5.0408	5.0537	5.0231	5.0118		
15	5.0402	5.0505	5.0205	5.0108		
16	5.0390	5.0475	5.0183	5.0091		
17	5.0379	5.0447	5.0163	5.0085		
18	5.0368	5.0419	5.0145	5.0079		
19	5.0361	5.0395	5.0129	5.0066		
20	5.0351	5.0372	5.0121	5.0061		

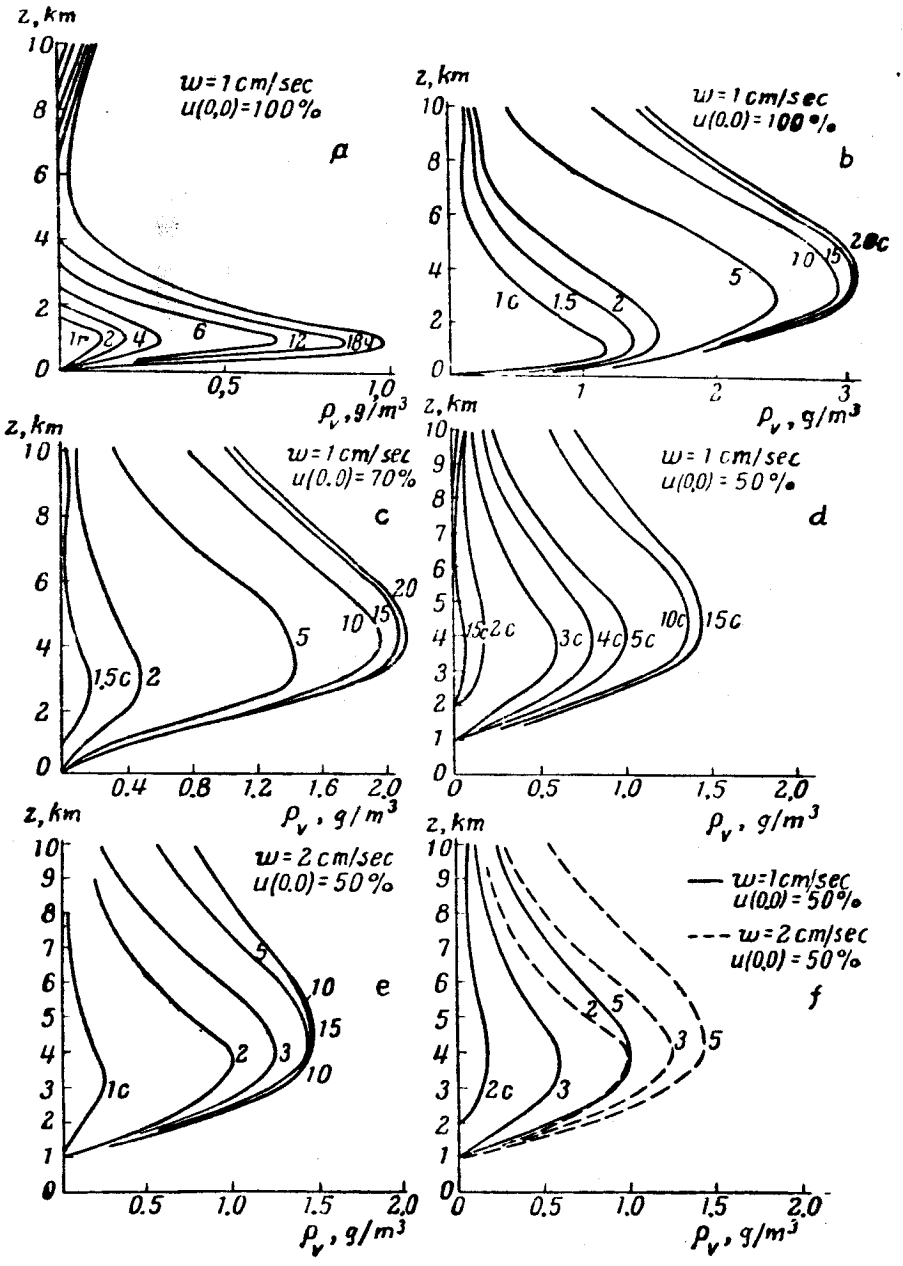

Fig.VII.4.1 Time Rate of Change in Liquid-Water Content in the Thickness of a Cloud at k = 10^5 cm^2/sec and for Various w and u(0, 0)

TABLE VII.4.1

z, km	t, hours							t, days					
	1	2	4	6	12	18	24	1.5	2	5	10	15	20
0	0	0	0	0	0	0	0	0	0	0	0	0	0
1	0.1291	0.1881	0.3096	0.6607	0.8664	0.9874	1.1688	1.3476	1.4644	1.8314	1.9098	1.9224	1.9258
2	0	0	0	0.0791	0.3960	0.5039	0.7809	1.3029	1.5366	2.2436	2.4428	2.4773	2.4853
3	0	0	0	0.0210	0.1388	0.2607	0.6056	1.0430	1.3286	2.4762	2.9286	2.9948	3.0104
4	0	0	0	0	0	0.0724	0.4094	0.6816	1.0438	2.2990	2.9137	3.0588	3.0847
5	0	0	0	0	0	0.0192	0.1394	0.4597	0.7657	1.9921	2.7521	2.9471	2.9865
6	0	0	0	0	0.0080	0.0399	0.1620	0.3582	0.5101	1.6006	2.4169	2.6349	2.7311
7	0	0	0	0	0.0180	0.0373	0.1071	0.2066	0.3417	1.2003	2.0302	2.3084	1.3767
8	0	0	0	0.0254	0.0303	0.0335	0.0835	0.1980	0.2463	0.8496	1.6631	1.9729	2.0560
9	0	0	0	0.0542	0.0842	0.0842	0.1207	0.1670	0.2549	0.6007	1.3498	1.6731	1.7648
10	0.0263	0.0458	0.0791	0.0918	0.1094	0.1167	0.1321	0.1381	0.1881	0.4368	1.0972	1.4239	1.5053

TABLE VII.4.2

z, km	t, hours							t, days					
	1	2	4	6	12	18	24	1.5	2	5	10	15	20
0	0	0	0	0	0	0	0	0	0	0	0	0	0
1	0	0	0	0	0	0	0	0	0.04	0.34	0.44	0.45	0.45
2	0	0	0	0	0	0	0	0.13	0.42	0.03	1.26	1.30	1.30
3	0	0	0	0	0	0	0	0.18	0.50	1.44	1.28	1.89	1.92
4	0	0	0	0	0	0	0	0.09	0.41	1.33	1.96	2.09	2.12
5	0	0	0	0	0	0	0	0.06	0.31	1.29	1.88	2.01	2.05
6	0	0	0	0	0	0	0	0.06	0.22	1.07	1.66	1.88	1.9201
7	0	0	0	0	0	0	0	0.03	0.15	0.827	1.443	1.637	1.6905
8	0	0	0	0	0	0	0	0.06	0.162	0.588	1.183	1.4043	1.4671
9	0	0	0.009	0.019	0.020	0.027	0.042	0.072	0.106	0.420	0.9575	1.1909	1.2606
10	0	0.012	0.019	0.023	0.027	0.030	0.040	0.063	0.0852	0.3209	0.7904	1.0076	1.0744

sible to conclude that, for the condition of sufficient moisture in the layer near the ground, the ascending vertical currents and the turbulent mixing lead to the formation of a two-layer cloud.

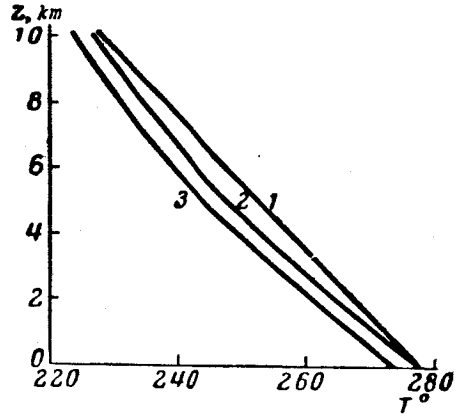

Fig.VII.4.2 Vertical Slope of the Initial Temperature (Curve 1) and of the Dew Point Corresponding to the Initial Distribution of Moisture with u(0, 0) = 100% (Curve 2) and u(0, 0) = 75% (Curve 3)

Basically, the process of cloud formation is determined by the development of the lower cloud. The upper cloud layer is so weak that it could be entirely disregarded were it not for the special effect of radiation on such a layer.

TABLE VII.4.3 /221

z, km	t, days							
	1	1.75	2	3	4	5	10	15
1	0	0	0	0	0	0	0	0
2	0	0	0	0.272	0.434	0.551	0.671	0.738
3	0	0.0478	0.160	0.548	0.739	0.903	1.189	1.242
4	0	0.0632	0.182	0.599	0.820	1.014	1.341	1.434
5	0	0.234	0.167	0.458	0.712	0.911	1.360	1.428
6	0	0.0186	0.107	0.351	0.566	0.729	1.206	1.322
7	0	0.0139	0.082	0.251	0.434	0.555	1.017	1.154
8	0	0.0122	0.065	0.187	0.301	0.417	0.820	0.988
9	0.0009	0.0372	0.067	0.136	0.214	0.300	0.678	0.842
10	0.0292	0.0526	0.069	0.116	0.172	0.238	0.566	0.718

There is also a second possibility. Some observational data show that Hann's formula overestimates the humidity of the air in the upper part of the troposphere. In this case, consideration of an upper cloud in our calculation does not reflect the true process of cloud formation.

TABLE VII.4.4

z, km	t, days					
	1	2	3	5	10	15
1	0	0	0	0	0	0
2	0.125	0.584	0.659	0.719	0.723	0.723
3	0.235	0.890	1.098	1.221	1.272	1.272
4	0.186	0.900	1.256	1.437	1.451	1.451
5	0.110	0.74	1.135	1.407	1.430	1.454
6	0.060	0.534	0.948	1.275	1.360	1.361
7	0.0319	0.389	0.701	1.075	1.201	1.203
8	0.0287	0.254	0.495	0.871	1.044	1.047
9		0.196	0.345	0.689	0.902	0.907
10			0.282	0.555	0.775	0.781

Section 5. Limiting Regime

At a sufficiently removed instant of time t, the second term in the expression (VII.3.39) becomes small with respect to the first term so that the solution assumes the form

$$\pi_i(z, t) = \tilde{\pi}_i(z) = \beta_i + \frac{v_i D}{cw} e^{-\frac{cw}{D}H}\left(e^{\frac{cw}{D}z} - 1\right). \qquad \text{(VII.5.1)}$$

Equation (VII.5.1) determines the stationary state of the clouds. The rate of creation of this state, as indicated in eq.(VII.3.39), depends on the quantity $\frac{cw}{D}$, i.e., on the ratio of the intensity of vertical currents to the turbulent exchange. Thus, according to another paper (Bibl.4), at $w = 0$ and $k_t = 10^5$ cm^2/sec, the stationary state is established after 73 days; according to our computations, this state is established, for the same value of k_t, after 20 days at $w = 1$ cm/sec and after 10 days at $w = 2$ cm/sec.

Therefore, at ratios of w to k_t, characteristic for a real atmosphere, the limiting regime is established during a time of the order of 10 days and is thus only of purely cognitive importance.

It follows from eq.(VII.5.1) that /222

1) at $\nu_i = 0$ and any $\frac{cw}{D}$,

$$\tilde{\pi}_i(z) = \beta_i; \qquad \text{(VII.5.2)}$$

2) at $\nu_i \neq 0$ and $\frac{cw}{D} \to 0$

$$\tilde{\pi}_i(z) = \mu_i + \nu_i z; \qquad \text{(VII.5.3)}$$

3) at $\nu_i \neq 0$ and $\frac{cw}{D} \to D$

$$\tilde{\pi}_i(z) = \mu_i. \qquad \text{(VII.5.4)}$$

Equations (VII.5.2) - (VII.5.4) show that, at a given value of the coefficient of turbulent mixing, the vertical currents not only determine the rate at which the stationary state is established but also regulate the penetration into the atmosphere of the conditions prevailing at the upper boundary.

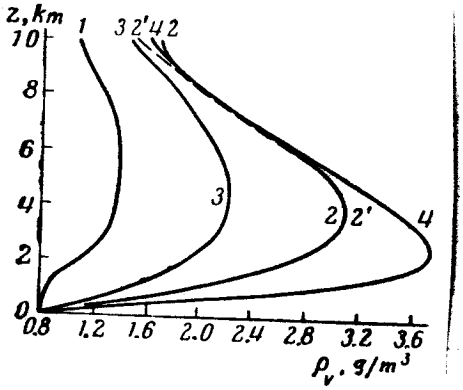

Fig.VII.5.1 Limit Distribution of Liquid-Water Content at $k = 10^5$ cm^2/sec.
1 - w = 0, $\nu_i \neq 0$; 2 - w = 1 cm/sec, $\nu_i \neq 0$; 2' - w = 1 cm/sec, $\nu_i = 0$; 3 - "semi-empirical" solution; 4 - solution for m = 0

Large ascending vertical currents impede the downward spread of fluxes passing through the upper boundary, which results in a heat and humidity regime in the limit, which is about the same as in the case of zero fluxes [cf. eqs. (VII.5.2) and (VII.5.4)]. At small w/D, the heat (moisture) passing through the upper boundary is redistributed into the depth of the layer, as shown in eq. (VII.5.3).

We recall that the condition

$$\tilde{\pi}_i(z) = \mu_i = \text{const}$$

indicates an equalization of potential temperature and potential humidity over the entire thickness of the atmosphere. Therefore, as compared with the initial distribution of heat and moisture, the atmosphere at the limit will be colder and more moist at all levels above the earth's surface, i.e., the conditions for

cloud formation will improve. As compared with this case, at small w/D and at $\nu_1 \neq 0$ and considering $\nu_1 > 0$ and $\nu_2 < 0$ [see eqs.(VII.3.11) and (VII.3.12)], we will obtain a less extensive cloudiness in accordance with eq.(VII.5.3).

All above statements confirm Fig.VII.5.1 which represents the limit distribution of liquid-water content under various conditions. Curve 1 corresponds to the case $w = 0$, $k_t = 10^5$ cm^2/sec, ν_1 is given by eq. (VII.3.11) and eq. (VII.3.12); Curve 2 (solid) corresponds to $w = 1$ cm/sec, other conditions being equal; Curve 2, with a broken segment, represents the previous case of $\nu_1 = 0$ and demonstrates the negligible effect of the heat and moisture fluxes through the upper boundary in the presence of extensive vertical currents. This also confirms the advantage of selecting the heat and moisture fluxes as the boundary condition for $z = H$.

Figure VII 5.1 also gives the "semi-empirical" solution of the problem (Curve 3): The moisture is determined from eq.(VII.3.36) ($i = 2$) and the temperature distribution is taken from observational data [see (Bibl.4)], while Curve 4 represents the solution of eqs.(VII.1.8) and (VII.1.9), disregarding the heat of condensation, i.e., for $m = 0$ [in this formulation, the problem /223 was considered in another paper (Bibl.10)]. Obviously, both last variants give all significant deviations of the results of solving the problem, in more general statements.

Section 6. Allowing for the Radiation

We will now consider eq.(VII.1.9) for $R(T) \neq 0$. Let us introduce a dimensionless constant

$$a = 2\pi \frac{t_0 \alpha_0 \rho_{w,0} B_0}{T_0 C_p \rho_0} = 7.6 \cdot 10^{-2}. \qquad \text{(VII.6.1)}$$

Here, as in Chapter VI, α_0 and B_0 are characteristic values for the absorption coefficient of water vapor and for the radiation of a black body; $\alpha_0 = 1$ cm^2/gm, $B_0 = 0.146$ cal/cm^2 · min, which corresponds to a temperature of $T_0 = 273^\circ$.

Let us use the notation

$$\bar{R}(T) = \frac{1}{2\pi \alpha_0 \rho_{w,0} B_0} R(T). \qquad \text{(VII.6.2)}$$

Then, eq.(VII.1.9) will assume the form

$$\frac{\partial \bar{\theta}}{\partial z} + c\bar{w} \frac{\partial \bar{\theta}}{\partial z} = D \frac{\partial^2 \bar{\theta}}{\partial z^2} + b \frac{\bar{m}}{\rho} + \frac{a}{\rho} \bar{R}(T), \qquad \text{(VII.6.3)}$$

where

(VII.6.4)

$$\rho(z) = \frac{1}{\rho} \rho(z) = e^{-0.15z}.$$

From eq.(VII.6.3), together with eqs.(VII.1.8) and (VII.2.3), we will again obtain equations of the type of

$$\frac{\partial \pi_i}{\partial t} + cw\frac{\partial \pi_i}{\partial z} = D\frac{\partial^2 \pi_i}{\partial z^2} + \Phi_i(z, t), \quad i = 1, 2, \qquad \text{(VII.6.5)}$$

where the symbols $\pi_i(z, t)$ retain their previous meaning, and

$$\Phi_1(z, t) = \frac{a}{b\rho}\overline{R}(T) = \frac{a}{b}\overline{R}(T)e^{0.18z}, \qquad \Phi_2(z, t) = 0. \qquad \text{(VII.6.6)}$$

The boundary and initial conditions of the problem also remain as before.

Let us select a sufficiently small interval of time Δt such that the variations in temperature, humidity, and water content during the time Δt will not lead to a considerable variation in $\overline{R}(t)$ and thus also in $\Phi_1(z, t)$. Over the interval Δt we will assume $\Phi(z, t)$ to be constant in time and equal to $\Phi_1(z, t_0)$ where t_0 is the initial instant of time.

For a free term independent of time, eq.(VII.6.5) can be solved simply by the Fourier method. As a result, we obtain

$$\pi_i(z, t) = \overline{\chi}(z) + e^{\frac{cwz}{2D}}\sum_{n=0}^{\infty}\frac{\sin\sqrt{\lambda_n}z}{N_n}e^{-\left(\lambda_n D + \frac{c^2w^2}{4D}\right)t} \times$$
$$\times\int_0^H [\pi_i(\xi, t_0) - \chi_i(\xi)]\, e^{-\frac{cw}{2D}\xi}\sin\sqrt{\lambda_n}\,\xi d\xi +$$
$$+ e^{\frac{cw}{2D}z}\sum_{n=0}^{\infty}\frac{1 - e^{-\left(\lambda_n D + \frac{c^2w^2}{4D}\right)t}}{\lambda_n D + \frac{c^2w^2}{4D}}\frac{\sin\sqrt{\lambda_n}z}{\Lambda}\int_0^H \Phi_i(\xi, t_0)\, e^{-\frac{cw}{2D}}\sin\sqrt{\lambda_n}\cdot\xi d\xi. \qquad \text{(VII.6.7)}$$

Here, t varies within the limits of /224

$$t_0 \leqslant t \leqslant t_0 + \Delta t.$$

If the solution obtained for the instant $t = t_0 + \Delta t$ is taken as the new initial condition it is possible, by repeating the computation with eq.(VII.6.7), to find the sought values at the instant $t = t_0 + 2\Delta t$ and so forth.

Consequently, the process of solution is accomplished in time steps* and can be represented in the form of the following algorithm:

* We used an analogous method before (see Chapter VI, Sect.9) which simultaneously took both turbulent and radiative heat exchange into consideration.

$$\pi_i(z, t_k) = \bar{\chi}_i(z) + e^{\frac{cw}{2D}z} \sum_{n=0}^{\infty} \frac{\sin \sqrt{\lambda_n}\, z}{N_n} e^{-\left(\lambda_n D + \frac{c^2w^2}{4D}\right)\Delta t} \times$$
$$\times \int_0^H [\pi_i(z, t_{k-1}) - \bar{\chi}_i(\xi)]\, e^{-\frac{cw}{2D}\xi} \sin \sqrt{\lambda_n}\, \xi d\xi +$$
$$+ e^{\frac{cw}{2D}z} \sum_{n=0}^{\infty} \frac{1 - e^{-\left(\lambda_n D + \frac{c^2w^2}{4D}\right)\Delta t}}{\lambda_n D + \frac{c^2w^2}{4D}} \frac{\sin \sqrt{\lambda_n}\, z}{N_n} \times$$
$$\times \int_0^H \Phi_i(\xi, t_{k-1}) e^{-\frac{cw}{2D}\xi} \sin(\sqrt{\lambda_n}\xi)\, d\xi. \qquad \text{(VII.6.8)}$$

Section 7. Calculation of the Radiative Heat Influx

The most difficult problem in calculations with eq.(VII.6.8) is derivation of the quantity $\Phi_1(z, t_k)$ which is connected with the radiative inflow of heat R(T) over the relations (VII.6.2) and (VII.6.6).

We note first that, unlike in Chapter VI, it is not permissible here to neglect the absorption of radiation by water vapor with respect to the absorption by droplet water, in view of the fact that we here consider the initial stage of the development of the cloud. For the same reason, it is not permissible to use the simplified procedure for calculating the radiative inflow of heat, proposed in Chapter VI.

If, as before, we neglect scattering* and introduce a mean absorption coefficient for water α_v as well as three absorption coefficients for water vapor α_j ($j = 1, 2, 3$), then R(T) can be presented in the following form [see eq. (I.2.45) for $k_t = 0$].

$$\bar{R}(z, t) = \frac{1}{\rho_{w,0}\alpha_0} \sum_{j=1}^{3} [a_{w,j}\rho_w(z, t) + a_v\rho_v(z, t)]\, K_j(T), \qquad \text{(VII.7.1)}$$

where

$$K_j[T(z, t)] = \left\{A_{1,j} + A_{2,j} + \int_0^{\tau_j^*} \bar{B}_j(\xi, t)\, E_1(|\tau_j - \xi|)\, d\xi - 2\bar{B}_j(\tau_j, t)\right\}; \qquad \text{(VII.7.2)}$$

$$\bar{B}_j = \frac{B_j}{B_0}; \qquad \text{(VII.7.3)}$$

$$\tau_j = \int_0^z [a_{w,j}\rho_w(\xi, t) + a_v\rho_v(\xi, t)]\, d\xi; \qquad \text{(VII.7.4)}$$

Here, $A_{1,j}$ is the radiation entering the medium from its lower boundary; /225
$A_{2,j}$ is the radiation penetrating from the upper boundary inward; $A_{1,j}$ and $A_{2,j}$ are determined by the boundary conditions.

* This is more justified here because of the small concentration of droplets in the nascent cloud.

If we assume that the earth's surface radiates like a black body, we obtain

$$A_{1,j} = \bar{B}_j(0,\ t)E_2(\tau_j). \qquad \text{(VII.7.5)}$$

The value of $A_{2,j}$ is usually assumed to be zero. However, recalling the statement made in Chapter I, Sect.3 as to the fluxes of long-wave descending radiation at the upper boundary of the atmosphere being other than zero* then it is natural to present this quantity in the form of

$$A_{2,j} = \int_0^{\tau_j^{(1)}} \bar{B}_j^{(1)}(\xi)\, E_1(\xi + \tau_j^* - \tau_j)\, d\xi. \qquad \text{(VII.7.6)}$$

Here $\bar{B}_j{}^{(1)}(\xi) = \bar{B}_j[T^{(1)}(\xi)]$; $T^{(1)}(\xi)$ is the temperature distribution with height at $z > H$; $\tau_j^{(1)}$ is the optical thickness of the layer $H \leq z \leq \infty$.

Equation (VII.7.6) represents (see Chapter VI) the influx of heat per unit volume in the investigated layer $0 \leq z \leq H$, due to the absorption of radiant energy arriving from the layer $z > H$ located above the cloud.

Stipulating that the top of the level $z = H$, receives primarily radiation from the immediately adjoining layer, we can limit the calculation to the simple assumption

$$\bar{B}_j^{(1)}(\xi) = \text{const} = \bar{B}_j(H).$$

$$A_{2,j} = \bar{B}_j(H)\,[E_2(\tau_j^* - \tau_j) - E_2(\tau_j^* + \tau_j^{(1)} - \tau_j)]. \qquad \text{(VII.7.7)}$$

A calculation on the basis of eqs.(VII.7.1) and (VII.7.2) at given $\rho_w(z)$, $\rho_v(z)$, and $T(z)$ is quite laborious and requires maintenance of a high accuracy for the levels z located within the clouds, in view of the fact that here $K_j(T)$ can be very small (see Chapter VI) while the factor at $K_j(T)$ in eq.(VII.7.1) is large (especially if ρ_v is sufficiently large).

Calculation of $K_j(T)$ with high accuracy is made difficult by the fact that $\int_0^{\tau} B(\xi)E_1(|\tau - \xi|)d\xi$ is an improper integral, [the function $E_1(x)$ has a logarithmic singularity at $x = 0$]. In order to increase the computational accuracy, this integral can be presented in the following form (the subscript j is omitted here)

$$\varphi(\tau) = \int_0^{\tau^*} B(\xi)\, E_1(|\tau - \xi|)\, d\xi = \int_0^{\tau^*} \Delta B(\xi, \tau)\, E_1(|\tau - \xi|)\, d\xi + B(\tau)\,[2 - E_2(\tau) - E_2(\tau^* - \tau)], \qquad \text{(VII.7.8)}$$

* By upper boundary of the atmosphere is meant here and above the level of the tropopause $z = H = 10$ km.

Here, $\Delta_k = \tau_{k+1} - \tau_k$.

Let us consider that

$$\Delta_k b_k = f(\tau_{k+1}) - f(\tau_k), \quad a_k = f(\tau_k)$$

and perform the simple transformations. We then obtain the following expression of the integral (VII.7.10) for the case $f(\xi) = \Delta B(\xi, \tau_p)$:

$$\begin{aligned}\int_0^{\tau^*} \Delta B(\xi, \tau_p) E_1(|\tau_p - \xi|)\, d\xi = \sum_{k=p}^{n-1} \{b_k [E_3(\tau_k - \tau_p) - E_3(\tau_{k+1} - \tau_p)] + \\ + \Delta B(\tau_k, \tau_p) E_2(\tau_k - \tau_p) - \Delta B(\tau_{k+1}, \tau_p) E_2(\tau_{k+1} - \tau_p)\} - \\ - \sum_{k=0}^{p-1} \{b_k [E_3(\tau_p - \tau_{k+1}) - E_3(\tau_p - \tau_k)] + \\ + \Delta B(\tau_k, \tau_p) E_2(\tau_p - \tau_k) - \Delta B(\tau_{k+1}, \tau_p) E_2(\tau_p - \tau_{k+1})\}. \end{aligned} \quad \text{(VII.7.16)}$$

To characterize the accuracy of calculation by eq.(VIII.7.16), two variants of dividing the interval $(0, \tau^*)$ into 12 and 36 parts of the points τ_k shown in the Table are given in Table VII.7.1. These values of τ_k were computed by means of eq.(VII.7.4) at $\rho_w(z, t)$ and $\rho_v(z, t)$, obtained in one of the examples in Section 4, namely, in the case of t = 36 hours, $\rho_w(0, 0) = 5$ gm/m^3, w = = 1 cm/sec (see Fig.VII.4.2). Corresponding values of z_k are also given in Table VII.7.1. /227

TABLE VII.7.1

First Variant		Second Variant					
z_k	τ_k	z_k	τ_k	z_k	τ_k	z_k	τ_k
0	0	0	0	1.2	12.89	4.0	19.66
0.5	6.08	0.1	1.22	1.3	13.25	4.5	20.14
1.0	12.16	0.2	2.43	1.4	13.62	5.0	20,62
1.5	13.98	0.3	3.65	1.5	13.98	5.5	20.92
2.0	15.80	0.4	4.86	1.6	14.34	6.0	21.23
3.0	18.16	0.5	6.08	1.7	14.71	6.5	21.42
4.0	19.66	0.6	7.30	1.8	15.07	7.0	21.62
5.0	20.62	0.7	8.51	1.9	15.43	7.5	21.76
6.0	21.23	0.8	9.73	2.0	15.80	8.0	21.89
7.0	21.62	0.9	10.94	2.5	16.98	8.5	21.99
8.0	21.89	1.0	12.16	3.0	18.16	9.0	22.08
9.0	22.08	1.1	12.52	3.5	18.91	9.5	22.81
10.0	23.50					10.0	23.53

The computation with eq.(VII.7.16) for a linear temperature distribution with height gives, in this case,

$$\int_0^{\tau^*} \Delta B(\xi, \tau_p) E_1(|\tau_p - \xi|)\, d\xi \begin{cases} -0.00255 & \text{for } n = 12, \\ -0.00261 & \text{for } n = 36. \end{cases}$$

Therefore, the formula of approximate integration (VII.7.16) is quite accurate when the interval $(0, \tau^*)$ is divided into a comparatively small number of parts.

Section 8. Calculation Samples

Some numerical results showing the effect of the radiative inflow of heat on the variations in water content of the cloud are given below.

The calculations were made first with eq.(VII.6.8) for n = 20. The laboriousness of the calculations and the low accuracy at $z \approx H$ made us change the method of solution and apply the finite-difference method (Bibl.11) directly to eqs.(VII.6.5). Here as before, the nonlinear term of the equation $\Phi_1(z, t)$ was assumed to be known while for $t = t_n$ it was to be calculated from eq.(VII.7.1) and consequently for the values $T(z, t_{n-1})$, $\rho_v(z, t_{n-1})$, $\rho_w(z, t_{n-1})$. The calculations were made on the "Ural-1" computer. The following variants were considered:

1. $w = 1$ cm/sec, $k_t = 10^5$ cm^2/sec, $R(T) = 0$, $R(T) \neq 0$;
2. $w = 2$ cm/sec, $k_t = 10^5$ cm^2/sec, $R(T) = 0$, $R(T) \neq 0$;
3. $w = 0$, $k_t = 10^5$ cm^2/sec, $R(T) = 0$,
4. $w = 0$, $k_t = 0$, $R(T) \neq 0$.

For t = 0, it was assumed that

$$T(z, 0) = T(0,0) - \gamma z,$$

$$\rho_w(z, 0) = \rho_w(0,0)\, e^{-az},$$

where $T(0,0) = 280°$, $\gamma = 50$ km^{-1}, $\rho_w(0,0) = 9.3$ g/m^3, $a = 0.45$ km^{-1}.

Table VII.8.1 gives the values of the liquid-water content $\rho_v(z, 0)$ of a cloud with the above-prescribed values of temperature and humidity at the /228

TABLE VII.8.1

	z, km										
	0	1	2	3	4	5	6	7	8	9	10
$\rho_v(z, 0)$, g/m^3	0	0.281	0.0276	0	0	0	0	0	0	0	0.00684

initial instant.

The following boundary conditions were assumed:

The calculations show that, under the influence of radiative cooling, the cloud develops upward.

TABLE VII.8.2

	$R=0$	$R\neq 0$	$R=0$	$R\neq 0$	$R=0$	$R\neq 0$	$R=0$	$R\neq 0$
t, hours	0		2		4		5	
z_s, km	2	2	2	3	3	5	5	6

Table VII.8.2 shows the heights of the upper boundaries of the cloud z_s at various instants of time at w = 1 cm/sec taking into account (R(T) ≠ 0) but neglecting (R(T) = 0) radiation.

TABLE VII.8.3

z, km	w=1 cm/sec			w=2 cm/sec		
	t, hours					
	1	2	3	1	2	3
1	7	6.8	5.3	3.2	1.8	1.5
2	104	50.5	37.5	13.7	8.6	6.7
3	—	—	189.7	—	30.6	37.8

The increment of water content, in percent, due to radiation is shown in Table VII.8.3. Here, z = 1 km corresponds to about the center of the cloud, while z = 2 km and 3 km refer to its upper part. The dashes in the Table refer to cases where, at a height of z = 3 km, there was as yet no cloud when neglecting the radiation but did appear when radiation was taken into consideration.

Table VII.8.3 also shows that the contribution to the liquid-water content made by radiation decreases with increasing velocity of ascending motion. This indicates the major role played by vertical currents in the formation of clouds. With an increase in the latter, the relative contribution of other factors is reduced.

To compare the radiative and turbulent inflow of heat, the absolute increase in water content with time computed by means of /229

$$\Delta\rho_v(t) = \rho_v(z,t) - \rho_v(z,t_0).$$

is shown in Table VII.8.4. (The quantities ρ_v and $\Delta\rho_v$ are given in gm/m^3.) In the computations, it is assumed that $w = 0$. The columns $k_t = 0$ correspond to pure radiation and the columns $R = 0$ refer to pure turbulence.

TABLE VII.8.4

z, km	t, hours					
	1		2		3	
	$k_t = 0$	$R = 0$	$k_t = 0$	$R = 0$	$k_t = 0$	$R = 0$
1	0.006	0.011	0.009	0.04	0.011	0.030
2	0.0307	0.0039	0.0459	0.0078	0.0722	0.0162

The Table shows that, in the center of the cloud, the influence of radiation is less than that of turbulence but that it is not negligibly small with respect to the latter. In the upper part of the cloud, the role played by radiative transfer becomes predominant.

Therefore, the generally accepted mechanism of formation of stratus clouds, which takes into account vertical ordered motions and turbulent transfer of heat and of moisture, is not complete. Radiative heat exchange plays an important role, especially in the upper part of the cloud.

The obtained results again confirm the decisive influence of radiation on the formation of upper layers of the cloud, revealed in Chapter VI. The conditions stipulated in Chapter VI (no reduction in water content toward the upper boundary) permitted a direct investigation of the thermal effect of radiation, namely, the development of a temperature inversion.

In this Chapter, the problem was formulated as to assume that the water content of a developing cloud rapidly diminishes in the direction toward the upper boundary. In this case, in accordance with the conclusions in Chapter VI, no inversion of radiative origin takes place.

Obviously, both effects will be found if the formulation of the problem is changed to state that the computed water content does not decrease in the upper part of the cloud.

BIBLIOGRAPHY

1. - A Course in Meteorology (Kurs meteorologii). P.N.Tverskoy, Ed. Gidrometeoizdat, 1951.
2. Shvets, M.Ye.: On the Condensation of Water Vapor in the Atmosphere (O kondensatsii vodyanogo para v atmosfere). Izv. Akad. Nauk SSSR, ser. geofiz., No.6, 1955.
3. Shvets, M.Ye.: On the Question of Precalculating the Field of Relative Humidity (K voprosu predvychisleniya polya otnositel'noy vlazhnosti). Trudy GGO (Main Geophysical Observatory), No.81, 1959.
4. Bogdanova, N.P. and Shvets, M.Ye.: On the Determination of the Lower Boundary within Mass Stratus Clouds (Ob opredelenii nizhney granitsy vnutri massovykh sloistykh oblakov). Trudy GGO, No.81, 1959.
5. Arrago, L.P. and Shvets, M.Ye.: On the Theory and Formation and Evolution of Nonconvective Cloudiness (K teorii obrazovaniya i evolyutsii nekonvektivnoy oblachnosti). Trudy GGO, No.121, 1961.
6. Matveyev, L.T. and Kozharin, V.S.: The Role of Turbulent Mixing in the Structure Formation of Stratus Clouds (Rol' turbulentnogo peremshivaniya v formirovanii struktury sloistoobraznykh oblakov). Izv. Akad. Nauk SSSR, ser. geofiz., No.11, 1956.
7. Matveyev, L.T.: Some Questions of the Theory of Formation and Evolution of Stratus Clouds (Nekotoryye voprosy teorii obrazovaniya i evolyutsii sloistoobraznoy oblachnosti). Trudy Arkt. i Antarkt. Inst., No.228, 1959.
8. Matveyev, L.T.: Conditions of Formation and Evolution of Clouds under the Influence of Vertical Currents and of Turbulent Exchange (Usloviya obrazovaniya i evolyutsii oblakov pod vliyaniyem vertikal'nykh tokov i turbulentnogo obmena). Izv. Akad. Nauk SSSR, ser. geofiz., No.1, 1961.
9. Feygel'son, Ye.M.: Origin and Development of Stratus Clouds (Voznikноveniye i razvitiye sloistoobraznykh oblakov). Izv. Akad. Nauk SSSR, ser. geofiz., No.2, 1963.
10. Klubovich, K.V.: On the Theory of Cloud Formation (K teorii obrazovaniya oblakov). Uchen. Zap. Minsk. Gos. ped. in-ta, ser. fiz.-mat. (Minsk State Pedag. Inst.), No.7, 1957.
11. Berezin, I.S. and Zhidkov, N.P.: Methods of Calculus, Vol.II (Metody vychisleniy, T. II). Fizmatgiz, 1959.